Australian Government
Geoscience Australia

Government of South Australia
Primary Industries and Resources SA

An assessment of the uranium and geothermal prospectivity of east-central South Australia

D. L. Huston and S. E. van der Wielen

With contributions by D.C. Champion, D. Connolly, G. Fraser, E. Gerner, D.L. Huston, A. Kirkby, A.J. Meixner, T.P. Mernagh, A. Schofield, R.G. Skirrow, R. Weber, and S.E. van der Wielen

Record
2011/34

GeoCat #
72666

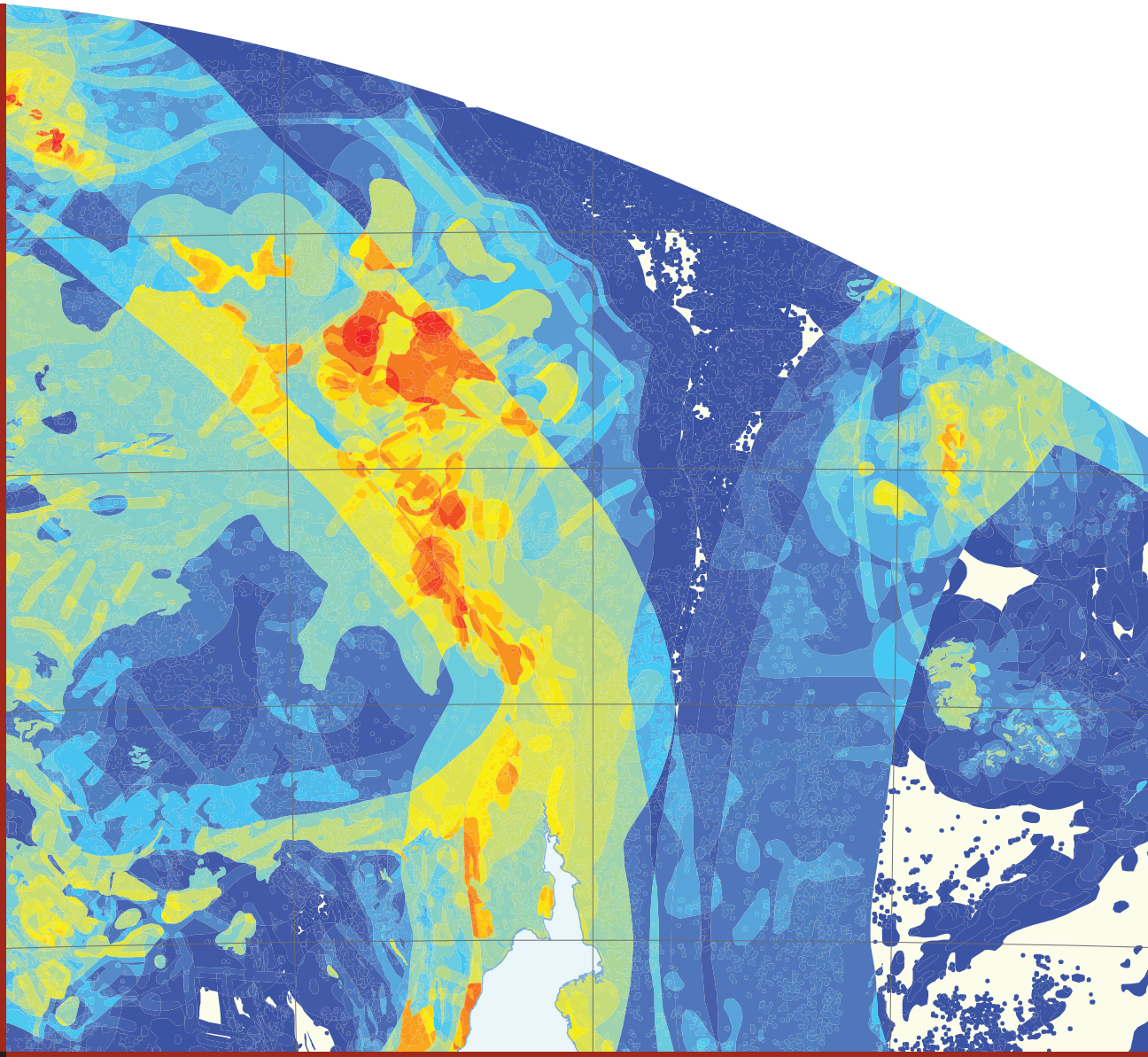

An assessment of the uranium and geothermal prospectivity of east-central South Australia

GEOSCIENCE AUSTRALIA
RECORD 2011/34

Edited by

D. L. Huston and S. E. van der Wielen

With contributions by D.C. Champion, D. Connolly, G. Fraser, E. Gerner, D.L. Huston, A. Kirkby, A.J. Meixner, T.P. Mernagh, A. Schofield, R.G. Skirrow, R. Weber, and S.E. van der Wielen

Onshore Energy and Minerals Division, Geoscience Australia, GPO Box 378, Canberra, ACT 2601

Department of Resources, Energy and Tourism
Minister for Resources and Energy: The Hon. Martin Ferguson, AM MP
Secretary: Mr Drew Clarke, PSM

Geoscience Australia
Chief Executive Officer: Dr Chris Pigram

ISSN 1448-2177
ISBN 978-1-921954-38-2 (Web)
978-1-921954-37-5 (Print)

GeoCat # 72666

Bibliographic reference: Huston, D. L., and van der Wielen, S. E. (eds), 2011. An assessment of the uranium and geothermal prospectivity of east-central South Australia. *Geoscience Australia Record*, **2011/34**, 229pp.

Contents

Executive summary

Assessments of the uranium and geothermal energy prospectivity of east-central South Australia have been undertaken using a GIS-based geological systems approach. Sandstone-hosted (including both roll-front and paleochannel varieties) uranium, iron oxide-copper-gold-uranium, unconformity-related uranium, magmatic-related (including intrusive and volcanic-related) uranium and sediment-hosted copper-uranium mineral systems were considered. For geothermal energy, both hot rock and hot sedimentary aquifer systems were considered.

A customised mineral prospectivity assessment methodology was developed for the uranium systems analysis. The approach utilised is knowledge-driven, and develops mappable geological criteria from a mineral systems model. The mineral systems model used consists of four key components:

- sources of metals and fluids;
- drivers of fluid flow;
- fluid pathways and architecture; and
- deposition sites.

Criteria weightings were assigned subjectively, and are a product of the importance, applicability and confidence of the given criterion. The final assessment combined each of the mappable criteria under its relevant uranium systems component, which was then normalised to the number of inputs to avoid over-representation of any of the mineral system components. The final map was produced by adding together the individual component weightings.

Prospectivity analysis for paleochannel and roll-front uranium deposits identified the highest prospectivity to be located to the east and northeast of the Mount Painter Inlier. The area corresponds with an area of known mineralisation including the Beverley and Beverley North mines and the Four Mile and Honeymoon deposits. Other areas identified in the analysis as having high to very high prospectivity include two areas in the far southwestern part of the study area (paleochannel sub-type) and an area to the north of Roxby Downs (roll-front sub-type).

Prospectivity analysis for uranium-rich iron oxide-copper-gold deposits highlighted areas of known deposits in the Olympic Dam and Prominent Hill districts. In addition to the two known districts, the analysis also identified an area to the north and west of Spencer Gulf. Although hematitic alteration assemblages have been reported in this area, no significant iron oxide-copper-gold deposits have been recognised. The modelling has also identified areas in the northern Curnamona Province, under extensive and deep cover, as having prospectivity for this mineral system.

Prospectivity analysis for unconformity-related uranium deposits highlighted the southern end and eastern margin of the Cariewerloo Basin, the southwest corner of the study area, and the Mount Painter and Mount Babbage Inliers and surrounding Callabona Sub-basin. The analysis also identified an area of moderate to high potential around Olympic Dam due to the potential for remobilisation of uranium which could lead to unconformity-related uranium deposits in this region.

The assessment for intrusive-related systems highlighted the area in the vicinity of Crocker Well, particularly the Basso Suite southeast of Crocker Well, and the Mount Painter Inlier as having high prospectivity in the Curnamona Province. In the Gawler Province, potential is dominated by Hiltaba Suite granites, with the highest favourability occurring in the southwest and northwest of the study area, as well as the region around Olympic Dam. In many cases, the same regions identified as having potential for intrusive-related systems also exhibit favourability for volcanic-related uranium. In addition, the analysis highlighted the central Benagerie Ridge Volcanics in the Curnamona

Province, as well as felsic components of the lower Gawler Range Volcanics in the Gawler Province.

Neoproterozoic rocks in the study area were assessed for copper-uranium prospectivity using a sediment-hosted mineral system model developed for the Adelaide Rift Complex. This analysis identified areas with known deposits as well as areas without significant known deposits. The latter areas included several areas to the south of Leigh Creek, three areas associated with diapirs to the northeast of Hawker, several areas east of Port Pirie and an area near the northern tip of the Stuart Shelf.

Hot rock and hot sedimentary aquifer geothermal prospectivity was mapped based on the results of 3D thermal modelling which was conducted on a 3D geological map constructed to a depth of 15 km from geological and geophysical data. Using thermal conductivity data, heat production data and the 3D geological map, thermal forward models were computed and the modelled temperature and heat flow results compared to measured surface heat flow values and down-hole temperatures. Some heat production values of basement units and thermal conductivities of cover sequences were modified to minimise the difference between the modelled and measured data.

Hot rock prospectivity was determined from a temperature at 4 km depth slice through the optimal thermal model. This modelling identified three broad regions with different prospectivity. Low prospectivity was determined in the southwest part of the study area, corresponding to the western part of the Gawler Province. Moderate to high prospectivity was indicated in the centre (eastern Gawler Province, the Adelaide Rift Complex, the Mount Painter and Mount Babbage Inliers) of the study area, and low to moderate prospectivity was indicated in the southeast (Curnamona Province). Localised regions of higher prospectivity occur across the entire assessment area and correspond to high-heat-producing granite bodies which have intruded into the basement. Hot sedimentary aquifer prospectivity is generally low because of the limited volume of permable aquifers in the thermal model at sufficient temperature for utilisation.

1 Introduction

As part of the Onshore Energy Security Program, Geoscience Australia, in collaboration with Primary Industries and Resources South Australia (PIRSA) has undertaken geological framework studies to provide information on the geodynamic and architectural controls on energy systems. These framework studies are targeted at key strategic regions of Australia and are linked to the acquisition of deep seismic and magnetotelluric data. The focus of fiscal year 2009-2010 was east-central South Australia, stretching between longitudes of 135.0° and 141.0° east and between latitudes 29.0° and 33.5° south (Figure 1.1). In addition to geophysical data acquisition and interpretation, these framework studies have included geochronology as well as uranium mineral system and geothermal system studies (Korsch *et al.*, 2010a,b; Fraser and Neumann, 2010; Skirrow *et al.*, 2011). The main goal of these studies is to provide pre-competitive data that can be used by the mineral and geothermal sectors for exploration. The data also provide new information which can be used in assessing the prospectivity of east-central South Australia for energy (uranium and geothermal) resources using geosystems (i.e. mineral and geothermal systems) methodologies in a GIS environment. This report is intended to provide such an assessment in a qualitative to semi-quantitative way. One of the goals of this analysis is to define the extent of areas or regions with known deposits. Another goal was to define areas with previously unrecognised prospectivity.

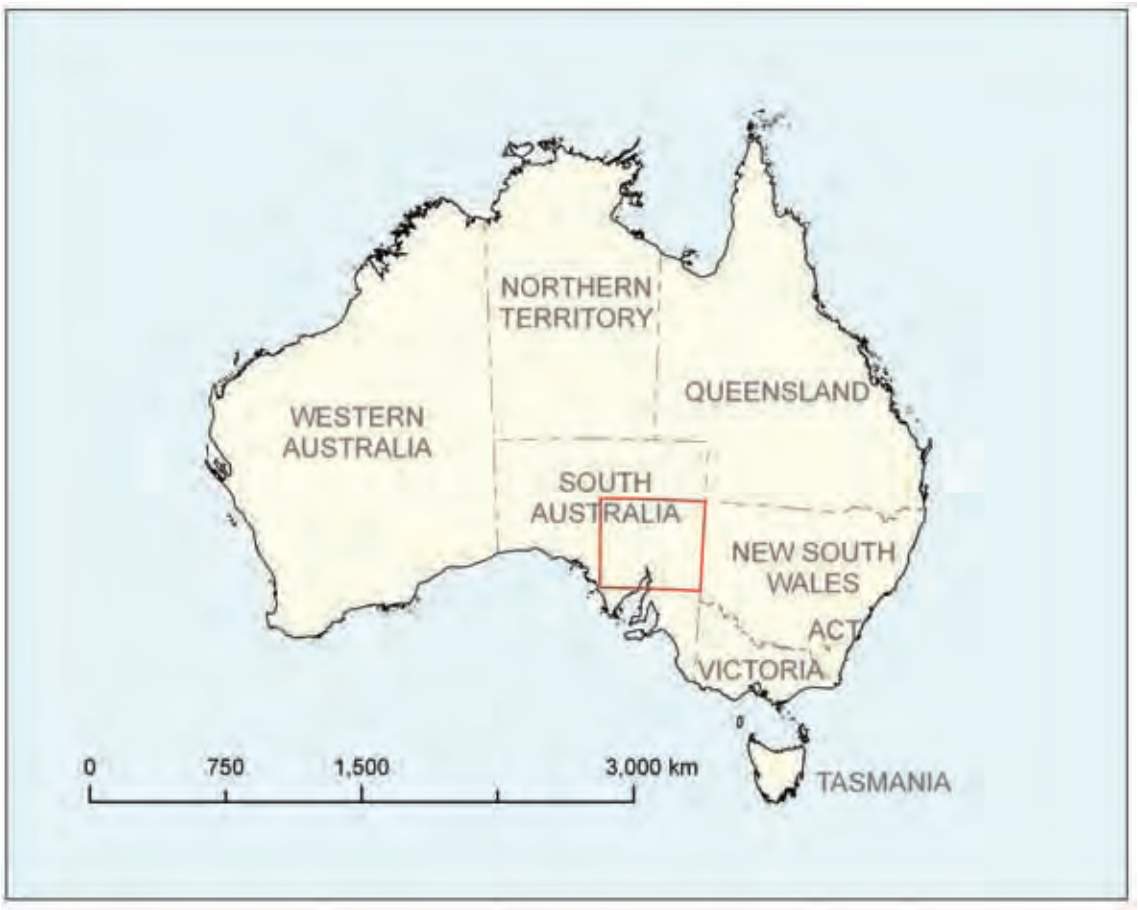

Figure 1.1: *Location of study area.*

2 Overview of Regional Geology

G. FRASER

2.1 INTRODUCTION

The geographic area considered in this report, in east-central South Australia, spans the geological provinces of the eastern Gawler Province, the Adelaide Rift Complex, and the western Curnamona Province (Figure 2.1). The northern part of the study area is covered by sedimentary rocks of the Arckaringa, Eromanga and Lake Eyre basins. The geological history of each of these geological provinces and basins is briefly reviewed here to provide context for the more detailed considerations of the energy and mineral systems components that follow.

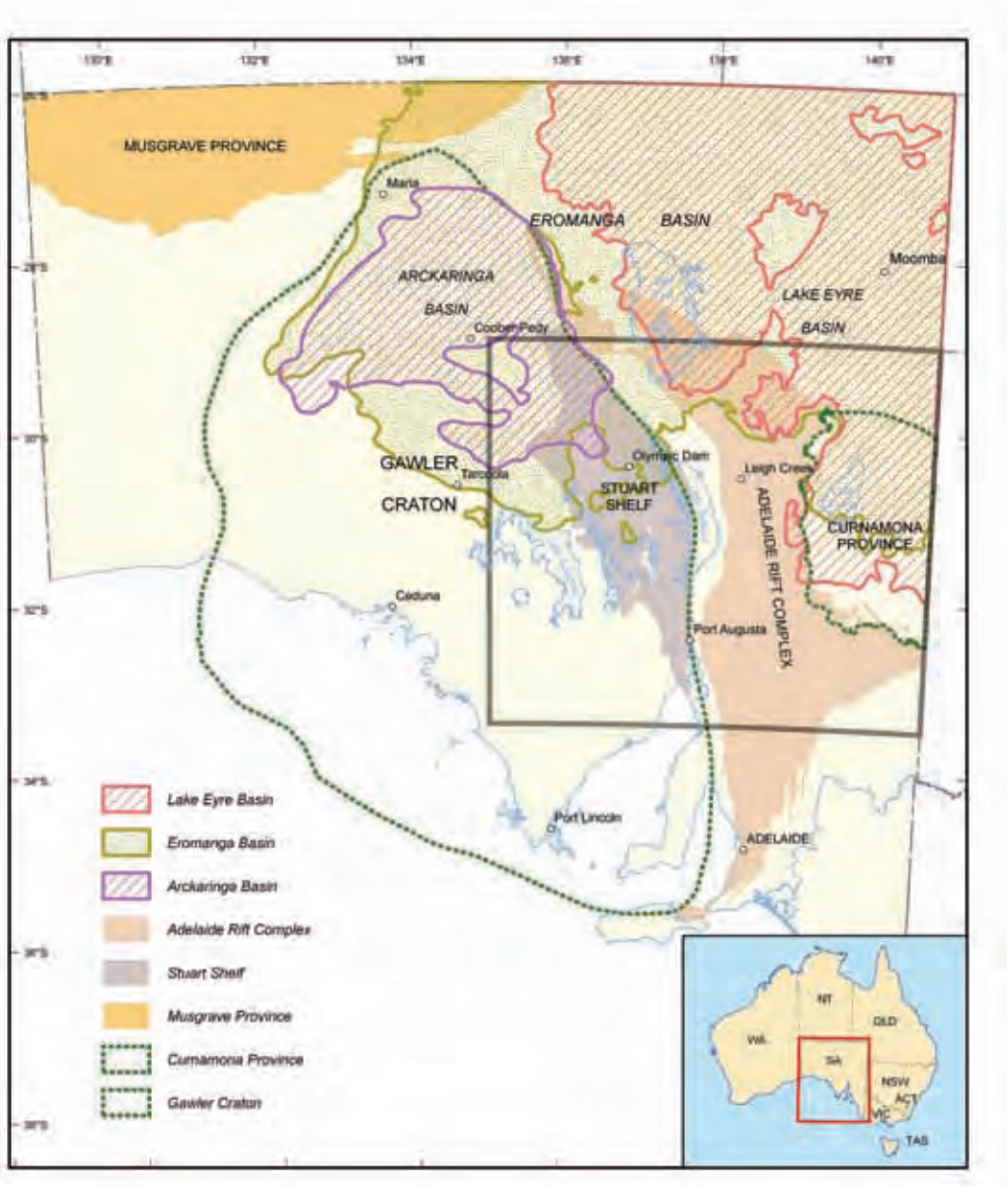

Figure 2.1: *Simplified geology of South Australia, showing the major provinces and regions. The box encloses the area considered in this study.*

2.2 THE GAWLER PROVINCE

The Gawler Province (Figures 2.2 and 2.3) consists of Mesoarchean to Mesoproterozoic rocks and has been subdivided into numerous geological domains comprised of rocks of similar ages and history, and/or bounded by major shear-zones (Ferris *et al.*, 2002). The geological components and history of the Gawler Province have been described in detail by Drexel *et al.* (1993), Daly *et al.* (1998), Ferris *et al.* (2002), Hand *et al.* (2007) and Kositcin (2010).

The oldest rocks known from South Australia are Mesoarchean (~3150 Ma) granitic gneisses identified in only a relatively restricted area of about 1500 km^2 within the northern Spencer Domain, near the eastern margin of the Gawler Province (Fraser *et al.*, 2010a). On geochemical grounds, and by analogy with post-tectonic potassic granites of the Pilbara and Yilgarn cratons of Western Australia, these rocks are regarded as the product of melting of a pre-existing trondjhemite-tonalite-granodiorite-like source region that has not been identified in surface outcrops. The location of these Mesoarchean potassic granites, with relatively elevated heat production values, broadly correlates with the western part of the South Australian heat flow anomaly (Neumann *et al.*, 2000) and has been tentatively suggested as an underlying control on high-heat flow with attendant implications for geothermal exploration (Fraser *et al.*, 2010a).

The period between ~3150 and ~2550 Ma is essentially unrepresented in the known rock record in the Gawler Province, although it is noted that numerous gneissic rocks from the Sleaford Complex contain pre~2600 Ma zircons, some of which may be of detrital origin, while others may represent igneous protolith ages (e.g., Coolanie Gneiss, Waddikee Rocks; Fraser and Neumann, 2010) and yield Nd model ages in the range ~3000 to ~2700 Ma (Daly and Fanning, 1993). This evidence suggests Mesoarchean crust may be present beneath considerable parts of the Gawler Province.

Supracrustal assemblages, including clastic and chemical sediments and volcanic rocks, were deposited between ~2550 and ~2480 Ma in both the north of the craton (Christie, Wilgena and Harris Greenstone domains), and in the south (Coulta Domain). Late Archean supracrustal rocks of the Gawler Province are variably metamorphosed, with many having reached granulite-facies conditions during the Sleafordian Orogeny between ~2470 and ~2410 Ma. These latest Archean to earliest Proterozoic rocks in the northern Gawler Province are termed the Mulgathing Complex, while similar aged rocks in the southern Gawler Province are known as the Sleaford Complex. These two complexes are now separated at the surface by the extensive, essentially flat-lying Gawler Range Volcanics and late Paleoproterozoic igneous rocks of the St Peter Suite in the Nuyts Domain and may be continuous at depth, forming an arcuate-shaped basement on which Paleoproterozoic sediments were deposited.

East of the Kalinjala Mylonite Zone, in the Spencer Domain, sedimentary rocks of the Middleback Group, including banded iron formations (BIF) which contain the iron ore deposits of the Middleback Ranges, were previously attributed to the Paleoproterozoic Hutchison Group but recently it has been suggested that these rocks were deposited in the late Archean (Szpunar *et al.*, 2011), making them contemporaneous with Sleaford and Mulgathing Complex supracrustal rocks.

No rocks with ages between ~2400 and ~2000 Ma are known from the Gawler Province. On eastern Eyre Peninsula the Miltalie Gneiss outcrops as a migmatitic, granodioritic gneiss, with magmatic zircon ages of ~2000 Ma (Fanning *et al.*, 2007; Fraser and Neumann, 2010). The map pattern is suggestive of a folded marker horizon, suggesting that the magmatic protolith to the Miltalie Gneiss may have formed as a flat-lying volcanic unit or extensive intrusive sill.

The late Paleoproterozoic between ~2000 and ~1700 Ma was a period of extensive sedimentation across large parts of the Gawler Province, punctuated by episodes of magmatism, deformation and metamorphism. On the eastern margin of the craton, sediments of the Hutchison Group are interpreted to have been deposited between ~2000 and ~1850 Ma, possibly along a passive margin

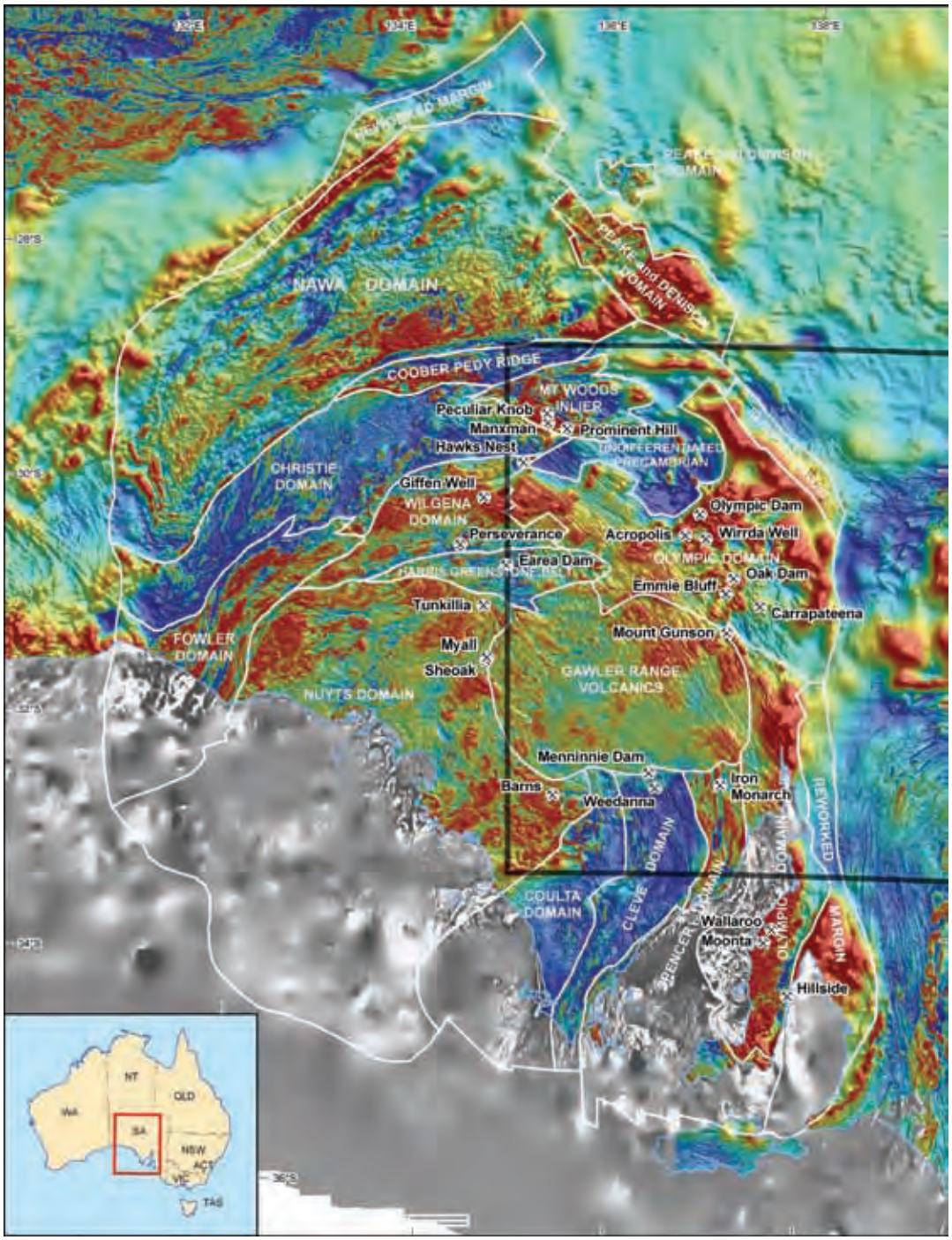

Figure 2.2: *Subdivision of the Gawler Province into geological domains (after Ferris et al., 2002) overlain on a Total Magnetic Intensity Image. The box encloses the area considered in this study.*

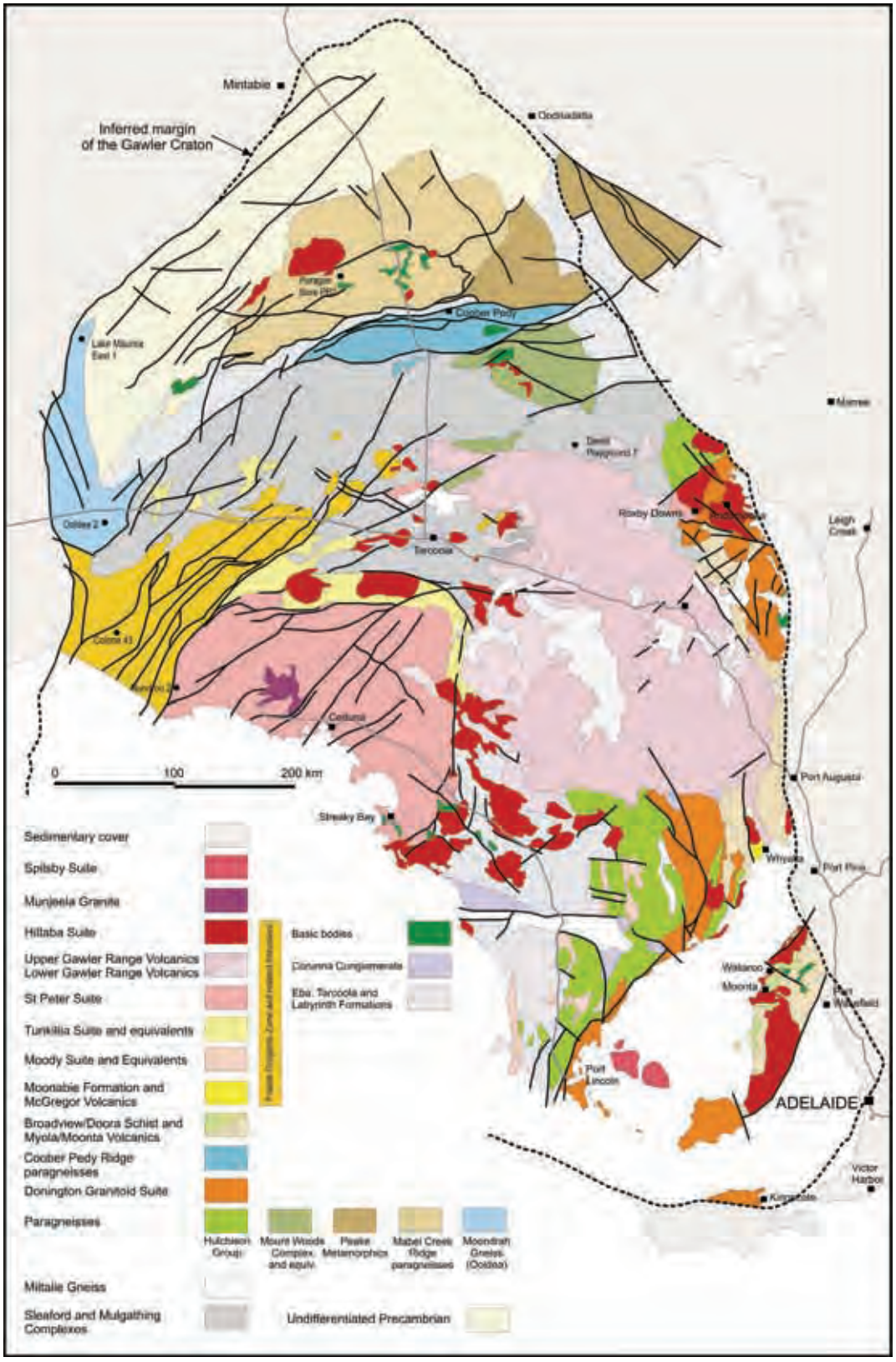

Figure 2.3: *Interpreted solid geology map of the Gawler Province (from Kositcin, 2010, and modified after Ferris et al., 2002).*

setting (Parker, 1993). Recently, however, the Hutchison Group stratigraphy has been extensively revised (Szpunar *et al.*, 2011) and subdivided into a late Archean Middleback Group and two Paleoproterozoic Groups, the ~1865 Ma Darke Peak Group and the ~1780 to ~1730 Ma Cleve Group. Sedimentary deposition of the Darke Peak and Cleve Groups was separated by intrusion of extensive granitoid plutons, collectively known as the Donington Suite, along the eastern margin of the Gawler Province, ~1850 Ma (Reid *et al.*, 2008).

Deposition of the Cleve Group was associated with deposition of the ~1750 Ma McGregor Volcanics and Moonabie Formation in the Spencer Domain of eastern Eyre Peninsula and was broadly synchronous with deposition of the Wallaroo Group sedimentary and bimodal volcanic rocks on Yorke Peninsula (Szpunar and Fraser, 2010). In common with the eastern Gawler Province, the interval between ~1780 and ~1730 Ma was also a period of sedimentary deposition in the northern and western parts of the craton, in the Nawa and Fowler Domains (Payne *et al.*, 2006; Howard *et al.*, 2011).

Sedimentary deposition in the interval ~1780 to ~1730 Ma in the Gawler Province appears to have been terminated by the Kimban Orogeny which spanned the interval ~1730 to ~1690 Ma and was responsible for high-grade metamorphism across much of the craton. In the southern Gawler Province the Sleaford Complex was extensively reworked during the Kimban Orogeny (Dutch *et al.*, 2010), and the Miltalie Gneiss and Hutchison Group were tightly folded and metamorphosed. Shearing along the Kalinjala Mylonite Zone on the eastern margin of Eyre Peninsula is inferred to have occurred in association with the Kimban Orogeny (Dutch *et al.*, 2009).

In the northern Gawler Province, relatively limited thermal and deformational reworking of the Mulgathing Complex was associated with the Kimban Orogeny, but high-grade metamorphism and deformation occurred in the Nawa Domain (Payne *et al.*, 2008) north of the Karari Shear Zone and in the Fowler Domain (Howard *et al.*, 2011). Significant magmatism also was associated with the Kimban Orogeny in both the southern Gawler Province west of the Kalinjala Mylonite Zone (Fanning *et al.*, 2007; Fraser and Neumann, 2010) and in the central and northern parts of the craton, including the ~1690 Ma Tunkillia Suite (Payne *et al.*, 2009).

Following the Kimban Orogeny, sedimentation of the Tarcoola Formation occurred in the central part of the craton ~1660 Ma (Fanning, 1990).

The latest Paleoproterozoic to early Mesoproterozoic was a time of very extensive magmatism in the Gawler Province. Magmatism in this interval initiated with the intrusion of the St Peter Suite granitoids in the southwestern part of the craton in the Nuyts Domain at ~1630 to ~1610 Ma, which was accompanied by contemporaneous volcanism of the Nuyts Volcanics.

Magmatism of the St Peter Suite was closely followed by the extrusion of the extensive Gawler Range Volcanics ~1595 to ~1590 Ma and Hiltaba Suite intrusive equivalents spanning the interval ~1595 to ~1575 Ma. Broadly contemporaneous with intrusion of the Hiltaba Suite granitoids, the northern domains of the Gawler Province, including the Mount Woods Domain, Coober Pedy Ridge and Mabel Creek Ridge were undergoing high-grade metamorphism at mid to deep crustal levels (Payne *et al.*, 2008; Cutts *et al.*, 2011).

Magmatism and/or metamorphism between ~1595 and ~1570 Ma marks the final tectonothermal event to have affected most of the Gawler Province. The exception is in the northwestern parts of the craton, where significant shearing is interpreted to have occurred along northeast-trending shear-zones ~1450 Ma (Fraser and Lyons, 2006), contemporaneous with high-grade metamorphism even

farther north in the central Nawa Domain (M. Hand, pers. comm.. 2010). In the eastern part of the craton, relatively flat-lying sandstones of the Pandurra Formation overlie the Gawler Range Volcanics, and underlie Neoproterozoic sediments of the Adelaide Rift Complex. A minimum depositional age for the Pandurra Formation of 1424 ± 51 Ma (Rb-Sr) was reported by Fanning *et al.* (1983).

2.3 THE CURNAMONA PROVINCE

The Curnamona Province (Figure 2.4) is situated in the east of the study area and straddles the border of South Australia and New South Wales. The Curnamona Province is separated from the Gawler Province to the west by Neoproterozoic to Cambrian rocks of the Adelaide Rift Complex. Compared with the Gawler Province, with its long and complex geological history as outlined in 2.2, rocks of the Curnamona Province span a relatively restricted part of the geological time-scale, from late Paleoproterozoic to early Mesoproterozoic. The southern part of the Curnamona Province is dominantly composed of metasedimentary rocks of the Willyama Supergroup, deposited between ~1720 and ~1640 Ma. The stratigraphy and geological setting of the Willyama Supergroup rocks has been extensively studied and debated and detailed descriptions and reviews can be found in Stevens *et al.* (1988), Page *et al.* (2005), Conor (2006), Conor and Preiss (2008) and Kositcin (2010). In the Olary Domain, constituting the southwestern part of the Curnamona Province, the Willyama Supergroup can be subdivided into a lower package, known as the Curnamona Group, and an upper package comprising the Saltbush Group and overlying Strathearn Group. The Curnamona Group consists of shallow-marine and/or lacustrine sediments and syndepositional felsic and lesser mafic volcanics deposited between ~1720 and ~1700 Ma, together with synchronous felsic intrusive sills. The overlying Strathearn Group, dominated by psammopelitic rocks, was deposited between ~1690 and ~1640 Ma. The Willyama Supergroup as a whole is interpreted to have been deposited in a progressively deepening basin. No basement rocks underlying the Willyama Supergroup have been identified.

Willyama Supergroup rocks were deformed and metamorphosed in the Olarian Orogeny ~1600 Ma. The Olarian Orogeny produced high temperature, low pressure metamorphism of the Willyama Supergroup and was associated with extensive magmatism, including the bimodal Benagerie Ridge Volcanics (~1585 to ~1580 Ma; Fanning *et al.*, 1998) and Ninnerie Supersuite granites (~1590 to ~1570 Ma; Fricke, 2009). Some workers have argued also for an earlier (~1690 to ~1670 Ma) episode of high temperature metamorphism within the Willyama Supergroup (Nutman and Ehlers, 1998; Gibson and Nutman, 2004) although this is contested by others (Page and Laing, 1992; Page *et al.*, 2005).

In the northwestern part of the Curnamona Province, the Mount Painter Province (Mount Painter Inlier and Mount Baggage Inlier) exhibits a significant post-Olarian Orogeny history that contrasts with the rest of the Curnamona Province. High-grade metasedimentary rocks of the Radium Creek Metamorphics yield maximum depositional ages of ~1600 and ~1590 Ma (Fraser and Neumann, 2010), indicating sedimentary deposition during, or after, the Olarian Orogeny. Sedimentary deposition of these rocks was closely followed by their deep burial and high-grade metamorphism by ~1555 Ma (Neumann *et al.*, 2009; Fraser and Neumann, 2010). Two granite suites were intruded in quick succession, the first including the Mount Neill and Box Bore granites ~1585 to ~1575 Ma, and the second, the Moolawatana Suite, including the Terrapinna and Wattleowie granites, ~1565 to ~1555 Ma (Fraser and Neumann, 2010).

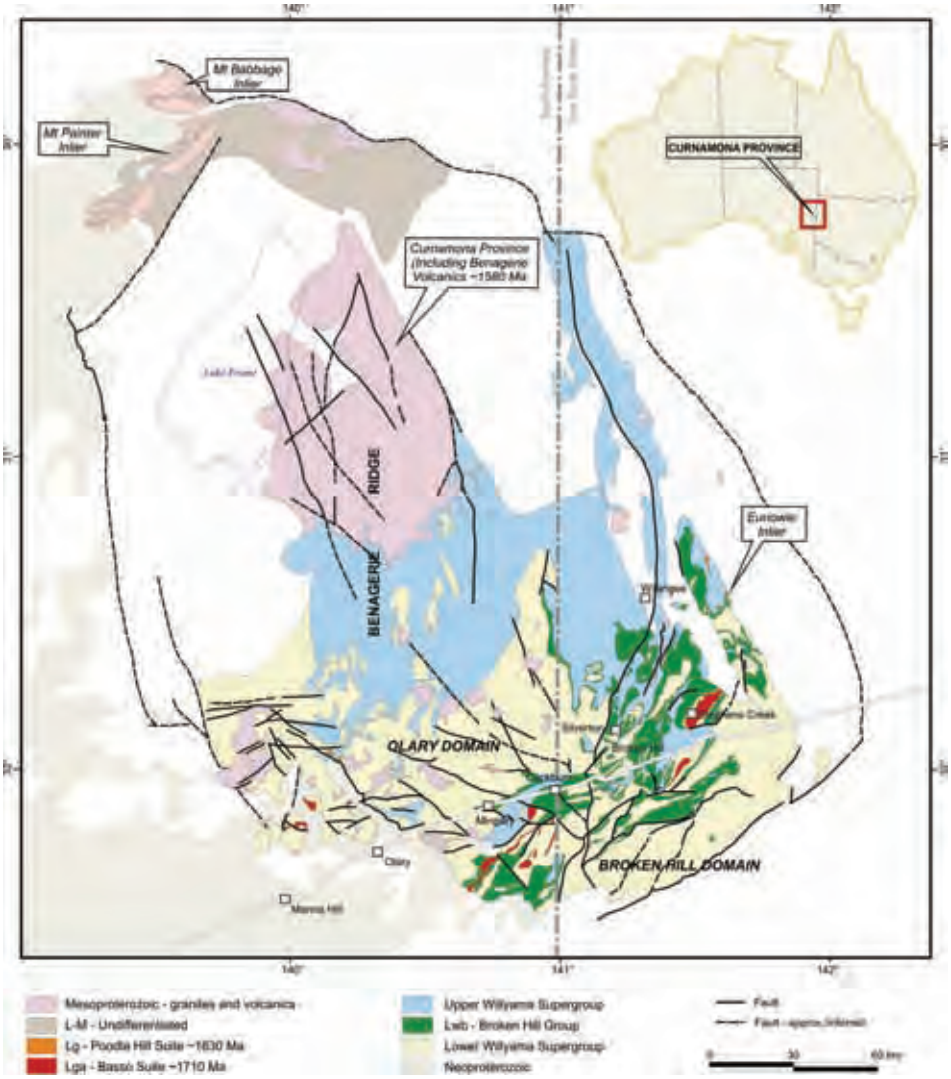

Figure 2.4: *Outcrop and interpreted solid geology map of the Curnamona Province (from Kositcin, 2010, and modified after Conor, 2006).*

2.4 SPATIAL AND TEMPORAL PATTERNS IN THE GAWLER AND CURNAMONA PROVINCES

As shown on Figure 2.2, the spatial arrangement of geological domains within the Gawler Province takes the form of a horseshoe-shaped late Archean to earliest Paleoproterozoic basement (the Sleaford and Mulgathing Complexes), with Paleoproterozoic sedimentary and less volcanic rocks situated around the outward-facing margins of the horseshoe. The interior of the basement horseshoe is dominated by late Paleoproterozoic felsic intrusive rocks of the Tunkillia Suite, St Peter Suite and Hiltaba Suite. The Paleoproterozoic sedimentary rocks of the Curnamona Province are consistent with this geometry and can be considered an easterly extension of Paleoproterozoic sedimentation on the eastern margin of the Gawler Province. Notable exceptions to this relatively simple geometric arrangement include the presence of a sliver of exposed Mesoarchean crust on the eastern margin of the Gawler Province, outboard of the basement horseshoe, and the position of the Fowler Domain,

dominated by Paleoproterozoic metasedimentary rocks but situated inboard of the basement horseshoe.

The horseshoe-shaped pattern described above is based on the ages of major constituent rock packages. Onto this pattern is superimposed the imprint of the major Proterozoic orogenic events which have reworked those rocks. The Kimban Orogeny (~1730 to ~1690 Ma) was responsible for high-grade metamorphism and intense ductile deformation in the southern Gawler Province in the region to the west of the Kalinjala Mylonite Zone as well as in the Fowler Domain and Nawa Domain in the west and north of the craton. The Kimban Orogeny in the Gawler Province was broadly synchronous with sedimentary deposition of the lower Willyama Supergroup to the east in the Curnamona Province. High-grade metamorphism and deformation affected most of the Curnamona Province later in the interval ~1600 to ~1550 Ma, while most of the Gawler Province was at upper crustal levels at this time. The exceptions are the northern terranes of the Gawler Province, including the Mount Woods Domain, Coober Pedy Ridge and Mabel Creek Ridge, which also experienced high-grade metamorphism at mid-crustal to lower-crustal conditions between ~1590 and ~1560 Ma.

2.5 THE ADELAIDE RIFT COMPLEX

The Adelaide Rift Complex (also termed the Adelaide Geosyncline) forms a zone at least 170 km wide separating the Gawler Province to the west from the Curnamona Province to the east. The rift complex is filled with Neoproterozoic to Cambrian sedimentary rocks which were subsequently deformed during the Cambro-Ordovician Delamerian Orogeny. The eastern margin of the Gawler Province is covered by a relatively thin veneer of Neoproterozoic and Cambrian sedimentary rocks in a region known as the Stuart Shelf, which represents the platform margin to the rift complex farther east. The Torrens Hinge Zone runs approximately north-south through the longitude of Port Augusta and forms the western boundary of the main rift complex. East of the Torrens Hinge Zone, the thickness of Neoproterozoic to Cambrian sedimentary rocks increases dramatically, with depth to basement reaching as deep as about 18 km, as indicated by the deep seismic reflection line 09GA-CG1 (Preiss *et al.*, 2010).

The stratigraphy of the Adelaide Rift Complex has been extensively studied and is described in detail by Preiss (1987; 1993; 2000) and is briefly summarised here, after the summary of Preiss (2010). Further details are provided in Section 3.6. Semi-continuous sedimentation occurred in the Adelaide Rift Complex through the interval between ~830 and ~500 Ma. Neoproterozoic sedimentation is subdivided into four groups, the Callana, Burra, Umberatana and Wilpena groups. Rifting commenced ~830 Ma, synchronous with intrusion of the extensive Gairdner Dolerite mafic dyke swarm in the Gawler Province to the west. Volcanic equivalents to the Gairdner dykes are found in the basal parts of the Adelaide Rift Complex, and are known as the Beda, Wooltana and Wilangee Volcanics. The Callana Group consists of these mafic volcanics interbedded with mixed evaporitic, clastic and carbonate facies. The base of the overlying Burra Group consists of immature clastic sedimentary rocks, interpreted to have been deposited in local grabens in an active rift setting. The upper siltstone and dolomite-dominated Burra Group is interpreted to have been deposited during a sag phase following the earlier rifting, and underlies a major unconformity ~660 Ma. The Umberatana Group was deposited following renewed rifting around the Curnamona Province and comprises Sturtian glacial deposits, interglacial siltstone, limestone and redbeds as well as Marinoan glacial deposits. The Wilpena Group is characterised by a widespread basal cap-dolomite unit, the Nucaleena Dolomite, overlain by silty to sandy clastic sediments which include Ediacaran fossil assemblages in the uppermost Pound Subgroup. The Pound Subgroup includes the Rawnsley Quartzite which forms the prominent cliff lines of Wilpena Pound in the central Flinders Ranges.

A depositional hiatus above the Wilpena Group marks the end of Neoproterozoic sedimentation in the Adelaide Rift Complex, and is overlain by Cambrian carbonate-dominated sediments of the Hawker Group followed by redbeds and minor limestone, including the Lake Frome Group. Renewed rifting in the south of the Rift Complex resulted in the deep Kanmantoo Trough filled with turbiditic sediments which form the eastern Adelaide Hills.

The Adelaide Rift Complex was inverted during the Cambro-Ordovician Delamerian Orogeny between ~515 and ~490 Ma, resulting in distinctive, arcuate fold patterns in the Fleurieu and Nackara Arcs. Rocks of this complex were variably metamorphosed during the Delamerian Orogeny with local regions reaching upper amphibolite facies while others areas were essentially unmetamorphosed. Syntectonic granites were intruded along the eastern margin of the Adelaide Hills and were followed by late- to post-tectonic A-type magmas.

2.6 LATE PALEOZOIC, MESOZOIC AND CENOZOIC BASINS

Neoproterozoic to early Paleozoic rocks of the Adelaide Rift Complex are overlain by late Paleozoic, Mesozoic and Cenozoic sedimentary rocks in a series of basins and sub-basins (Drexel and Preiss, 1995). In the region of interest for this study, these basins include the Arckaringa, Eromanga and Lake Eyre Basins.

The early Permian Arckaringa Basin is situated in the northwest of the study area, and overlies the northern Gawler Province in the Nawa, Coober Pedy and Mount Woods Domains as well as the northern Olympic Domain. Stratigraphy of the Arckaringa Basin has been subdivided into:

- the glacial to marine Boorthanna Formation,
- the Stuart Range Formation, composed dominantly of quiet water marine shales, and
- the Mount Toondina Formation, composed of siltstone and sandstone, interbedded with coal in the upper part of the formation (Hibburt, 1995).

Over most of its extent, the Arckaringa Basin lies on a relatively flat platform of underlying basement rocks, typically less than 500 m deep. Exceptions include the northwest-trending Phillipson Trough, overlying the northern Christie Domain, and the northwest-trending Boorthana Trough along the western margin of the Peak and Denison Domain (Figure 2.2). In each of these troughs the thickness of the Arckaringa Basin reaches more than1000 m and includes significant coal deposits.

The early Jurassic to mid-Cretaceous Eromanga Basin covers western Queensland, northwestern New South Wales and northeastern South Australia and extends into the northern part of the current study area, skirting the northern margins of Lake Gairdner and Lake Torrens and extending beneath Lake Frome (Figure 2.1). The stratigraphy of the Eromanga Basin is subdivided into:

- a lower terrestrial sequence,
- a middle transgressive marine sequence, and
- an upper terrestrial sequence (Krieg *et al.*, 1995).

The lower sequence consists of fluvial sands of the Poolowanna Formation overlain by fluvial to lacustrine sands and silts of the Algebuckinga Sandstone, from which plant fossils indicate deposition between Upper Jurassic to Lower Cretaceous Epochs. The overlying marine sequence reaches about 1000 m in thickness and includes the shoreline facies Cadna-owie Formation, fossiliferous mudstone of the Bulldog Shale and carbonaceous mudstone of the Toolebuc Formation. Fossil content indicates that the marine sequence was deposited over an interval of about 40 million years during the Lower Cretaceous. The upper, non-marine sequence consists of the shale, siltstone,

sandstone and minor coal seams of the Winton Formation and the Mount Howie Sandstone, together reaching about 1200 m in thickness and deposited in low-energy fluvial to lacustrine environments over an interval of ~8 Ma in the early Upper Cretaceous.

Overlying the Eromanga Basin in the northeastern part of the study area is the Paleogene to Quaternary Lake Eyre Basin (Callen *et al.*, 1995). The basal unit is the Eyre Formation, consisting of sandstone, carbonaceous sandstone, and conglomerate, deposited largely in braided streams between the late Paleocene and mid-Eocene. The Eyre Formation is, in turn, overlain by late Oligocene to Pliocene clay, fine sand and carbonate of the Etadunna and Namba formations. The most recent sediments in the study area are red and yellow-brown lacustrine sands and clays of Pliocene to Quaternary age, together with aeolian and evaporitic deposits and calcrete and gypsum horizons in soils.

2.7 A BRIEF OVERVIEW OF MAJOR ENERGY AND MINERAL SYSTEMS

The region of interest in this study, spanning the Gawler Province, Adelaide Rift Complex and Curnamona Province, contains several known mineral provinces of current and/or historical economic importance. These are briefly introduced here.

2.7.1 The Olympic iron oxide-copper-gold province

The Gawler Province hosts numerous significant iron oxide-copper-gold±uranium deposits and prospects, forming a broadly north-south oriented belt along the eastern margin of the craton. The largest of these is the supergiant Olympic Dam deposit, and hence the belt has been termed the Olympic iron oxide-copper-gold Province (Skirrow *et al.*, 2002, 2006). Other significant deposits in this metallogenic province include Prominent Hill and Carrapateena. The south of this mineral province includes the historically important mines in the Moonta-Wallaroo district and currently is the focus of intense exploration interest, in part sparked by the recent discovery of the Hillside prospect on eastern Yorke Peninsula. All the known deposits and prospects in the province appear to have formed ~1590 to ~1580 Ma, synchronous with magmatism of the Hiltaba Suite and Gawler Range Volcanics and associated hydrothermal alteration (Skirrow *et al.*, 2007).

2.7.2 The central Gawler gold province

Contemporaneously with copper-gold±uranium mineralisation in the Olympic iron oxide-copper-gold province, several gold-dominated deposits and prospects formed farther west in the Gawler Province, including Tarcoola, Tunkillia and Barns (Drown, 2003, Ferris and Schwarz, 2003, Fraser *et al.*, 2007; Budd and Skirrow, 2007). These deposits and prospects form an arcuate-shaped belt around the western and southern margins of the Gawler Range Volcanics and have been termed the central Gawler gold province (Ferris and Schwarz, 2003).

2.7.3 Middleback Ranges iron ore

On northeastern Eyre Peninsula, iron ore has been mined for more than 100 years in the Middleback Ranges and active exploration and development continues in the region today. This district was the major source of iron ore in Australia until the discoveries in the Hamersley Ranges of Western Australia in the 1960s. Several mines are located along a north-south strike orientation in synclinal keels and are hosted in banded iron formation and dolomitic marble of the Middleback Subgroup. The host sediments have been mapped as part of the Paleoproterozoic Hutchison Group, although recent work (Szpunar *et al.*, 2011) has subdivided the Hutchison Group and suggested that the

Middleback Subgroup may in fact be late Archean in age and potentially correlates with the Hamersley Group in the Pilbara Craton, Western Australia.

2.7.4 Broken Hill lead-zinc-silver

In the eastern part of the Curnamona Province the Broken Hill lead-zinc-silver deposit, the largest deposit of its type in the world, is hosted in Paleoproterozoic Willyama Supergroup metasedimentary rocks. This suggests that other parts of the Willyama Supergroup may also be prospective for similar base metal deposits.

2.7.5 Copper-gold in the Adelaide Rift Complex

Although recent production has been limited, the Adelaide Rift Complex historically has been a globally important copper province, during the mid-1800s. Copper was initially discovered in the early- to mid-1840s at Kapunda, about 80 km northeast of Adelaide and at Burra, around 150 km north of Adelaide. Underground mining of ore at Burra took place through the remainder of the 19th century, and was later followed by open cut mining in the 1970s and 1980s. Currrently, copper is being mined at several deposits in the vicinity of Leigh Creek. Although present throughout the Adelaide Rift Complex, copper is most concentrated at three stratigraphic levels:

- the Callana Group, including the Arkaroola and Curdimurka Subgroups;
- the Mundallio Subgroup of the Burra Group, and
- the Nepouie to basal Yerelina Subgroups of the Umberatana Group.

Of these, the third and youngest level has seen most production, with a global resource (i.e. production plus geological resources) of just under 900 kt, mostly from the Mount Gunson district. The deposits are typically stratabound at the broad scale, but at the outcrop scale the ores are hosted in veins and as disseminations within the host units. Although uranium production has not occurred in the Adelaide Rift Complex, many of the copper deposits and prospects have elevated uranium concentrations (Section 3.6).

2.7.6 Lake Frome region sandstone-hosted uranium

Cenozoic sandstones in the Lake Frome region east of the Mount Painter Province host economically viable uranium deposits, including the Beverley, Four Mile and Honeymoon deposits which are either being currently mined, or are expected to be mined in the near future via in-situ leach methods. The region remains prospective for further sandstone-hosted uranium discoveries. For example, Cauldron Energy Ltd recently announced the discovery of uranium mineralisation at the Blanchewater prospect to the northwest of the Mount Babbage Inlier. The uranium deposits of the Lake Frome region are in relatively close proximity to Proterozoic basement rocks of the Mount Painter Province, which are highly enriched in uranium and thorium and most exploration models assume that uranium in the Cenozoic sandstones is sourced from this proximal uranium-rich basement.

2.7.7 The South Australian heat flow anomaly – a geothermal province

A broad, approximately north-south trending belt through central South Australia exhibits anomalously high surface heat flow and has been termed the South Australian heat flow anomaly (Neumann *et al.*, 2000). The South Australian heat flow anomaly extends from the eastern Gawler Province, across the Adelaide Rift Complex and into the western Curnamona Province. The region of elevated surface heat flow corresponds with Proterozoic granites and gneisses which yield high-

heat production values as a result of an abundance of the radiogenic heat-producing elements uranium, thorium and potassium. In addition to the implications for uranium prospectivity briefly mentioned above, the radiogenic basement rocks mean that the region is highly prospective also for geothermal energy systems.

3 Uranium mineral systems

With the discovery in 1975 of the Olympic Dam deposit, the largest single known economic accumulation of uranium in the world, east-central South Australia became one of the two or three most significant uranium provinces in the world. Subsequent discoveries of uranium in Cenozoic basins, combined with known uranium deposits in the Mount Painter Inlier, have highlighted the diversity of uranium mineralisation in this area.

The styles of uranium deposits in east-central South Australia have been assigned to quite different groups using the existing International Atomic Energy Agency (IAEA) classification scheme (IAEA, 2009: Figure 3.0.1). However, some deposits have broad similarities suggesting linked genetic origins. In the following discussion a combination of the IAEA classification and a continuum classification presented by Skirrow *et al.* (2009) is used. Following the classification of Skirrow *et al.* (2009), the mineral systems are discussed in the following order:

- basin and surface-related uranium systems (including sandstone-related and unconformity-related systems);
- hybrid systems (including iron oxide-copper-gold systems), and
- magmatic-related systems (including orthomagmatic and magmatic-hydrothermal systems).

In addition there is discussion on the potential of the sediment-hosted copper minerals systems, which are known to have concentrations of uranium within the Adelaide Rift Complex.

The continuum classification links a number of IAEA deposit types together and progresses from basin-related processes of diagenesis and early fluid flow, through basin inversion and metamorphism to magmatism and related hydrothermal activity. Figure 3.0.1 shows the location of the east-central South Australian deposit types on the ternary classification of Skirrow *et al.* (2009), which highlights similar processes and possible continua between uranium systems.

In this study we have revised the methodology of uranium prospectivity assessment from that used in the energy prospectivity analysis in north Queensland (Huston, 2010). A custom methodology was developed following discussions with the Centre for Exploration Targeting at the University of Western Australia. The methodology used is described below.

3.1 PROSPECTIVITY ANALYSIS METHODOLOGY

A. SCHOFIELD

Mineral deposits form as a result of the coincidence of favourable geological conditions within a given spatial setting, constrained by geological time. At its most basic level, a prospectivity analysis study seeks to identify and map relevant geological evidence to assess where the greatest potential is for previously unrecognised mineralisation to occur. Typically, individual evidence maps will be assigned a weighting (either subjectively or by statistical methods) to reflect the importance in the targeted mineral system. The final map of mineral potential is a function of the input evidence maps (Bonham-Carter, 1994). Numerous methods have been proposed to integrate the disparate input evidence maps, ranging from simple Boolean approaches to sophisticated Bayesian methods (Bonham-Carter, 1994). These may be simplified to two broad categories; knowledge-driven and data-driven (Bonham-Carter, 1994; Knox-Robinson and Wyborn, 1997).

Data-driven prospectivity analysis methodologies include logistical regression, weights of evidence and neural networks (Bonham-Carter, 1994). They are typically applied in areas where there are a number of known deposits. Model parameters are calculated using known deposits as a training dataset (via statistics). The parameters are determined by examining the spatial relationships between different geological features and the training data and then applying them to the whole study area (Knox-Robinson and Wyborn, 1997). Knowledge-driven methodologies on the other hand may be applied to areas where known deposits may be sparse, or even lacking. Examples of knowledge-driven methodologies include fuzzy logic and index overlay (Bonham-Carter, 1994). Prospectivity criteria for these methods are developed based on a conceptual model which, in the case of metallic ore deposits, is represented by a mineral systems model. Criteria weightings are assigned subjectively by an expert.

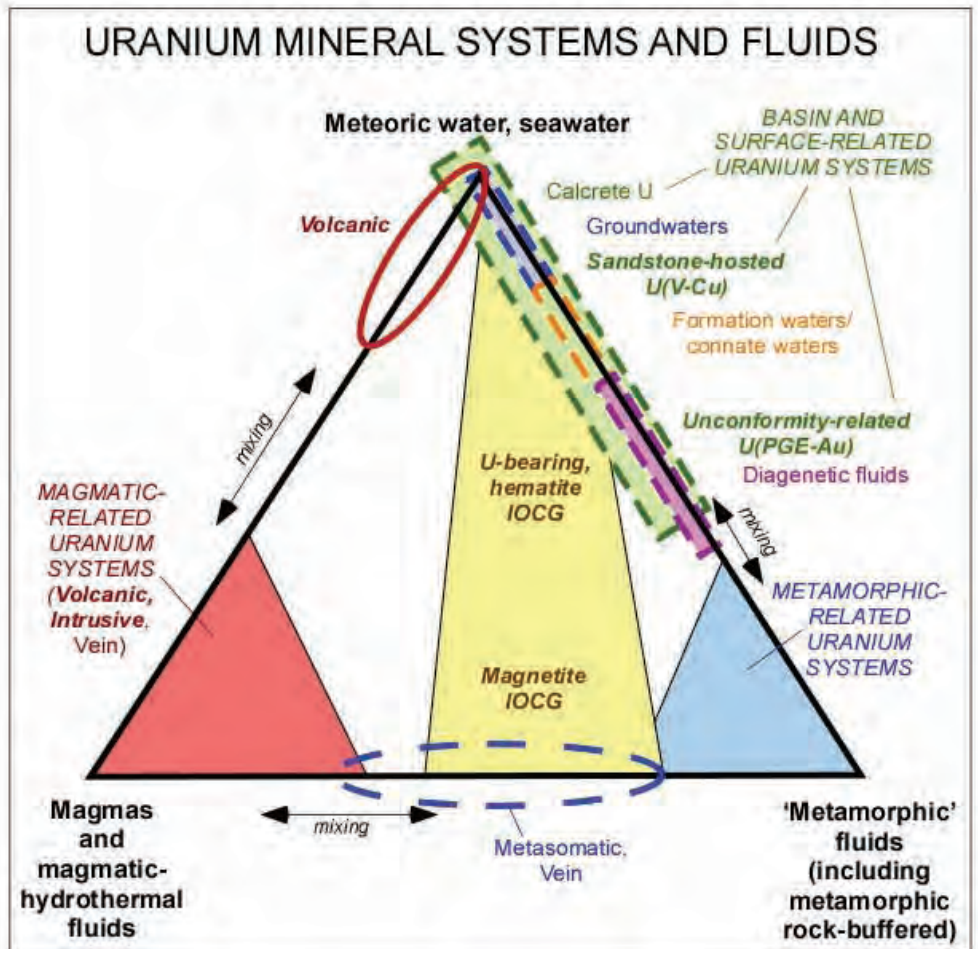

Figure 3.0.1: *Ternary diagram illustrating the location of uranium deposits in east-central South Australia (sandstone-hosted, unconformity-related, iron oxide-copper gold (IOCG) and magmatic-related) on the continuum classification of uranium deposits of Skirrow et al. (2009).*

There are a number of advantages associated with employing a mineral systems model. Criteria developed using existing deposits are likely to be biased towards local geological controls which are significant at the mine-scale. In contrast, the processes involved in a mineral system are mappable at large scales (Knox-Robinson and Wyborn, 1997). Furthermore, through using criteria based on process rather than empirical relationships to known mineralisation, the mineral potential of greenfield areas is able to be assessed and previously unknown styles of mineralisation may be

assessed in brownfield areas. For these reasons, this investigation has adopted a conceptual mineral system-based approach.

3.1.1 Mineral systems framework

Following the success of a systems approach to understanding and discovering petroleum accumulations (Magoon and Dow, 1994) and previous process-based analyses of mineral deposits (e.g., Lacy, 1974), Wyborn *et al.* (1994) first formalised a construct for analysing processes linked to the accumulation of mineral resources. Wyborn *et al.* (1994) proposed that a mineral system had seven geological factors:

- sources of the mineralising fluids and transporting ligands;
- sources of the metals and other ore components;
- migration pathway;
- thermal gradient;
- energy source;
- a mechanical and structural focussing mechanism at the potential depositional site; and
- chemical and/or physical mechanisms for ore precipitation.

These were subsequently adapted into the Five Questions of mineral systems (Walshe *et al.*, 2005; Barnicoat, 2008) and later simplified by Skirrow *et al.* (2009) into four mineral systems components (Figure 3.1.1). Following Skirrow *et al.* (2009), the four system components used in this assessment are:

- sources of metals and fluids;
- drivers of fluid flow;
- fluid pathways and architecture; and
- depositional sites.

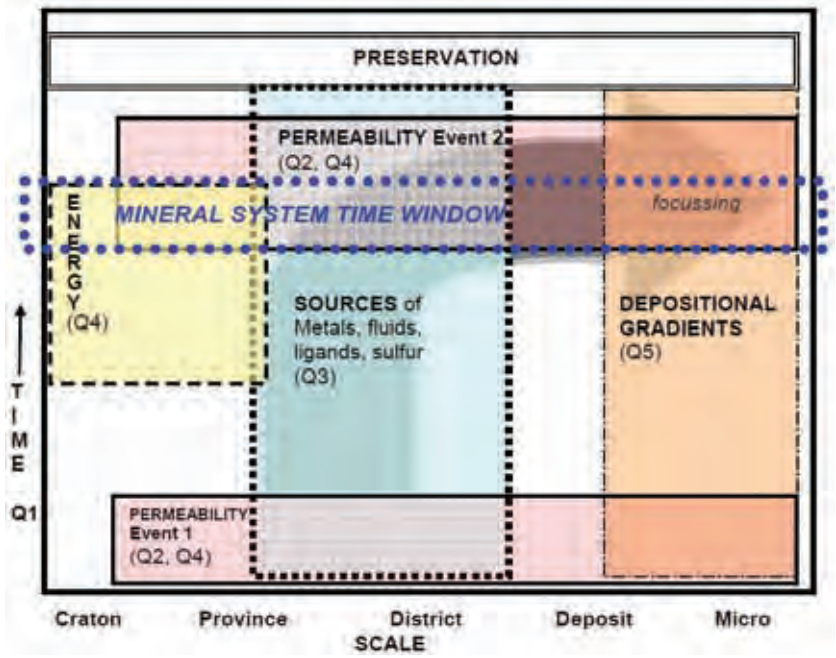

Figure 3.1.1: *Generalised mineral systems model from Skirrow (2009). The Five Questions have been mapped to the revised mineral systems components.*

3.1.2 Methodology used during this study

The prospectivity analysis methodology used in this study has been custom-developed to meet requirements of ease of application, robustness and transparency. Assignment of criteria weightings is similar to that employed for a fuzzy logic approach, whereas combination of criteria is similar to index overlay. The details of the methodology adopted during this study are presented below.

3.1.2.1 Assignment of criteria weightings

This study uses a mineral systems approach to develop theoretical geological criteria for mineral system components. These criteria were translated into mappable proxies and given weightings. This work flow is similar to that of McCuaig *et al.* (2010). The final weighting of each individual criterion is the product of the importance, its applicability and the confidence in the data quality.

The importance (I) is the overall importance of the criterion to the mineral system. The applicability (A) concerns the certainty that the mappable proxy reflects the desired process. The confidence (C) is the confidence in the data source, both spatially and in terms of overall data quality. The C factor should not be confused with spatial data coverage. Values for I, A and C are assigned subjectively on a scale of 0 to 1, with 0.25 corresponding to a low rating, 0.5 to a moderate rating, 0.75 to a high rating and 1.0 as total or critical. Table 3.1.1 gives an illustration of how weightings are applied for potential fluid flow pathways. Decisions concerning other aspects of the criteria used, such as the selection of buffer distances and cut-off values, were also made subjectively, based on the judgement of the analyst.

3.1.2.2 Combining prospectivity criteria

Since it is unlikely that each mineral systems component will be represented by an equal number of criteria, a purely additive approach will result in some mineral systems components being disproportionately represented in the final mineral potential map. To address this issue, individual mappable criteria are combined into intermediate maps corresponding to mineral systems components (Figure 3.1.2) before producing the final mineral potential map. Intermediate maps represent the average of the weighting for all input criteria. As such, values will range between 0 and 1 for each intermediate map. Finally, the four mineral systems component maps are added together to produce the final mineral potential map.

Table 3.1.1: Example of the application of I, A and C values to a hypothetical fault dataset used to map fluid flow pathways. The importance of faults to the mineral system (I) is constant, whereas the applicability (A) varies based on distance from the fault, since areas distal to the fault have a lower likelihood of being influenced by hydrothermal fluids. The confidence value (C) varies based on data quality, and hence inferred faults receive a lower value than mapped faults. The final weighting (WF) is the product of I, A and C.

CRITERION		I	A	C	WF
Fault distance (mapped faults)	2 km buffer	0.75	0.75	0.75	0.422
	4 km buffer	0.75	0.50	0.75	0.281
	6 km buffer	0.75	0.25	0.75	0.141
Fault distance (inferred faults)	2 km buffer	0.75	0.75	0.25	0.141
	4 km buffer	0.75	0.50	0.25	0.094
	6 km buffer	0.75	0.25	0.25	0.047

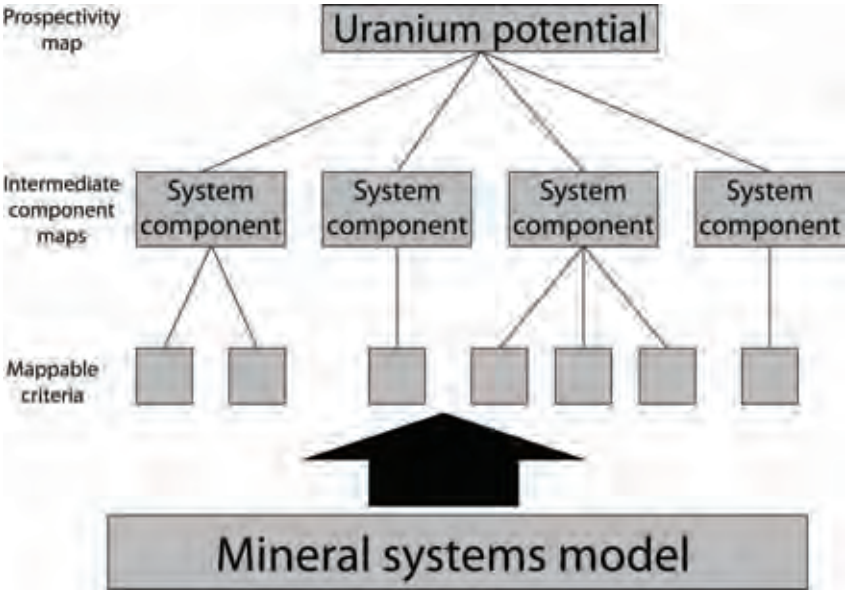

Figure 3.1.2: *Schematic process for developing uranium potential maps.*

In the following sections, an outline is provided of known deposits and the present models for the formation of each uranium system considered in the study. The components and resulting prospectivity mapes, or percentage errors, are then presented and discussed. The following systems were considered:

- sandstone-hosted (including both roll-front and paleochannel varieties) uranium;
- iron oxide-copper-gold-uranium;
- unconformity-related uranium;
- magmatic-related (including intrusive and volcanic-related) uranium; and
- sediment-hosted copper-uranium.

3.2 SANDSTONE–HOSTED URANIUM SYSTEMS

S. E. VAN DER WIELEN, D. L. HUSTON AND D. CONNOLLY

Sandstone–hosted uranium mineral systems are an important type of uranium deposit, accounting for one quarter of the world uranium production and one third of global resources (OECD Nuclear Energy Agency, 2008). Currently in Australia there are only two operating sandstone–hosted uranium mines, the Beverley and Beverley North mines, which are located in the northeastern corner of the assessment area (Figure 3.2.1). Beverley in the past has accounted for up to for 7% of Australia's uranium production (McKay, 2008) with several other similar deposits in various stages of feasibility (i.e. Yeelirrie deposit in Western Australia, and Four Mile and Honeymoon deposits in South Australia). This section assesses the potential for sandstone–hosted uranium systems in the study area by:

- describing known sandstone–hosted uranium deposits within the study area;
- documenting conceptual sandstone–hosted uranium system models;
- outlining essential components and mappable criteria; and
- presenting and discussing the results of the mineral prospectivity analysis.

3.2.1 Known sandstone–hosted uranium systems within the assessment area

There are three significant sandstone–hosted uranium deposits, Beverley (and Beverly North), Four Mile and Honeymoon, in the study area (Figure 3.2.1), all of which are in the Lake Frome region. Table 3.2.1 summarises the main characteristics of each deposit. These deposits are all hosted by the Lake Eyre Basin, with Four Mile also extending into the underlying Eromanga Basin, and are located mainly within paleochannels. The main uranium minerals are uraninite and coffinite, with pyrite (and marcasite), phosphate minerals (some of which are uraniferous), clays (kaolinite and montmorillonite) and alunite also present (Table 3.2.1). Mineralisation is thought to have occurred in two, or possibly three events, in the intervals 105 to 55 Ma, 36 to 20 Ma and 5 to 1 Ma (Jaireth, 2009). These events may be associated with periods of uplift and erosion after deep weathering.

3.2.2 Model for sandstone–hosted uranium mineral systems

Two models have been proposed for the formation of sandstone–hosted uranium deposits, a single–fluid model and a two–fluid model (Figure 3.2.2; Jaireth *et al.*, 2008). In the single–fluid model, oxidised meteoric water migrates through a confined reduced sandstone aquifer progressively oxidising and dissolving uranium from the sandstone. The uranium is subsequently deposited and concentrated at a redox boundary, the roll–front (Figure 3.2.2). In the two–fluid model (Figure 3.2.2), oxidised meteoric water migrates through a clean sandstone aquifer, dissolving uranium from the sandstone. A reduced basinal fluid (hydrocarbon– and/or H_2S–bearing) from underlying petroleum basins migrates upwards along faults and mixes with the oxidised fluid, resulting in the precipitation of uranium adjacent to the fault (Jaireth *et al.*, 2008; Figure 3.2.2). It is important to note in the two–fluid model that there are little to no *in situ* reductants so that uranium–bearing oxidised fluids can migrate much deeper into the basin where there is greater opportunity for interaction with a reduced fluid.

The sandstone–hosted system produces two broad deposit types, roll-front deposits in which uranium deposition occurs within a laterally continuous sandstone aquifer at depth in a basin and paleochannel–related deposits in which uranium deposition occurs within laterally restrictive fluvial channels. Both of these deposit types have been considered as separate mineral systems. However,

as many of the mineral systems components are similar, the mappable criteria used in the two analyses overlap.

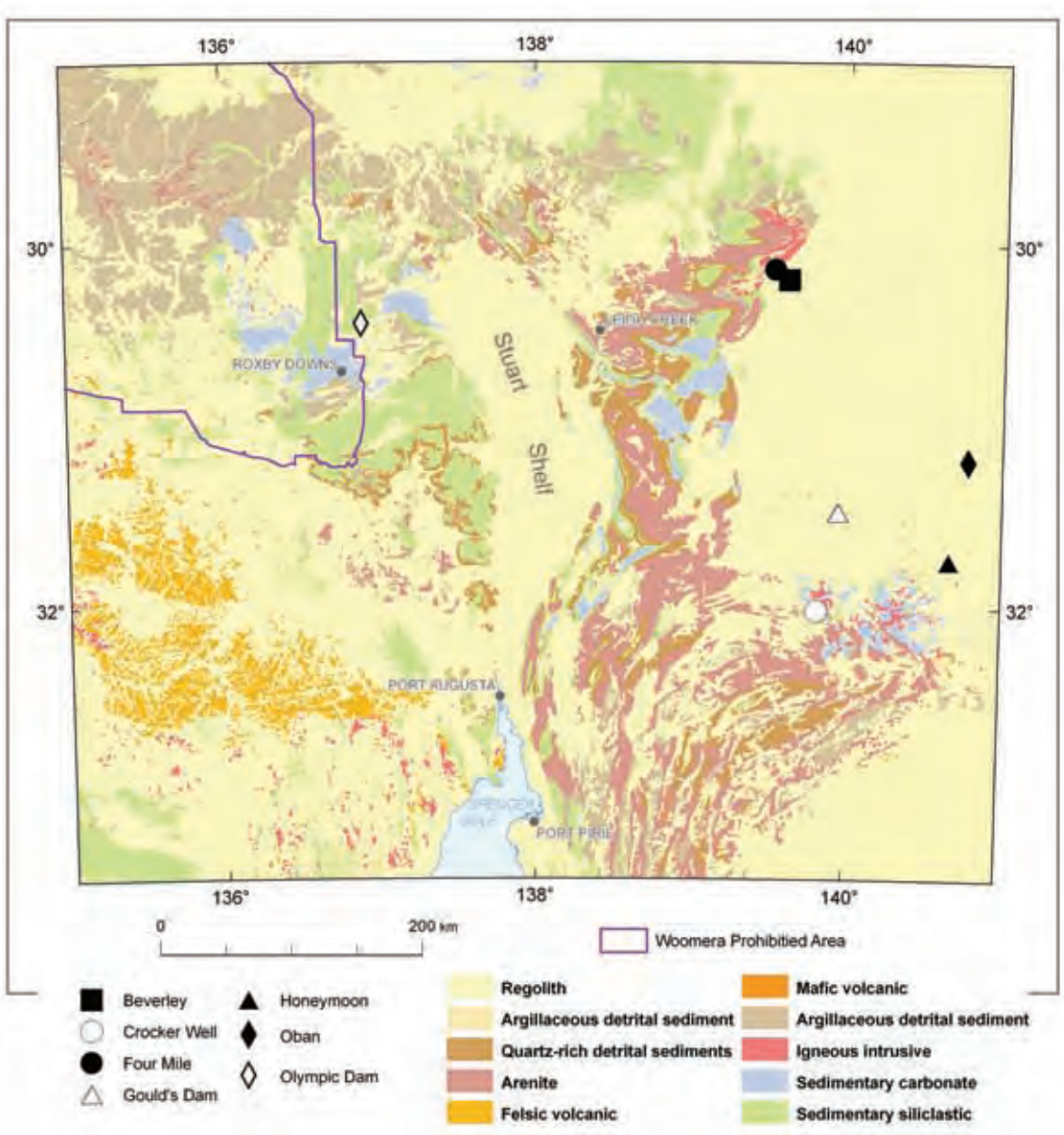

Figure 3.2.1: *Surface geology of the study area (after Whitaker et al., 2008) showing the locations of roll-front and paleochannel–hosted deposits (filled symbols) and other uranium depostis (open symbols). The purple line encloses the Woomera Prohibited Area.*

Table 3.2.1: Main features of the major sandstone- and paleochannel-hosted uranium deposits in the study area.

DEPOSIT	LOCATION (LATITUDE, LONGITUDE)	RESOURCE	DISCOVERY	PROVINCE	HOST ROCKS	REDUCTANTS	GEOMETRY	MINERALISATION	TIMING OF MINERALISATION	REFERENCES
Beverley	139.59891, -30.19138	16.3 kt of U_3O_8 at 0.23% U_3O_8.	1969	Lake Eyre Basin	Mineralisation occurs in the Beverley Clay, Beverley Sands and Alpha Mudstone units of the late Oligencene to Miocene Namba Formation, with the majority of mineralisation occurring in basal portion of the Beverley Sands.	The Beverley Sands are organic poor (0.05% to 0.5%) whereas the underlying Alpha Mudstone is organic rich (plant fragments and large pieces of carbonised wood).	The paleochannel that hosts the Beverley deposit is associated with a northeast-trending half–graben that is controlled by the Paralana–Wertaloona fault system. The north-south paleochannel system has been cross–cut by several faults.	Uranium is predominately in the form of coffinite which fills voids and forms coatings on quartz grains. There are also minor occurrences of uraninite. The ore zone also contains pyrite, marcasite, feldspars, clays (kaolinite and montmorillonite), gypsum and alunite. The ores contain traces of Th, Rb, Sr, Cu, Zn, Mo, V, Se and As, which are typical for sandstone-hosted deposits.	Two potential mineralisation periods have been recognised for mineralisation in the Eyre Formation, 5–1 Ma and 36–20 Ma related to deep weathering, uplift and erosion.	Brunt (pers. comm., 2005), McConachy *et al.* (2006), Marsland–Smith (2005), Curtis *et al.* (1990), Haynes (1975), Wülser (2009), Jaireth (2009) and Geoscience Australia (2009).
Four Mile	139.59058, -30.183047	Four Mile West: 15.0 kt U_3O_8 at 0.37% U_3O_8 Four Mile East: 14.4 kt U_3O_8 at 0.314% U_3O_8	2005	Lake Eyre Basin and underlying Eromanga Basin	Four Mile West is hosted in Early Cretaceous sediments of the Eromanga Basin, most likely Bulldog Shale equivalent. Four Mile East mineralisation occurs within Eyre Formation.	Unknown	Tabular, very close to the range–front and appears to be fault controlled.	At Four Mile East uraninite is the dominant ore mineral. Pyrite, kaolinite, REE– and U–bearing phosphate minerals are present within the ore.	Two potential mineralisation periods have been recognised for mineralisation in the Eyre Formation, 5–1 Ma and 36–20 Ma (Skirrow, 2009). The Four Mile West mineralisation may be also associated with an earlier (105–55 Ma) deep weathering, uplift and erosion event (Skirrow, 2009).	Schofield *et al.* (2009), Jaireth (2009), Stoian (2010) and Geoscience Australia (2009)
Honeymoon	140.653931, -31.746788	2.88 kt U_3O_8 at 0.20% U_3O_8	1972	Lake Eyre Basin	Mineralisation occurs within Eyre Formation sediments in the Yarramba Paleo-channel which is overlain by Namba Formation and underlain by the uranium–rich, Meso-proterozoic Willyama Supergroup.	Carbonaceous *in situ* reductant.	Yarramba Paleochannel is a northwest– to north–trending paleochannel system which is strongly controlled by stratigraphy and structure of under-lying basement. Honey-moon is located on bend in the paleochannel.	The uranium is usually present as uraninite or coffinite coating on sands, and the ore is often pyritic and carbonaceous.	Two potential mineral-isation periods have been recognised in the Eyre Formation, 5–1 Ma and 36–20 Ma, related to deep weathering, uplift and erosion.	Skidmore (2005); Haynes (1975); Curtis *et al.* (1990); Jaireth (2009).

Table 3.2.2. Theoretical and mappable criteria for sandstone–hosted uranium systems

MINERAL SYSTEM COMPONENT	CRITERIA		DATASET	IMPOR-TANCE	APPLIC-ABILITY	CONFI-DENCE	WEIGHT	COMMENTS
	THEORETICAL	MAPPABLE						
1. Source of uranium	Presence of U–enriched rocks - either in the basement (or within the basin?) **Both systems**	Basement rocks with ≥10 ppm uranium (radiometrics) 10 km buffer around U–enriched basement rocks 30 km buffer around U–enriched basement rocks 100 km buffer around U–enriched basement rocks	Radiometric Map of Australia (Minty *et al.*, 2010)	1.00 1.00 1.00 1.00	1.00 0.75 0.50 0.25	1.00 1.00 1.00 1.00	1.000 0.750 0.500 0.250	Uranium values ≥10 ppm were extracted from the filtered uranium band and converted to a polygon shape file. A spatial query was used to select values for crystalline basement only.
2. Drivers	Topographic relief (slope) **Both systems**	10 km buffer in basin around basement with high slope 30 km buffer in basin around basement with high slope 100 km buffer in basin around basement with high slope	9 second DEM	0.50 0.50 0.50	1.00 0.75 0.50	0.25 0.25 0.25	0.125 0.094 0.063	High slopes (upper decile) were measured from DEM and then clipped to areas of basement . Buffers are extended into basins from the areas of high topographic gradients.
3. Architecture of potential fluid pathways	Distribution of Cenozoic sedimentary basins **Both systems**	10 km (internal) buffer of basin margin 30 km (internal) buffer of basin margin 100 km (internal) buffer of basin margin	Sedimentary basins (ANZCW-0703002747)	0.50 0.50 0.50	1.00 0.75 0.50	1.00 1.00 1.00	0.500 0.375 0.250	Unconformity interpreted from solid geology map.
	Distribution of Mesozoic sedimentary basins **Roll-front only**	10 km (internal) buffer of basin margin 30 km (internal) buffer of basin margin 100 km (internal) buffer of basin margin	Sedimentary basins (ANZCW-0703002747)	0.50 0.50 0.50	1.00 0.75 0.50	1.00 1.00 1.00	0.500 0.375 0.250	Unconformity interpreted from solid geology map.
	Distribution of Cenozoic alluvium and/or fluvial units **Paleochannel only**	Evidence of Paleochannels	Surface Geology of Australia 1:1 000 000 scale (Whitaker *et al.*, 2008)	1.00	0.75	1.00	0.750	
	Distribution of paleochannels **Paleochannel only**	Evidence of Paleochannels	South Australia paleochannels map	1.00	1.00	0.50	0.500	
	Distribution of aquifers **Roll-front only**	Distribution of Algebuckina Formation at surface and in the subsurface	3D Eromanga model (Van der Wielen *et al.*, 2011)	1.00	1.00	1.00	1.000	
	Distribution of aquifers **Roll-front only**	Distribution of Cadna-owie Formation at surface and in the subsurface	3D Eromanga model (Van der Wielen *et al.*, 2011)	1.00	1.00	1.00	1.000	
4. Depositional mechanisms and environment	Redox gradient **Both systems**	Interpreted redox gradient 5 km buffer 10 km buffer 15 km buffer	Hydrogeochemistry (Radke *et al.*, 2000)	1.00 1.00 1.00 1.00	1.00 0.75 0.50 0.25	0.50 0.50 0.50 0.50	0.500 0.375 0.250 0.125	
	pH gradient **Both systems**	Interpreted pH gradient 5 km buffer 10 km buffer 15 km buffer	Hydrogeochemistry (Radke *et al.*, 2000; https://sarig.pir.sa.gov.au/sarig/frameSet.jsp)	0.75 0.75 0.75 0.75	1.00 0.75 0.50 0.25	0.50 0.50 0.50 0.50	0.375 0.281 0.188 0.094	
	Groundwater salinity (see text) **Both systems**	Electrical conductivity (µS/cm) 58384 – 380666 34965 – 58384 11545 – 34965 0 – 11545	Hydrogeochemistry (Radke *et al.*, 2000; https://sarig.pir.sa.gov.au/sarig/frameSet.jsp	0.25 0.25 0.25 0.25	1.00 0.75 0.50 0.25	0.50 0.50 0.50 0.50	0.125 0.094 0.063 0.032	
	Evidence of uranium deposition **Both systems**	Basin rocks with 10 ppm uranium (radiometrics) 10 km buffer around U–enriched basin rocks 20 km buffer around U–enriched basin rocks 30 km buffer around U–enriched basin rocks	Radiometric Map of Australia (Minty *et al.*, 2010)	1.00 1.00 1.00 1.00	1.00 0.75 0.50 0.25	1.00 1.00 1.00 1.00	1.000 0.750 0.500 0.250	Uranium values ≥10 ppm were extracted from filtered uranium band and converted to a polygon shape file. A spatial query was used to select values for Mesozoic to Cenozoic basins only.
	Source of reducing fluids (two–fluid model) **Roll-front only**	Distribution of coal basins		0.50	0.50	0.50	0.125	
	Source of reducing fluids (two–fluid model) **Roll-front only**	Distribution of petroleum basins		0.50	0.50	0.50	0.125	

3.2.3 Mineral systems components

Mineral systems can be subdivided into four critical components, and without any of critical components a deposit cannot form. The critical components are:

- sources of metals, fluids and ligands;
- drivers;
- fluid pathways and architecture; and
- depositional mechanisms.

Table 3.2.2 summarises the theoretical and mappable criteria for sandstone–hosted uranium systems. This table also indicates which mappable criteria were used for the paleochannel and roll-front systems.

3.2.3.1 Sources

In sandstone–hosted uranium systems sources of leachable uranium and oxidised fluids are important source ingredients for a potent ore fluid. There are two potential sources of uranium for this system:

- Uranium leached from the hinterland.
- Uranium leached from detrital uranium minerals within aquifers.

As a source of uranium is considered important for both systems, this criterion was used in analysing both paleochannel and roll-front systems.

Australian Proterozoic rocks are elevated in uranium compared to crustal averages (Budd *et al.*, 2001) and, as such, they are likely to have provided the source of uranium in both systems. Consequently, the presence of uranium–enriched basement rocks is a good indicator of a uranium source, either leached directly from the basement or leached from sediment sources derived from the basement. Figure 3.2.3 and Plates 3.1 and 3.2 illustrate the distribution of these potential source rocks, including buffers into basin successions likely to host mineralisation.[1] This diagram highlights the proximity of the Frome Embayment, an embayment of the Eromanga Basin and younger rocks which host the known sandstone–hosted deposits, to an extensive area of uranium–enriched basement in the Mount Painter area. It also indicates smaller areas of uranium–enriched basement with buffers which extend into basins to the north of Crocker Well, to east of Roxby Downs and in the northern Eyre Peninsula.

Meteoric water is the main fluid in these systems. It is typically low temperature (20° to 60°C), initially highly oxidised (air saturated) and weakly acidic to neutral (pH 4 to 7), but it is progressively buffered by wallrock interaction to become reduced and alkaline. In the two fluid model, hydrocarbon and/or hydrogen sulfide (H_2S) rich connate water may be the source of reductants and it is likely to be highly reduced, warm (60° to 100°C) and have variable pH. This second fluid is discussed in the section on deposition as fluid mixing may be an important mechanism for uranium deposition. With respect to the source of ore fluids, that is evolved meteoric water, criteria which could map this mineral system component were not identified.

[1] For uranium concentrations calculated from radiometric data, 10 ppm was chosen as the cut off because it is two standard deviations from the mean. Anything above two standard deviations from the mean is considered to be anomalous. Three buffers were chosen based on empirical evidence. The main deposits (i.e. Beverley and Four-Mile) in Frome Embayment are less than 10 km from the range front. Mound springs, the likely discharge zone for the system on the eastern margin of Lake Frome, are 30 km from potential source rocks in Mount Painter. The 100 km buffer is based on the theoretical modelling based on Kazakhstan deposits.

3.2.3.2 Drivers

Drivers are associated with the energy required to move metals, fluids and ligands to the deposition site. Topographic gradient is the main driver for fluids in sandstone–hosted uranium systems. Meteoric water migrates downward along gravitational gradients until it reaches hydraulic equilibrium. In the case of the two fluid model, where a hydrocarbon and/or H_2S rich fluids is involved, then natural buoyancy of the fluid may be an important driver for the migration of fluids. An example of this would be hydrocarbons migrating up dip along permeable lithologies and faults. Other possible drivers for fluid movement include convection and deformation–related forcing. In this analysis, topographic gradient was used as a criterion to map fluid flow driver. The use of modern topography as a proxy for a topographic driver is considered valid owing to the young age (5 to 1 Ma) of the major mineralising event in the Frome Embayment. Figure 3.2.4 and Plates 3.1 and 3.2 illustrate the results of this analysis, which identifies areas within Mesozoic and Cenozoic basins adjacent to high topographic gradients, particularly adjacent to the northern Flingers Ranges, along the western margin of the Stuart Shelf and in the southwestern part of the study area. This criteria was used in analysing both paleochannel and roll-front systems.

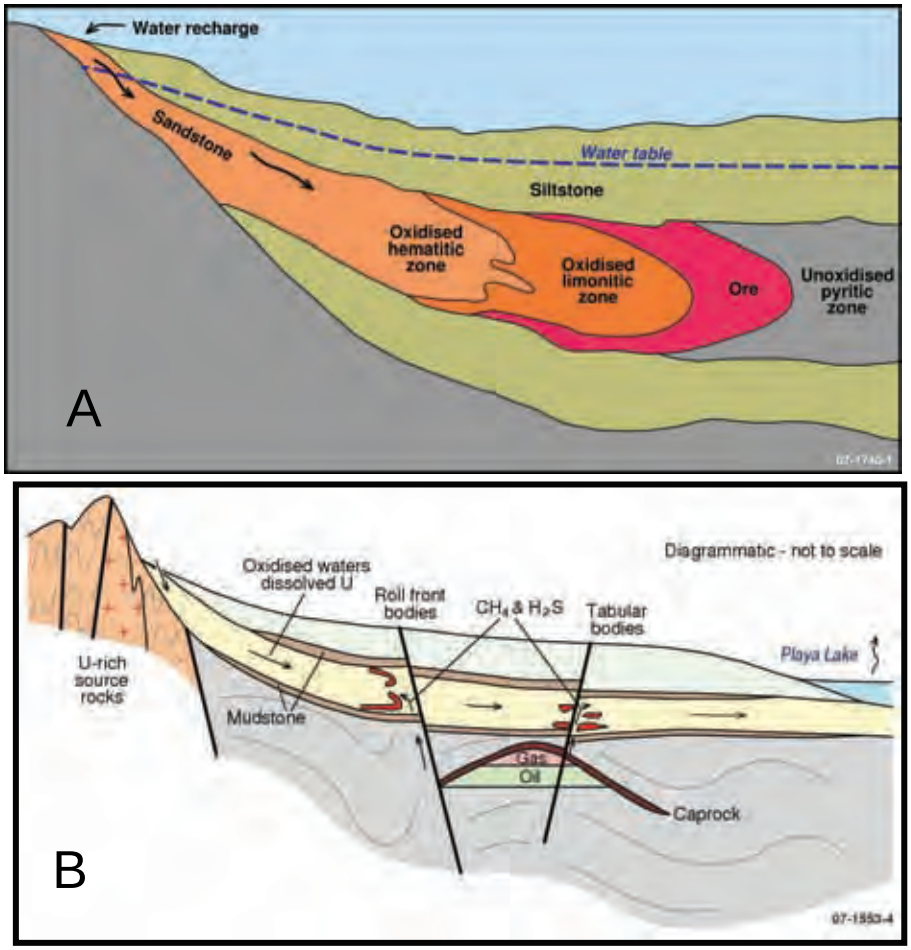

Figure 3.2.2: *Mineral system models for the formation of roll-front/paleochannel uranium deposits: (A) single fluid model and (B) two–fluid model (after Jaireth et al., 2008).*

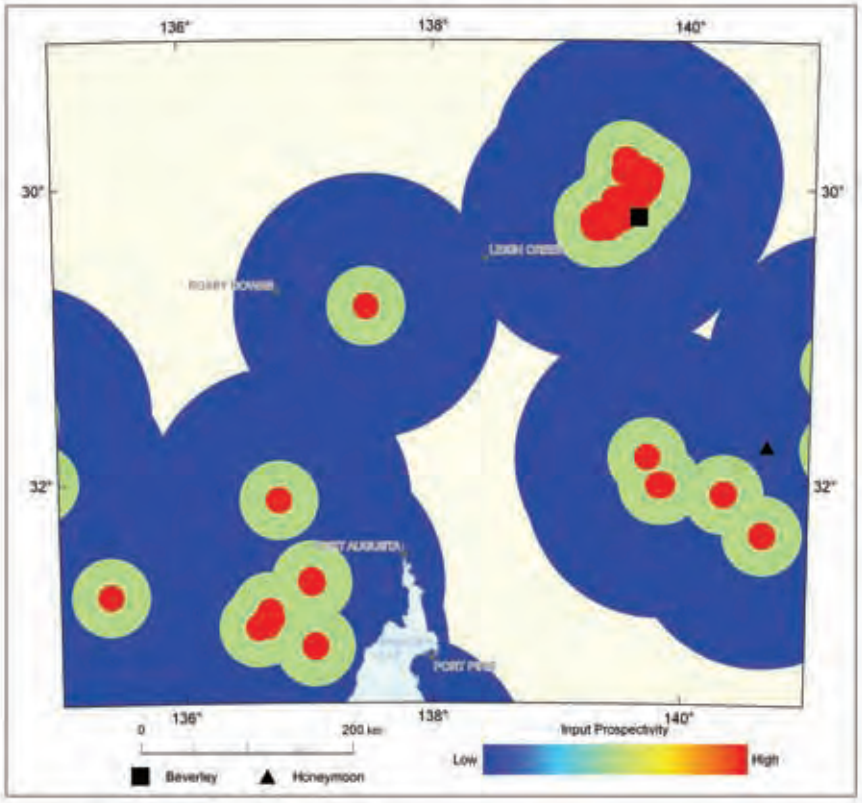

Figure 3.2.3: *Variations in the weighting of basement uranium source.*

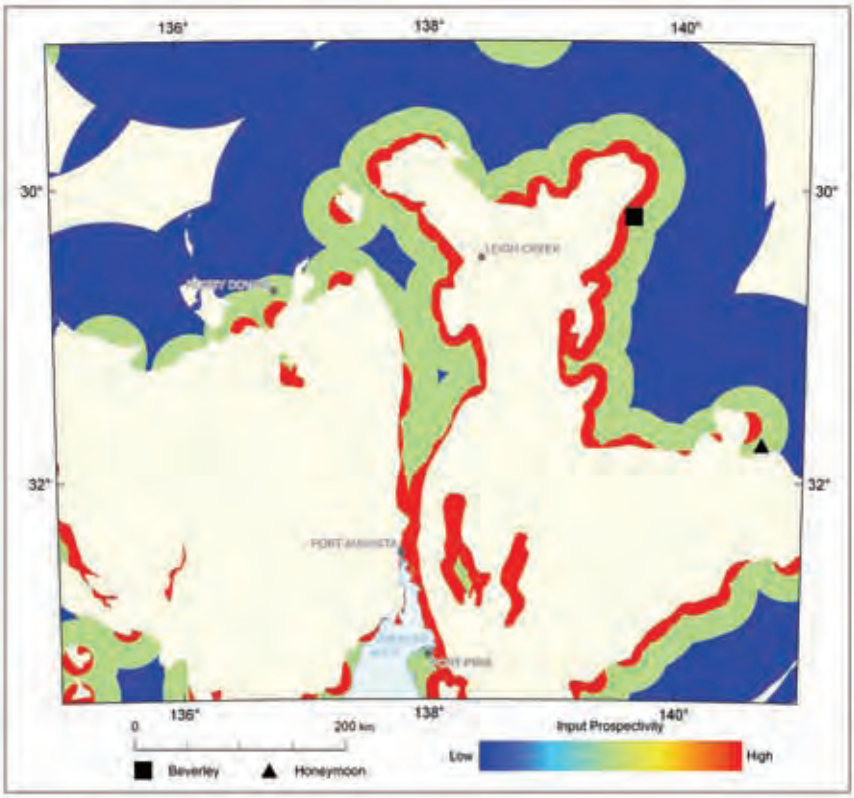

Figure 3.2.4: *Variations in the weighting of topographic driver.*

3.2.3.3 Fluid pathways and architecture

Variations in permeability and porosity play a role in controlling fluid flow pathways. Likely fluid flow pathways include:

- High permeability faults;
- Permeable sandstone units that are confined by low permeability lithologies; and
- Paleochannels.

Growth and basin margin faults are important in sandstone–hosted uranium systems because they can control the distribution and shape of sandstone lithologies (i.e. wedge–shape sandstone lithologies proximal to permeable faults and/or uranium–rich basement), paleochannels and basin morphology. Variations in permeability and porosity play a role in controlling the fluid flow regime for sandstone–hosted uranium systems (i.e. permeable sandstone units which are confined by less permeable fine-grained lithologies). As criteria to map fluid flow pathways, the following criteria were used:

- Distribution of Cenozoic (Figure 3.2.5; used in both analyses) and Mesozoic (Figure 3.2.6; used in roll-front analysis) sedimentary basins;
- Distribution of Cenozoic alluvium and/or fluvial units (Figure 3.2.7; used in paleochannel analysis);
- Distribution of paleochannels (Figure 3.2.8; used in paleochannel analysis);
- Surface and subsurface distribution of Algebuckina Formation (Figure 3.2.9; used in roll-front analysis); and
- Surface and subsurface distribution of Cadna-owie Formation (Figure 3.2.10; used in roll-front analysis).

The datasets used and weightings given are summarised in Table 3.2.2. This analysis has highlighted the distribution of paleochannels near the margins of basins (Plate 3.1) and the subsurface distribution of sandstone aquifers (Plate 3.2).

3.2.3.4 Depositional mechanisms

Depositional elements can take the form of *in situ* carbonaceous material within the sediments as in the case of the single fluid model or as a hydrocarbon and/or H_2S–bearing fluid. In the latter case locations of known hydrocarbon fields will be important in determining sandstone–hosted uranium prospectivity.

Reduction of the oxidised uranium–bearing fluid is the primary depositional mechanism for sandstone–hosted mineral system. Changes in redox state can be achieved either by wall rock interactions (i.e. single fluid model with an *in situ* reductant) or by mixing of two fluids (i.e. an oxidised fluid carrying uranium in solution and a second reduced, hydrocarbon and/or H_2S–bearing fluid). However, the distribution of reductants, generally organic carbon, in basins is difficult to map. The availability of a large quantity of hydrogeochemical data from potential aquifers to uranium–rich fluid flow may allow mapping of redox gradients. Figure 3.2.11 shows the distribution of these redox gradients interpreted from the hydrogeochemistry of Radke *et al.* (2000). In addition to redox gradients, changes in pH may also cause uranium deposition (Bastrakov *et al.*, 2010). Figure 3.2.12 indicates the distribution of pH gradients, again based on the hydrogeochemistry data (Radke *et al.* 2000; https://sarig.pir.sa.gov.au/sarig/frameSet.jsp). Figure 3.2.13 shows electrical conductivity (µS/cm), which was used as a proxy for total dissolved solids (TDS). There is empirical evidence to suggest that the TDS increases at sites of uranium deposition (Spalding *et al.*, 1984). All three of these hydrochemical parameters were used in both analyses.

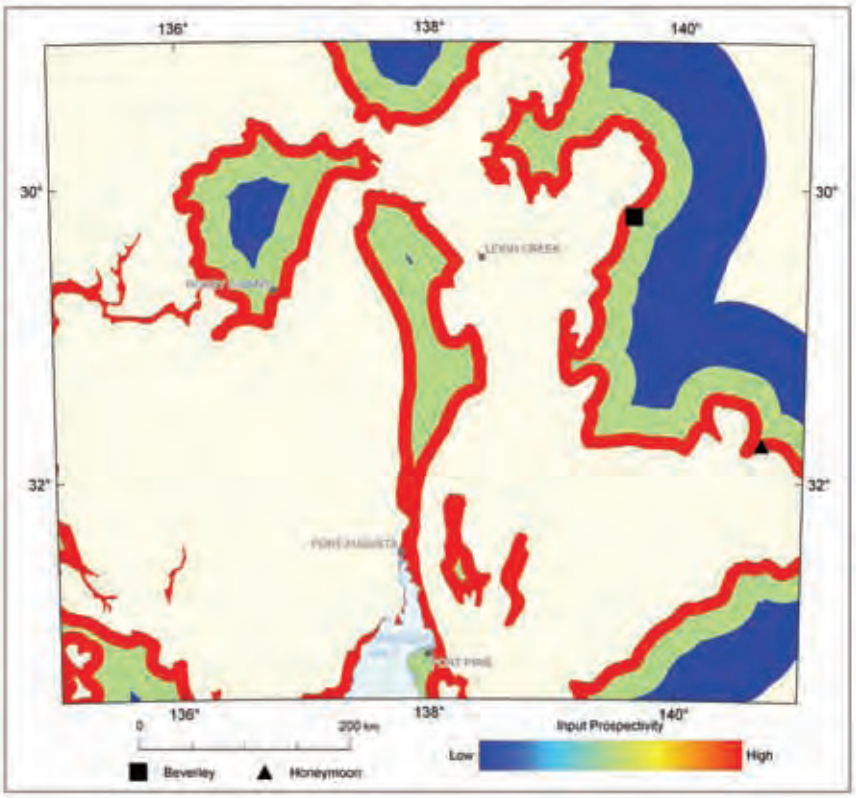

Figure 3.2.5: *Variations in the weighting of Cenozoic sedimentary basins.*

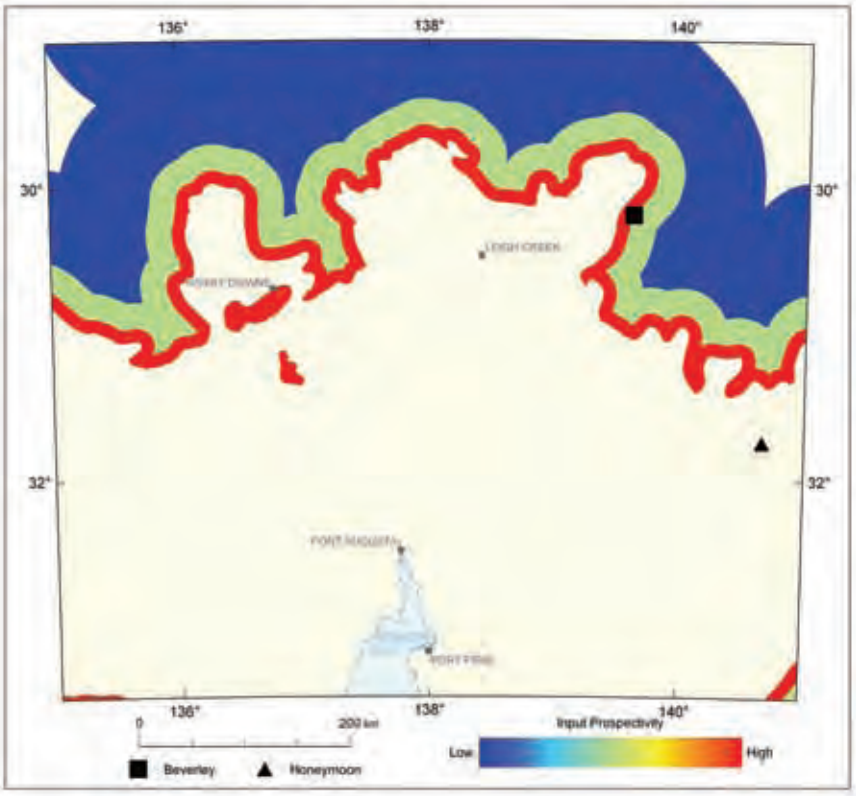

Figure 3.2.6: *Variations in the weighting of Mesozoic sedimentary basins.*

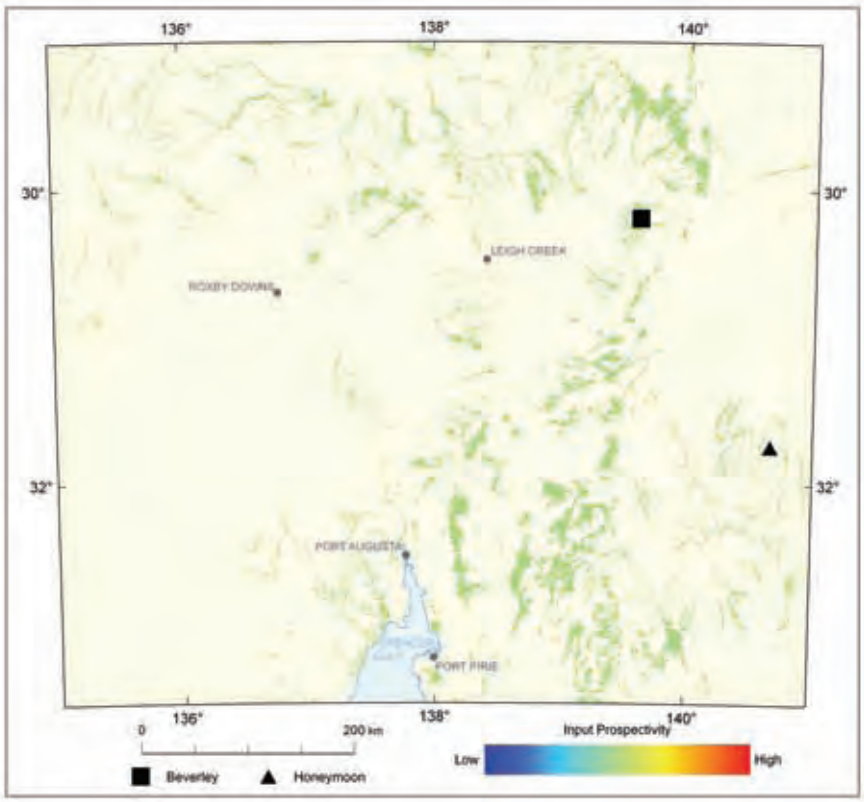

Figure 3.2.7: *Variations in the weighting of distribution of Cenozoic alluvial and fluvial units.*

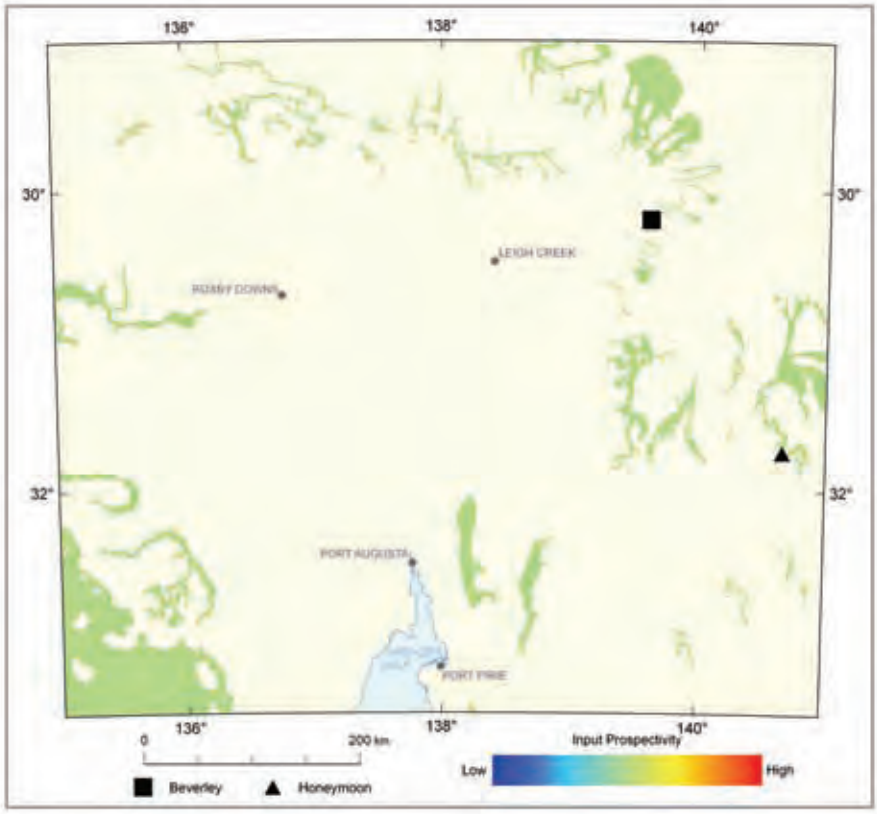

Figure 3.2.8: *Variations in the weighting of paleochannels.*

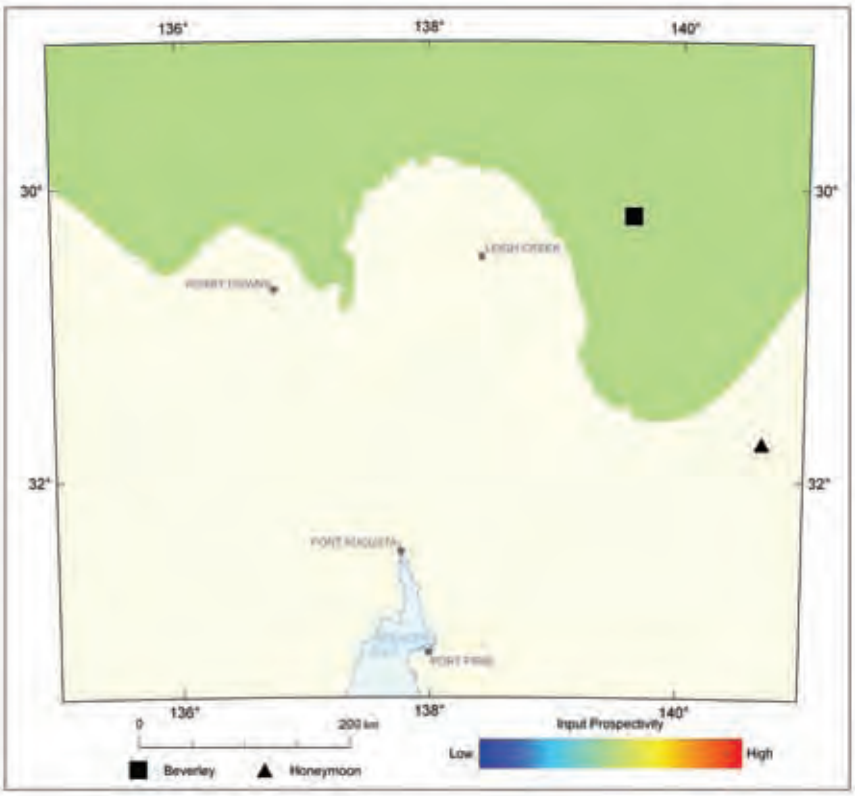

Figure 3.2.9: *Variations in the weighting of the subsurface distribution of the Algebuckina Formation.*

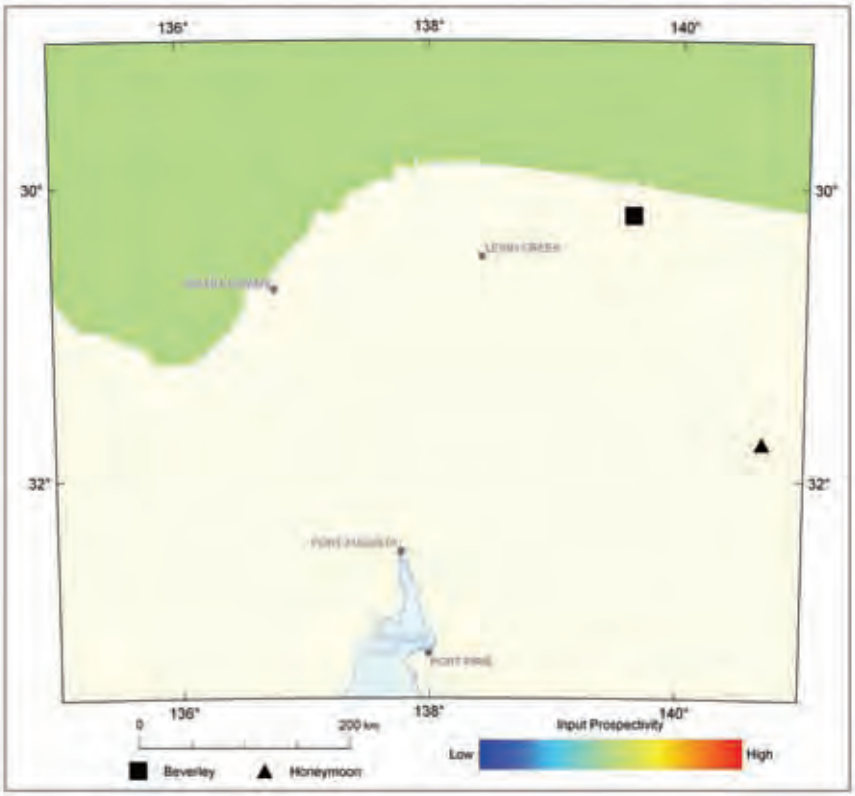

Figure 3.2.10: *Variations in the weighting of the subsurface distribution of the Cadna-owie Formation.*

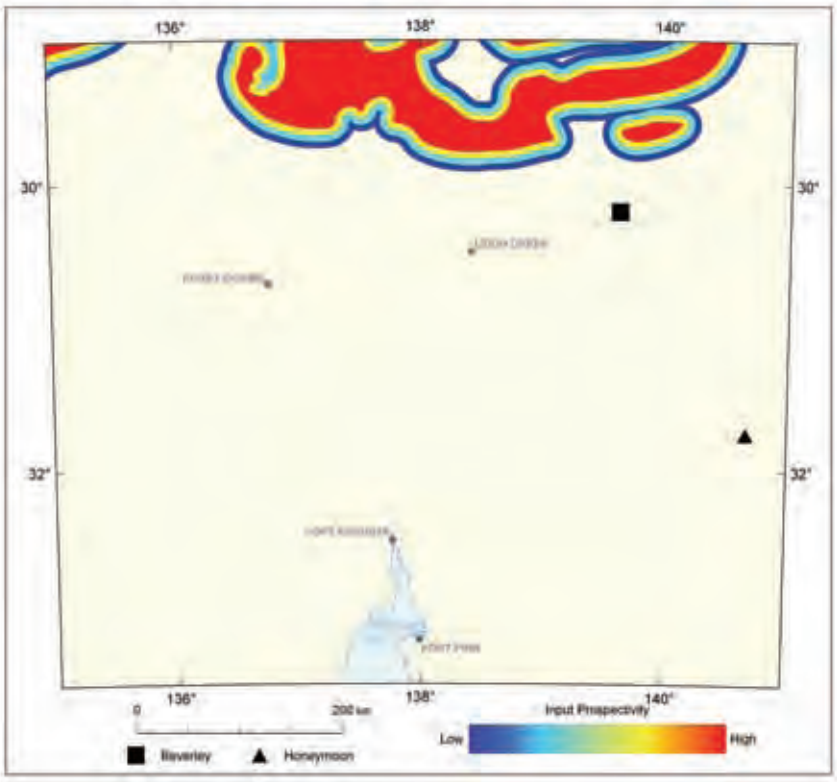

Figure 3.2.11: *Variations in the weighting of redox gradient as determined from hydrogeochemical data.*

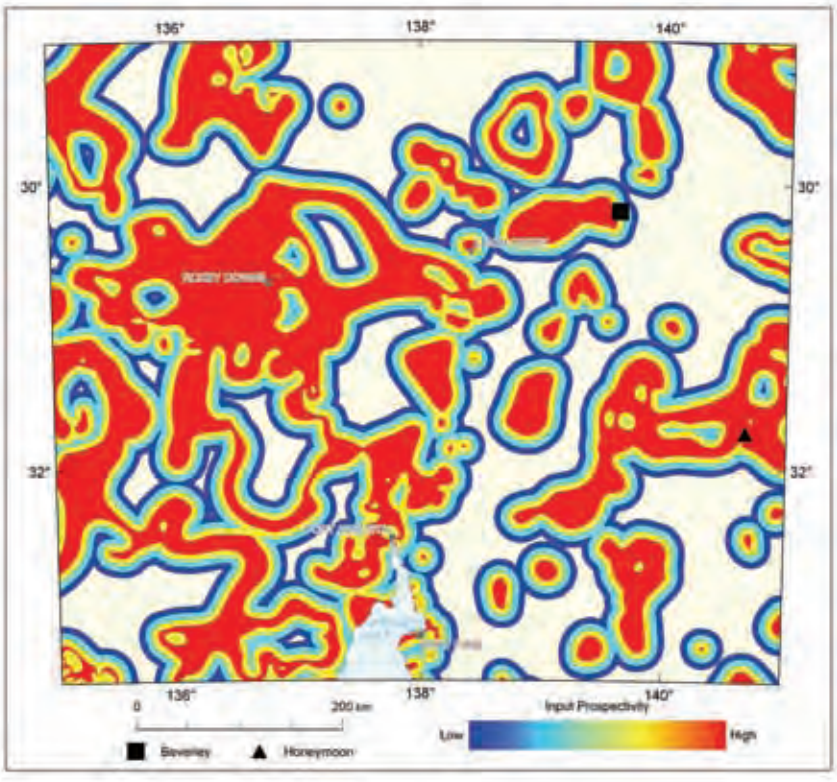

Figure 3.2.12: *Variations in the weighting of pH gradient as determined from hydrogeochemical data.*

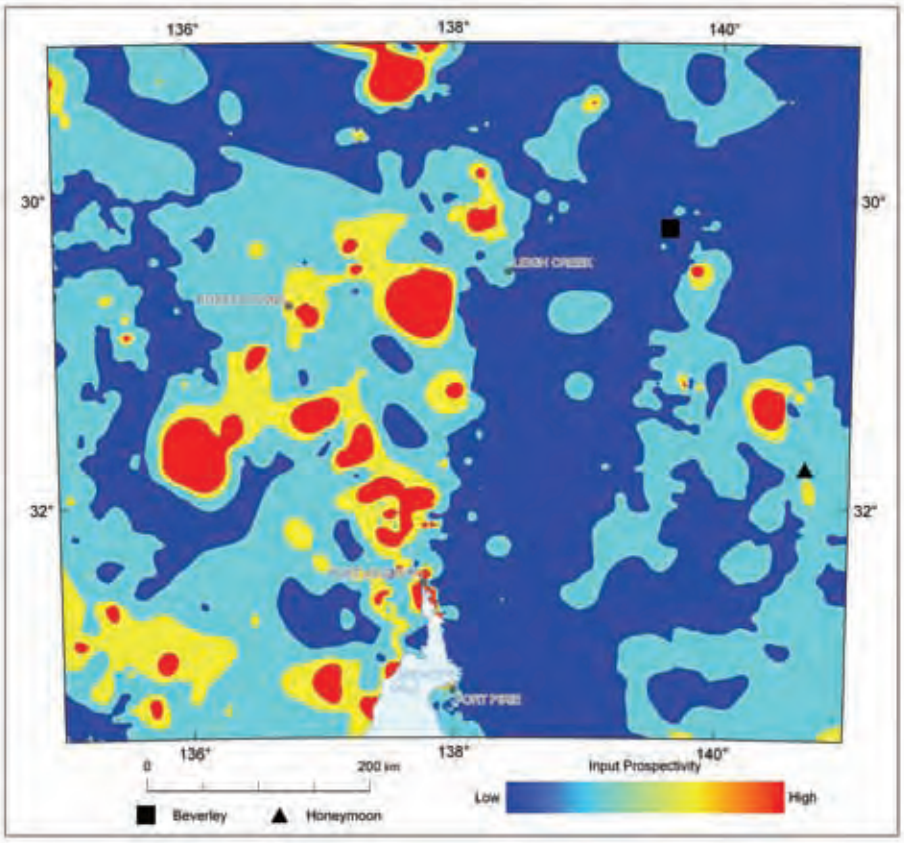

Figure 3.2.13: *Variations in the weighting of total groundwater electrical conductivity.*

In addition to these criteria, radiometric data were used to identify uranium surface anomalies of more than 10 ppm in Mesozoic and Cenozoic basins. The anomalies and buffers, as described in Table 3.2.2, are shown in Figure 3.2.14. This parameter was used in both analyses.

Following the two–fluid model for sandstone–hosted uranium deposits, wherein a second fluid sourced from either a petroleum field or from a coal field acts as a reductant to deposit uranium (Figure 3.2.2), the distributions of known petroleum and coal fields were considered in the mineral potential analysis of roll-front deposits. However, petroleum fields are not known within the study area and known coal fields are restricted to the vicinity of Leigh Creek (in the Arkaringa Basin). Consequently, the distribution of these mappable criteria did not affect the depositional component of the roll-front system and the distributions of these features are not shown.

Together, these data sets indicate areas of potential uranium deposition along the northern part of the study area, particularly in the Frome Embayment (Plates 3.1 and 3.2). Additional potential depositional sites are present in the southwestern corner of the study area and the area around Port Pirie.

3.2.4 Results

Based on the analysis of paleochannel prospectivity, four areas have been highlighted as having high to very high prospectivity, and are indicated on Figure 3.2.15 and Plate 3.1:

A) The Lake Eyre Basin to the east and northeast of Mount Painter Inlier;

B) An area north of outcropping basement of the Curnamona province in the eastern part of the study area;
C) An area in the far southwest of the study area (western Eyre Peninsula); and
D) An area to the north of area C.

In addition to these four areas, a paleochannel in the west–central portion of the study area southwest of Tarcoola has been highlighted as having moderate to high potential (area E). This area was also highlighted as having high potential in the Woomera Prohibited Area assessment (Geoscience Australia, 2010).

Based on the analysis of roll-front prospectivity, two areas were identified as having high to very high prospectivity, and are indicated in Figure 3.2.16 and Plate 3.2:

A) The Eromanga Basin to the east and northeast of the Mount Painter Inlier; and
B) An area near Olympic Dam in the north–central part of the study area.

In addition to these areas, several others have moderate potential, including Eromanga Basin rocks in the northern part of the study area (area C). This area overlaps an area of moderate prospectivity identified in the Woomera Prohibited Area assessment (Geoscience Australia, 2010).

The area which has been highlighted as being most highly prospective for both systems is the area adjacent to the Mount Painter Inlier. This region hosts the Beverley and Four Mile sandstone–hosted uranium deposits. The area has been highlighted for the following reasons: proximity to uranium–enriched source rocks in the Mount Painter Inlier, high topographic relief which can drive uranium fluids into the adjacent basins and the presence of both *in situ* (organic–rich material) and mobile (hydrocarbons in the Cooper and Arrowie Basins) reductants within the basin. The western side of the Eyre Peninsula is prospective for paleochannel–style uranium mineralisation because it drains the uranium-rich source rocks of the Gawler Range Volcanics. The area has moderate relief (i.e. driver of fluids) and higher rainfall than the northern areas of South Australia (i.e. fluid source). The potential reductants in this area are unclear and, as a result, uranium may be carried in solution some distance from the source. The third area lies in a paleochannel in the Woomera Prohibited Area. Potential uranium sources are likely to come from the Peak and Denison Inliers or directly from the sandstone units of the Eromanga Basin. The area has low relief and is a confined system, draining into Lake Eyre. Sources of reductants are likely to be both *in situ* (i.e. coal measures in the Arckaringa Basin) and mobile (i.e. reduced hydrocarbon–bearing groundwater within the Eromanga Basin).

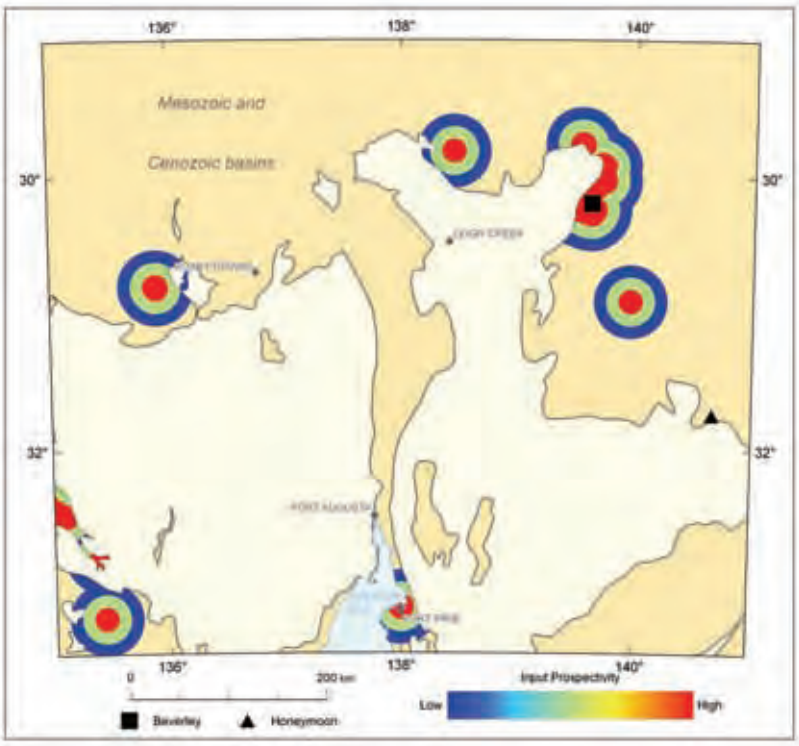

Figure 3.2.14: *Variations in the weighting of basin–hosted uranium anomalies as determined from radiometric data. The shaded area indicates the distribution of Mesozoic to Cenozoic basins.*

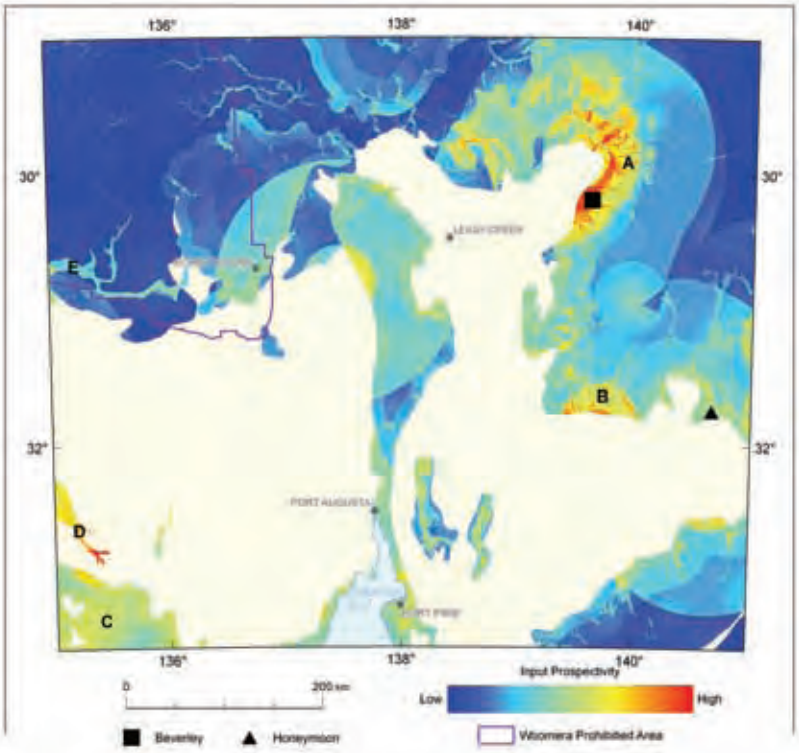

Figure 3.2.15: *Variations in assessed prospectivity, paleochannel mineral system. The letters indicate prospective areas discussed in the text. The purple line encloses the Woomera Prohibited Area.*

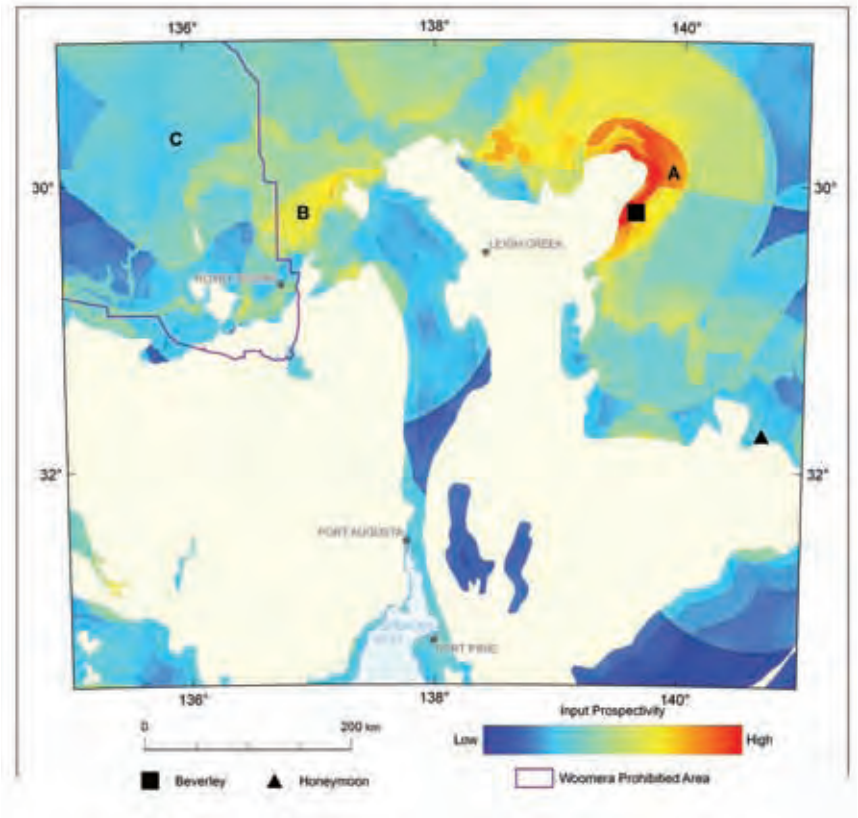

Figure 3.2.16: *Variations in assessed prospectivity, roll-front mineral system. The letters indicate prospective areas discussed in the text. The purple line encloses the Woomera Prohibited Area.*

3.3 URANIUM-RICH IRON OXIDE-COPPER-GOLD

R. S. SKIRROW, A. SCHOFIELD AND D. CONNOLLY

Iron oxide-copper-gold deposits (Hitzman *et al.*, 1992) are a diverse family of mineral deposits characterised by the following features:

- copper with or without gold, as economic metals;
- hydrothermal ore styles and strong structural controls;
- abundant magnetite and/or hematite;
- iron oxides with Fe/Ti greater than those in most igneous rocks; and
- no clear spatial associations with igneous intrusions as, for example, displayed by porphyry and skarn ore deposits (Williams *et al.*, 2005).

In addition, most iron oxide-copper-gold deposits display a broad space-time association with batholithic granitoids, occur in crustal settings with very extensive and commonly pervasive alkali metasomatism and many are enriched in a distinctive, geochemically diverse suite of minor elements, including various combinations of fluorine, phosphorous, cobalt, nickel, arsenic, molybdenum, silver, barium, light rare-earth-elements and uranium (Williams *et al.*, 2005).

Uranium-rich iron oxide-copper-gold deposits in which uranium is an economic metal are an important, yet rare subset of the iron oxide-copper-gold family (Hitzman and Valenta, 2005). Currently the Olympic Dam deposit is the only iron oxide-copper-gold deposit in which uranium is extracted as a major economic commodity. Nevertheless, this deposit is the world's largest single resource of uranium ore (BHP Billiton, 2010 Annual Report, www.bhpb.com). In a global context, most of the other iron oxide-copper-gold deposits containing higher grades of uranium are also located in the Gawler and Curnamona provinces of southern Australia (Hitzman and Valenta, 2005; Skirrow, 2011).

In terms of uranium mineral systems, uranium-bearing iron oxide-copper-gold deposits are considered to represent a hybrid deposit type involving both surface-derived and deep-sourced (magmatic-hydrothermal and/or metamorphic) fluids (see Figure 3.0.1). Iron oxide-copper-gold deposits form a continuum in terms of iron oxide contents between magnetite-dominated and hematite-dominated end-member styles. Uranium-rich iron oxide-copper-gold deposits are most closely associated with the hematite-rich style although not all hematite-dominated deposits contain high uranium contents (Skirrow, 2010, 2011).

3.3.1 Gawler Province uranium-bearing iron oxide-copper-gold systems

This section describes the uranium-bearing iron oxide-copper-gold metallogenic province in the Gawler Province, the major iron oxide-copper-gold deposits and resources, hydrothermal alteration and the timing of mineralisation (modified from Hayward and Skirrow, 2010).

3.3.1.1 Olympic iron oxide-copper-gold province

The Olympic iron oxide-copper-gold Province along the eastern margin of the Gawler Province is defined by the distribution of known early Mesoproterozoic iron oxide-copper-gold±uranium mineralisation and alteration (Figure 3.3.1; Skirrow *et al.*, 2002; Hayward and Skirrow, 2010). The Olympic Province is generally very poorly exposed, and Neoproterozoic to Cenozoic cover sediments and regolith commonly exceed several hundred metres in thickness (e.g., less than 350 m at Olympic Dam, Reeve *et al.*, 1990). This metallogenic province encompasses three known districts containing iron oxide-copper-gold±uranium deposits (from north to south), Mount Woods Inlier with

the Prominent Hill deposit immediately to the south, Olympic Dam district hosting the Olympic Dam and Carrapateena deposits and the historic Moonta-Wallaroo copper-gold mining district with the recently discovered Hillside deposit (Figure 3.3.1). The Olympic Province is superimposed on older geological domains (Figure 2.2). From north to south these geological domains include the Peake and Denison, Coober Pedy Ridge, Mount Woods Inlier, Olympic and Spencer geological domains. The Olympic geological domain in the eastern Gawler Province hosts most of the known iron oxide-copper-gold deposits.

Boundaries of the iron oxide-copper-gold metallogenic province remain uncertain, particularly in the north. The western boundary of the Olympic iron oxide-copper-gold Province is marked by the Elizabeth Creek Fault Zone and by the Kalinjala Shear Zone in the central and southern portions of the iron oxide-copper-gold province respectively (Figure 3.3.1). These structures are believed to represent fundamental controls on the location of the iron oxide-copper-gold systems (see also below). The eastern boundary is defined as a major linear discontinuity in magnetic and gravity data which is buried beneath Neoproterozoic and younger cover sequences. This discontinuity has been commonly identified as the eastern margin of the Gawler Province. In the southern Olympic and Spencer geological domains, the eastern boundary of the Olympic iron oxide-copper-gold Province is defined by the Pine Point Fault Zone along the eastern shore of Yorke Peninsula, although in this region the boundary is inboard of the province margin.

The distribution of iron oxide-copper-gold deposits and prospects in the Olympic Province is shown in Figure 3.3.1 and resource data are summarised in Table 3.3.1. The Olympic Dam deposit is currently the world's fourth largest copper resource, fifth largest gold resource and the world's largest uranium resource by far, with all resources contained in a single deposit of less than 25 km^2 (BHP Billiton Annual Report 2009). The only other currently producing iron oxide-copper-gold mine in the province is the Prominent Hill open pit where production commenced in 2009, although historical copper production also came from several small open pits and underground mines in the Moonta-Wallaroo iron oxide-copper-gold district on the Yorke Peninsula (Figure 3.3.1). The Cairn Hill deposit in the Mount Woods Inlier is in the early stages of pit development and will be mined for iron with copper as a by-product. Carrapateena and Wirrda Well are significant deposits buried under relatively deep cover (less than 450 m). A resource was recently announced by OzMinerals for the Carrapateena deposit: 203 Mt at 1.31% copper, 0.56 g/t gold, and 270 ppm uranium, with a cutoff of 0.7% copper (April 2011, www.ozminerals.com).

Iron oxide-copper-gold deposit styles and mineralogy vary systematically along the Olympic iron oxide-copper-gold Province (Skirrow *et al.*, 2002). Deposits in the central-northern part of the province (Prominent Hill, Olympic Dam, Carrapateena; Figure 3.3.1) mostly comprise hematite-rich breccias with disseminated hypogene chalcopyrite-bornite±chalcocite mineralisation, interpreted to have formed at shallow crustal levels (Reeve *et al.*, 1990; Fairclough, 2005; Belperio *et al.*, 2007). Deposits in the southern third of the province (Moonta-Wallaroo, Hillside) and far north (Mount Woods Inlier) mostly comprise magnetite-rich alteration systems with hypogene chalcopyrite mineralisation. These systems are interpreted to have formed at deeper crustal levels. These variations are considered to reflect different levels of post-mineralisation exhumation and syn-mineralisation fluid redox conditions (Skirrow *et al.*, 2002; Skirrow, 2010). In detail, hematite-rich alteration overprints earlier magnetite-rich alteration (see below), and both magnetite and hematite rich deposit styles occur in close proximity within some districts. Furthermore, the range of secondary elements (gold, silver, uranium, rare-earth-elements) is highly variable between deposits and shows little district scale zonation, with the possible exception of uranium which appears most enriched in hematite-rich iron oxide-copper-gold systems in the central part of the Province (e.g.,

Olympic Dam, Oak Dam). The magnetite-rich deposits in general contain lower concentrations of uranium.

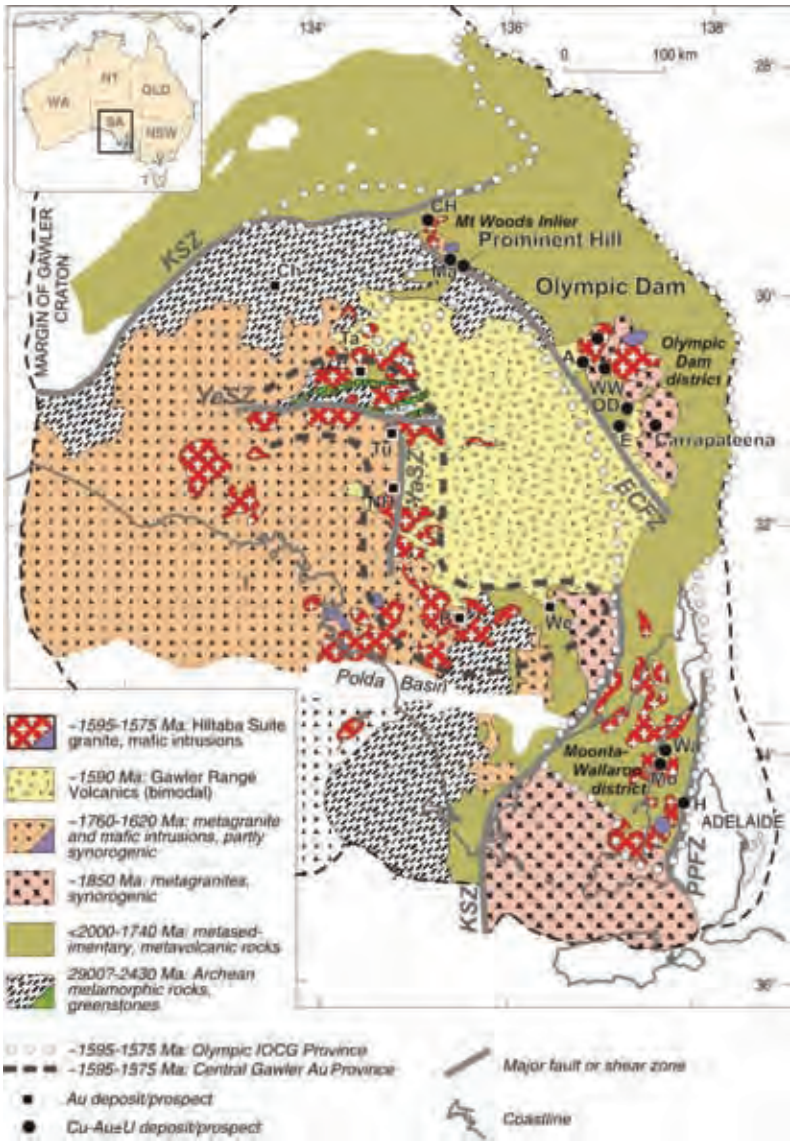

Figure 3.3.1: *Geology of the Gawler Province (pre-Neoproterozoic, excluding Mesoproterozoic Pandurra Formation), regional fault zones, and principal iron-oxide copper-gold±uranium and Au deposits and prospects in the Olympic iron-oxide copper-gold Province and Central Gawler Gold Province. Regional faults: ECFZ: Elizabeth Creek Fault Zone, KFZ: Kalinjala Fault Zone, KRFZ: Karari Fault Zone, PPFZ: Pine Point Fault Zone, GFZ: Gregory Fault Zone, YFZ: Yerda Fault Zone. iron-oxide copper-gold deposit abbreviations from north to south: Ch – Cairn Hill, Ma – Manxman, A – Acropolis, WW – Wirrda Well, OD – Oak Dam, E – Emmie Bluff, Wa – Wallaroo, Mo – Moonta, H – Hillside. Gold deposit abbreviations: Ch – Challenger, Ta – Tarcoola, Tu – Tunkillia, NH – Nuckulla Hill, B – Barns, We – Weednanna. From Hayward and Skirrow (2010).*

3.3.1.2 Olympic Dam deposit

The Olympic Dam deposit is hosted by the Olympic Dam Breccia Complex within the Roxby Downs Granite, a member of the Hiltaba Suite. Aspects of the geology of the Dam Breccia Complex are shown in Figure 3.3.2 and are described in detail elsewhere (Reeve *et al.*, 1990; Oreskes and Einaudi, 1992; Cross *et al.*, 1993; Haynes *et al.*, 1995; Reynolds, 2000). In brief, the zoned funnel-shaped Olympic Dam Breccia Complex comprises multi-phase heterolithic breccias ranging from granite-rich to hematite-rich. The core zone of hematite-quartz breccias lacks major copper mineralisation but has high levels of rare-earth-elements, barium and locally uranium. The core zone also contains ultramafic to felsic igneous dykes and diffuse zones of fragmented intrusive rocks interpreted as phreatomagmatic diatreme breccias (Reeve *et al.*, 1990; Cross *et al.*, 1993). Large blocks of altered volcaniclastic rocks are present within the inferred maar craters. The margins of the core zone contain native gold and copper mineralisation with low temperature illite and local silicification, and grade outwards and downwards into hematite-granite breccias hosting the bulk of the copper-gold-uranium mineralisation. The distribution of individual hematitic breccia bodies partly controls copper grades. However, grades are also controlled by an important deposit-wide sharp interface between bornite and chalcopyrite which is broadly funnel shaped and, in detail, highly convoluted. Bornite-chalcocite mineralisation above the interface commonly attains grades of 4 to 6% copper, whereas chalcopyrite mineralisation below the interface rarely exceeds 3% copper (Reeve *et al.*, 1990). The deeper and peripheral zones of the Olympic Dam Breccia Complex contain

Table 3.3.1: *Iron oxide copper-gold(uranium-silver) deposits and prospects.*

Name	Total Resources[1]	Status	Fe oxide Style	Reference
Olympic Dam[2]	9231 Mt @ 0.86% Cu, 0.33 g/t Au, 1.5 g/t Ag, 0.027% U_3O_8	Underground production	Hematite breccias	BHP Billiton Ltd Annual Report 2009
Prominent Hill[3]	297.7 Mt @ 0.93% Cu, 0.78 g/t Au, 2.49 g/t Ag	Open pit production	Hematite breccias	Belperio *et al* (2007) OZ Minerals ASX Resource Statement 23/12/2008
Wirrda Well	Best intersection: 248 m @ 0.86% Cu, 4.6 g/t Ag (from 419m in WRD9)	Prospect delineation	Hematite breccias	WMC Limited unpublished memoranda (1985)
Carrapateena	203 Mt @ 1.31% Cu, 0.56 g/t Au, 270ppm U	Resource delineation	Hematite breccias	Fairclough (2005) www.OzMinerals.com
Oak Dam	(~300 Mt @ 0.2% Cu) Best intersection: 5 m @ 7.1 kg/t U_3O_8 within 63 m @ 0.7 kg/t U_3O_8, 0.3%Cu (in AD1)	Subeconomic prospect	Hematite breccias and mantos	Davidson *et al* (2007)
Moonta-Wallaroo[4]	10.1 Mt @ 3.7% Cu, 0.42 g/t Au	Closed Mines	Magnetite-bearing veins	Conor (2003)
Hillside	170 Mt @ 0.7% Cu, 0.2 g/t Au	Resource delineation	Magnetite-bearing veins	Rex Minerals Limited Annual Report 2009
Cairn Hill	Fe resource with 11.4 Mt @ 0.37% Cu, 0.11 g/t Au	Open Pit development	Magnetite-rich breccias and stratabound replacement	IMX Resources Limited Annual Report 2007
Punt Hill	Best intersection: 159 m at 0.47% Cu, 5.3 g/t Ag, 0.12 g/t Au, 0.48% Zn, 0.12% Pb (from 846 m, GHDD6)	Prospect delineation	Hematite breccias and veins	Monax Mining Limited Annual Report 2008

1 Total for Measured, Indicated and Inferred Resources, Reserves and Production, or best downhole drill intersection results.
2 Includes Au-only resource.
3 Total for Cu, Au and Western Cu resources.
4 Combined production only.

greater proportions of magnetite and chlorite relative to hematite and sericite, and siderite is locally abundant. Uranium mineralisation is present throughout the hematite-rich breccias broadly in association with copper mineralisation, but higher grade zones occur at the upper margin of the bornite-chalcocite zone. Uraninite (as pitchblende) is the dominant uranium mineral, whereas minor coffinite and brannerite occur in upper/shallower and deeper/peripheral zones respectively (Reynolds, 2000).

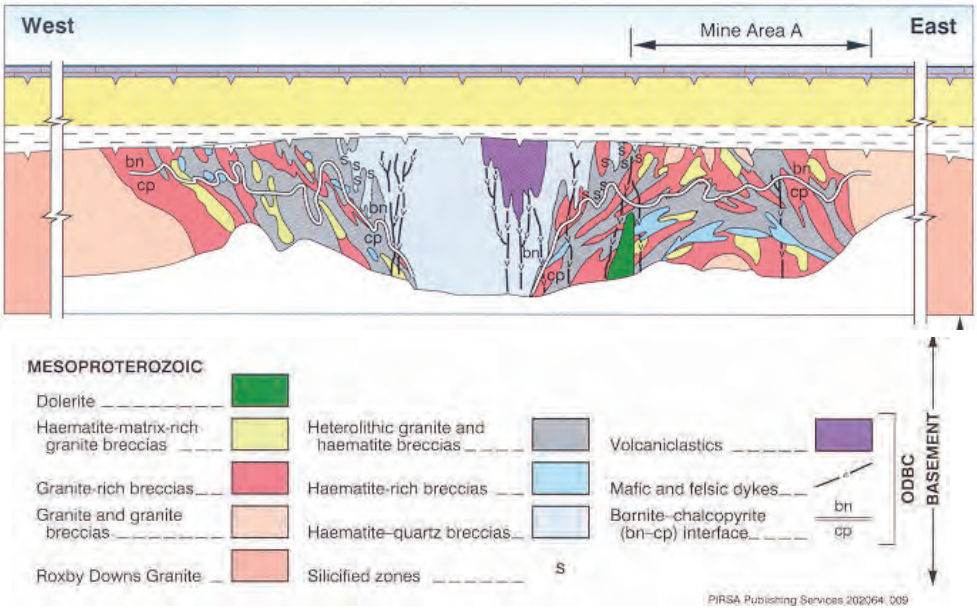

Figure 3.3.2: *Cross section of the Olympic Dam deposit (from Reynolds, 2000).*

3.3.1.3 Prominent Hill deposit

The Prominent Hill copper-gold deposit is situated on the southern flank of the Paleo- to Mesoproterozoic Mount Woods Inlier, concealed beneath ~100 m of Mesozoic sediments and regolith (Figs 3.3.1, 3.3.3). Few descriptions have been published, and the following summary is based on that of Belperio *et al.* (2007). The geology of the Prominent Hill deposit appears to be quite different to that of the Mount Woods Inlier in terms of metamorphic grade and lithologies, and we therefore suggest that the Prominent Hill deposit is situated in either the northernmost Olympic geological domain or within a lower metamorphic grade part of the Mount Woods Inlier.

The major hosts to mineralisation at Prominent Hill are hematitic breccias, which are themselves hosted by a sequence of andesitic to rhyodacitic volcanic rocks and sedimentary strata, including sandstone, greywacke, argillite and carbonate rock. The age of this sequence is unknown, although Belperio *et al.* (2007) correlated it with the Gawler Range Volcanics and parts are intruded by a dacitic porphyry with an age of 1585 ± 8 Ma (M. Fanning, in Belperio *et al.*, 2007). A variety of other intrusive rocks are present also, including dolerite, andesite, diorite, and granite. Hematitic breccias were emplaced within, and replaced, the sedimentary and volcanic strata as a series of steeply north-dipping tabular zones. Drilling and gravity data indicate the hematite-rich rocks extend at least 2 km east-west and are up to about 400 m wide. This zone contrasts with a strongly magnetic skarn domain immediately to the north of the hematitic breccias, which is characterised by the presence of magnetite, actinolite, chlorite, phlogopite, serpentine, talc, antigorite, carbonate, pyrite and minor chalcopyrite. The highest grade copper-gold mineralisation occurs within the hematitic breccias to the south of the magnetic domain. The breccias are multi-stage and heterolithic with sedimentary and/or volcanic clasts and hematite-rich matrix. They were attributed by Belperio *et al.*

(2007) to hydrothermal brecciation and explosive volcanism. In places, the breccias are almost entirely hematite and cryptocrystalline silica. Gold-only mineralisation occurs in this type of breccia and is typically on the margins of the copper mineralisation. Chalcopyrite, chalcocite and bornite are the principal copper minerals. Chalcocite-bornite breccia zones have higher copper grades (average 2.5% copper, 0.5 g/t gold) than chalcopyrite±uranium breccia zones (average 1.4% copper, 0.6 g/t gold) although the latter are volumetrically dominant. As at Olympic Dam, chalcocite and chalcopyrite are not observed together, although zoning at Prominent Hill has not been reported for the deposit as a whole. Uranium grades are higher in the chalcopyrite zone than in the chalcocite zone, and locally exceed 5000 ppm. Uranium is hosted by coffinite and uraninite. Elevated rare-earth-element (mainly cerium and lanthanum) concentrations are widespread in the hematitic breccias and average about 3000 ppm (Belperio *et al.*, 2007). In addition to hematite, the principal hydrothermal alteration minerals associated with copper-gold-uranium mineralisation are sericite, chlorite, silica, fluorite and barite.

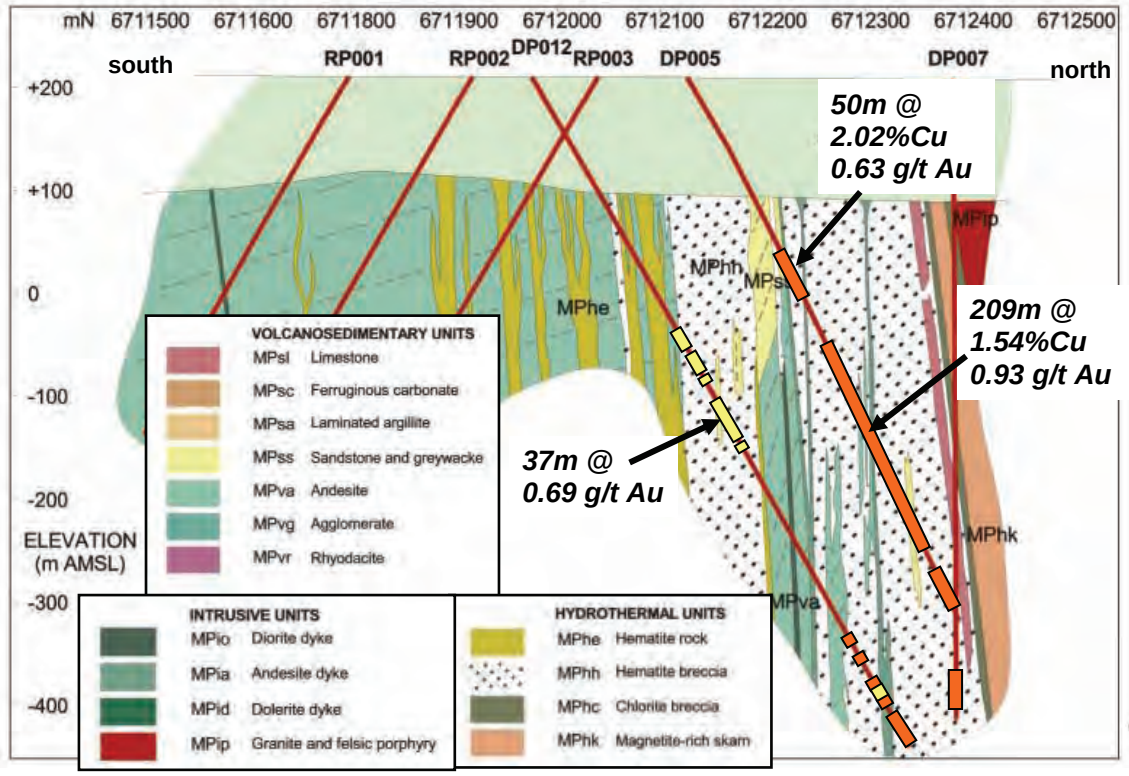

Figure 3.3.3: *Cross section of the Prominent Hill deposit (courtesy Minotaur Resources and PIRSA).*

3.3.1.4 Hillside deposit

The Hillside deposit is a major new iron oxide-copper-gold discovery in the Moonta-Wallaroo district, about 50 km southeast of the historic Moonta mining field (Figure 3.3.1). Discovered by Rex Minerals Ltd in 2008, the resource currently stands at 170 Mt at 0.7% copper and 0.2 g/t gold (Rex Minerals, 2011, www.rexminerals.com.au). The following summary is based on descriptions on the Rex Minerals website and by Conor *et al.* (2010). Mineralisation and alteration occur within intensely deformed metasedimentary rocks of the Paleoproterozoic Wallaroo Group and within gabbroic and granitic rocks assumed to be associated with the Hiltaba Suite. The Hillside deposit is spatially associated with the north-northeast trending regional Pine Point (Ardrossan) Fault, and with linear magnetic and gravity anomalies broadly parallel to the fault. Mineralised Proterozoic

basement rocks are concealed by 1 to 30 m of Cenozoic cover at the Hillside deposit and deep weathering has resulted in supergene mineralisation in weathered basement above some hypogene zones (Conor *et al.*, 2010).

Copper and gold mineralisation occurs as a series of sub-parallel, sub-vertical to steeply west-dipping, sheet-like bodies extending to depths of at least 600 m, which are generally associated with prograde and retrograde skarn alteration of the metasedimentary and felsic and mafic igneous host rocks (Conor *et al.*, 2010). From published descriptions, iron oxides in the alteration appear to be dominated by magnetite, with lesser hematite replacing the magnetite. Prograde skarn comprises garnet rock and magnetite±quartz±pyrite±garnet, replaced by clinopyroxene, potassium-feldspar, epidote, actinolite, allanite and biotite. Chalcopyrite and lesser hypogene bornite and chalcocite are closely associated with hematite replacement of magnetite, along with late-stage carbonate, chlorite and quartz. Although uranium mineralisation has not been described in detail and appears to be relatively minor in comparison with that in the hematite-dominated deposits of the iron oxide-copper-gold province, uraninite and pitchblende are described as commonly associated with carbonate-rich zones and light rare-earth-elements mineralisation is hosted by allanite (Conor *et al.*, 2010).

Titanite from the alteration has yielded a uranium-lead (U-Pb) isotope age of 1570 ± 8 Ma (Reid, 2010), which is within uncertainty of the youngest of the Hiltaba Suite granite ages from the region.

3.3.1.5 Carrapateena deposit

The Carrapateena deposit was discovered in 2005 by RMG Services with joint funding from Primary Industries and Resources South Australia (PIRSA) and, after a joint venture with Teck Australia Ltd, was acquired by OzMinerals in early 2011. Published information is very limited to date and the following summary is based on the description by Fairclough (2005) and recent OzMinerals information released to the ASX (www.ozminerals.com). Copper-gold mineralisation occurs in a roughly cylindrical, pipe-like, vertically plunging body and is hosted by heterolithic hematite-rich breccias corresponding to a gravity anomaly in an area where depths to basement are more than 470 m. A weak magnetic anomaly to the north may correspond to mafic volcanic rocks intersected in drillhole CAR001. There is both vertical and lateral zonation of sulfide minerals, with chalcocite-bornite zones developed at the top and central portions of the deposit, flanked by chalcopyrite mineralisation. Breccia clasts are predominantly of medium grained gneissic diorite which is variably altered to chlorite, sericite and hematite, as well as hematite-dominated clasts of earlier breccia phases. Sulfides occur mainly in the breccia matrix with hematite. Some parts of the breccia are noticeably vuggy and there is no evidence in CAR002 of a tectonic fabric within the hematitic breccias. Available geochemical data indicate elevated concentrations of silver, light rare-earth-elements, fluorine, barium and uranium in addition to copper and gold.

3.3.1.6 Summary of regional and proximal hydrothermal mineral assemblages

Iron oxide-copper-gold-related alteration and mineralisation assemblages in the Olympic iron oxide-copper-gold Province occur in a wide range of rock types, including metasiltstones and calcareous protoliths of the Wallaroo Group and granitoids of the Donington Suite and Hiltaba Suite as well as the Gawler Range Volcanics (Reeve *et al.*, 1990; Conor, 1995; Skirrow *et al.*, 2002). Despite the large extent of the metallogenic province (more than 500 km in length) and limitation of observations to mainly widely spaced drillholes, the iron oxide-copper-gold related alteration is remarkably consistent in its mineralogy, paragenetic sequence and timing throughout the province. Four key assemblages have been recognised, although not all occur within any particular

hydrothermal system (Skirrow *et al.*, 2002, 2007; Bastrakov *et al.*, 2007). Additionally, there are systematic regional differences described below, which are interpreted to relate to crustal depth of formation and preservation. The assemblages in generalised paragenetic order from earliest to latest, are:

- Albite-calc-silicate±magnetite alteration, representing sodium-calcium-iron metasomatism, is well developed in the Mount Woods Inlier and Moonta-Wallaroo districts as kilometre-scale regional alteration zones. Albitic alteration is rare in the Olympic Dam district, but it may be present at deeper levels where large scale magnetite-rich alteration zones are interpreted from geophysical inversion modelling (Williams *et al.*, 2004; Hayward and Skirrow, 2010). Actinolite, clinopyroxene (generally diopside or salite) and minor titanite and scapolite occur in places in assemblage (1). This alteration appears to be paragenetically the earliest of the alteration assemblages in the iron oxide-copper-gold province, and is similar to the sodium-calcium alteration observed in the Cloncurry district (Williams *et al.*, 2005), the Olary Domain in the Curnamona Province to the east of the Gawler Province and in other iron oxide-copper-gold provinces globally (Hitzman *et al.*, 1992; Williams *et al.*, 2005). The only available isotopic age for the albite-actinolite±magnetite assemblage in the Gawler Province is from the Mount Woods Inlier where titanite yielded a U-Pb ion probe age of 1567 ± 10 Ma (Skirrow *et al.*, 2007). However, this is considered a minimum age and may represent re-setting during local or regional metamorphism, as recorded in leucogabbro-hosted zircon overgrowths at 1576 ± 7 Ma (Jagodzinski, 2005).

- Biotite-magnetite alteration, representing Fe^{2+}-potassium metasomatism, has been observed in the Mount Woods Inlier and Moonta-Wallaroo districts where it shows mutually cross-cutting relationships with Hiltaba Suite granitoids (Conor, 1995; Hampton, 1997; Conor *et al.*, 2010). Biotite-magnetite alteration zones may be very extensive and are clearly imaged in regional aeromagnetic data (Raymond, 2003). Albite appears to be a stable phase during this iron-potassium metasomatism and, in some areas, minor quantities of pyrite, chalcopyrite, pyrrhotite, monazite and titanite were deposited at this stage. Copper±gold mineralisation associated with biotite-magnetite alteration is generally low grade (less than 0.5% copper), but at the Wallaroo deposit small higher grade zones have been mined. Biotite-magnetite altered rocks typically contain a cleavage which developed during alteration, particularly in the Moonta-Wallaroo district, indicating syntectonic formation under generally brittle-ductile conditions (Conor, 1995; Skirrow, 2010). U-Pb ion probe dating of titanite and monazite in biotite-magnetite alteration in the Moonta-Wallaroo district has revealed a range of ages from ~1620 to ~1570 Ma (Raymond *et al.*, 2002), and a rhenium-osmium (Re-Os) age 1575 ± 6 Ma for molybdenite cross-cutting the biotite-magnetite alteration provides a minimum age constraint (Skirrow *et al.*, 2007).

- Magnetite - potassium-feldspar ± actinolite ± carbonate alteration, also representing Fe^{2+}-potassium metasomatism, is an important alteration assemblage in the Olympic Dam district, but based on current knowledge is not present in other parts of the Olympic iron oxide-copper-gold province. Minor pyrite, quartz, carbonate, chalcopyrite, apatite and titanite are present in places. The very large magnetite-rich alteration systems at the Acropolis, Wirrda Well and Murdie Murdie prospects are representatives of this alteration assemblage and relicts of it are observed in many of the iron oxide-copper-gold systems (e.g., Davidson *et al.*, 2007). In most of this alteration copper±gold±uranium mineralisation is generally low grade (less than 0.5% copper), although long intervals of such mineralisation may be present. At the Olympic Dam deposit its is suggested that the hydrothermal magnetite with siderite observed in peripheral and deeper parts of the deposit

(Reeve *et al.*, 1990; Haynes *et al.*, 1995) may have affinities with the magnetite – potassium-feldspar ± actinolite ± carbonate alteration assemblage seen regionally. Inversion modelling of gravity and magnetic data indicate that magnetite alteration could extend beneath the Olympic Dam deposit to depths of at least 10 km (Hayward and Skirrow, 2010; see also Williams *et al.*, 2005). Isotopic ages for minerals in this assemblage are presently limited to an apatite U-Pb TIMS age of 1604 ± 7 Ma for the Acropolis prospect (Mortimer *et al.*, 1988) and two titanite U-Pb ion probe ages from the Murdie Murdie prospect yielding a pooled age of 1576 ± 5 Ma (Skirrow *et al.*, 2007).

- Hematite-sericite-chlorite-carbonate alteration, a form of water and carbon dioxide metasomatism involving oxidation of Fe^{2+} to Fe^{3+}, is the critical alteration assemblage associated with higher grade copper-gold-uranium mineralisation in the Olympic iron oxide-copper-gold Province. Chalcopyrite, pyrite, bornite, chalcocite, gold, and uranium-bearing minerals are characteristically deposited with hematite, sericite, chlorite and carbonate, although only rarely are all of these minerals present in any given sample. Other phases present locally are barite, fluorite, native copper and rare-earth-elements phosphate minerals (Reeve *et al.*, 1990; Gow *et al.*, 1994; Bastrakov *et al.*, 2007; Belperio *et al.*, 2007; Davidson *et al.*, 2007). This assemblage is most extensively developed in the Olympic Dam district and at the Prominent Hill deposit immediately south of the Mount Woods Inlier, although it occurs sporadically in the Moonta-Wallaroo district (e.g., Hillside prospect) and Mount Woods Inlier. Hematite of assemblage (4) replaces magnetite or is developed separately from magnetite (e.g., Prominent Hill, Belperio *et al.*, 2007). Sericite replaces igneous, metamorphic or earlier hydrothermal, potassium-bearing phases such as potassium-feldspar, whereas chlorite replaces iron-magnesium silicates such as actinolite and biotite. However, in many cases no precursor minerals are evident and in these cases hematite, sericite, chlorite and carbonate grew in veins and breccia matrix. Hematite-sericite-chlorite-carbonate alteration is similar to the hydrolytic alteration described in iron oxide-copper-gold districts elsewhere (Hitzman *et al.*, 1992; Williams *et al.*, 2005) although the use of the more descriptive mineralogical terminology is preferred here. The absolute (radiometric) age of hematite-sericite-chlorite-carbonate alteration has been established in only a few localities in the Olympic iron oxide-copper-gold Province. Sericite alteration associated with weak copper-gold mineralisation in the Torrens prospect yielded an argon-argon (^{40}Ar-^{39}Ar) age of 1575 ± 11 Ma (Skirrow *et al.*, 2007). In the Moonta-Wallaroo district, molybdenite in chalcopyrite-bearing veins with chloritic alteration aureoles, possibly related to the hematite-sericite-chlorite-carbonate event, gave Re-Os ages of 1574 ± 6 and 1577 ± 6 Ma.

3.3.1.7 Summary of timing of iron oxide-copper-gold-uranium mineralisation and alteration

The timing of iron oxide-copper-gold ± uranium mineralisation at the Olympic Dam deposit has been the subject of debate since its discovery in 1975. Two principal scenarios have been proposed:

- approximately coeval timing of brecciation, iron oxide development and copper-uranium-gold mineralisation during or immediately following deposition of the Gawler Range Volcanics between 1595 and 1585 Ma (Reeve *et al.*, 1990; Haynes *et al.*, 1995; Johnson and Cross, 1995; Jagodzinski, 2005; Skirrow *et al.*, 2007); and
- later introduction of copper-uranium-gold mineralisation post-dating brecciation, Fe oxide development and the Gawler Range Volcanics by up to 160 m.y. (Oreskes and Einaudi, 1992) or more (Meffre *et al.*, 2010; McPhie *et al.*, 2010).

It is considered that the available geochronological and geological data are most consistent with iron oxide-copper-gold ± uranium mineralisation and alteration at Olympic Dam and elsewhere in the Olympic iron oxide-copper-gold Province developing between ~1595 and ~1585 Ma during the Hiltaba-Gawler Range Volcanics magmatic event when dyke emplacement, intense hydrothermal brecciation and iron oxides also developed. The iron oxide-copper-gold deposits have been disrupted by post-mineralisation reverse fault movements along east-west to east-north-east trending faults, which have been attribute to the distal effects of the 1570 to 1540 Ma Kararan orogeny. Disturbance of some isotopic systems is apparent during younger thermal events, along with minor hydrothermal remobilisation of metals, and may account for some of the young ages reported for Olympic Dam and other deposits in the region.

3.3.2 Curnamona Province iron oxide-copper-gold±uranium deposit characteristics

Iron oxide-bearing copper-gold deposits in the Curnamona Province are unified by several characteristics, namely the association of copper-gold±molybdenum mineralisation with abundant iron oxides, potassic alteration (represented by potassium-feldspar and biotite), syn-tectonic timing (~1600 Ma), moderate temperatures of hydrothermal activity (about 300º to 450ºC), and involvement of both hypersaline and carbonic fluids. Styles of mineralisation vary from ironstone-hosted high grade copper-rich deposits (e.g., Wilkins, Green and Gold prospects), through to generally lower grade stratabound copper-gold±molybdenum systems in which magnetite is confined largely to footwall zones (e.g., Kalkaroo, North Portia, Waukaloo deposits). The White Dam gold deposit (9.6 Mt at 1.05 g/t gold, Exco, 2010, www.excoresources.com.au) in the southern Curnamona Province (Olary Domain) contains minor copper-molybdenum mineralisation within iron oxide poor quartzo-feldspathic gneiss and has a similar age to the iron oxide-copper-gold deposits in the district (based on Re-Os molybdenite ages, Skirrow *et al.*, 2000). Its relationship to the iron oxide-copper-gold deposits remains unclear. The northernmost of the known iron oxide-copper-gold deposits, North Portia, appears to be the most hematite and uranium-rich of the iron oxide-copper-gold deposits in the Olary Domain and Benagerie Ridge region (Teale and Fanning, 2000).

Stratabound replacement and vein networks styles in the northern Olary Domain and Benagerie Ridge region (e.g., North Portia, Kalkaroo, Waukaloo deposits) are hosted predominantly by amphibolite or upper greenschist facies albitic and calc-albitic metesedimentary rocks of the lower Willyama Supergroup. In places, copper-gold±molybdenum mineralisation and associated potassic±sodic alteration extend upwards across the regional interface into carbonaceous pelites of the upper Willyama Supergroup. This interface in part corresponds to a redox boundary, which is evident in regional aeromagnetic data, although in detail the redox boundary transgresses the stratigraphy (Conor, 2006). In contrast, the White Dam deposit and some ironstone-hosted copper-gold occurrences, such as Wilkins and Green and Gold prospects, occur in upper amphibolite facies gneisses at a lower stratigraphic position within the lower Willyama Supergroup (Conor, 2006). Syn-tectonic potassium-feldspar–albite–biotite–quartz veins, or segregations host gold-chalcopyrite-pyrite-molybdenite mineralisation at White Dam, representing possibly a high-temperature and deeper (magmatic-hydrothermal) expression of the copper-gold-molybdenum regional mineralising system (Skirrow *et al.*, 2000; Williams and Skirrow, 2000).

Syndiagenetic to late-diagenetic regional albitisation ± magnetite alteration (see below) was overprinted by a characteristic suite of hydrothermal assemblages associated directly with iron oxide-copper-gold mineralisation. Some chalcopyrite–pyrite ± molybdenite (e.g., deeper part of Kalkaroo) occurs within veins and replacements comprised of magnetite–actinolite ± potassium-feldspar ± quartz ± albite ± titanite ± allanite. Most chalcopyrite (rare bornite), gold and molybdenite

were deposited in association with biotite–quartz–pyrite ± potassium-feldspar potassic alteration, or biotite–albite, that overprinted the magnetite-actinolite assemblages (e.g., upper parts of Kalkaroo; North Portia). White mica typically is absent from these assemblages, but carbonate is locally abundant. Magnetite-biotite and copper-gold deposition were coeval and spatially coincident in some deposits with strong structural controls (e.g., the shear-related Copper Blow, Walparuta, Green and Gold, and Wilkins deposits), whereas magnetite is restricted to footwall alteration zones in stratabound systems of the Benagerie Ridge region (e.g., Kalkaroo, North Portia). Late-stage chloritisation, carbonate replacements and sericitisation are locally significant, along with fluorite, hematite and rutile development.

3.3.2.2 Regional alteration

A defining characteristic of the Curnamona Province is the exceptionally widespread sodium-rich lithologies, particularly in the lower parts of the Willyama Supergroup (Stevens and Stroud, 1983; Cook and Ashley, 1992; Ashley *et al.*, 1998; Ashley, 2000). Regional alteration occurs in two principal styles, pre-tectonic to early-tectonic stratabound sodium ± iron metasomatism, and syntectonic stratabound to discordant sodium ± calcium ± iron metasomatism. Both are distinguished from generally localised potassium ± iron alteration (Ashley and Plimer, 1998); this biotite ± potassium-feldspar ± magnetite ± hematite alteration is associated in places with copper-gold mineralisation, as noted above. Textural evidence in low grade metasedimentary rocks of the Benagerie Ridge bracket the timing of the regional sodium ± iron-oxide alteration to a period after diagenetic formation of carbonate ± evaporite(?) nodules and before or during metamorphic recrystallisation to albite ± magnetite during D1 and D2 (Cook and Ashley, 1992; Skirrow and Ashley, 1998; Teale and Fanning, 2000).

Syntectonic sodium ± calcium-iron alteration was localised by shearing and folding mainly during the D3 regional deformation event and is mostly restricted to upper parts of the Curnamona Group in the Olary and Mulyungarie Domains. Styles include calc-silicate-matrix breccias and calc-silicate vein networks, brecciated ironstones and intensely albitised zones affecting diverse lithologies, with assemblages including sodium-plagioclase, clinopyroxene, clinoamphibole, quartz, magnetite, hematite, garnet and titanite (Ashley *et al.*, 1997, 1998; Lottermoser and Ashley, 1996; Skirrow and Ashley, 1998). Hypersaline high temperature (450 to 550ºC) fluids were involved (Yang and Ashley, 1994; Kent *et al.*, 2000; Skirrow *et al.*, 2000; Clark *et al.*, 2005; Schmidt Mumm *et al.*, 2006). Oxygen, hydrogen and samarium-neodymium isotopic data for the albitised and calc-silicate altered rocks indicate the fluids were of similar origin and were either metamorphic or were magmatic-hydrothermal fluids which had reacted with metamorphic rocks at elevated temperatures (Skirrow *et al.*, 2000; Clark *et al.*, 2005).

3.3.2.3 Ages of mineralisation and alteration

Relative timing of copper-gold±molybdenumintroduction varies from pre-metamorphic or syn-peak metamorphic at the White Dam gold-copper-molybdenum prospect, through syn-metamorphic and post-peak metamorphic at the Kalkaroo, Waukaloo, Mundi Mundi, Lawsons, Wilkins, Dome Rock, Green and Gold, Copper Blow and Walparuta prospects. Rhenium-osmium (Re- Os) isotopic dating of molybdenite from mineralisation in the Kalkaroo, White Dam, Waukaloo, and North Portia areas yielded nine Re-Os ages clustering in two groups, ~1632 to ~1624 Ma and ~1616 to ~1612 Ma, with errors of 1 to 8 Ma (K. Suzuki, unpublished data; Skirrow *et al.*, 2000; Williams and Skirrow, 2000). Re-Os dating of one of the samples from the younger age group yielded a slightly lower age of ~1603 Ma (R. Creaser, unpublished data). Molybdenite is paragenetically associated with chalcopyrite in most of the dated assemblages, although molybdenite also occurs separately from

copper-gold in some prospects. The Re-Os dating results are remarkably consistent with uranium-lead (U-Pb) SHRIMP dating of hydrothermal monazite in the North Portia area. Teale and Fanning (2000) reported ages of ~1630 Ma for monazite associated with early invasive albitisation and molybdenite, and ~1605 Ma for monazite in copper-gold assemblages.

Both the Re-Os and U-Pb results imply molybdenum and initial copper-gold introduction in the dated systems prior to, or coeval with the metamorphic peak at 1600 ± 8 Ma, as determined from zircon U-Pb dating in medium and high grade areas (Page and Laing, 1992; Page *et al.*, 2000).

Titanite from albitised and calc-silicate regional alteration assemblages yielded U-Pb SHRIMP ages in the range of ~1588 to ~1583 Ma (Skirrow *et al.*, 2000), which are similar to a samarium-neodymium (Sm-Nd) age for massive garnet-epidote replacement zones (1575 ± 26 Ma, Sm-Nd, Kent *et al.*, 2000). The titanite ages are considered to be minima for regional syntectonic Na±Ca-Fe metasomatism. Monazite from albitised rock, dated by the electron microprobe chemical method, also yielded an age within uncertainty of previous results (1582 ± 22 Ma, Clark *et al.*, 2005). These results suggest that at least some of the regional syn-D3 sodic and calc-silicate alteration developed late within the Olarian Orogeny and may not be directly related to the earlier iron oxide-copper-gold mineralisation ~1600 to ~1610 Ma. However, propagation of uncertainties when comparing different geochronological methods (e.g., up to ±1.0% for the Re-Os ages because of decay constant uncertainties), allowing it to be concluded that copper-gold±molybdenum mineralisation and regional sodium-iron and calcium-iron metasomatism developed broadly contemporaneously with the Olarian Orogeny.

3.3.2.4 Ore fluid characteristics and origins

Temperatures obtained from oxygen isotope geothermometry at the Kalkaroo and Waukaloo prospects indicate formation of early magnetite–quartz–actinolite–chalcopyrite ± potassium-feldspar assemblages about 420º to 450ºC (Skirrow *et al.*, 2000; Skirrow *et al.*, 2000). Halite dissolution temperatures (total homogenisation) in fluid inclusions from the same copper-bearing assemblages at Kalkaroo are ~350º to 380ºC. As in many other iron oxide-copper-gold provinces globally, there is a common association of iron oxide-copper-gold deposits in the Curnamona Province with hypersaline sodium-calcium-potassium-chlorite and carbonic fluid inclusions (Williams *et al.*, 2005). Brine inclusions contain multiple daughter minerals, including halite, sylvite, nahcolite, mica, carbonate, gypsum, anhydrite, hematite, and possibly sulfide (Bierlein *et al.*, 1996; R. Skirrow, unpublished data). Both carbon dioxide-rich and methane-rich carbonic fluid types were recognised by Bierlein *et al.* (1996), as well as a range of low to moderate salinity inclusion fluids.

Fluids involved in copper-gold-molybdenum mineralisation have calculated $\delta^{18}O$ compositions of 4.2-8.5‰ (n=12, calculated ~300º to 450°C), which are significantly lower than $\delta^{18}O$ values of syntectonic regional alteration fluids (8-11‰, n=25, calculated about 450º-500°C; Skirrow *et al.*, 2000, Williams and Skirrow, 2000; Clark *et al.*, 2005). There is no distinction between calculated δD for fluids in regional alteration and copper-gold-molybdenum mineralisation (-44 to -67‰; n=14). The oxygen and hydrogen isotopic compositions of fluids involved in and copper-gold-molybdenum mineralisation are consistent with a significant input of magmatic water (i.e., fluids equilibrated at high temperature with felsic magmas or igneous rocks). It should be noted, however, that no causative intrusions have been identified so far proximal to iron oxide-copper-gold deposits in the Curnamona Province with the same age as the mineralisation. Input of fluids equilibrated with metamorphic rocks was subordinate in the ore fluids, whereas metamorphic waters may have been dominant in fluids responsible for syntectonic regional alteration.

Oxidation-reduction conditions during sulfide-oxide deposition varied greatly between individual copper-gold deposits of the Curnamona Province, as also observed in other iron oxide-copper-gold districts globally (Williams *et al.*, 2005). Copper-gold related assemblages range from reduced pyrrhotite-magnetite ± arsenopyrite (e.g., Copper Blow, Dome Rock, Lawson, upper pelitic intervals at Kalkaroo and Waukaloo), to hematitic and sulfate-bearing oxidised assemblages (e.g., Portia). Notwithstanding this variation, the intermediate-redox assemblage of magnetite-pyrite-biotite is dominant in many deposits (e.g., Kalkaroo, Waukaloo, Walparuta, Green and Gold, Mundi Mundi). The wide range of sulfide depositional conditions may reflect compositional variations in the host sequences. Ore fluids may have been of near-neutral to weakly acid pH (potassium-feldspar stable) and of intermediate oxygen fugacity in the main, with local variations imposed by reaction with, for example, carbonaceous host units or oxidised hematitic ± meta-evaporitic strata, or mixing with oxidised fluids. Given this range of conditions, it is perhaps no surprise that sulfur isotope compositions of sulfides vary widely, from $\delta^{34}S$ values of –19‰ to +10‰ (Bierlein *et al.*, 1996).

3.3.2.5 Mount Painter Inlier uranium-bearing iron oxide-copper-gold systems

The following section is based on descriptions of the Mount Gee uranium-rare-earth-elements deposits and geological setting summarised in Skirrow *et al.* (2011).

Crystalline basement in the Mount Gee–Mount Painter area of the Mount Painter Inlier comprises the Radium Creek Metamorphics and associated metagranitic rocks, which were emplaced and metamorphosed in the early Mesoproterozoic before being intruded by unmetamorphosed and undeformed Ordovician granites (Elburg *et al.*, 2003; McLaren *et al.*, 2006). The area is characterised by the presence of extensive breccias and hydrothermal rocks, which are the host to iron oxide-rich uranium-rare-earth-elements mineralisation at the Mount Gee and nearby Armchair deposits (Lambert *et al.*, 1982; Drexel and Major, 1987, 1990). The breccia zones measure up to about 3 km in length within a 12 km long northeast-trending zone and occur within the Mesoproterozoic rocks. The breccias have been grouped into two major lithological types:

- the Radium Ridge Breccias (also known as Radium Creek Breccia), including granitic breccia, hematite-rich breccia, and chlorite-rich breccia; and
- quartz±hematite-rich rocks of the Mount Gee Sinter (also known as the Mount Gee Unit) and quartz veins.

Most of the uranium-rare-earth-elements mineralisation is hosted by hematite-rich breccias (Lambert *et al.*, 1982; Drexel and Major, 1987, 1990).

An indicated and inferred resource of 51 Mt at 615 ppm U_3O_8, yielding 31 300 tonnes of U_3O_8, with a 300 ppm cutoff, was reported by Marathon Resources (2009, Annual Report). Additionally, a resource of 44 Mt at 0.12% lanthanum + cerium was reported by Marathon Resources (2005, Annual Report). The main uranium mineralisation at the Mount Gee deposit occurs as shallow-dipping zones within hematitic breccia which is generally enclosed within granitic breccia. Some of the higher grade intersections occur on the flanks of a body of Mount Gee Sinter, although this unit contains lower grades internally. In contrast, the Armchair deposit appears to have not been strongly affected by the late-stage Mount Gee Sinter. In other respects the breccias and mineralisation appear to be similar at the Mount Gee and Armchair deposits.

Drexel and Major (1990) reported geochemical results for 81 samples of hematitic breccia, chloritic breccia, Mount Gee Sinter and local granitic and metasedimentary basement. Uranium values are up to 1900 ppm, averaging 660 ppm in hematitic breccias, but are only 60 ppm in the Mount Gee Sinter. Drill-hole intersections reported by Marathon Resources include 54 m at 1578 ppm at the

Mount Gee deposit, and 16m at 1169 ppm at the Armchair deposit. The rare-earth-elements are highly enriched in the hematitic breccias, with up to 1.37% cerium and average values of 6100 ppm reported by Drexel and Major (1990). Although lower in rare-earth-elements than the hematitic breccias, the Mount Gee Sinter is also very anomalous in rare-earth-elements with an average cerium content of 2500 ppm. Mineralogical studies indicate the rare-earth-elements are hosted mainly by monazite (Drexel and Major, 1990). Copper values average 1100 ppm in the hematitic breccias but only 250 ppm in the Mount Gee Sinter. Gold is weakly anomalous with values up to 0.2 ppm, and molybdenum contents are up to 500 ppm (Drexel and Major, 1990). Uranium and molybdenum assay values are strongly correlated (Marathon Resources, unpublished data; see also Skirrow *et al.*, 2011).

Three main hydrothermal stages have been recognised (Skirrow *et al.*, 2011), pre-brecciation, syn-brecciation and post-brecciation. Prior to brecciation the host igneous and metamorphic rocks were partly replaced by biotite-apatite-fluorite assemblages, magnetite-pyrite (±chalcopyrite-bornite?) and some early hematite. It is possible that at least some of the widespread potassium-feldspar in the host rocks is also a pre-brecciation alteration phase. The main brecciation stage was characterised by almost complete replacement of early magnetite by hematite (martite) together with new (specular) hematite, chlorite, monazite, fluorite, pyrite, molybdenite and uraninite. Late-stage post-brecciation alteration involved formation of secondary copper minerals, quartz, chalcedony, hematite, and clay minerals. This last stage may correlate with the formation of the Mount Gee Sinter unit.

Three molybdenite Re-Os isotope ages were obtained from the Armchair deposit: 360.8 ± 1.7 Ma, 361.6 ± 1.5 Ma and 364.6 ± 1.5 Ma (Skirrow *et al.*, 2011). These are interpreted to represent the age of molybdenite crystallisation, hematite breccia formation and uranium mineralisation at the Armchair deposit and, by inference, at the Mount Gee deposit.

The Re-Os ages are significantly younger than the U-Pb ages of Ordovician granitic intrusions in the region (~460 to ~440 Ma, Elburg *et al.*, 2003; McLaren *et al.*, 2006), titanite-diopside veins (~440 Ma, Elburg *et al.*, 2003), and some of the imprecise monazite ages from uranium mineralised breccias (e.g., 440 ± 50 Ma, Pidgeon, 1979; ~460 Ma, Elburg *et al.*, 2003). The 367 ± 13 Ma brannerite U-Pb age obtained by Wülser (2009), however, is within uncertainty of the molybdenite Re-Os ages, and points to a Devonian uranium mineralising event, not only at Mount Gee, but also affecting other parts of the Mount Painter Inlier.

No information is available on the nature or origins of the fluids involved in formation of the hematite-rich uranium-rare-earth-elements mineralisation. Although copper and gold are present at only low levels in the known systems near Mount Gee, based on the limited published data, there appear to be many similarities with aspects of iron oxide-copper-gold deposits globally (e.g., Williams *et al.*, 2005). These include:

- the element association of uranium and light rare-earth-elements with copper, gold, molybdenum, fluorine and phosphorous;
- the close spatial and temporal association of mineralisation with abundant hydrothermal iron oxides;
- epigenetic breccias hosting mineralisation;
- alteration mineral assemblages and paragenetic sequence from early magnetite-pyrite±copper sulfides to later hematite, chlorite, uraninite;
- the low abundance of hydrothermal quartz during the iron oxide stages (Mount Gee Sinter post-dates the hematite breccias); and
- lack of proximal igneous intrusions, although major iron oxide-copper-gold provinces are characterised by regional syn-iron oxide-copper-gold felsic and mafic magmatism.

Based on studies to date, it is concluded that the iron oxide uranium-rare-earth-elements (±copper-gold) mineralisation in the Mount Gee district may represent a copper-gold-poor, uranium-rich end-member in the spectrum of iron oxide-copper-gold deposits. The distribution of uranium and rare-earth-elements in the Olympic Dam and Prominent Hill deposits have not been described in detail in the literature, but in both deposits there are light rare-earth-element-rich and hematite-rich zones (with or without elevated gold) which appear to be separate from the high grade copper-gold zones (Reeve *et al.*, 1990; Reynolds, 2000; Belperio *et al.*, 2007). Therefore the possibility of copper-gold-rich zones in the Mount Gee district should not be dismissed if the system is zoned. Alternatively, major copper and gold may be absent because of a lack of suitable source rocks such as coeval mafic igneous rocks (Johnson and McCulloch, 1995).

3.3.3 Mineral system model for Mesoproterozoic uranium-rich iron oxide-copper-gold systems of the Gawler and Curnamona Provinces

Figure 3.3.5 shows a generalised model for uranium-rich iron oxide-copper-gold mineral systems. The geodynamic setting for the Olympic iron oxide-copper-gold Province has been widely debated (see Hayward and Skirrow, 2010, and references therein). The preferred setting here is a distal continental retroarc environment in which earlier subduction-related processes (possibly ~1850 Ma, Kositcin, 2010) led to metasomatism of the upper mantle. Melts derived from this enriched mantle, driven by a mantle plume or perhaps by removal of lithospheric mantle (via convective processes or delamination; Skirrow, 2010), resulted in extensive crustal melting and production of high-temperature A-type and I-type magmas associated with potassium-rich mafic melts between ~1595 and ~1575 Ma. The felsic melts are represented by the Hiltaba Suite and Gawler Range Volcanics, which are temporally and spatially linked to iron oxide-copper-gold deposits in the Olympic iron oxide-copper-gold Province. The Benagerie Volcanics and A-type granites on the northern Benagerie Ridge are likely the igneous equivalents in the Curnamona Province (Schofield, 2010a).

A key event in the geodynamic evolution of the Gawler and Curnamona provinces appears to have been a switch from compression ~1600 Ma to extension ~1590 to ~1585 Ma, followed by a return to compression, at least in the northern Gawler Province (Skirrow, 2010; Hayward and Skirrow, 2010). Extension may lead to down-thrown blocks above mafic-underplated regions, where volcanic rocks are deposited and preserved. These downthrown blocks are favourable also for preservation of hematite-uranium-rich iron oxide-copper-gold deposits that formed in the near-surface (Figure 3.3.5). In contrast, the surrounding upthrown regions are less likely to preserve uppermost crustal levels and the deeper, magnetite-rich iron oxide-copper-gold deposit styles are predicted to characterise such regions.

Key characteristics and controls on the formation of uranium-rich iron oxide-copper-gold are as follows (after Hitzman and Valenta, 2005; Skirrow, 2010, 2011).

- Higher grade uranium is associated spatially with hematite-rich, oxidised hydrothermal alteration assemblages, but it occurs at trace or low levels in the more reduced magnetite-rich style of iron oxide-copper-gold systems. Only a subset of hematite-rich deposits contain significant uranium.
- Uranium-rich mineralisation occurs generally in breccia-hosted iron oxide-copper-gold deposits where there is evidence for involvement of relatively low temperature fluids.
- Zoning of uranium versus copper and gold mineralisation is present in most uranium-rich iron oxide-copper-gold deposits, with some of the higher grade uranium spatially separate from copper and gold. In some cases uranium-rich iron oxide deposits occur with only low grade copper-gold (e.g., Mount Gee).
- There is generally a strong spatial association with light rare-earth-elements and fluorine.

- Felsic igneous rocks are the main host rocks of the uranium-rich iron oxide-copper-gold deposits, with the richer uranium mineralisation occurring in hosts of unusually high magmatic uranium contents (e.g., Olympic Dam). Other hematite-rich deposits in the same districts hosted by metasedimentary or low-uranium igneous rocks contain lower grade uranium mineralisation.
- The larger uranium-rich iron oxide-copper-gold deposits occur in districts where there was coeval high-temperature A-type or I-type felsic and mafic magmatism.
- Volcanic rocks coeval with intrusive magmatism are preserved in districts with uranium-rich iron oxide-copper-gold deposits.

3.3.3.1 Mesoproterozoic iron oxide-copper-gold±uranium system components and mappable criteria

Based on this general model, the theoretical requirements for each of the four components of the iron oxide-copper-gold-uranium mineral system are shown in Table 3.3.2. Although the focus has been on the Mesoproterozoic systems, it is recognised that there may be potential for Paleozoic uranium-rich iron oxide systems with or without copper-gold in the northern Curnamona Province (i.e., Mount Gee type). For the assessment of iron oxide-copper-gold-uranium prospectivity, mappable criteria which represent each of the theoretical requirements have been identified. The mappable criteria and their derivations for each mineral system component are described below.

3.3.3.2 Sources of metals, fluids, ligands, sulfur

Multiple fluids are required to form uranium-rich iron oxide-copper-gold deposits, including highly oxidised uranium-rich fluids (e.g., meteoric/ground waters), deep-sourced, high-temperature brines (magmatic-hydrothermal fluids and/or fluids reacted with metamorphic rocks) and possibly separate sulfur-bearing fluids (see review by Williams *et al.*, 2005, and references therein). Figure 3.3.6 shows sources for both deep-sourced and shallow hydrothermal fluids, the latter leaching uranium from uranium-rich granitoid or volcanic rocks. Alternatively, a direct magmatic-hydrothermal source of uranium is also possible in these iron oxide-copper-gold systems. The sources of copper, gold, sulfur, chlorine and carbon dioxide may be either coeval magmas (felsic and/or mafic) or sedimentary and igneous rocks that were leached by the ore fluids, as marked by the presence of sodic-calcic regional alteration zones (Oreskes and Einaudi, 1992; Johnson and McCulloch, 1995; Haynes *et al.*, 1995; Williams *et al.*, 2005; Oliver *et al.*, 2004; Skirrow *et al.*, 2007).

Pre-iron oxide-copper-gold basins hosting major iron oxide-copper-gold provinces tend to lack major reduced (e.g., deep marine) sections (Haynes, 2000) and commonly show evidence for the (former) presence of evaporite minerals. Rift basin sequences may supply some of the iron, chlorine, and sulfur to iron oxide-copper-gold deposits, particularly those of overall oxidised character with subaerial to shallow marine depositional settings. Potential geodynamic settings include continental back-arc basins and foreland basins. Low metamorphic grade of these basins prior to iron oxide-copper-gold formation is favourable because of potentially higher permeability and fluid content than basins metamorphosed to medium or high grade. In models involving non-magmatic fluids, exposure near, or at the paleosurface of uranium-rich source rocks is favourable for sourcing highly oxidised, surface-derived waters capable of leaching and transporting uranium. Topographic depressions (e.g., calderas, grabens, maar complexes, etc) are conducive to mixing of shallow-crustal and deep-sourced fluids.

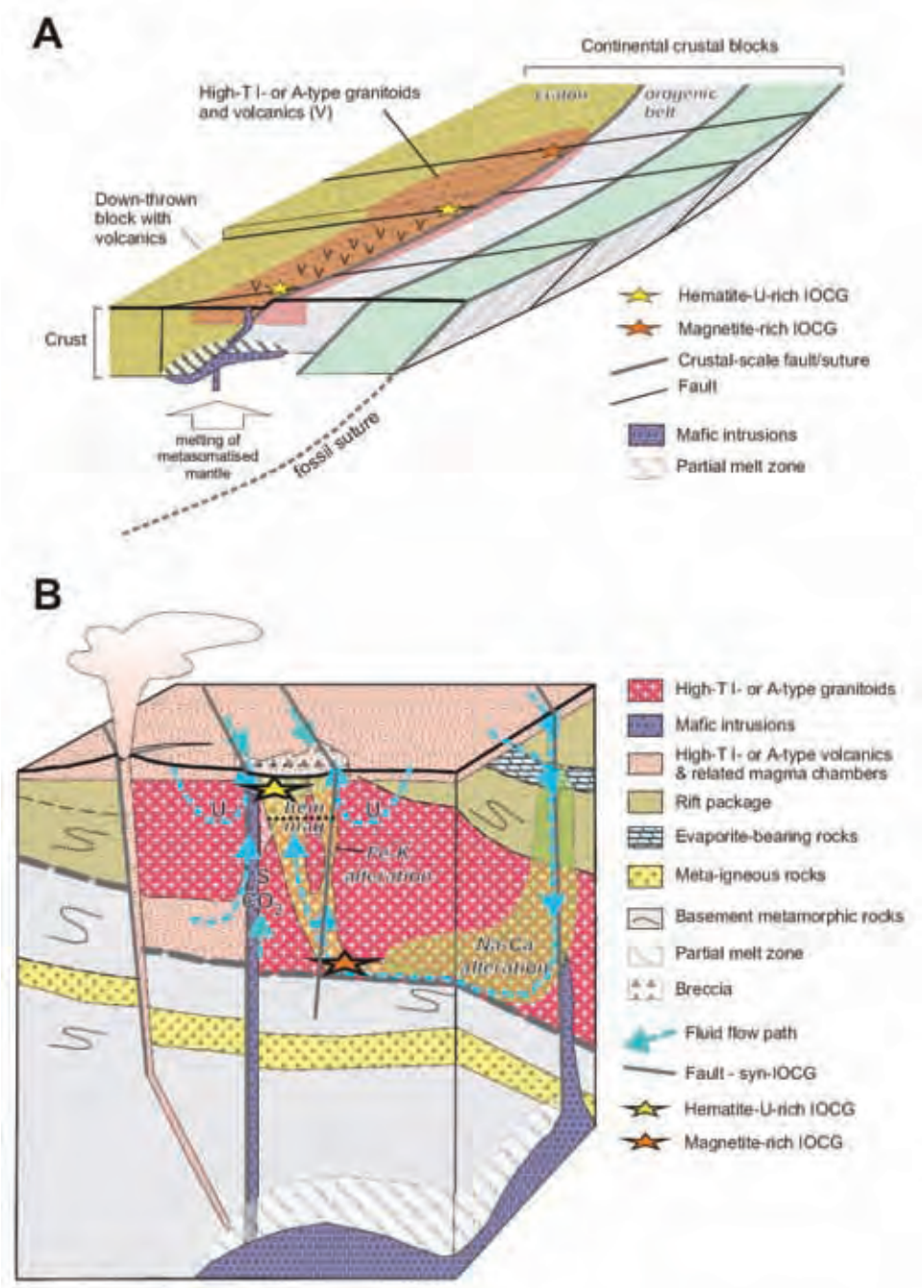

Figure 3.3.5: *Mineral system model for uranium-bearing iron oxide copper-gold deposits. A: Schematic oblique view of crustal-scale section across idealised iron-oxide copper-gold-uranium province. B: Schematic oblique section of iron-oxide copper-gold-uranium deposit in (A), viewed from the right, showing district-scale features.*

Table 3.3.2. Mappable criteria and weights used for mineral potential analysis for uranium-rich iron oxide-copper-gold deposits.

MINERAL SYSTEM COMPONENT	CRITERIA		DATASETS	IMPOR-TANCE	APPLIC-ABILITY	CONFI-DENCE	WEIGHT	COMMENTS
	THEORETICAL	MAPPABLE						
Sources of U, Cu, Fe, fluids, ligands, sulfur	Sources of brines, Fe, Cl, S	Fe-rich back-arc or other basins	Solid Geology of South Australia (Cowley, 2006)	0.75	0.50	0.75	0.28125	Wallaroo Group + Myola Volcanics which includes Moonabie Formation
	Sources of U: presence of U-enriched igneous rocks	Igneous rocks with high U contents	Solid Geology of South Australia (Cowley, 2006); geochemical data (Schofield, 2009; OZCHEM)	0.75	0.50	0.25 - 1.00	0.09375-0.375	High U defined as greater than the 75th percentile for each rock class (intrusive and volcanic)
	Sources of U: high-T breakdown of U-bearing minerals in magma source region	Igneous rocks with high zircon saturation temperatures	Solid Geology of South Australia (Cowley, 2006); geochemical data (Schofield, 2009; OZCHEM)	0.75	0.50	0.25 – 0.75	0.09375-0.28125	Temperatures are based on zircon saturation temperature (see Schofield, 2010b). High temperatures are defined as greater than the 75th percentile for intrusive rocks
	Sources of Cu	Mafic or ultramafic intrusions and volcanics	Solid Geology of South Australia (Cowley, 2006)	0.75	0.75	0.75	0.421875	
	Sources of F	Igneous rocks with high F	Solid Geology of South Australia (Cowley, 2006); geochemical data (Schofield, 2009; OZCHEM)	0.50	0.50	0.25 – 0.75	0.0625-0.1875	High F defined as greater than the 75th percentile for each rock class (intrusive and volcanic). Rocks with accessory fluorite are also deemed to be high in F (see Schofield, 2010b)
Drivers/energy sources	High paleo-geothermal gradient	Units with good evidence for high-level intrusion	Surface Geology of Australia (Raymond & Retter, 2010)	0.75	0.75	0.75	0.421875	High-level magmas are likely associated with higher geothermal gradients, for effective fluid circulation
		Units with moderate evidence for high-level intrusion		0.75	0.50	0.75	0.28125	
		Units with poor evidence for high-level intrusion		0.75	0.25	0.75	0.140625	
	Volatile/fluid release	Breccias of unknown origin in intrusive rocks; excludes fault breccias	Solid Geology of South Australia (Cowley, 2006); input from literature, Stratindex etc	0.50	0.75	0.75	0.28125	
	Large-volume high-T crustal melts	A- and high-temp I-type felsic intrusive rocks, with 20 km buffer	Solid Geology of South Australia (Cowley, 2006)	0.75	0.75	0.75	0.421875	
		A- and high-temp I-type felsic volcanic rocks, with 20 km buffer		0.75	0.75	0.75	0.421875	Volcanics also represent high paleo-geothermal gradients
	Mantle (metasomatised) melts	Mafic or ultramafic intrusions and volcanics, with 20 km buffer		1.00	0.75	0.75	0.5625	
Pathways and architecture	Fluid flow along permeable structures	Late Paleo to early Mesoprot faults with 2.5 km buffer	Solid Geology of South Australia (Cowley, 2006)	0.75	0.50	0.50	0.1875	For Gawler Craton, Archean to Mesoprot attributed faults ("AM" faults in Cowley, 2006)
	Crustal-scale weak zones guiding mantle to crust magmatism and fluid fluid	Crustal domain boundaries, incl. margin of Archean, with 30 km and 100 km buffers (see comments)	New interpretation using Sm-Nd data, solid geology of Cowley (2006), seismic & MT data (Korsch & Kositcin, 2010a, b)	1.00	0.50	0.50	0.25	30 km buffer in footwall
				1.00	0.75	0.50	0.375	100 km buffer in hangingwall
Ore depositional gradients	Direct evidence of elevated U	U^2/Th values 1σ above the mean for each unique geological unit - igneous only?	Radiometric Map of Australia (Minty *et al*., 2010)	0.25	0.50	0.75	0.09375	
		U^2/Th values 2σ above the mean for each unique geological unit		0.25	0.75	0.75	0.140625	
	Chemical gradient sites	Inversion model volumes of magnetite alteration	Geoscience Australia's new inversion model of magnetite alteration	0.75	0.75	0.75	0.421875	High percentage of magnetite
				0.75	0.50	0.75	0.28125	Low percentage of magnetite
		Inversion model volumes of hematite alteration	Geoscience Australia's new inversion model of hematite alteration	1.00	0.75	0.75	0.5625	High percentage of hematite
				1.00	0.50	0.75	0.375	Low percentage of hematite
		Ironstones, iron formations; dominant and present	Solid Geology of South Australia (Cowley, 2006)	0.50	0.75	0.75	0.28125	
		IOCG alteration - observed hematite-ser-chl-carb with 10 km buffer	IOCG potential map (Skirrow *et al*., 2006)	1.00	0.75	1.00	0.75	Observation point are drillholes
		Sericite alteration as mapped by ASTER AlOH group content - 1σ above mean	New Gawler-Curnamona ASTER dataset	0.50	0.25	0.50	0.0625	

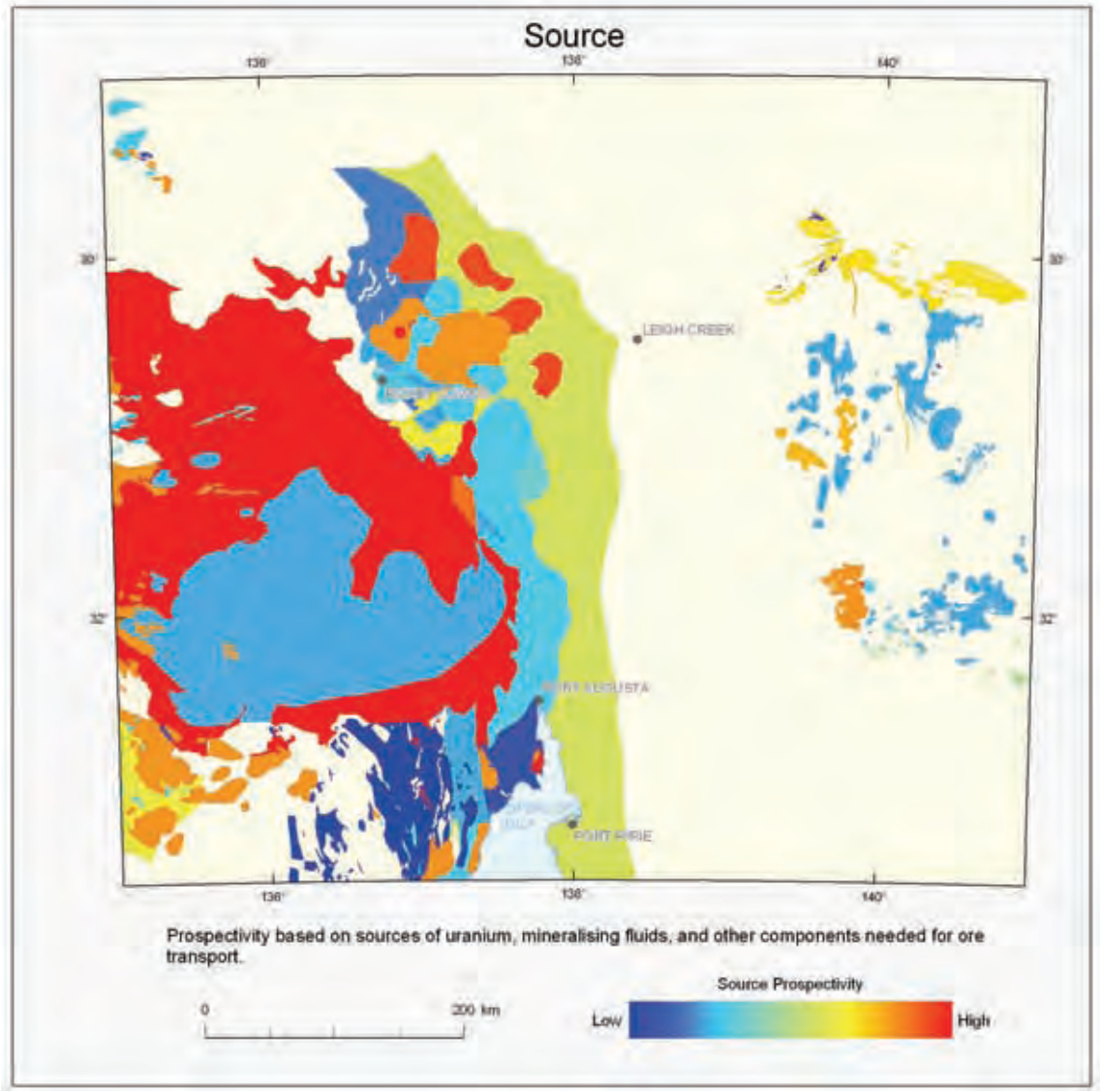

***Figure 3.3.6**. Map of the study area showing results of the prospectivity assessment for the source component.*

Based on these processes and theoretical criteria relating to sources of ore components, the following mappable criteria (underlined) were considered in the iron oxide-copper-gold-uranium prospectivity assessment (Table 3.3.2):

- Uranium-rich igneous rocks represent potential source rocks for uranium-rich iron oxide-copper-gold deposits. High temperature A-type and I-type crustal melts are especially favourable because they are commonly enriched in the high field strength elements including uranium as a result of the breakdown of refractory minerals such as zircon. Igneous whole rock geochemistry and radiometric data may effectively map uranium-rich compositions. These are represented in the study area principally by the Hiltaba Suite granitoids, felsic members of the Gawler Range Volcanics and Benagerie Ridge Volcanics, as well as other early Mesoproterozoic high temperature A-type and I-type felsic igneous rocks. The role of the Donington Suite as a uranium source, emplaced ~1850 Ma along the eastern margin of the Archean core of the craton, is unclear, but it may have been important

as a uranium-enriched source from which uranium and other high field strength elements of the Hiltaba Suite were partly derived (Creaser, 1995).

- Basins of likely continental back-arc or foreland settings, existing prior to the early Mesoproterozoic, with evidence of evaporite minerals, or their former presence. These include the Wallaroo Group and equivalents (e.g., Moonabie Formation) in the eastern Gawler Province, in which chlorine-bearing scapolite has been identified (Conor, 1995; Skirrow *et al.*, 2007). McPhie *et al.* (2010, 2011) suggested that a pre-ore basin existed above the Olympic Dam deposit, from which some of the fluids involved in ore formation may have been derived. The Hutchison Group is relatively reduced overall, having been deposited on a passive margin and as a result is less conducive for the hydrothermal transport of copper and uranium, although, as a source of iron, this basin cannot be dismissed.
- Mafic or ultramafic igneous rocks represent potential sources of copper, gold, sulfur and carbon dioxide, either via leaching of pre-iron oxide-copper-gold to syn-iron oxide-copper-gold igneous rocks or directly via magmatic-hydrothermal fluids (Johnson and McCulloch, 1995; Campbell *et al.*, 1998; Skirrow *et al.*, 2007). Because the present prospectivity analysis is focussed on uranium-rich iron oxide-copper-gold systems, this source criterion (i.e. copper, gold, sulfur, carbon dioxide) has been given a lower weighting than the source criteria for uranium. As noted in Section 3.3.3.3, the proxies for copper-gold- sulfur-carbon dioxide sources in the Gawler Province are: syn-Hiltaba mafic/ultramafic intrusions, and pre-iron oxide-copper-gold to syn-iron oxide-copper-gold mafic rocks which may have been available to be leached by the ore fluids. Importantly these include mafic components of the Gawler Range Volcanics and Benagerie Ridge Volcanics.
- High-fluorine igneous rocks are considered a useful indicator of potential sources of fluorine, which is locally abundant (e.g., as fluorite) in the major uranium-rich iron oxide-copper-gold deposits such as Olympic Dam, Prominent Hill, and Carrapateena. Whether fluorine acted as a ligand for the ore metals in the hydrothermal fluids, or played a role in acid leaching of sources rocks (Chambefort *et al.*, 2009), remains to be resolved.

The role of felsic magmas of the Hiltaba Suite and Gawler Range Volcanics as a direct source of metals, fluids and ligands (via exsolution of magmatic-hydrothermal fluids) remains unclear and is one of the key unresolved questions regarding the genesis of the iron oxide-copper-gold deposits in the Olympic iron oxide-copper-gold Province. Studies of stable and radiogenic isotopes and fluid inclusions point to three possible contributing sources of fluids; magmatic-hydrothermal, metasedimenary rock-reacted and surface derived (see discussion and references in Bastrakov *et al.*, 2007 and Skirrow *et al.*, 2007). High temperature magnetite-forming brines are interpreted to have undergone extensive geochemical and isotopic exchange with the Wallaroo Group or other metasedimentary rocks, although the data are permissive of an ultimately magmatic-hydrothermal origin. On the other hand, lower temperature hematite-forming fluids appear to have had two distinct sources; one similar to that of the magnetite-forming fluids and one surface-derived (e.g., meteoric or lake waters). From the available evidence (e.g., Oreskes and Einaudi, 1992; Haynes *et al.*, 1995; Gow *et al.*, 1994, Morales Ruano *et al.*, 2002; Bastrakov *et al.*, 2007) it has been suggested that one of the key differences between the major deposits such as Olympic Dam and the barren and weakly mineralised iron oxide-copper-gold prospects is the greater involvement of surface-derived fluids in the major deposits (Skirrow *et al.*, 2007). Sulfur as sulfate in this highly oxidised fluid may have been critical in the formation of the major iron oxide-copper-gold deposits and particularly for the higher grade chalcocite-bearing mineralisation (Haynes *et al.*, 1995; Bastrakov *et al.*, 2007).

Regional sodic-calcic alteration zones may represent source regions for iron, copper, gold and other ore components (Oliver *et al.*, 2004), as well as parts of the fluid pathways. Such alteration is well

known in the Moonta-Wallaroo district, Mount Woods Inlier, and southern Curnamona Province. This criterion has not been specifically included in the source component in the current assessment of iron oxide-copper-gold-uranium potential because it is not clear that uranium was sourced from sodic-calcic alteration zones. Nevertheless, some of the rock volumes identified in the inversion modelling of gravity and magnetic data may include areas of dense non-magnetic alteration as represented by hematite alteration (see Depositional gradients, below) or weakly magnetic socic-calcic alteration (represented by magnetite alteration). This alteration is characterised by the presence of albite, clinopyroxene (e.g., diopside) and/or amphibole (e.g., actinolite) and may contain minor magnetite, scapolite and titanite. It should be noted that the inversion modelling at the scale applied does not discriminate between sodic-calcic alteration and hematite±sulfides.

3.3.3.3 Drivers/energy sources

High to extreme paleogeothermal gradients are considered to be a key driver of regional-scale upper crustal fluid flow in iron oxide-copper-gold systems. Regional- to crustal-scale (hydro)thermal systems are necessary to explain the huge scale of the alteration systems and the masses of hydrothermal precipitates (e.g., 10^7 to 10^{10} tonnes of ore rich in hydrothermal Fe oxides, sulfides and silicates) in individual deposits. All known districts with major iron oxide-copper-gold deposits in the Olympic iron oxide-copper-gold Province contain mafic intrusions that are roughly coeval with iron oxide-copper-gold formation. These igneous rocks may mark the locus of crustal-scale thermal anomalies, as well as providing a source of copper and/or sulfur to iron oxide-copper-gold systems (Johnson and McCulloch, 1995; Skirrow *et al.*, 2002, 2007). Additionally, high-temperature A-type or I-type crustal melts, emplaced at high levels in the crust or at surface, are considered to have augmented the thermal flux provided by mantle magmatism, and so their presence is considered as an indicator of a favourable driver or energy source in the iron oxide-copper-gold systems. These igneous associations and tectonic context are shown schematically in Figure 3.3.5A.

For the Gawler Province, these components of the mineral system are represented by early Mesoproterozoic mafic and ultramafic intrusions, as well as the high temperature Hiltaba Suite and Gawler Range Volcanics units (temperatures based on zircon saturation conditions which in turn are derived from whole rock geochemical compositions; see also Section 3.5). Some of the key syn-Hiltaba mafic intrusive units in the eastern Gawler Province are the Curramulka gabbronorite in the Yorke Peninsula, dioritic and ultramafic intrusions in the Olympic Dam district and the White Hill complex in the Mount Woods Inlier. In the central Gawler Province near the Tarcoola gold deposit, the Lady Jane Diorite has hornblende with an argon-argon (^{40}Ar-^{39}Ar) age of 1582 ± 5 Ma, which is interpreted as an emplacement age (Budd and Fraser, 2004). Several other mafic intrusive complexes of poorly constrained age include the Bills Lookout Gabbro in the Olympic Dam district (~1760 Ma U-Pb zircon age, Johnson, 1993) and various mafic intrusions thought to be associated with the St Peter Suite in the central and western Gawler Province.

In the Curnamona Province, early Mesoproterozoic mafic intrusive rocks appear to be less abundant than in the eastern Gawler Province, with known units identified only in the Billeroo alkaline igneous complex and Crocker Well area (western Olary Domain). Syenite, ijolite and lamprophyre dykes in the Billeroo complex are interpreted to be early Mesoproterozoic in age (Rutherford *et al.*, 2007). Their relationship to diorites, alkaline granitoids (emplaced at 1579 ± 1.5 Ma, Ludwig and Cooper, 1984) and uranium mineralisation in the nearby Crocker Well area is not clear. Additionally, several concealed bodies of inferred mafic composition, possibly related to the ~1580 to ~1595 Ma Bimbowrie Suite, have been interpreted in the central-western and northern Curnamona Province (Cowley, 2006). The Bimbowrie Suite itself is mostly plutonic, with S-type compositions

yielding low magmatic temperatures based on zircon saturation constraints, and so is less favourable as a driver of near-surface hydrothermal activity.

High temperature A-type and I-type igneous rocks of early Mesoproterozoic age in the Curnamona Province are known mainly from the Mount Painter Inlier, Benagerie Ridge, and possibly in the Crocker Well area. The depth of emplacement of most of these intrusive rocks is presently unconstrained. However, the important recent discovery of an A-type granitic porphyry on the northern Benagerie Ridge (Schofield, 2010a) with an emplacement age of 1590 ± 5 Ma (Fraser and Neumann, 2010) strongly suggests an affinity with Hiltaba Suite in the northern Curnamona Province. The shallow depth of emplacement of the porphyry, together with the presence of the ~1585 Ma A-type felsic and mafic Benagerie Volcanics (Fricke, 2008; Schofield, 2010a), provide good evidence of an environment with high paleogeothermal gradients in parts of the northern Curnamona Province during the early Mesoproterozoic.

Critically, for uranium-bearing iron oxide-copper-gold systems, a very shallow crustal setting has been preserved in the Benagerie Ridge region, as evidenced from the presence of early Mesoproterozoic volcanic and subvolcanic rocks, and possibly low metamorphic grade of the Willyama Supergroup. In contrast, the southern Curnamona Province appears to expose deeper, mid-crustal levels represented by medium to high grade metamorphic rocks, plutonic granitoids and mostly ductile deformation fabrics during the Olarian Orogeny (e.g., Clark *et al.*, 1987; Korsch and Kositcin, 2010a).

3.3.3.4 Fluid pathways/permeability architecture of the system

Terrane boundary zones initiated during earlier orogenic belt formation are believed to form part of the crustal-scale magma and fluid pathways for major iron oxide-copper-gold systems including those rich in uranium. This inference is based largely on interpretation of geophysical data, including seismic and magnetotelluric studies near the Olympic Dam deposit (Lyons and Goleby, 2005; Heinson *et al.*, 2006; Direen and Lyons, 2007). Groves *et al.* (2010) extended this concept to other major iron oxide-copper-gold deposits globally. Major iron oxide-copper-gold systems may preferentially occur in the hangingwall of boundary zones between crustal blocks, above zones of partial crustal melting and mafic underplating (Figure 3.3.5A). Fluid flow is enhanced by juxtaposition of earlier rift basins with this high-temperature melt province. Pre-existing basinal structures and second-order cross structures (e.g., conjugate fault sets) localise dilational deformation, brecciation (at high crustal levels) and fluid flow. The intersections of second-order faults with crustal-scale terrane boundaries are favoured locations for iron oxide-copper-gold systems, as illustrated in Figures 3.3.5A and 3.3.5B.

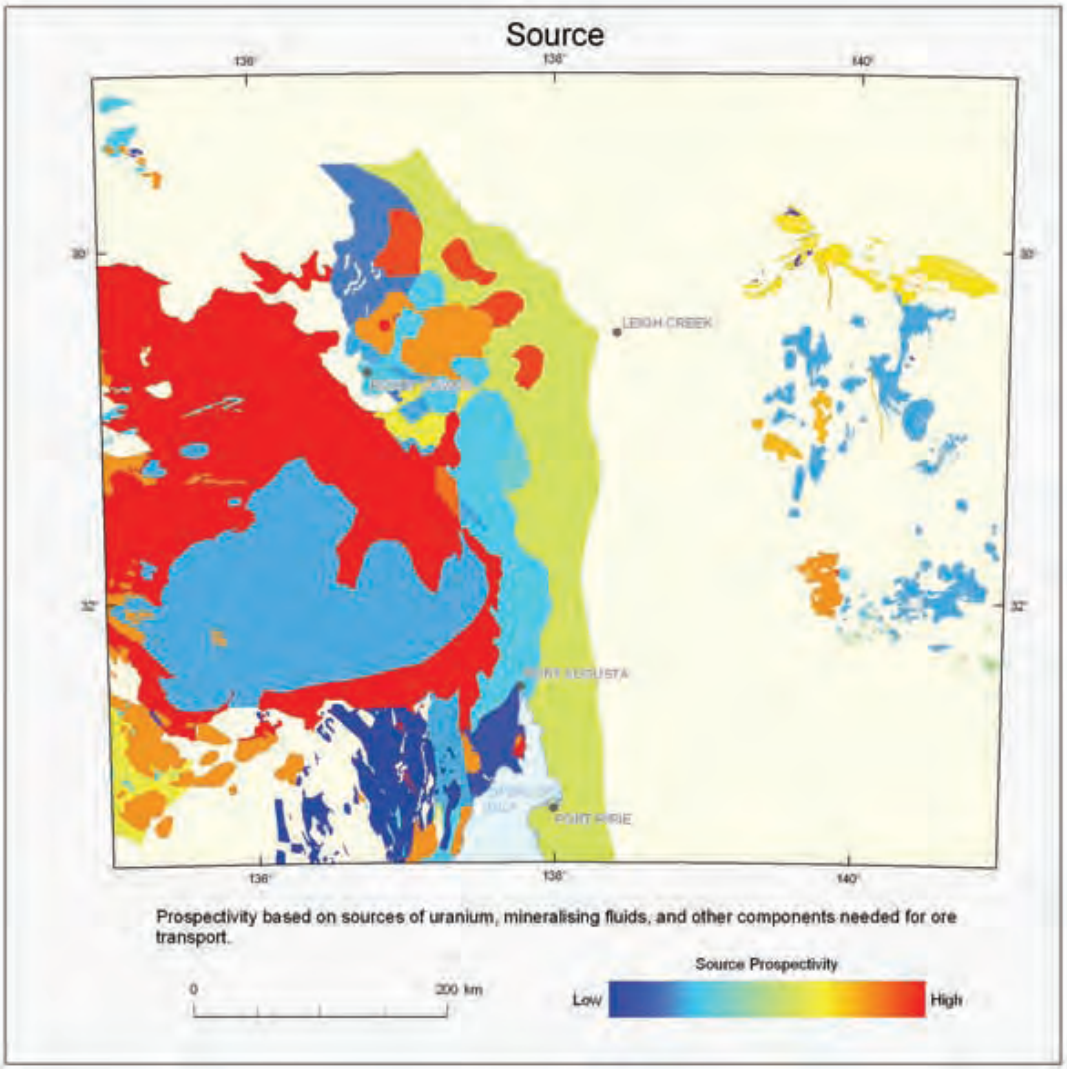

Figure 3.3.7. *Map of the study area showing results of the prospectivity assessment for the Driver component.*

Based on these processes and favourable characteristics of the fluid pathways/architecture, the following mappable criteria (underlined) were considered in the iron oxide-copper-gold-uranium prospectivity assessment:

- Major crustal domain boundary zones, such as craton margins, with greatest potential in the hangingwall (hence the higher weighting of the 100 km buffer on the hangingwall side than for the 30 km buffer on the footwall side; Figure 3.3.8). In the Gawler Province, the crustal domain boundary zone identified beneath the Olympic Dam deposit (Lyons and Goleby, 2005) is believed to correspond to the northwest-trending Elizabeth Creek Fault Zone. New seismic and magnetotelluric data obtained since the Olympic Dam survey (Korsch and Kositcin, 2010b), along with interpretation of compiled samarium-neodymium (Sm-Nd) isotope data (Kositcin, 2010), have allowed the structure beneath Olympic Dam to be interpolated to the south and to the northwest. In the south it probably links with the Kalinjala Shear Zone, which dips at depth to the east and separates Mesoarchean and Neoarchean domains to the west from Paleoproterozoic domains to the east. South of the Carrapateena deposit, seismic data clearly image two extensional half-graben, partly filled by interpreted mafic Gawler Range Volcanics, in the position of the Elizabeth Creek Fault Zone (Korsch and Kositcin, 2010a). To the northwest of Olympic Dam, a seismic traverse

northwards from Tarcoola images a north-dipping zone separating Archean to the south from the Paleoproterozoic Coober Pedy Ridge to the north (Korsch and Kositcin, 2010b). This boundary is interpreted to represent the northwestern continuation of the Elizabeth Creek Fault Zone where it meets the Karari Fault Zone, enveloping the Archean core of the Gawler Province on its eastern and northern flanks. The crustal domain boundary is interpreted as a long-lived fundamental structure which controlled basin formation (e.g., Wallaroo Group), magmatism (e.g., Donington Suite and parts of the Hiltaba Suite and Gawler Range Volcanics) and hydrothermal activity in the Olympic iron oxide-copper-gold Province.

- A second possible crustal domain boundary has been identified from seismic data to the east of the Gawler Province, separating the Mount Painter and Babbages inliers from other parts of the Curnamona Province. This is tentatively correlated with the east-dipping Aliena Fault Zone to the south, which separates mid-crustal to lower-crustal seismic provinces beneath the Adelaide rift (Korsch and Kositcin, 2010a). The northern Benagerie Ridge may be situated in the hangingwall of this crustal domain boundary.

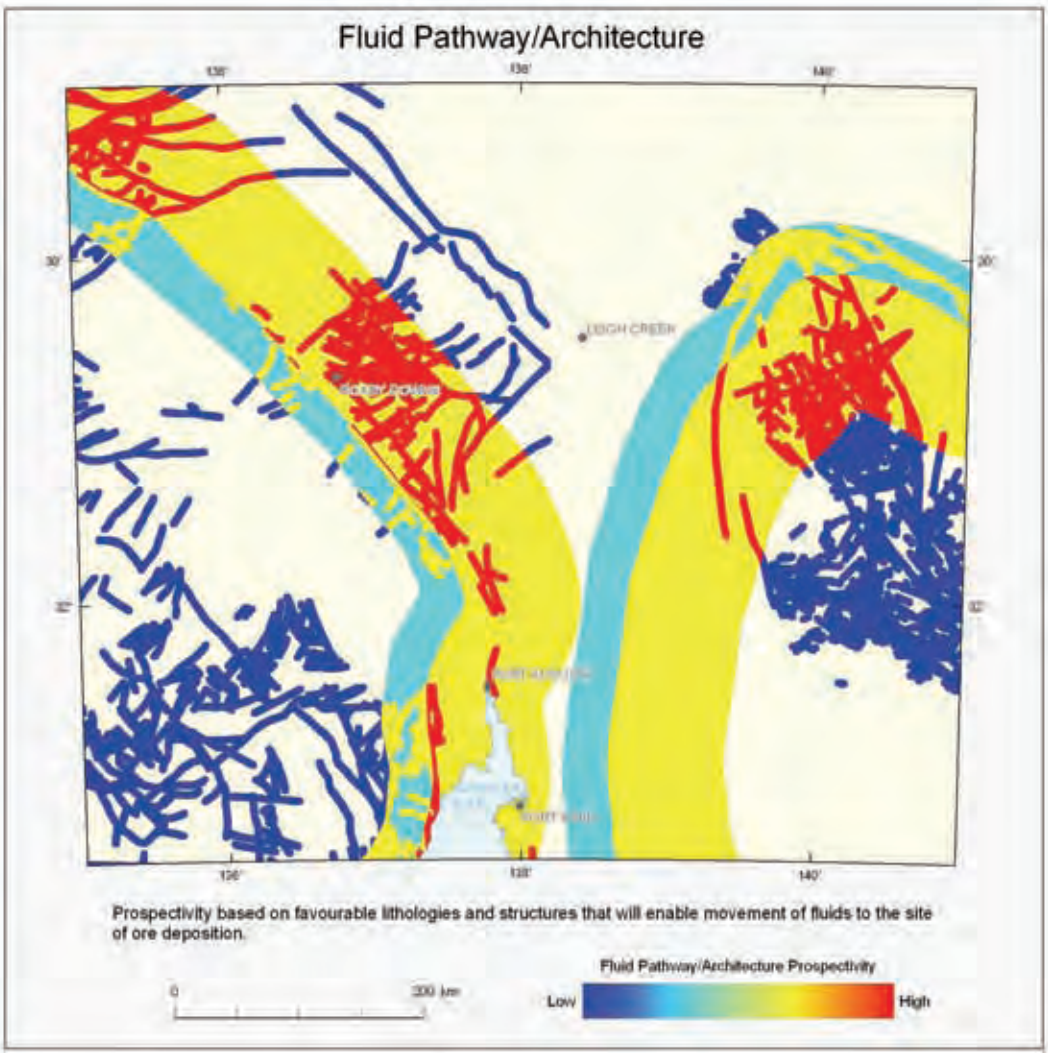

Figure 3.3.8: *Map of the study area showing results of the prospectivity assessment for the fluid pathways / architecture component.*

Networks of syn-orogenic major fault/shear zones, reactivated during high-temperature magmatic events, may represent fluid flow pathways for iron oxide-copper-gold-related fluids. In the Gawler Province they include the north-northwest faults and conjugate northeast trending faults interpreted in the Olympic Dam district.

Hydrothermal alteration zones mark the passage of fluids and hence map fluid flow pathways. Magnetite-biotite, magnetite – potassium-feldspar and hematite-rich alteration zones represent proximal iron oxide-copper-gold settings, and thus, not only mark fluid flow paths but also represent the sites of physico-chemical gradients proximal to the sites of ore deposition. For this reason it has been decided to include the proxies for magnetite-bearing and hematite-bearing alteration in the ore depositional gradients component of the iron oxide-copper-gold mineral system, rather than in fluid pathways/permeability architecture.

3.3.3.5 Ore depositional gradients

Uranium is highly mobile as U^{6+} in oxidised fluids over a wide range of temperatures, and forms complexes with chloride, hydroxy, carbonate, phosphate and fluoride ions (see reviews by Skirrow *et al.*, 2009; Bastrakov *et al.*, 2010; Rozsypal, 2009). Under reduced conditions concentrations of uranium (as U^{4+}) sufficient to form major ore deposits appear to be restricted to high temperature highly acidic conditions where the fluids are fluorine-rich and/or chlorine-rich.

It is unclear in iron oxide-copper-gold systems whether the high temperature brines of intermediate redox state or the lower temperature oxidised fluids carry the bulk of the uranium. In the Olympic Dam district, the high temperature brines carried at least 300 ppm copper in places, but uranium was not analysed (Bastrakov *et al.*, 2007). If it is assumed that the uranium was transported mainly by the oxidised fluids, then removal of uranium from the fluid may be achieved through reduction or, depending on the complexing ligand, by changes in temperature, pressure, pH or ligand activity (Bastrakov *et al.*, 2010). Based on iron oxide-copper-gold-uranium systems of the eastern Gawler Province, a key copper-gold-uranium depositional process was mixing of large volumes of oxidised groundwaters, or shallow basinal waters, with deep-sourced iron-rich brines of intermediate redox state (Haynes *et al.*, 1995). This process will result in reduction of oxidised uranium-rich fluids as well as possible changes in pH, temperature and ligand activity. Additionally, reaction of the oxidised fluids with rocks containing abundant iron-rich minerals such as magnetite, siderite and chlorite, or with reduced sulfur in sulfide minerals, or with reduced carbon, may also lead to uranium as well as copper-gold deposition. Chemical modelling by Bastrakov *et al.* (2007) showed that higher grade copper and gold mineralisation are expected in zones where hematite has replaced earlier magnetite. Other modelling by Bastrakov *et al.* (2010) suggests that uranium will be deposited upstream of the copper, potentially in hematitic zones lacking significant copper mineralisation. The implication of these findings is that hematite-rich alteration zones in iron oxide-copper-gold systems are more favourable for uranium (as well as copper-gold) mineralisation in comparison to magnetite-rich zones, but the juxtaposition of hematite with magnetite is potentially the most favourable (Bastrakov *et al.*, 2007). The hematite may occur above the magnetite (e.g., Olympic Dam) or laterally adjacent to the magnetite (e.g., at the Prominent Hill deposit, Belperio *et al.*, 2007; see also Hayward and Skirrow, 2010). The uranium mineralisation may occur in overlapping and/or separate zones relative to copper-gold mineralisation.

Based on these processes and theoretical criteria, the following mappable criteria (underlined) representing ore depositional gradients were considered in the iron oxide-copper-gold-uranium prospectivity assessment (Table 3.3.2):

- Observed hematite-rich alteration, based on previous mapping, drill core logging and petrological studies (from iron oxide-copper-gold potential map, Skirrow *et al.*, 2006).
- Hematite-rich alteration as represented by inversion models of regional gravity and magnetic data which identify volumes of dense rock with low magnetic susceptibility. The volumes may also include other dense non-magnetic minerals such as sulfides, some silicates and possibly some carbonates and oxides. It is therefore possible that the volumes of hematite alteration also include zones of regional sodic-calcic alteration. The uppermost voxets in the 3D inversion models were selected to best represent the near-surface distribution of hematite-rich alteration. The hematite alteration mappable criterion is weighted more heavily than magnetite alteration in the assessment (Table 3.3.2) because of the known association of higher grade uranium with hematite in iron oxide-copper-gold systems of the Gawler Province, as noted above. However, it should be noted that the inversion modelling used in the mineral potential assessment is not able to discriminate between shallow-crustal low-temperature and deeper mid-crustal high-temperature hematite-rich alteration. Hematite-bearing iron formations also would be included in the inversion volumes.
- Magnetite-rich alteration as represented by inversion models of regional gravity and magnetic data that identify volumes of dense rock with high magnetic susceptibility and may include other dense magnetic minerals such as pyrrhotite. This mappable criterion represents the magnetite-biotite and magnetite – potassium-feldspar types of iron oxide-copper-gold-related alteration, but also may include lithologies such as banded iron formation and some mafic igneous rocks. More detailed, district-scale, constrained inversions are necessary to discriminate between magnetite-bearing iron oxide-copper-gold-related alteration and these other lithologies.
- Ironstones and iron formations, identified from regional geological mapping and in inversion modelling (see above). These lithologies, if present in the host rocks prior to iron oxide-copper-gold development, may act as chemical depositional sites because of the possible presence of Fe^{2+} reductant in magnetite, carbonates or silicates.
- Elevated uranium values as shown by the U^2/Th ratio calculated from airborne radiometric survey data. High values emphasise areas where uranium may have been preferentially enriched relative to thorium, as expected in uranium-rich mineralisation in iron oxide-copper-gold systems. However, the high values may have many other causes unrelated to iron oxide-copper-gold systems and so this criterion is given a relatively low weighting in terms of *Applicability* (Table 3.3.2).

3.3.4 Results

The potential for uranium-bearing iron oxide-copper-gold systems is shown for the study area in South Australia in Plate 3.3 and Figure 3.3.10. The mineral potential map should be regarded as a guide towards prospective provinces requiring further investigation, rather than as a detailed deposit targeting map. Nevertheless, two key outcomes are as follows: (a) the modelling successfully highlights many of the areas of known iron oxide-copper-gold mineralisation (e.g., Olympic Dam, Prominent Hill), which is suggested as a validation of the method used, and (b) the modelling highlights a number of regions with significant potential for undiscovered uranium-bearing iron oxide-copper-gold deposits. These are discussed below.

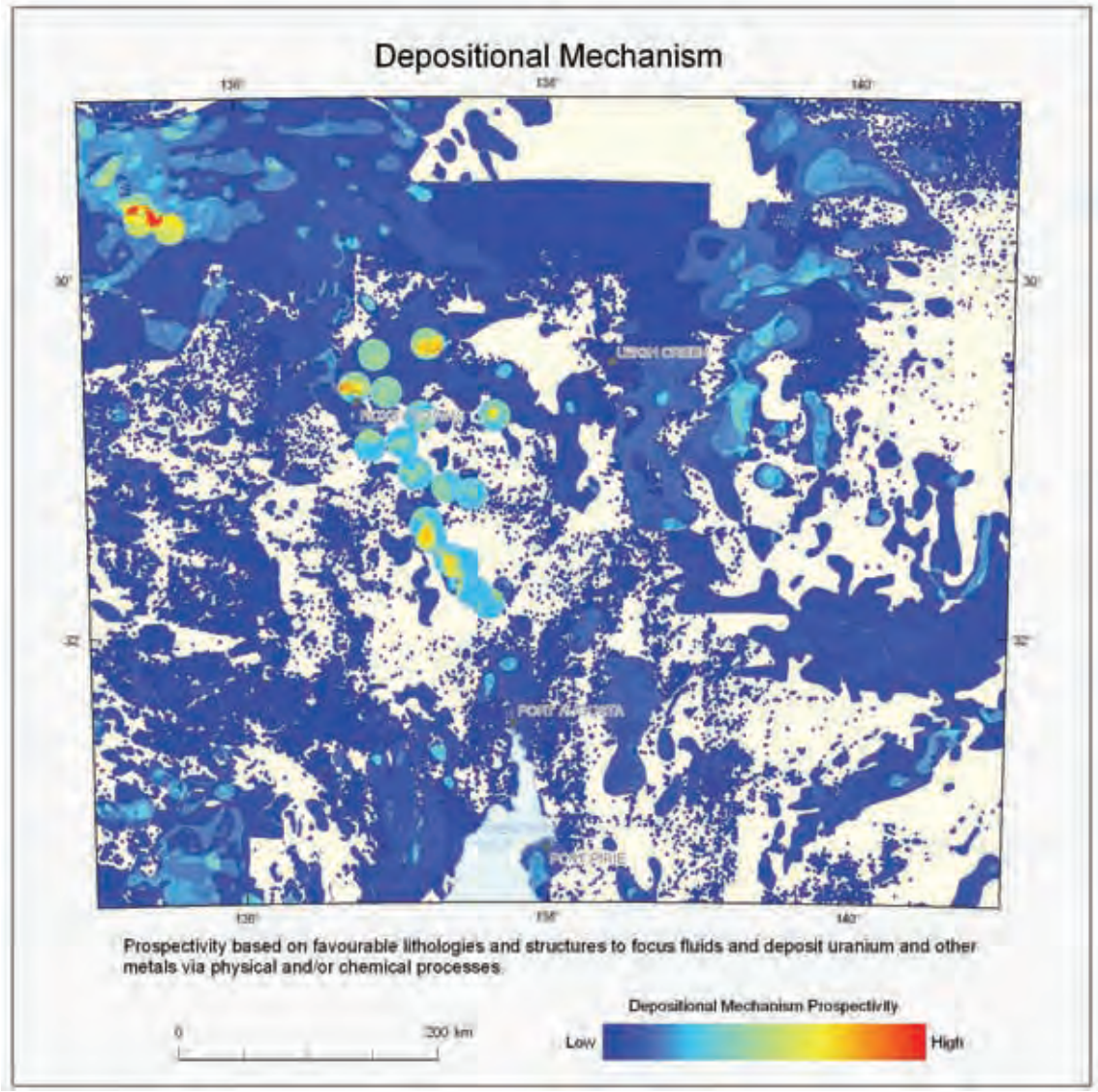

Figure 3.3.9: *Map of the study area showing results of the prospectivity assessment for the ore depositional gradient component. Areas in white are areas with no indication of prospectivity.*

The area of the Carrapateena deposit is not highlighted as an unusually prospective area. This may be because there are no mapped Hiltaba Suite or Gawler Range Volcanics rocks in the area, lowering the prospectivity model scores for driver and source. Additionally, the relatively coarse cell size used in the inversion modelling of the widely spaced gravity and magnetic data in this area resulted in no major anomalies in either the magnetite alteration or hematite alteration datasets, even though it is known from more detailed company data that such anomalies are present at the local scale. The moderate score for depositional gradients is largely because of the presence of hematitic alteration. Consequently, the overall prospectivity ranking in the map for the Carrapateena area is only moderate. This underlines how the prospectivity modelling may be improved in future; with better and closer spaced data inputs. The map is considered therefore to represent the minimum prospectivity for the study area.

Two broad regions of elevated prospectivity have been outlined in the study. The largest and best known is the Olympic iron oxide-copper-gold-uranium Province along the eastern margin of the

Gawler Province. The area outlined in Figure 3.3.10 and Plate 3.3 corresponds closely to the iron oxide-copper-gold province shown in the 2006 iron oxide-copper-gold-uranium potential map of the Gawler Province (Skirrow *et al.*, 2006). The second area, in the northern Curnamona Province, is a newly identified region with potential for uranium-rich iron oxide-copper-gold deposits, and represents a northerly extension of the known iron oxide-copper-gold province, which includes the North Portia and Kalkaroo deposits. While the boundaries of both provinces remain uncertain, the mineral potential modelling has clearly highlighted regions warranting follow-up by the minerals exploration industry.

Within each of these iron oxide-copper-gold-uranium metallogenic provinces there are areas of enhanced potential, labelled A to E, as described below.

Area A contains the Olympic Dam and Carrapateena deposits and many other as-yet uneconomic, but significant deposits and prospects such as Wirrda Well, Acropolis, Emmie Bluff and Oak Dam. This large iron oxide-copper-gold-uranium district potentially extends at least 80 km south from Carrapateena following major crustal structures and is known to host areas of hematitic alteration. Inversion modelling of regional gravity and magnetic data suggests the presence of several large hematite alteration and/or magnetite alteration volumes in this southern extension area. To the east and southeast of Olympic Dam the mineral potential modelling highlights a broad area of high potential, including the Torrens area. The more detailed inversion modelling of this district by Williams *et al.* (2004) and reported by Skirrow *et al.* (2007) shows many areas with anomalous hematite and magnetite alteration, many of which have not been thoroughly drill tested.

Area B is the Mount Woods Inlier–Prominent Hill district. It should be noted that much of the inlier to the north of the Prominent Hill deposit was subjected to high metamorphic grade in the early Mesoproterozoic, whereas at Prominent Hill the metamorphic grade of the host rocks appears to be low (Belperio *et al.*, 2007). Insufficient geochronological data are currently available for the Prominent Hill deposit to understand whether copper-gold and low grade uranium mineralisation was pre-metamorphic, syn-metamorphic or post-metamorphic in timing. If the Mount Woods Inlier to the north of Prominent Hill was exhumed after formation of iron oxide-copper-gold-uranium mineralisation, which appears likely from available data, then the potential of this high grade metamorphic domain for uranium-rich, shallow-crustal, iron oxide-copper-gold deposits would be low because such systems would have been removed by erosion. Nevertheless, the mineral potential modelling shows elevated prospectivity because of the presence of Hiltaba Suite granitic and coeval mafic intrusions (contributing to driver and sources), presence of favourable structures and volumes of iron oxide alteration (mainly magnetite). A more sophisticated treatment of geological setting in the mineral potential modelling, in which preserved shallow crustal settings are discriminated from deeper crustal settings (e.g., using metamorphic grade, presence of volcanics, etc), would probably result in the shallow-crustal Prominent Hill area having a higher potential for uranium-bearing iron oxide-copper-gold systems than the mid-crustal inlier to the north. Copper-gold-magnetite-rich systems such as that at Manxman, Joes Dam and Cairn Hill (immediately west of the study area) are indicative of the potential for such mid-crustal iron oxide-copper-gold systems in the Mount Woods Inlier.

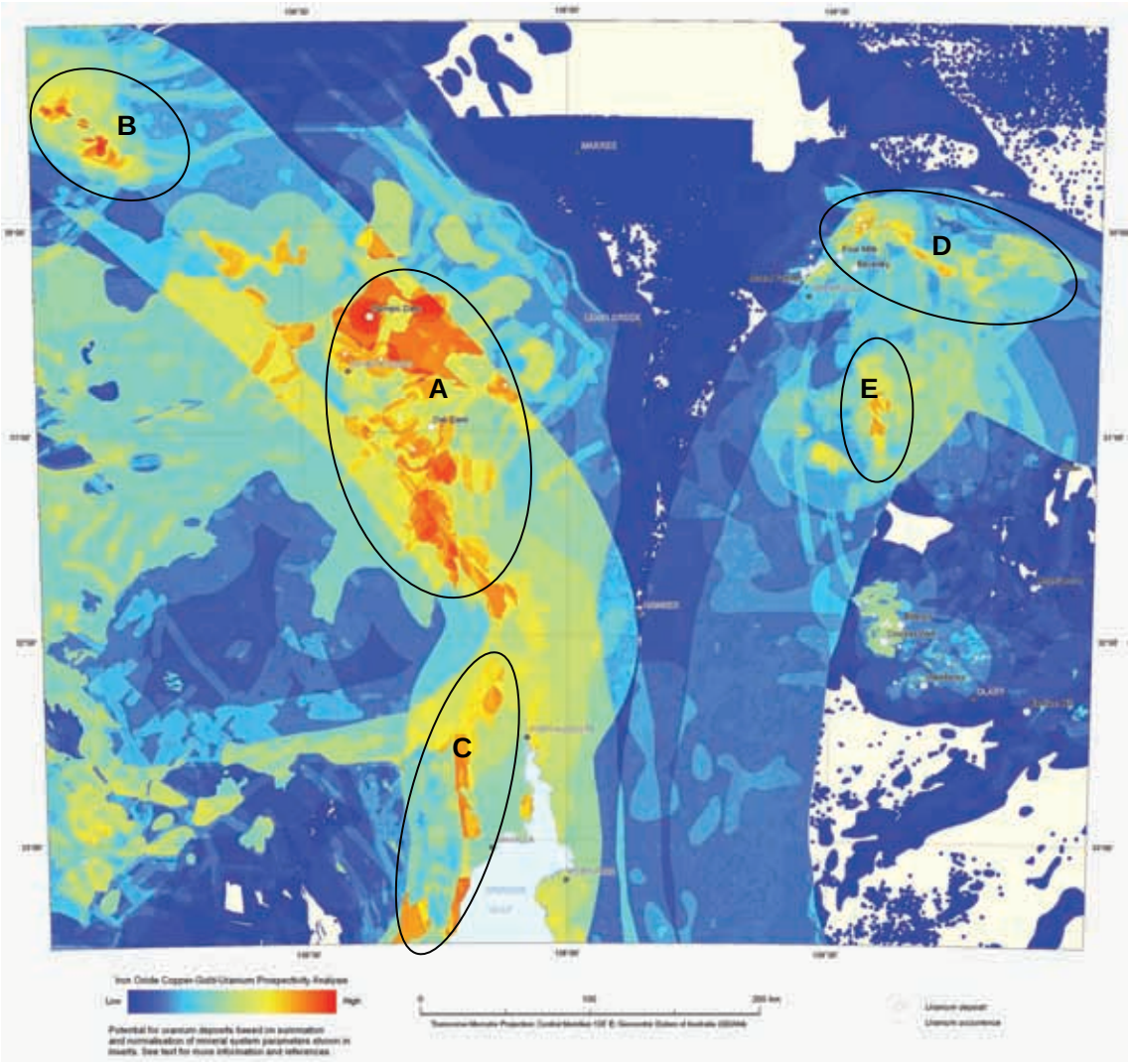

Figure 3.3.10: *Map of the study area showing results of the overall prospectivity assessment for uranium-bearing iron-oxide copper-gold deposits.*

Area C in the south of the study area shows elevated prospectivity because of the combined presences of Hiltaba Suite granites, Gawler Range Volcanics mafic rocks and favourable structures corresponding to possible splays of the Kalinjala Mylonite Zone (e.g., Roopena Fault). The Kalinjala Mylonite Zone has been interpreted to be the southern extension of the Elizabeth Creek Fault Zone, which is itself inferred to be the shallow-crustal expression of the boundary zone between the Archean core of the Gawler Province and Paleoproterozoic terranes to the east. This boundary zone is a fundamental control on the location of the Olympic iron oxide-copper-gold-uranium Province, as discussed earlier.

Weste (1996) reported hematitic alteration in the Roopena district, and, if included in the mineral potential modelling, would have enhanced the prospectivity of Area C. The presence of Gawler Range Volcanics in the district is also a very favourable indicator of preservation of shallow crustal levels. However, based on the relatively coarse inversion modelling of regional gravity and magnetic data in this study, Area C does not display large volumes of intense iron oxide alteration. More

detailed inversion modelling is recommended for this district, which may highlight as-yet unrecognised iron oxide-copper-gold-uranium targets.

Areas D and E in the northern Curnamona Province are largely in areas of extensive and deep cover where the identity of basement rock types is poorly understood. In the mineral potential modelling, the enhanced prospectivity in Areas D and E is a result of the known and inferred presence of high-uranium, high-temperature Mesoproterozoic granitoids and felsic volcanics and inferred mafic intrusions (driver and sources), favourable crustal structure based on recent seismic reflection data, and several large volumes of magnetite and hematite alteration mapped from inversion modelling of regional gravity and magnetic data. The recent discovery of a ~1590 Ma A-type granite in the region (Schofield, 2010a), together with the presence of the apparently undeformed ~1585 Ma Benagerie Ridge Volcanics, indicate a highly favourable crustal setting for the preservation of uranium-rich iron oxide-copper-gold systems, not unlike that of the Olympic Dam district. There are very few mineral exploration drill-holes in most of the northern Curnamona Province, particularly in areas distant from the Mount Painter and Mount Babbage Inliers and to the north of the well known prospects on the Benagerie Ridge, such as North Portia and Kalkaroo. These iron oxide-copper-gold deposits are magnetite-rich and probably represent the deeper parts of iron oxide-copper-gold systems exhumed since their formation ~1600 Ma (Williams and Skirrow, 2000). It is predicted that to the north of these known deposits, iron oxide-copper-gold systems, if they exist, will be hematite-rich with greater development of breccias and higher uranium contents than their southern cousins.

3.4. UNCONFORMITY-RELATED URANIUM

T. P. MERNAGH AND D. CONNOLLY

Unconformity-related uranium systems produce the largest known high-grade uranium deposits and currently constitute about 33% of the western world's uranium resources (World Nuclear Association, 2010). All unconformity-related uranium deposits currently being exploited occur in the Athabasca Basin in Canada or the Kombolgie Basin, a sub-basin of the McArthur Basin in northern Australia. The deposits in the Kombolgie Basin account for 19% of Australia's known in-ground uranium resources (Lambert *et al.*, 2005).

Cuney (2010) has defined four major periods of uranium deposition throughout Earth's history. Unconformity-related uranium deposits occur in the third period which began with the strong increase in oxygen content of the atmosphere ~2200 Ma, making possible the oxidation of U^{4+} to U^{6+}. These deposits formed mainly after 1750 Ma during a long period of relative tectonic quiescence recorded by numerous highly-oxidised (red-bed) intracontinental siliciclastic basins of broad geographic extent (Lambeck *et al.*, 2011). The unconformity-related deposits are hosted either within the basement to these basins or just above the unconformity in the overlying sediments. Most of the prescribed basins are approximately 1 to 3 km thick, flat lying, unmetamorphosed and pervasively altered. The sedimentary units of these basins are mainly fluvial sandstone sequences which overly basement rocks that have been paleoweathered, with variable preservation of a clay-altered, haematitic regolith grading down through a chloritic zone into fresh rocks. However, the basin fill can be absent and completely removed by later erosional processes.

Although the formation of the major unconformity-related uranium deposits may be associated with the initial oxygenation of the Earth's atmosphere, a second oxygenation event occurred ~600 Ma as indicated by the colonisation of the oceans by animal life (Farquhar *et al.*, 2010). This resulted in the development of new sedimentary successions comprising alternating oxidised and reduced layers which became the major setting for sandstone-hosted uranium deposits. However, these basins still retain all the parameters needed for the formation of unconformity-related deposits. Therefore, the prospectivity of the study area has been assessed for the existence of unconformity-related uranium deposits over two time periods, the Precambrian and the Phanerozoic. The former accounts for the main period of unconformity-related mineralisation and the latter explores the potential for this style of mineralisation in younger host rocks.

3.4.1 Deposit overview

3.4.1.1 Unconformity-related uranium mineralisation in the Northern Territory

Because possible occurrences of unconformity-related mineralisation in South Australia are not well documented at present, a brief overview of unconformity-related uranium deposits in the Northern Territory is included. Since 1980, most of this uranium has been mined from two deposits, Nabarlek (now mined out) and Ranger 1 and 3. Unconformity-related uranium deposits are known to occur in the Alligator Rivers Uranium Field, and the South Alligator Valley in the northern part of the McArthur Basin, while a similar style of mineralisation associated with intrusive units occurs in the Westmoreland region in the southern McArthur Basin.

The northern McArthur Basin is represented by the Kombolgie sub-basin which overlies steeply dipping Paleoproterozoic basement metasedimentary rocks. The Kombolgie Subgroup consists of sandstone and conglomerate, as well as interlayered volcanic units of the Nungbalgarri Formation

and Gilruth Member. Economic deposits of uranium have primary mineralisation ages of 1675 to 1650 Ma (Maas, 1989; Polito *et al.*, 2005a; Polito *et al.*, 2005b) and are hosted in the Paleoproterozoic basement rocks, but near the unconformity between the basement and overlying Kombolgie Subgroup. The sediments of the Kombolgie Subgroup were deposited in fluvial and eolian environments, with occasional marine incursions which deposited marine sandstone and evaporite. Shallow marine to evaporative conditions dominated in the McKay Formation, as suggested by the presence of glauconite, halite crystal casts and wave ripple marks in sandstone. Sandstone of the McKay Formation shows minimal diagenesis relative to the rest of the units in the Subgroup.

The generalised paragenetic sequence recorded in the lower Kombolgie Subgroup sandstone layers is characterised by the formation of early stage quartz overgrowths which formed at 80 to 130ºC from low salinity sodium chloride (NaCl) fluids with less than 10 wt.% NaCl having δD values typical of evaporated seawater (Derome *et al.*, 2007; Polito *et al.*, 2006). The next paragenetic stage is associated with filling of the remaining pore space with diagenetic illite and euhedral quartz or less commonly, chlorite, coincident with peak diagenesis. Chlorite follows, and is coeval with illite in the lowermost parts of the Kombolgie Subgroup, indicating a change of fluid properties in some parts of the basin to one which contained magnesium (Polito *et al.*, 2006). The third stage in the fluid evolution is related to fracturing, faulting and quartz vein formation. Veins filling heavily fractured and slightly desilicified sandstone have primary fluid inclusions with δD values near -30‰, homogenisation temperatures between 200 and 400ºC and salinities of 22 wt.% equivalent. The fluids are sodium-magnesium-calcium-chloride brines. The final stage of alteration of the Kombolgie Subgroup is pervasive kaolinite which permeates to several hundreds of metres depth. This late stage kaolinite had isotopic compositions typical of those expected from modern weathering (i.e. past 50 million years) associated with the development of the vast Australian regolith.

3.4.1.2 Unconformity-related uranium mineralisation in South Australia

In the Gawler Province, uranium mineralisation is intimately associated with copper mineralisation but no unconformity-related uranium deposits are currently positively identified in this region. Several weak uranium anomalies occur in sheared gneiss and silicified, brecciated Katunga dolomite at Benbuy, generally along a northwest trending fault (Parker and Fanning, 1998). The Katunga dolomite occurs at the base of the Paleoproterozoic Middleback Subgroup. A conglomerate of unknown age overlies the Katunga Dolomite in the Benbuy area, with silicification and alteration of the Katunga Dolomite at this contact interpreted as possibly resulting from regolith processes. In the immediate vicinity of the Benbuy uranium occurrence, the Blue Range Beds, consisting of a basal conglomerate and overlying sandstone, unconformably overlies Archaean and Late Proterozoic sequences. The significance of the unconformity below the Blue Range Beds is not known. However, Parker and Fanning (1998) suggest it may be analogous to the unconformity below the Kombolgie Formation of the Alligator Rivers region in the Northern Territory. Additional uranium occurrences near Benbuy include the Poonana Mine (Figure 3.4.1), also on a northwest trending fault, and trace torbernite in a granite quarry near Yeldulknie Weir (Parker and Fanning, 1998). At the nearby Emu Plain Mine (Figure 3.4.1) there is minor uranium mineralisation associated with copper mineralisation in Hutchison Group metasediments.

Local high-grade uranium mineralisation associated with copper also occurs at the Calcookara Mine (Figure 3.4.1). The mine workings are within calc-silicate, marble, amphibolite and banded iron formation of the lower Middleback Subgroup where that sequence has been disrupted by a north–

south trending, possibly Tertiary fault, although the latter is not clearly delineated on the ground (Parker and Fanning, 1998).

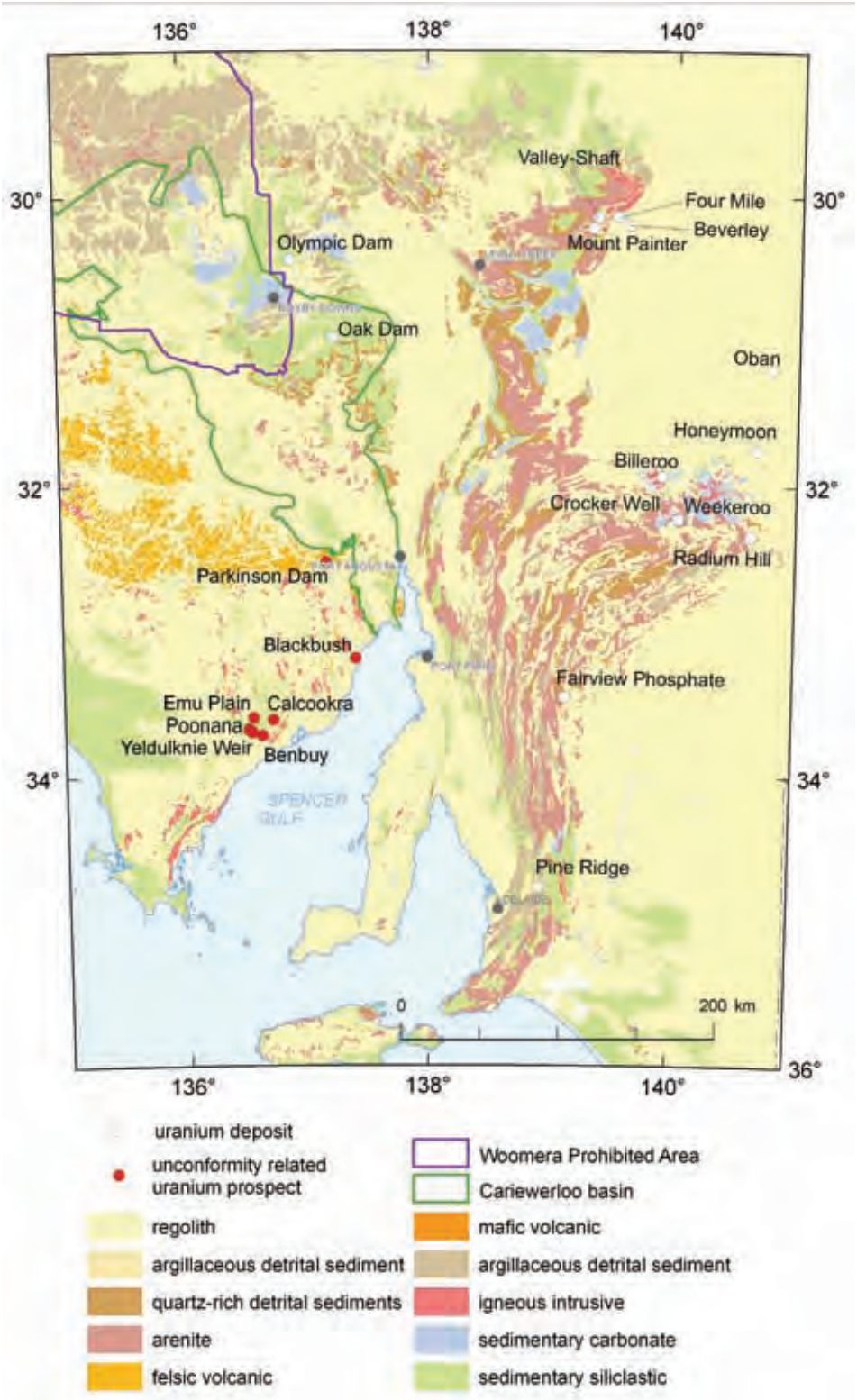

Figure 3.4.1: *Geological map (from Whitaker et al., 2008) showing locations of selected unconformity-related uranium prospects in South Australia.*

There has been exploratory drilling for sandstone-hosted uranium mineralisation in the Cadna-owie Formation and Algebuckina Sandstone flanking the Peake and Denison Inliers which indicated anomalous uranium results at the unnamed uranium occurrence 8874 (28.0590º S and 135.8050º E). Anomalous uranium concentrations with associated vanadium, nickel and copper suggest enrichment processes occurring immediately below the Mesozoic sequences within the underlying weathered basement (Johnston, 2007; Wilson and Fairclough, 2009).

Exploration by Tasman Resources at the Parkinson Dam project (Figure 3.4.1) approximately 60 km west of Port Augusta has identified lead-zinc mineralisation in the Mesoproterozoic Corunna Conglomerate (Tasman Resources NL Annual Report, 2010). Fine-grained uraninite was also found in outcrop within close proximity to a regional unconformity. Several airborne radiometric anomalies exist nearby, in addition to anomalous surface geochemical values (Tasman Resources NL Annual Report, 2006).

3.4.1.2.1 The Cariewerloo Basin

The intracratonic Cariewerloo Basin (Figure 3.4.1), overlying the northeast margin of the Gawler Province, has long been considered an exploration target for unconformity-related uranium deposits in South Australia (Fairclough *et al.*, 2006; Wilson and Fairclough, 2009). The Cariewerloo Basin is an elongate, 120 km wide, northwest-trending basin bounded by major northwest-trending faults bordering basement highs. Younger northeast-trending faults disrupt the faulted eastern margin. Consistent internal stratigraphy, regardless of depth to basement, suggests that the basin formed prior to the faulting that produced the present half-graben morphology (Wilson *et al.*, 2010).

The Cariewerloo Basin is in-filled by the Pandurra Formation, a medium to coarse grained, poorly sorted, subangular quartz and lithic sandstone which also includes intervals of moderately well-sorted, very fine to medium-grained sandstone, granule to pebble conglomerates, mudstones and siltstones. The red, red-brown or purple kaolinite/sericite matrix, ochreous hematite and minor illite have typically undergone some reduction, displaying spotting or mottling in grey or white. Yellow or green reduction spotting is also observable in the interbedded mudstones and siltstones towards the lower part of the formation (Wilson *et al.*, 2010).

Recent hyperspectral logging of drillholes throughout the Cariewerloo Basin has shown that the Pandurra Formation has pervasive muscovite throughout. Dickite occurs in the upper sequence and paragonite, illite, phengite and montmorillonite are commonly present as well. Siderite and highly crystalline kaolinite are also a significant component of the formation while iron-chlorites and magnesium-chlorites are characteristic of the basement units (Wilson *et al.*, 2010). Montmorillonite is often present at the unconformity surface and possibly may represent a paleoweathering surface, an important parameter for unconformity-related uranium mineralisation. Phengite occurs at the base of the formation, varying upwards into muscovite-dominated mineralogy. Dickite occurs above the muscovite in drill core, sometimes with highly crystalline kaolinite in the middle of the dickite zone (Wilson and Fairclough, 2009).

Uranium enriched source rocks are known to occur within the vicinity of the Cariewerloo Basin. The presence of altered potassium-feldspar, chert, ferruginous chert, ironstone, muscovite and acid volcanics in the Pandurra Formation suggests that the sediments were derived from the Gawler Range Volcanics (Drexel *et al.*, 1993). Additionally, the basement is intruded by A-type granites and co-magmatic volcanics, including the Hiltaba Suite, which have elevated uranium contents of around 15 to 20 ppm uranium (Neumann *et al.*, 2000). Several possible sources of reductant lithologies are recognised in the region, including the graphitic schists of the Hutchison Group equivalent,

carbonaceous metasediments of the Wallaroo Group, graphitic shear zones, mafic rocks and iron formations (Cowley, 1993; Wilson and Fairclough, 2009).

The potential for unconformity-related mineralisation in the Pandurra Formation is also suggested by the results of recent exploration. At the Westopolis prospect, 30 km southwest of Olympic Dam and 5 km west of the Acropolis Prospect, drilling has intersected sediments of the Stuart Shelf unconformably overlying the Pandurra Formation, which in turn unconformably overlies haematitic breccias within the basement. Anomalous copper and uranium were reported for the breccias. Uranium mineralisation is confined to narrow zones of secondary oxidation within coarse-grained sandstones associated with localised concentrations of iron and manganese over widths of a few centimetres (Wilson and Fairclough, 2009).

3.4.2 Mineral system model

Skirrow *et al.* (2009) have proposed a classification scheme which describes a continuum of possible deposit styles based on three end-member uranium mineral systems. In this scheme (Fig. 3.0.1) unconformity-related uranium deposits are classified as part of basin and surface-related uranium systems as they involve mixing of fluids derived from dehydration reactions during metamorphism/diagenesis and surface-derived fluids. Previously, Mernagh *et al.* (1998) also defined the essential components associated with some of the unconformity-related uranium deposits in the McArthur Basin in the Northern Territory. The following discussion describes the key features of the unconformity-related mineral system model used in this study.

3.4.2.1 Sources

Current models for the formation of unconformity-related uranium deposits can be divided into two general types. The first involves the basement as the source of uranium and the basins as the source of the fluids (e.g., Cuney *et al.*, 2003; Derome *et al.*, 2005; Johnston, 1984; Mernagh *et al.*, 1994). The second involves the overlying basin as a source for both the uranium and fluid (e.g., Hoeve *et al.*, 1980; Kyser, 2007; Ruzicka, 1993). The first model sources uranium from the breakdown of monazite along fault zones as basinal brines interact with the basement. Uranium is precipitated when the oxidised fluid carrying uranium interacts with a reduced basement lithology (Hoeve *et al.*, 1980), or encounters reductants in the basin such as volcanic units (Ahmad and Wygralak, 1990), or mixes with reduced fluids derived from the basement (Johnston, 1984; Mernagh *et al.*, 1994). In some cases, fluid interaction with feldspathic or calcareous rocks may cause only a moderate increase in pH and a decrease in the oxidation state (fO_2), leading to precipitation of other metals (e.g., gold and platinum group metals), but little or no uranium (e.g., the Coronation Hill deposit).

In the basin model the source of uranium is from the breakdown of uranium-bearing detrital minerals, such as monazite, zircon, phosphates, tourmaline and uraninite by basinal fluids in deep basin paleoaquifers (e.g., Hoeve *et al.*, 1980; Kyser, 2007; Ruzicka, 1993). These fluids flow laterally along paleoaquifers, but may also flow downward because of the density of the highly saline fluid. Some models allow part of the fluid to enter faults and fracture zones in the basement rocks and, as a result, become reduced before ascending again along faults and fractures where they mix with laterally moving oxidised fluids. Precipitation of the uranium (and other metals) takes place at the interface between the oxidising and reducing fluids (i.e. at the redox front). High-grade uranium or polymetallic mineralisation forms directly at the unconformity. Medium-grade uranium mineralisation may form below the unconformity and low-grade uranium mineralisation may form within the overlying sediments at some distance above the unconformity.

3.4.2.1.1 Precambrian Source Map

The Precambrian source map (Figure 3.4.2) includes mappable criteria indicating potential sources of uranium and other metals, mineralising fluids and other components needed for ore transport (see Table 3.4.1). Three datasets were combined to produce the source map. The first dataset was a map of uranium-enriched Precambrian igneous rocks (intrusive or volcanic). Uranium concentrations (in ppm) for each lithological unit were obtained from Geoscience Australia's OZCHEM database (http://www.ga.gov.au/meta/ANZCW0703011055.html) and only those igneous rocks greater than the 75th percentile for each rock class were kept in the dataset. The second dataset was a map of uranium-enriched Precambrian sediments. As the composition of the sediments was more variable, the uranium-rich sediments were selected by comparing their distribution with the uranium channel of the Radiometric Map of Australia (Minty *et al*., 2010) and selecting units which corresponded with above average concentrations of uranium. The third dataset was a map of Precambrian evaporate-bearing units or shallow water units which may act as a source of basinal brines. These units were selected from the literature (e.g., Drexel *et al*., 1993).

The Precambrian source map highlights uranium-rich rocks in the Curnamona Province, including the Mount Painter and Mount Babbage inliers and the region north of Roxby Downs in the Gawler Province. Most of the central and southern Gawler Province has medium-high source potential owing the presence of the uranium-rich rocks of the Hiltaba Suite and Gawler Range Volcanics.

3.4.2.1.2 Phanerozoic Source Map

The Phanerozoic source map (Figure 3.4.7) includes the uranium-rich basement rocks shown in the Precambrian source map (Figure 3.4.2) plus uranium-rich sedimentary rocks in the Phanerozoic. As before, the uranium-rich sediments were selected by comparing their distribution with the uranium channel of the Radiometric Map of Australia and selecting units which corresponded with above average concentrations of uranium. The third dataset included was a map of Phanerozoic evaporite-bearing units or shallow water units which may act as a source of basinal brines. These units were selected from the literature (e.g., Drexel *et al*., 1993). The Phanerozoic source map shows that the basement rocks in the Gawler Province and the Curnamona Province all have moderate potential. A region of high source potential occurs just north of Roxby Downs where uranium-rich sediments of the Bulldog Shale overly the Hiltaba Granite. Similar areas of high source potential occur in the Curnamona Province where uranium-rich source rocks were identified in the radiometrics.

3.4.2.2 Drivers

Migration of oxidised, uranium-bearing fluids in deep-basinal settings may be driven by gravity (topography or salinity-related density controls), diagenesis/compaction, convection/temperature variations or tectonic processes (e.g., basin inversion). During basin inversion, fluid flow patterns will be significantly different, and, in some cases, reversed relative to directions during extension. Switches in fluid flow direction may be partly responsible for the variations in local settings and characteristics of basement-hosted unconformity-related uranium deposits versus basin-hosted styles of unconformity-related uranium deposits. Additionally, the role of basement fluid in unconformity-related systems may vary in importance with switches in fluid flow direction (Cuney *et al*., 2003). Paleomagnetic studies in the McArthur Basin also support a link between tectonic processes and uranium mineralisation in the McArthur Basin. Changes in the apparent polar wander path at 1680 to 640 Ma (Idnurm, 2000) correspond with uranium mineralisation ages, indicating that these tectonic processes may have stimulated fluid flow in the McArthur Basin.

Table 3.4.1. Theoretical and mappable criteria for unconformity-related uranium in the Precambrian Eon

MINERAL SYSTEM COMPONENT	CRITERIA		DATASET	IMPOR-TANCE	APPLIC-ABILITY	CONFI-DENCE	WEIGHT	COMMENTS
	THEORETICAL	MAPPABLE						
1. Source of uranium	Presence of U-enriched igneous rocks (intrusive or volcanic)	10 km buffer around U-enriched basement rocks 30 km buffer around U-enriched basement rocks 100 km buffer around U-enriched basement rocks	OzChem database	1.00 1.00 1.00	0.75 0.50 0.25	1.00 1.00 1.00	0.750 0.500 0.250	
	Presence of U-enriched sedimentary rocks of Precambrian age	Presence of U-enriched sedimentary rocks of Precambrian age	Radiometric Map of Australia (Minty *et al*., 2010)	0.50	0.50	0.50	0.125	
1. Source of ligands	Presence of evaporite minerals of Precambrian age indicating production of basinal brines	Lithological unit	Drexel *et al.* (1993)	0.5	0.25	1.00	0.125	
2. Drivers	Presence of thick, intracratonic, epicontinental or foreland basin of Precambrian age.	Cariewerloo Basin Cariewerloo Basin + 40 km buffer Corunna conglomerate Corunna Conglomerate + 40 km buffer	Surface Geology of Australia (Raymond and Retter, 2010)	1.00 1.00 0.50 0.50	0.75 0.50 0.75 0.50	1.00 1.00 1.00 1.00	0.750 0.500 0.375 0.250	
	Diagenesis creating oxidised fluids as shown be presence of hematite	ASTER ferric oxide content - 1σ above mean ASTER ferric oxide content - 2σ above mean	Gawler-Curnamona ASTER Project	0.50 0.50	0.25 0.50	0.50 0.50	0.063 0.125	
	Diagenesis indicated by sericite alteration associated with fluid flow in aquifers	ASTER AlOH group content - 1σ above mean ASTER AlOH group content - 2σ above mean	Gawler-Curnamona ASTER Project	0.50 0.50	0.25 0.50	0.50 0.50	0.063 0.125	
	Diagenesis indicated by kaolinite alteration associated with fluid flow in aquifers	ASTER advanced argillic - 1σ above mean ASTER advanced argillic - 2σ above mean	Gawler-Curnamona ASTER Project	0.50 0.50	0.25 0.50	0.50 0.50	0.063 0.125	
3. Architecture	Presence of basal unconformity of Precambrian age	Distribution of unconformities in solid geology + Cariwerloo Basin + Corunna conglomerate - 10 km buffer 20 km buffer 40 km buffer	Solid Geology of South Australia (Cowley, 2006)	1.00 1.00 1.00	1.00 0.75 0.50	1.00 1.00 1.00	1.000 0.750 0.500	
	Distribution of extensional faults	Archean to Mesoproterozoic faults Middle Mesoproterozoic faults	http://www.pir.sa.gov.au/minerals/sarig	0.50 0.50	0.75 0.50	1.00 1.00	0.375 0.250	
3. Fluid pathways	Demagnetisation of rock units caused by oxidised fluids	Demagnetised zones - 1σ above mean Demagnetised zones - 2σ above mean	Magnetic Map of Australia	0.50 0.50	0.25 0.50	1.00 1.00	0.125 0.250	
	Distribution of hematite as evidence of oxidised fluids	ASTER ferric oxide content - 1σ above mean ASTER ferric oxide content - 2σ above mean	Gawler-Curnamona ASTER Project	0.50 0.50	0.25 0.50	0.50 0.50	0.063 0.125	
	Sericite alteration associated with fluid flow	ASTER AlOH group content - 1σ above mean ASTER AlOH group content - 2σ above mean	Gawler-Curnamona ASTER Project	0.50 0.50	0.25 0.50	0.50 0.50	0.063 0.125	
	Kaolinite alteration associated with fluid flow	ASTER advanced Argillic - 1σ above mean ASTER advanced Argillic - 2σ above mean	Gawler-Curnamona ASTER Project	0.50 0.50	0.25 0.50	0.50 0.50	0.063 0.125	
4. Depositional mechanisms and environment	Evidence of uranium deposition	U^2/Th radiometric maps - 1σ above mean U^2/Th radiometric maps - 2σ above mean	Radiometric Map of Australia (Minty *et al*., 2010)	1.00 1.00	0.50 0.75	0.50 0.50	0.250 0.375	
	Thoriium enrichment that may indicate uranium deposition at depth	Th enrichment - 1σ above mean Th enrichment - 2σ above mean	Radiometric Map of Australia (Minty *et al*., 2010)	0.50 0.75	0.25 0.25	0.50 0.50	0.063 0.094	
	Redox gradients along and below basal unconformity	Carbonaceous rocks of Hutchison Group Carbonaceous rocks in Corunna Conglomerate Other carbonaceous rocks of Precambrian age Fe2+-rich rocks of Precambrian age	PIRSA 1:100 000 scale surface geology	1.00 1.00 0.75 0.75	1.00 1.00 0.75 0.50	0.50 0.50 0.50 0.50	0.500 0.500 0.281 0.188	

Diagenesis and concurrent compaction of basinal sediments was an important driver also of fluid flow in these basins. The ages of diagenetic phases extracted from aquifer lithologies reveals that fluid migration in the diagenetic aquifers effectively covers the period of formation of unconformity-related uranium deposits (Polito *et al.*, 2006). Sequence stratigraphic analysis and models of fluid flow also indicate that basinal reservoirs were likely sources for mineralising fluids. Thus, diagenetic aquifer lithologies were being drained of fluids at the same time as the deposits were forming from fluids which were chemically and isotopically similar, thus linking diagenesis and fluid flow events within the basins to the formation of the unconformity-related uranium deposits.

3.4.2.2.1 Precambrian Driver Map

The Precambrian driver map (Figure 3.4.3) includes criteria which denote energy gradients capable of mobilising sufficient quantities of ore-bearing fluids to the site of deposition. Four datasets were combined to produce the driver map. The first mappable criterion is the presence of thick, intercratonic, epicontinental or foreland basins. Ideally these basins should have been greater than 3 to 4 km thick initially in order to generate fluids with temperatures above the 150ºC typically associated with unconformity-related uranium deposits. The Cariewerloo Basin was given the highest weighting factor (Table 3.4.1) because it is greater than 3000 m thick and contains unmetamorphosed, oxidised sediments of the Mesoproterozoic Pandurra Formation. The Corunna Conglomerate, which contains fluvial to marine sediments, was given a lower weighting factor because of the more reduced nature of the marine sediments and the fact that it is not as thick as the sediments in the Cariewerloo Basin. In the Alligator Rivers Uranium Field, most known uranium deposits are situated within 40 to 50 km of the present day margins of the overlying basin. Hence, a buffer of 40 km has been added to the margins of the Cariewerloo Basin and the Corunna Conglomerate to account for the fact that the margins of these units have been eroded away over time.

The other datasets consist of the ferric oxide content, AlOH bonding group content and the advanced argillic group content all derived from the ASTER images of this region. It was not possible to divide these datasets into Precambrian and Phanerozoic groups. These products are used as proxies for hematite, sericite and kaolinite all of which may indicate where diagenesis has led to the generation of oxidised fluids. However, these datasets are given a low weighting factor because of the age uncertainty and the fact that they are severely affected by surface weathering.

The Precambrian driver map indicates that the highest potential for favourable drivers is where the buffers of the Cariewerloo Basin and the Corunna Conglomerate overlap. A zone of moderate to high potential also occurs where the buffer around the Cariewerloo Basin overlaps with the Corunna Conglomerate. The whole Cariewerloo Basin has moderate potential as a driver because of the thickness of the basin. The region outside the buffer around the Cariewerloo Basin has much lower potential as a fluid flow driver. Other tectonic events such as basin inversion are also important fluid drivers, but these could not be readily expressed as mappable components.

3.4.2.2.2 Phanerozoic Driver Map

The Phanerozoic driver map is presented in Figure 3.4.8. Regions of moderate to high driver potential occur where one or more sedimentary basins overlie older basins. The regions of highest driver potential occur around Roxby Downs where the Eromanga Basin overlaps the Cariewerloo Basin. Other regions of moderately-high potential occur where the Eromanga Basin (≤3000 m thick) overlaps the Warburton Basin (≤1800 m thick) and the Arrowie Basin (≤5000 m thick). Although the

Arrowie Basin consists mainly of marine sediments it also contains some red-bed sediments in the Lake Frome Group which are favourable for the passage of uranium-bearing oxidised fluids.

3.4.2.3 Fluid Pathway/Architecture

Unconformity-related uranium systems are generally located in intracratonic, epicontinental or foreland basins which unconformably overly uranium-rich basement rocks. A critical element in these systems is a major disconformity (generally an unconformity) between the basement containing relatively reduced rocks and the overlying basin which contains oxidised, highly permeable sedimentary rocks. There is often an onlapping relationship between the basin and basement. Periodic reactivation of basement faults during and after basin development creates the faults and architecture for later fluid flow pathways. The faults generally exhibit relatively small displacement (less than a few hundred metres) and form conjugate networks, but may also include fault strands with strike lengths of tens to hundreds of kilometres. The deposits sometimes also show a close association with gravity highs and/or ridges, which may reflect major structures in the basement that control later fluid flow in the system.

The migration of fluids into deep-basinal settings requires particular architectures to maintain the high oxidation state necessary for the transport of uranium. The fluids may be buffered and/or maintained at high oxidation states by the presence of Fe^{3+}-bearing minerals such as hematite and goethite, or by sulfate minerals, provided that reductants are in low abundance. Consequently, redbed evaporite sequences may be favourable reservoirs for the storage of oxidised fluids deep within basins. Fluid flow pathways are influenced by the formation of aquifers and aquitards during diagenesis, as well as other lateral and vertical variations in permeability caused by faulting and shearing during episodes of basin extension and basin inversion. The aquifers are typically defined by illite-kaolinite alteration or hematite-bearing oxidised assemblages or aquitards with intense silicification. Basement penetrating faults are often defined by illite-kaolinite and/or chloritic alteration.

3.4.2.3.1 Precambrian Fluid Pathway/Architecture Map

This Precambrian fluid pathway/architecture map (Figure 3.4.4) includes favourable lithologies and structures which enable movement of fluids to the site of ore deposition. Of particular importance to unconformity-related uranium deposits are basal unconformities which separate oxidised and reduced lithologies. To partially account for the extension of the unconformities below the basins and for possible erosion of the basins, 10, 20 and 40 km buffers were added to the unconformities. Archean–Mesoproterozoic faults were included as important fluid flow pathways that may channel uranium-rich fluids into the vicinity of the basal unconformities

Highly oxidised fluids are required to transport uranium in solution (Skirrow *et al.*, 2009) and such fluids would be expected to oxidise any rocks along their pathways. Therefore, strongly demagnetised zones (up to two standard deviations below the mean) were used to indicate possible oxidation as a result of fluid flow. In addition, derivatives from the ASTER data were used to indicate the presence of hematite, sericite and kaolinite that may also form from oxidised fluid flow. However, the ASTER groups were given relatively low weighting factors (Table 3.4.1) because of the strong overprinting effects of surface weathering in many parts of the study area.

Regions of high fluid pathway potential occur where the faults intersect the buffers around the unconformities. Thus the northwestern edge of the Cariewerloo Basin is highlighted, as is the region around Roxby Downs. There is also a north-northwest trending zone of high potential north of Port

Augusta corresponding with the eastern margin of the Cariewerloo Basin. An outcropping part of the Corunna Conglomerate in the southwest corner of the map also has moderate to high fluid pathway potential.

3.4.2.3.2 Phanerozoic Fluid Pathway/Architecture Map

The Phanerozoic fluid pathway/architecture map (Figure 3.4.9) includes favourable lithologies and structures which enable movement of fluids to the site of ore deposition. A dataset of Neoproterozoic-Ordovician faults also was added to the map. However, a dataset of more recent faults was not available. In addition, derivatives from the ASTER data were used to indicate the presence of hematite, sericite and kaolinite that may also form from oxidised fluid flow, but again were given relatively low weighting factors (Table 3.4.2) because of the strong overprinting effects of surface weathering in many parts of the study area.

The fluid pathway/architecture map highlights the unconformities around the Phanerozoic sedimentary basins with regions of highest potential occurring where faults and other favourable criteria intersect the unconformities. This has resulted in regions of high potential around the town of Roxby Downs and to its north, particularly where unconformities of the Eromanga and Lake Eyre basins occur. The region to the east of Leigh Creek (along the western margin of the Arrowie Basin) is also an area of high fluid pathway potential. Other regions of high fluid pathway potential occur along the eastern margin of the Cariewerloo Basin, around the Stuart Shelf and along the northwestern margin of the Adelaide Rift Complex.

3.4.2.4 Deposition

Uranium has the ability to complex with a large number of ligands depending on the pH and oxidation state of the fluid. It can be transported as oxy-hydroxy, chloride, fluoride, sulfate, phosphate, carbonate and other complexes. Uranium ions in aqueous solution can form very complex species due to the four possible oxidation states, as well as hydrolytic reactions which lead to the formation of polymeric ions. For example, in oxidised aqueous fluids, U^{6+} readily forms the linear polar uranyl ion, UO_2^{2+}. Uranium is deposited when these oxidised fluids come in contact with reductants in the basin or in the basement rocks. Examples of possible reductants include carbonaceous shales, Fe^{2+}-rich rocks, hydrocarbons and hydrogen sulfide in reduced fluids. Zones of faulting and brecciation, particularly in the basement, are important for focusing the fluids and enhancing their interaction with reduced rock assemblages. There is a general association also of calcareous rocks with reduced rocks in the basement, which may indicate that changes in pH are also important during the depositional process.

Because most unconformity-related uranium deposits occur close to the basal unconformity between the sedimentary basin and the basement rocks, there is a good chance of preservation for this style of mineralisation. Most of the fertile basins which still exist are 1 to 3 km thick, flat-lying and essentially unmetamorphosed. However, in some cases, the basin fill can be absent, having been removed by erosion to leave the basement rocks outcropping at the surface and exposing the ore to possible leaching by surface waters.

Table 3.4.2. Theoretical and mappable criteria for unconformity-related uranium in the Phanerozoic Eon

MINERAL SYSTEM COMPONENT	CRITERIA		DATASET	IMPOR-TANCE	APPLIC-ABILITY	CONFI-DENCE	WEIGHT	COMMENTS
	THEORETICAL	MAPPABLE						
1. Source of uranium	Presence of U-enriched igneous rocks (intrusive or volcanic)	10 km buffer around U-enriched basement rocks 30 km buffer around U-enriched basement rocks 100 km buffer around U-enriched basement rocks	OzChem database	1.00 1.00 1.00	0.75 0.50 0.25	1.00 1.00 1.00	0.750 0.500 0.250	
	Presence of U-enriched sedimentary rocks of Phanerozoic age	Presence of U-enriched sedimentary rocks of Phanerozoic age	Radiometric Map of Australia (Minty *et al*., 2010)	0.50	0.50	0.50	0.125	
1. Source of ligands	Presence of evaporite minerals of Precambrian age indicating production of basinal brines	Lithological unit	Drexel and Preiss (1995)	0.5	0.25	1.00	0.125	
2. Drivers	Presence of thick, intracratonic, epicontinental or foreland basin of Precambrian age.	Eromanga Basin Lake Eyre Basin Stuart Shelf - Wilpenna Group Arckaringa Basin Arrowrie Basin Warburton Basin Billa Kalina Basin	Surface Geology of Australia (Raymond and Retter, 2010)	1.00 0.75 0.75 0.50 0.50 0.50 0.25	0.75 0.75 0.75 0.75 0.75 0.75 0.75	1.00 1.00 1.00 1.00 1.00 1.00 1.00	0.750 0.563 0.563 0.375 0.375 0.375 0.188	
	Diagenesis creating oxidised fluids as shown be presence of hematite	ASTER ferric oxide content - 1σ above mean ASTER ferric oxide content - 2σ above mean	Gawler-Curnamona ASTER Project	0.50 0.50	0.25 0.50	0.50 0.50	0.063 0.125	
	Diagenesis indicated by sericite alteration associated with fluid flow in aquifers	ASTER AlOH group content - 1σ above mean ASTER AlOH group content - 2σ above mean	Gawler-Curnamona ASTER Project	0.50 0.50	0.25 0.50	0.50 0.50	0.063 0.125	
	Diagenesis indicated by kaolinite alteration associated with fluid flow in aquifers	ASTER advanced argillic - 1σ above mean ASTER advanced argillic - 2σ above mean	Gawler-Curnamona ASTER Project	0.50 0.50	0.25 0.50	0.50 0.50	0.063 0.125	
3. Architecture	Presence of basal unconformity of Phanerozoic age	Distribution of unconformities in solid geology - 1 km buffer 5 km buffer 10 km buffer	Solid Geology of South Australia (Cowley, 2006)	1.00 1.00 1.00	1.00 0.75 0.50	1.00 1.00 1.00	1.000 0.750 0.500	Unconformities at the bases of the Eromanga, Lake Eyre, Arckaringa, Arrowrie, Warburton and Billa Kalina basins and at the base of the Wilpenna Group in the Stuart Shelf
	Distribution of extensional faults	Neoproterozoic-Ordovician faults	http://www.pir.sa.gov.au/minerals/sarig	0.50	0.75	1.00	0.375	
3. Fluid pathways	Demagnetisation of rock units caused by oxidised fluids	Demagnetised zones - 1σ above mean Demagnetised zones - 2σ above mean	Magnetic Map of Australia	0.50 0.50	0.25 0.50	1.00 1.00	0.125 0.250	
	Distribution of hematite as evidence of oxidised fluids	ASTER ferric oxide content - 1σ above mean ASTER ferric oxide content - 2σ above mean	Gawler-Curnamona ASTER Project	0.50 0.50	0.25 0.50	0.50 0.50	0.063 0.125	
	Sericite alteration associated with fluid flow	ASTER AlOH group content - 1σ above mean ASTER AlOH group content - 2σ above mean	Gawler-Curnamona ASTER Project	0.50 0.50	0.25 0.50	0.50 0.50	0.063 0.125	
	Kaolinite alteration associated with fluid flow	ASTER advanced Argillic - 1σ above mean ASTER advanced Argillic - 2σ above mean	Gawler-Curnamona ASTER Project	0.50 0.50	0.25 0.50	0.50 0.50	0.063 0.125	
4. Depositional mechanisms and environment	Evidence of uranium deposition	U^2/Th radiometric maps - 1σ above mean U^2/Th radiometric maps - 2σ above mean	Radiometric Map of Australia (Minty *et al*., 2010)	1.00 1.00	0.50 0.75	0.50 0.50	0.250 0.375	
	Thorium enrichment that may indicate uranium deposition at depth	Th enrichment - 1σ above mean Th enrichment - 2σ above mean	Radiometric Map of Australia (Minty *et al*., 2010)	0.50 0.75	0.25 0.25	0.50 0.50	0.063 0.094	
	Redox gradients along and below basal unconformity	Carbonaceous rocks of Phanerozoic age Fe^2+-rich rocks of Phanerozoic age	PIRSA 1:100 000 scale surface geology	0.75 0.75	0.75 0.50	0.50 0.50	0.281 0.188	

3.4.2.4.1 Precambrian Deposition Map

The Precambrian deposition map (Figure 3.4.5) includes favourable lithologies and structures which can focus fluids and deposit uranium and other metals via physical and/or chemical processes. The U^2/Th ratio derived from gamma-ray spectrometry has been found to be a useful method of identifying uranium enrichment in the near surface (Mernagh *et al.*, 1998) and was used as an indicator of uranium deposition (Table 3.4.1). Identifying mineralisation at depth is more difficult, but thorium enrichment at the surface can occur when uranium is leached by meteoric fluids. As a result, regions of above average thorium concentration may indicate uranium mineralisation at depth. Deposition of uranium typically occurs by reduction of U^{6+} to U^{4+} (Bastrakov *et al.*, 2010) in the vicinity of a basal unconformity, and hence, the presence of reducing lithologies such as carbonaceous rocks and Fe^{2+}-rich rocks is necessary for these chemical reactions to occur. Thus, Fe^{2+}-rich rocks and carbonaceous sediments were selected from the Surface Geology of South Australia (Cowley 2006). The Hutchison Group and the Corunna Conglomerate were considered the most favourable groups and given a higher weighting (Table 3.4.1). The Hutchison Group consists of various types of schists that locally contain graphite and graphitic lithologies. The Corunna Conglomerate contains a coarser basal unit, but fines upwards to thick carbonaceous siltstone and sandstone.

The Precambrian deposition map has areas of moderate to high potential in the southern Gawler Province associated mainly with the Hutchison Group and the Corunna Conglomerate. Another region of moderate potential occurs north of Roxby Downs associated with the Hutchison Group or a similar lithological unit. The Gawler Range Volcanics are also highlighted as having low to moderate potential due to their Fe^{2+}-rich nature.

3.4.2.4.2 Phanerozoic Deposition Map

The Phanerozoic deposition map presented (Figure 3.4.10) has an area of moderate to moderately-high potential in the northern section of the map, corresponding mostly with the Bulldog Shale and other sources of uranium-enrichment mentioned above. The Bulldog Shale consists mainly of bioturbated and fossiliferous mudstone with very fine sand intervals which commonly show cross-lamination or irregular interlamination with mudstone. Carbonaceous matter and pyrite are also present, both of which may act as reductants for U^{6+} (Bastrakov *et al.*, 2010). Another region of low to moderate potential coincides with the Gawler Range Volcanics as a result of their Fe^{2+}-rich nature and because they contain anomalously elevated uranium and thorium concentrations relative to global Proterozoic averages (Neumann *et al.*, 2000) and hence have high uranium and thorium responses in the radiometric map.

3.4.3 Results

The prospectivity of the study area for unconformity-related uranium deposits has been carried out for two time periods, the Precambrian and the Phanerozoic. The former accounts for the main period of unconformity-related mineralisation and the latter explores the potential for this style of mineralisation in younger successions.

3.4.3.1 Unconformity-related uranium in the Precambrian Eon

The assessment for the Precambrian Eon (Figure 3.4.6) was produced by combining the separate Precambrian prospectivity maps for the sources, drivers, fluid pathway/architecture and depositional mechanisms as discussed above (Plate 3.4). The results show that most of the prospectivity is

associated with the Cariewerloo Basin. Region A at the southern end of the Cariewerloo Basin denotes a large region with high potential for unconformity-related uranium deposits. This is because of the presence of favourable drivers such as the Cariewerloo Basin and the Corunna Conglomerate as well as potential uranium-rich source rocks and carbonaceous units of the Hutchison Group which are capable of precipitating uranium from the fluids. Region B south of Oak Dam is associated with the unconformity on the eastern side of the Cariewerloo Basin and the prospectivity is increased by the presence of cross-cutting faults which create favourable fluid flow pathways. Regions C and D near Roxby Downs have high prospectivity because of their proximity to the unconformity on the eastern side of the Cariewerloo Basin, the presence of favourable faults and the underlying carbonaceous rocks of the Hutchison Group. Region E in the southwest corner of the map has high prospectivity because of the presence of possible uranium-rich source rocks, favourable structures and the Corunna Conglomerate.

The Olary Domain in the east of the study area is also highlighted as having low to moderate prospectivity for unconformity-related uranium mineralisation. This area contains a number of magmatic-related uranium deposits hosted by sodic granite, trondhjemite, sodic alaskite and associated felsic gneiss or in pegmatites within these lithologies. The magmatic-related uranium deposits are associated with the ~1590 Ma Ninnerie Supersuite granitoids, but if uranium was remobilised from these deposits at a later date there is the potential for formation of unconformity-related deposits as well. Basal unconformities are also present in this region. The region is also cross-cut by a large number of faults and shear zones which would provide suitable fluid flow pathways. The basal units of the Willyama Supergroup are also locally enriched in iron sulfides and graphite, which may act as a suitable reductant for uranium.

The Mount Painter and Mount Babbage Inliers are also highlighted as having low to moderate prospectivity for unconformity-related uranium mineralisation for similar reasons to those of the Olary Domain. This area contains a number of hybrid and metamorphic-related uranium systems associated with granitic bodies and hematitic breccias. Unconformities separate the inliers from adjacent sediments of the Eromanga and Lake Eyre Basins. The Lake Eyre basin also contains a number of sandstone-hosted uranium deposits with uranium possibly being derived from the Mount Painter Inlier.

The Neoproterozoic to Middle Cambrian Adelaide Rift Complex is assessed as having low potential for unconformity-related uranium deposits, despite the presence of numerous faults and unconformities. This was because of the absence of identified uranium-rich source rocks in this region and the absence of large, relatively flat-lying sedimentary sequences. The uranium and copper potential of the Adelaide Rift Complex is discussed in more detail in Section 3.6.

A region of moderate to high unconformity-related uranium potential in Section 3.6 corresponds with Region C in this study. Region D corresponds with the southern part of a region of moderate potential on the boundary of the Woomera Prohibited Area. Because of the lower weighting factors given to the buffers further away from the unconformity in this study, the northern part of this Region D is given a lower prospectivity in the Precambrian prospectivity map. This accounts for the fact that the prospectivity decreases as the distance from the unconformity increases. The part of the Cariewerloo Basin which lies within the Woomera Prohibited Area was given a low to moderate potential in the Mineral Resource Potential Assessment (Geoscience Australia, 2010), which agrees fairly well with the low to moderate prospectivity given to that part of the Cariewerloo Basin in this study.

3.4.3.2 Unconformity-related uranium in the Phanerozoic Eon

The assessment for the Phanerozoic Eon (Figure 3.2.11 and Plate 3.5) was produced by combining the four key Phanerozoic mineral system components:

- source;
- driver;
- fluid pathway/architecture; and
- depositional mechanism.

The highest potential occurs in Region A which highlights the Mount Painter and Mount Babbage Inliers and surrounding regions. This area contains a number of hybrid and metamorphic-related uranium systems associated with granitic bodies and hematitic breccias which could act as a source of uranium for later unconformity-related deposits. Regions B, C and D highlight areas where unconformities exist between overlapping parts of the Arrowie, Eromanga and Lake Eyre basins and, as a result, are potential sites for unconformity-related uranium deposits. The Lake Eyre Basin also contains a number of sandstone-hosted uranium deposits, with uranium most likely being derived from the Mount Painter Inlier.

Region E highlights an area of moderate to high potential around Olympic Dam. Although this region is better known as a host for iron oxide-copper gold deposits, this study has shown that it also contains all the components needed to form unconformity-related uranium deposits. Thus any remobilisation of uranium in the Phanerozoic could have potential to generate unconformity-related uranium deposits in this region.

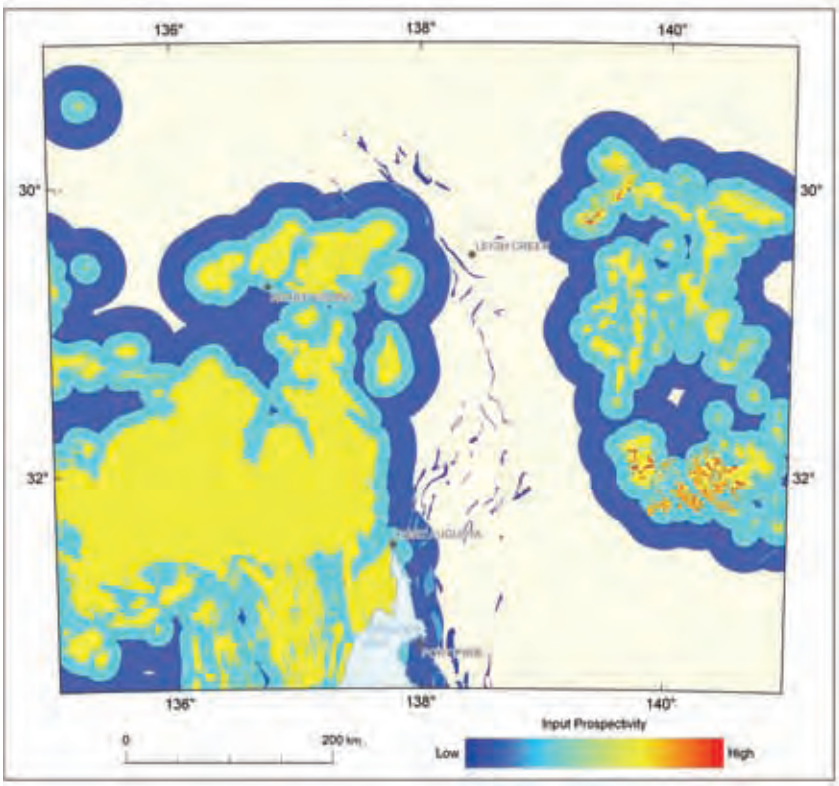

Figure 3.4.2: *Prospectivity for uranium-rich Precambrian source rocks based on sources of uranium, mineralising fluids and other components needed for ore transport (see text for details).*

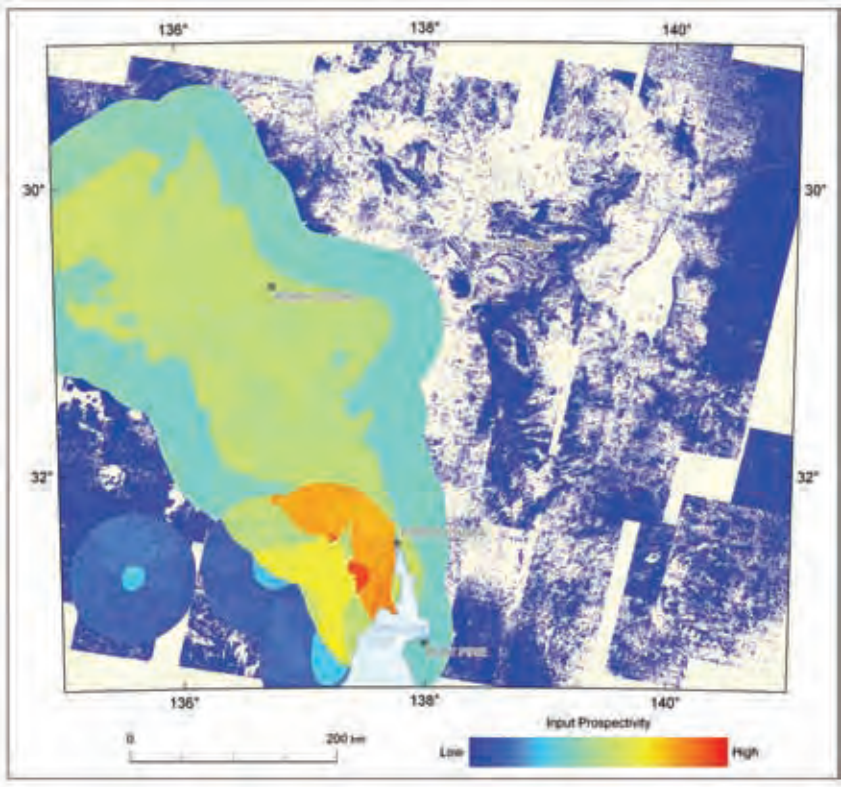

Figure 3.4.3: *Prospectivity for uranium-rich Precambrian drivers based on energy gradients that will mobilise sufficient quantities of ore-bearing fluids to the site of deposition (see text for details).*

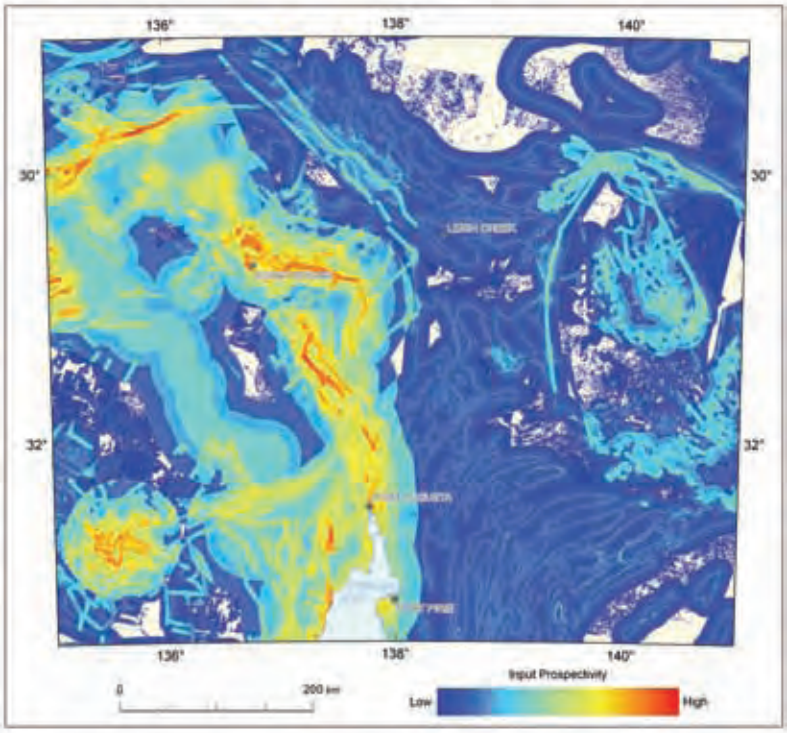

Figure 3.4.4: *Prospectivity for uranium-rich Precambrian fluid pathways/architecture based on favourable lithologies and structures that will enable movement of fluids to the site of ore deposition (see text for details).*

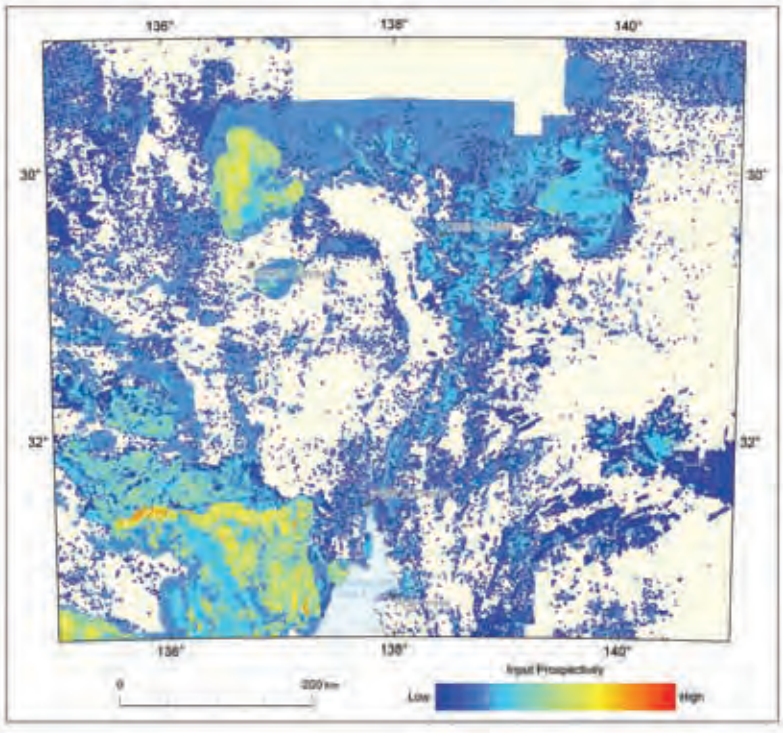

Figure 3.4.5: *Prospectivity for uranium-rich Precambrian depositional mechanisms based on favourable lithologies and structures to focus fluids and deposit uranium and other metals via physical and/or chemical processes (see text for details).*

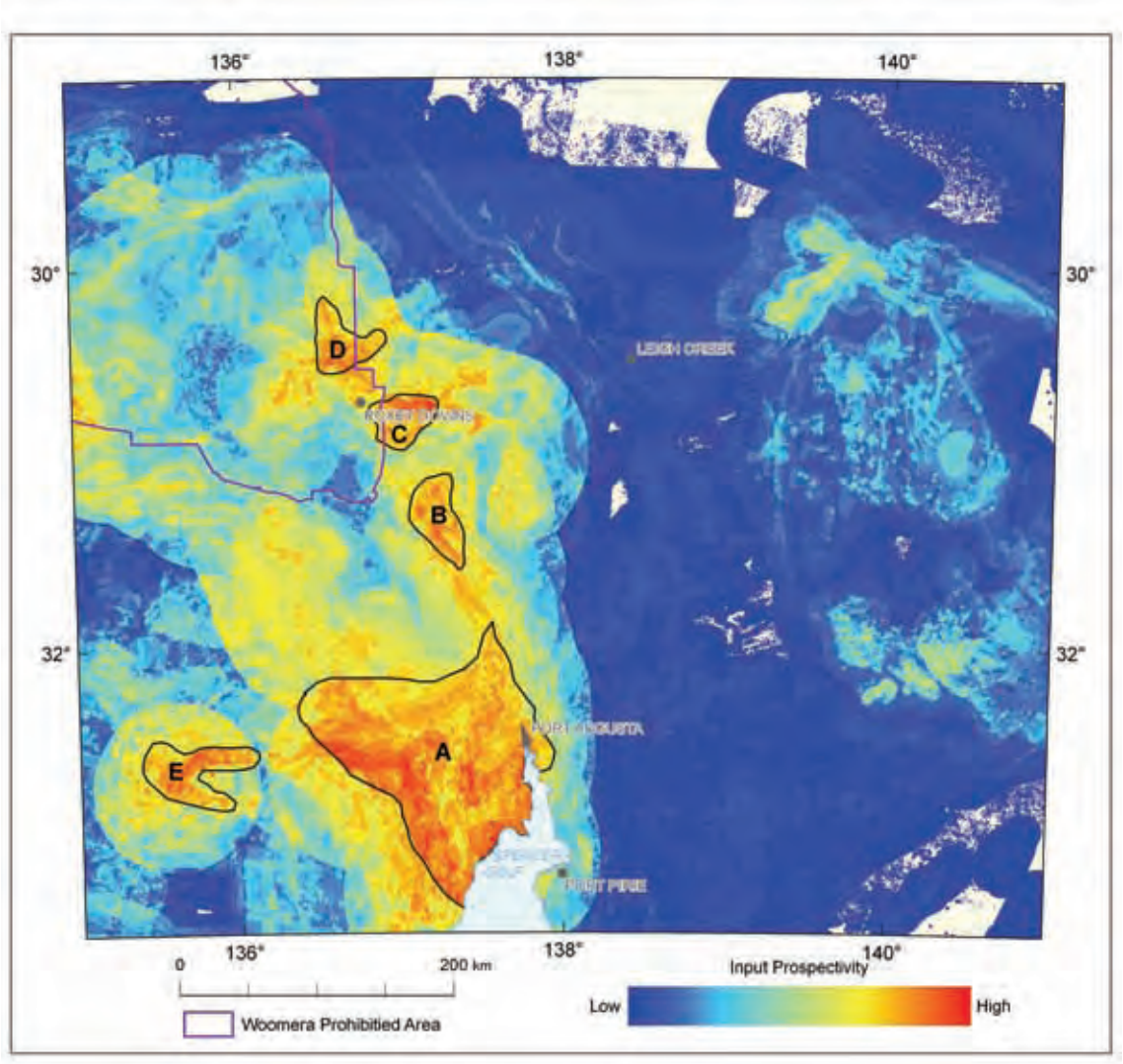

Figure 3.4.6: *Combined prospectivity for unconformity-related uranium in the Precambrian Eon (see text for details and Figure 3.4.1 for location of Cariewerloo Basin).*

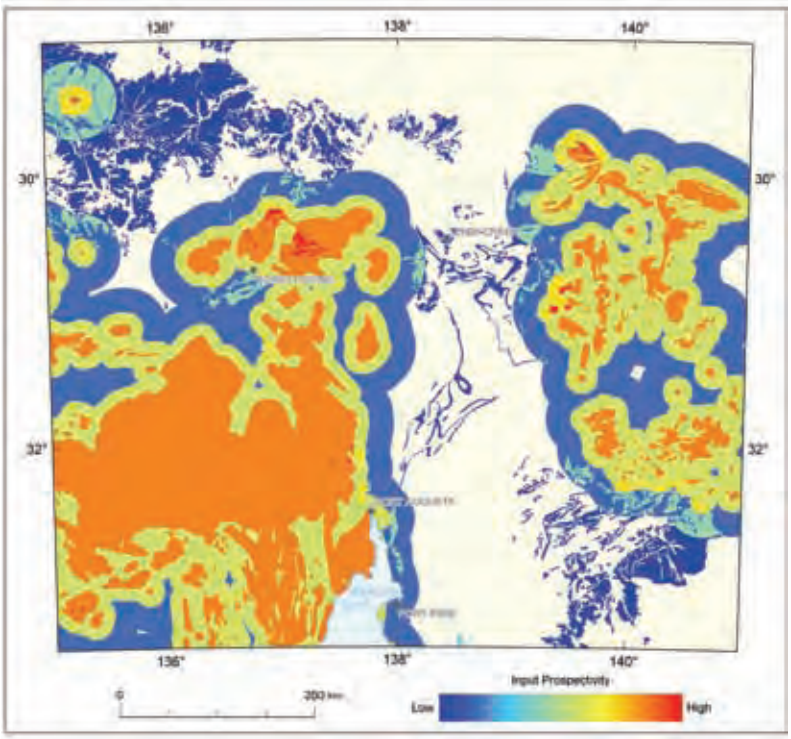

Figure 3.4.7: *Prospectivity for uranium-rich Phanerozoic source rocks based on sources of uranium, mineralising fluids and other components needed for ore transport (see text for details).*

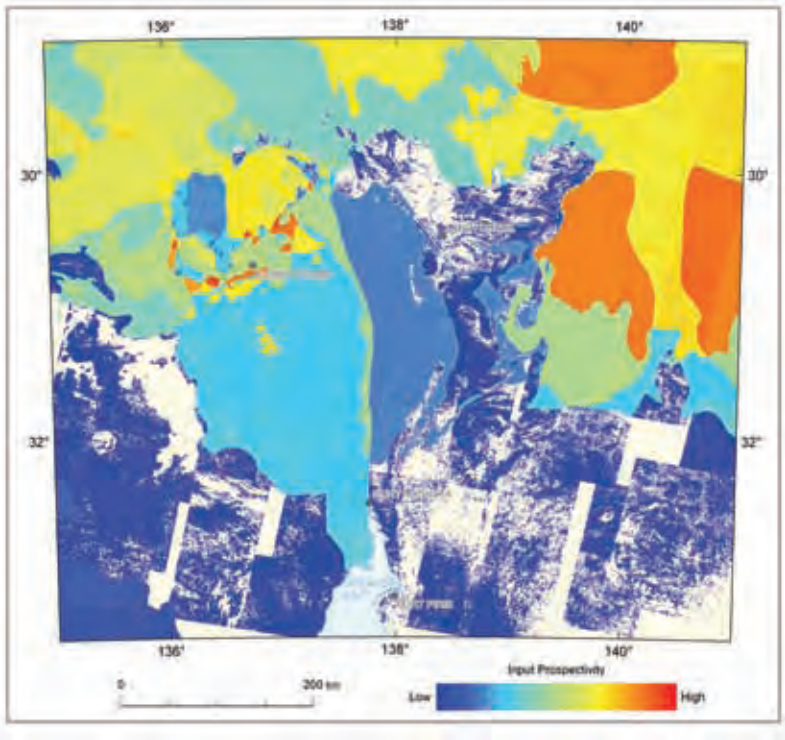

Figure 3.4.8: *Prospectivity for uranium-rich Phanerozoic drivers based on energy gradients that will mobilise sufficient quantities of ore-bearing fluids to the site of deposition (see text for details).*

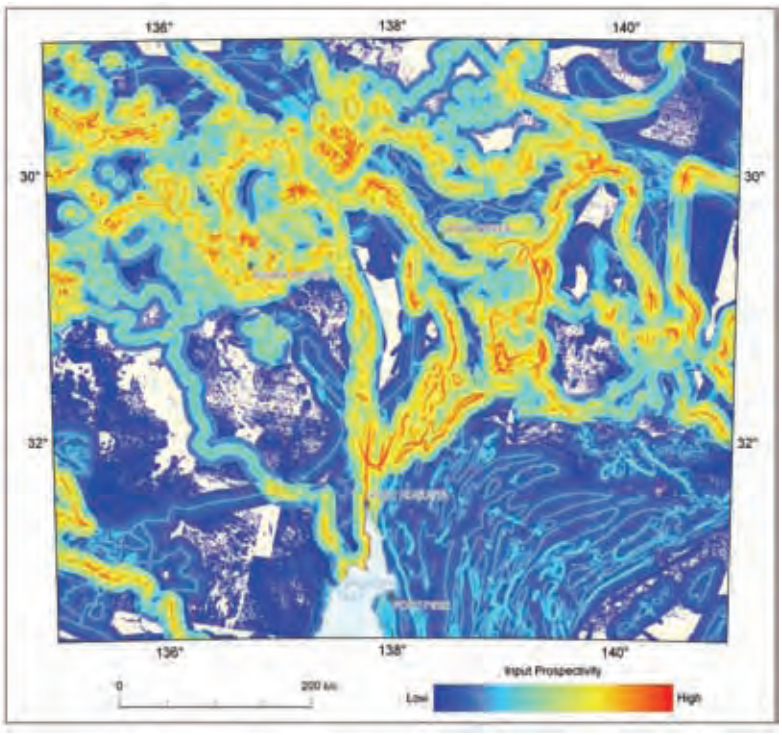

Figure 3.4.9: *Prospectivity for uranium-rich Phanerozoic fluid pathways/architecture based on favourable lithologies and structures that will enable movement of fluids to the site of ore deposition (see text for details).*

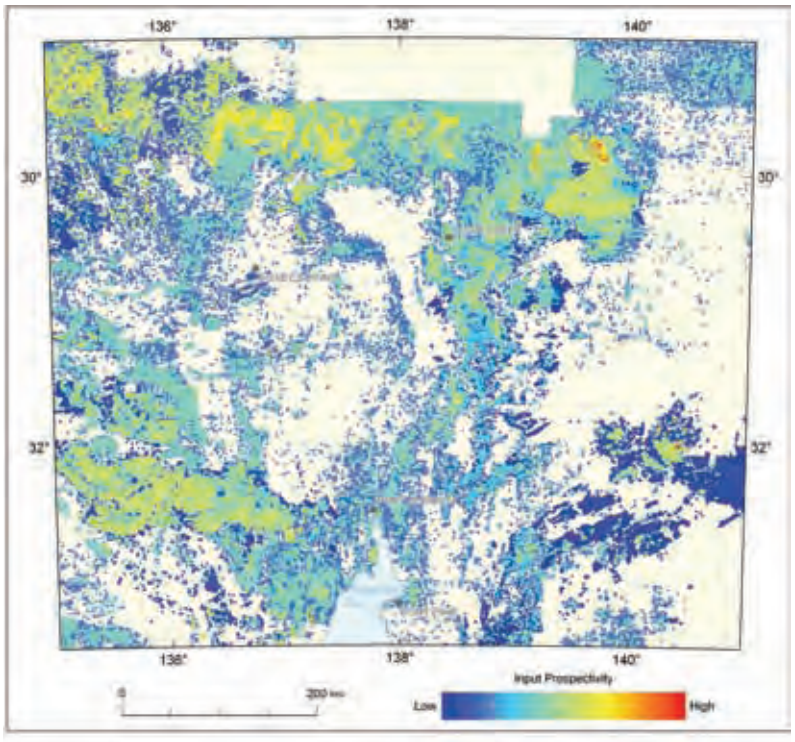

Figure 3.4.10: *Prospectivity for uranium-rich Phanerozoic depositional mechanisms based on favourable lithologies and structures to focus fluids and deposit uranium and other metals via physical and/or chemical processes (see text for details).*

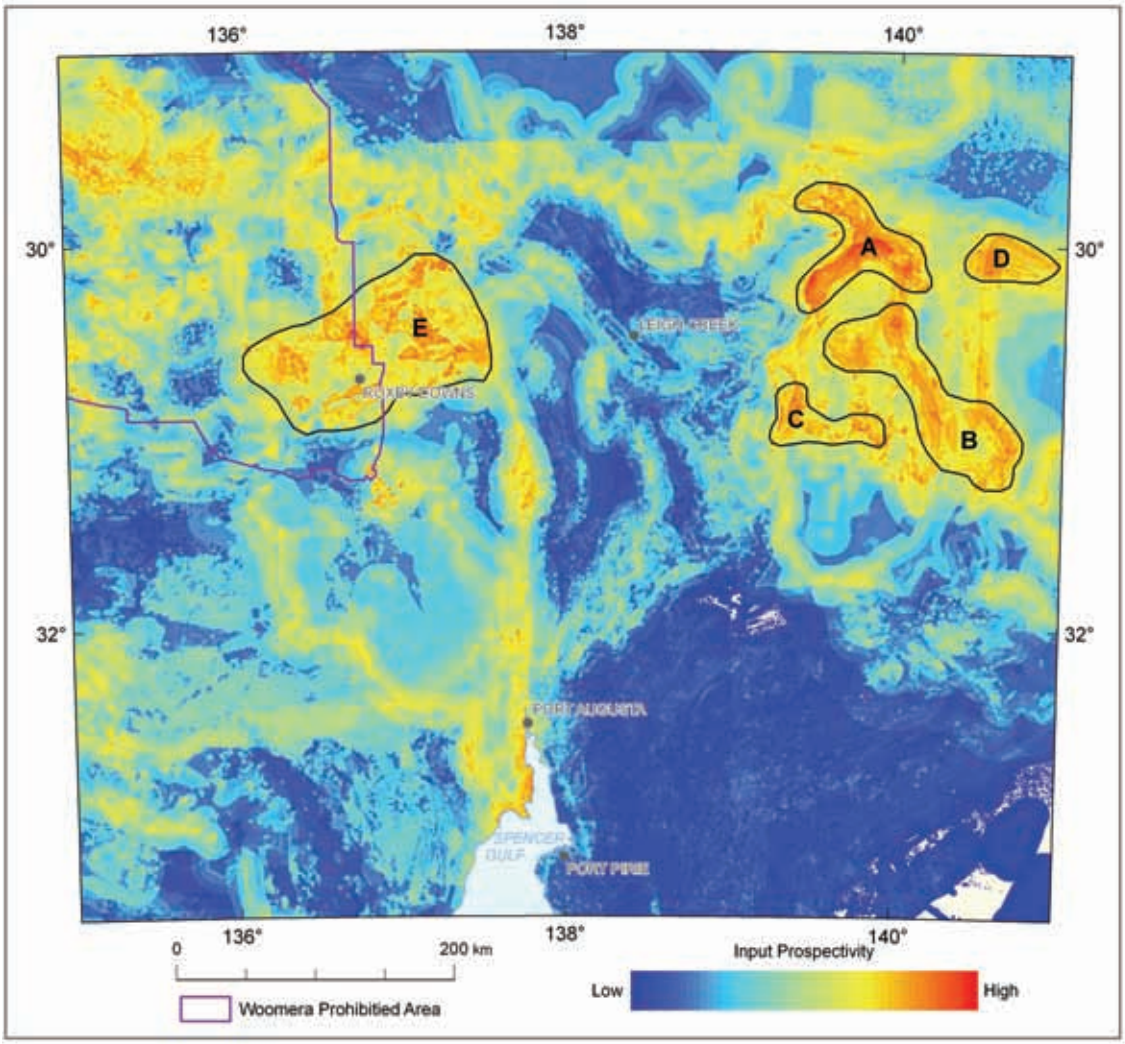

Figure 3.4.11: *Combined prospectivity for unconformity-related uranium in the Phanerozoic Eon (see text for details).*

3.5 MAGMATIC-RELATED URANIUM MINERAL SYSTEMS

A. SCHOFIELD AND D. CONNOLLY

Recent re-examination of the established International Atomic Energy Agency (IAEA) classification scheme of uranium deposit styles by Skirrow *et al.* (2009) has led to the identification of three broad families of uranium mineral systems. Of these, magmatic-related (and magmatic-hydrothermal) uranium systems are one end member. These systems fundamentally involve igneous processes, including partial melting and magmatic evolution. Uranium deposition may take place directly from the magma or from a hydrothermal fluid exsolved from the magma. This differentiates magmatic-related uranium systems from other deposits also involving a genetic link with igneous rocks such as iron oxide-copper-gold-uranium and metasomatic systems (Figure 3.0.1).

On a simplistic level, magmatic-related uranium mineral systems may be subdivided into two broad categories, orthomagmatic and magmatic-hydrothermal. In reality, true orthomagmatic uranium mineral systems are probably exceedingly rare because most deposits genetically associated with igneous rocks show evidence of fluid interaction. No distinction has been made during this assessment between true orthomagmatic mineral systems and those which incorporate some kind of hydrothermal fluid phase. This more inclusive approach differs slightly from that employed during the assessment for magmatic-related uranium mineral systems in north Queensland (Schofield and Huston, 2010).

3.5.1 Deposit overviews

Several notable examples of magmatic-related uranium mineralisation occur globally. The best known are the intrusive-related deposits at Rössing in Namibia (e.g., Berning *et al.*, 1976), Ross Adams in Alaska (Thompson *et al.*, 1982; Thompson, 1988) and Kvanefjeld in Greenland (e.g., Sørensen, 2001), along with the volcanic-related deposits associated with the Streltsovka caldera in Russia (e.g., Chabiron *et al.*, 2003). Although Australia possesses widespread uranium-rich igneous rocks spanning a wide range of geological time (Lambert *et al.*, 2005; Schofield, 2009), magmatic-related uranium deposits are rare. Uranium mineralisation related to volcanics is known from north Queensland, while South Australia is host to most of the known occurrences of intrusive-related uranium mineralisation in Australia (McKay and Miezitis, 2001).

3.5.1.1 Magmatic-related uranium deposits of the Olary Domain

The Olary Domain forms a component of the Proterozoic Curnamona Province and is host to a number of uranium deposits genetically related to felsic igneous magmatism. The largest and best known of these is the Crocker Well deposit which was detected initially during an airborne radiometric survey flown in 1951 by the Department of Mines, South Australia (now Primary Industries and Resources South Australia (PIRSA)). Following the initial detection of the radiometric anomaly, the deposit was the subject of extensive fieldwork and diamond drilling during the 1950s by the Department of Mines. Exploration was continued by a number of mineral exploration companies. Latest estimates indicate a total resource of 4.75 Mt of U_3O_8 at a grade of 513 ppm U_3O_8 (www.pepinnini.com.au).

The Crocker Well deposit is hosted by metaluminous to slightly peraluminous, sodic trondhjemite to monzogranite (Fricke, 2008). The granites were emplaced during the waning stages of the Olarian Orogeny (Fricke and Conor, 2010) and are thought to be derived from melting of Willyama Group metasediments, with some mantle input (Barovich and Foden, 2002; Fricke, 2008; Fricke and Conor,

2010). The granitic rocks are intruded by numerous alaskitic dykes, which show elevated radioactivity and correspond closely to the distribution of mineralisation (King, 1954). The depth of granite emplacement was approximately 7 to 10 km (Ashley, 1984). The granitic rocks hosting mineralisation have been dated at 1579.2 ± 1.5 Ma (Ludwig and Cooper, 1984). Brannerite from Crocker Well yielded scattered and discordant ages, but results are broadly consistent with the age of the host granite (Ludwig and Cooper. 1984). As well as this temporal link between magmatism and mineralisation, early workers inferred a genetic link as well (Campana and King, 1958).

The main uranium-bearing mineral is predominately thorium-rich brannerite, and is hosted in phlogopite-rich breccias (considered to be syn-magmatic by King, 1954 and Campana and King, 1958) and in veins and fractures, with minor amounts of disseminated ore (King, 1954; Campana and King, 1958; Ashley, 1984). Ashley (1984) considers the disseminated mineralisation to have affinities with porphyry copper and stockwork molybdenum deposits, although hydrothermal alteration at Crocker Well is not well developed (Ashley, 1984). Uranium mineralisation is associated with phlogopite, rutile, apatite, fluorite and xenotime (King, 1954; Whittle, 1954). Faults appear to have a control on the distribution of mineralisation (King, 1954; Campana and King, 1958; Wilson and Fairclough, 2009).

Despite the lack of pervasive alteration, mineralisation at Crocker Well is considered to be magmatic-hydrothermal in origin. The following genetic history is suggested by Ashley (1984).

- Local fluid saturation occurred at depth, leading to an increase in volatile (F and Cl) activity. Due to the depth of emplacement, mechanical fracturing was minor.
- The exsolved volatiles facilitated transfer of uranium from the host magma to the fluid phase.
- Deposition of uranium was facilitated by destabilisation of ligands and temperature reduction, resulting in brannerite mineralisation.

Other uranium prospects in the Olary Domain (Mount Victoria and Radium Hill) have been described as metamorphic-related systems, but bear a close relationship to intrusive igneous rocks (McKay and Miezitis, 2001; Wilson and Fairclough, 2009).

3.5.1.2 The Rössing deposit

The Rössing deposit in Namibia is the best known example of orthomagmatic uranium mineralisation globally, and more than 90 000 tonnes of uranium have been extracted to date (Cuney and Kyser, 2008). Although high in tonnage the Rössing deposit is low grade, with an average uranium grade of 300 ppm (Cuney and Kyser, 2008). Other examples of mineralisation similar to that at Rössing include Steward Lake in Canada, the Litsk district in Russia and the Mortimer Hills prospect in the Gascoyne Region of Western Australia (Carter, 1982; Cuney and Kyser, 2008).

Mineralisation is hosted by alaskitic pegmatites emplaced during the final stages of peak metamorphism (Kinnaird and Nex, 2007). The alaskites are interpreted to be derived from low degree partial melting of underlying metasediments (for example, see Cuney and Kyser, 2008). Calculated zircon saturation temperatures suggest that magmatic temperatures were low (about 675° to 700^{o}C; McDermott *et al.*, 1996).

Uranium does not correlate with other elements, which has led some (Nex *et al.*, 2001; Kinnaird and Nex, 2007) to interpret that uranium enrichment did not result from fractional crystallisation processes. However, the observed geochemical trends may be expected with post-magmatic remobilisation of uranium, which has been observed at Rössing (Nex *et al.*, 2002). These features have led Cuney and Kyser (2008) to propose a genetic model for the Rössing deposit consisting of

low degree partial melting of uraniferous metasedimentary basement. This liberated large quantities of uranium into the melt, which was locked into the alaskites when they were rapidly crystallised. Thus, Rössing may be defined as truly orthomagmatic, with some secondary remobilisation of uranium. This being the case, efficient liberation of uranium from a radiogenic source region becomes important.

Several difficulties are associated with the model outlined above. Although the geochemical evidence suggests that fractionation was not an important process in uranium concentration, the other geochemical features of the Rössing alaskites are similar to those found in strongly fractionated granites, if post-magmatic redistribution of uranium is allowed for. Further, the aluminium saturation index of the Rössing alaskites is low for rocks derived from melting of sedimentary protoliths (Cuney and Kyser, 2008), although the authors explain this by invoking partial melting of weakly peraluminous quartzofeldspathic sediments or acidic volcanics. Because of the persistent uncertainty in the genetic model and the lack of datasets available to indicate the key components of the Rössing deposit (e.g., alaskite distribution), this particular style of magmatic uranium system will not be dealt with in this study.

3.5.1.3 The Ross Adams and Kvanefjeld deposits

The Ross Adams deposit, situated in the Bokan Mountain Granite Complex in Alaska and the Kvanefjeld deposit located in the Ilímaussaq alkaline complex of Greenland are similar in many aspects and, as a result, are treated together. Both deposits are hosted by peralkaline granites with high sodium (Thompson *et al.*, 1982; Bailey *et al.*, 2001). This feature leads to high solubility levels for high field strength elements, including uranium. This feature, coupled with very high degrees of differentiation (up to 99% at Ilímaussaq; Thompson *et al.*, 1982; Bailey *et al.*, 2001), has resulted in magmas high in high field strength elements, rare-earth-element and volatiles (Bailey *et al.*, 2001; Cuney and Kyser, 2008). Both deposits are also hosted in igneous rocks emplaced at high crustal levels of 2 to 4 km for Ross Adams (Thompson *et al.*, 1982) and 2 to 3 km for Kvanefjeld (Sørensen, 2001).

Uranium mineralisation at Ross Adams occurs predominately in pipe-like orebodies along granite phase contacts and syn-magmatic faults and is localised in fractures (Thompson, 1988). Mineralisation also occurs as veins (the I and L vein system; Staatz, 1978) which extend up to 2.6 km from the granite margin. Mineralisation is thought to have occurred coincidentally with devolatilisation of the magma chamber as it ascended to a high crustal level, resulting in the release of water, carbon dioxide, hydrogen sulfide and fluorine (Thompson, 1982). Alteration consists mainly of albitisation, as well as chlorite, fluorite, calcite, quartz, sericite and tourmaline (Thompson *et al.*, 1982; Thompson, 1988). Stable isotope studies on hydrothermal calcite are consistent with a magmatic origin (Thompson, 1988). Because calcite is associated with fluorite, and because of the overall high fluorine nature of the magma, it is reasonable to suggest that uranium may have been transported as a fluoro complex. Ore deposition is interpreted to have occurred as a response to cooling and the development of localised reducing conditions (Thompson, 1988).

Mineralisation at Kvanefjeld is largely hosted by disseminated steenstrupine ($Na_{14}Ce_6Mn_2Fe_2(Zr,Th,U)(Si_6O_{18})_2(PO_4)_7.3H_2O$; Cuney and Kyser, 2008), which presents metallurgical difficulties in extracting uranium. Mineralised veins are also present at Kvanefjeld, and reflect the exsolution of a late magmatic fluid phase (Cuney and Kyser, 2008).

3.5.1.4 Volcanic-related uranium deposits

Uranium mineralisation bearing a genetic association with volcanic rocks constitutes an important expression of the magmatic-related family of uranium systems globally. The Streltsovka Caldera in Russia is the largest uranium deposit related to volcanic rocks (Chabiron *et al.*, 2003) and has a uranium resource of greater than 232 000 tonnes (Laverov *et al.*, 1992, cited in Cuney and Kyser, 2008). A recent review of deposits associated with volcanic rocks has been published by Nash (2010) and, as a result, a description of deposit examples will not be included here. However, the following describes some of the key geological and geochemical features common to many volcanic-related uranium systems.

Mineralisation in volcanic-related uranium systems is typically associated with rhyolitic rocks, especially those with alkaline affinities and high fluorine (Nash, 2010). For example, peralkaline rhyolites from Streltsovka have Na+K/Al exceeding 1.04 and fluorine contents greater than 1.4% (Chabiron *et al.*, 2001). These geochemical features allow for extremely high uranium solubilities in the magma (Peiffert *et al.*, 1996). Such magmas remain strongly undersaturated with respect to uranium, allowing it to partition into the matrix rather than phenocryst phases.

Observations from known volcanic-related uranium deposits reveal a strong correlation between uranium and the glassy matrix of the volcanics (George-Aniel *et al.*, 1991; Chabiron *et al.*, 2003). Located in such a way, uranium is highly available to leaching by hydrothermal fluids and may form concentrated deposits. Mass balance calculations by Chabiron *et al.* (2003) show that approximately 300 000 tonnes of uranium may have been leached from the Streltsovka rhyolites. Fluid flow along structural pathways is common to many volcanic-related deposits (Nash, 2010), and may express itself in clay and mica alteration (George-Aniel *et al.*, 1991; Cunningham *et al.*, 1994; Chernyshev and Golubev, 1996). Deposition of uranium from the fluid may occur via a range of potential mechanisms, including reduction, destabilisation of ligands or other physical processes (Nash, 2010). As a result, volcanic-related uranium systems may not be truly orthomagmatic, but rather magmatic-hydrothermal, and may have considerable hybrid characteristics, depending on the origin of the fluid phase (Figure 3.0.1).

3.5.2 Mineral systems model for magmatic-related uranium mineral systems

Summary mineral systems models for both intrusive-related and volcanic-related uranium mineral systems have been given by Schofield (2010b). This has only been slightly modified in the present study and, as a result, only a brief summary of each will be given.

3.5.2.1 Mineral systems model for intrusive-related uranium systems

The mineral systems model for intrusive-related uranium systems is relatively simple. The source magmas for both the Kvanefjeld and Ross Adams deposits in Greenland and Alaska respectively are peralkaline in composition and are derived from partial melting of the upper mantle. Crustally-derived magmas may also be favourable, especially high-temperature I-type and A-type magmas. S-type magmas, derived from partial melting of sedimentary or supracrustal rocks, are considered less favourable (Plant *et al.*, 1999), despite the association of uranium mineralisation with S-type melts at Rössing in Namibia.

Initial uranium content in these melts will be governed by the magma source region. Those melts derived from radiogenic regions are more favourable. Melting at high temperature is desirable because it allows uranium in the source region to be liberated into the melt. If magmatic temperature

is low, then a significant quantity of uranium will be locked up in restite phases, such as zircon, and will be unavailable to progressive concentration. Magmatic-stage concentration of uranium is most commonly associated with fractional crystallisation in the presence of high uranium solubility. Fluid phases exsolved from the magma also may contain appreciable uranium.

Fractionation alone is not likely to generate sufficient enrichment of uranium, necessitating a means of preferentially depositing uranium in a concentrated way. The processes of uranium deposition at high temperature are poorly understood. Uranium deposited from uranium-bearing magmatic-hydrothermal fluids may occur within the igneous rock itself, in the surrounding host rocks or in hydrothermal veins, such as the I and L vein system at Ross Adams (Staatz, 1978).

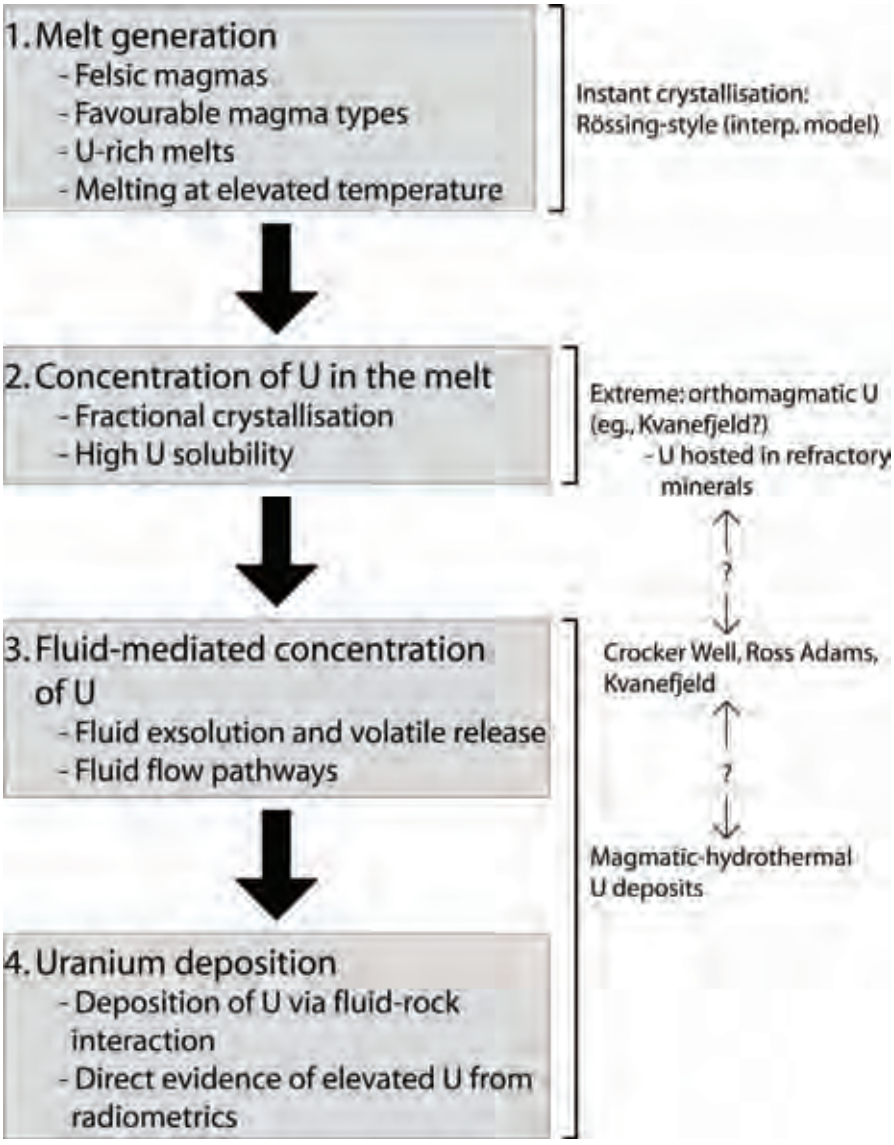

Figure 3.5.1: *Schematic mineral systems model for intrusive-related uranium systems.*

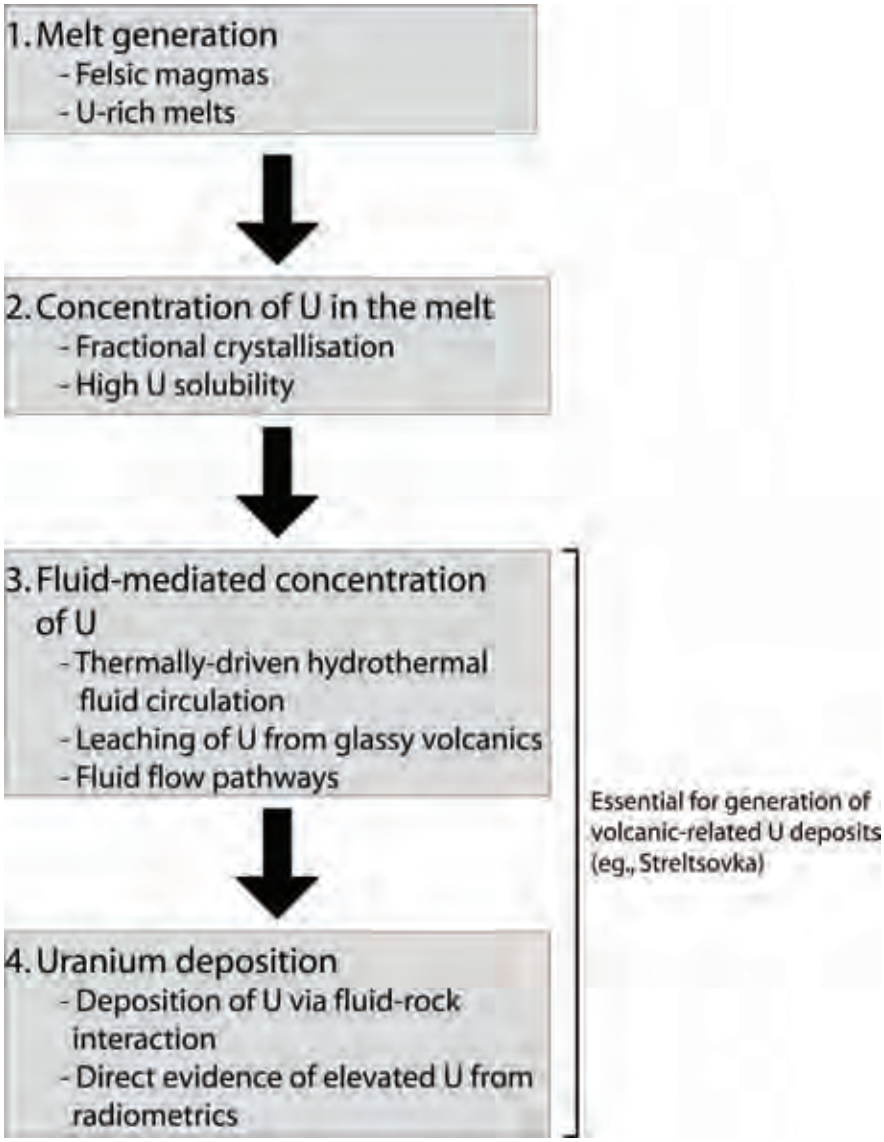

Figure 3.5.2: *Schematic mineral systems model for volcanic-related uranium systems.*

3.5.2.2 Mineral systems model for volcanic-related uranium systems

The volcanic-related uranium mineral system requires, at a fundamental level, the presence of suitable volcanic rocks. These will be of a broadly felsic composition and will ideally be extruded in a caldera setting. It is not entirely necessary that these volcanics contain very high uranium, because unaltered volcanics associated with uranium mineralisation in Mexico typically contain up to 10 ppm uranium (George-Aniel *et al.*, 1991). However, those magmas which have undergone uranium enrichment via fractional crystallisation will be more favourable targets.

The most important component of the volcanic-related uranium mineral systems model is leaching by hydrothermal fluids. This is most easily accomplished in volcanic rocks with a high proportion of finely crystalline matrix, or in highly glassy rocks. High uranium solubility allows for uranium to be partitioned into this glassy matrix, allowing it to be readily stripped out and concentrated. These magmas will be highly alkaline and/or have high fluorine.

Leaching and redeposition of uranium may take place broadly contemporaneous with igneous activity, or may occur post-volcanism. Likewise, the fluids involved in leaching uranium may be derived from diverse sources. Faults, zones of rheological contrast, breccia zones or fractures may act as fluid flow pathways. Deposition of uranium may occur as a result of pressure-temperature variations, changes in ligand stability or other localised chemical controls, such as reduction (Skirrow *et al.*, 2009).

Using these mineral systems frameworks, the generalised mineral systems models shown in Figures 3.5.1 and 3.5.2 are able to be translated into prospectivity criteria. These are outlined below.

3.5.3 Mineral systems assessment

The final assessment for magmatic-related uranium is shown in Plates 3.6 (intrusive-related) and 3.7 (volcanic-related). These have been produced by combining separate prospectivity maps for the sources, drivers, fluid pathways and architecture and deposition as discussed in Section 3.1. Table 3.5.1 lists the mappable criteria used to derive the individual systems component maps.

Largely, mappable criteria for magmatic-related uranium systems have been developed using solid geology and geochemical data. The solid geology coverage used in this assessment has been slightly modified from that of Cowley (2006). Igneous units, or units with a major igneous component, have been extracted from this dataset for the purposes of this study. Three main modifications have been made:

- Reclassification of the Crocker Well Suite as a distinct entity to the Bimbowrie Suite;
- Reclassification of the Hiltaba Suite into an east and west component as a result of varying geochemical characteristics (Neumann *et al.*, 2000; D. Champion, *pers. comm.*). (Hiltaba Suite granitoids east of 136.55° are designated as eastern Hiltaba Suite); and
- Reclassification of one unit of the Bimbowrie Suite as a separate entity, as suggested by Schofield (2010a).

Because the solid geology dataset used often lists greater than one unit present in a polygon, individual polygons have been given an overall rating for each criterion. The value assigned to the polygon is the highest value of the units present within it. As a result, although a polygon may contain some lowly-rated units, it may still be given a high rating because of the presence of a favourable constituent unit.

Geochemical data have been compiled from Geoscience Australia's OZCHEM dataset and PIRSA's geochemical dataset (accessed via http://www.pir.sa.gov.au/minerals/sarig). Geochemical data were filtered for non-igneous samples and duplicate data, and were combined into a single consistently-formatted dataset.

Where geochemical data are used, the confidence factor has been determined based on the number of samples used for the criterion. Units with ≤4 data points were given a C value of 0.25, 5-9 data points were assigned a value of 0.5, 10-19 data points correspond to a value of 0.75, and ≥20 data points are given a value of 1.0.

A number of criteria require the identification of high values from geochemical datasets. For the present study, the threshold for high values has been set at the 75th percentile value. To calculate this value, geochemical samples were subdivided into intrusive and extrusive rocks and unsuitable samples (e.g., altered or weathered rocks, mafic rocks) were excluded from the analysis as far as possible. Geochemical data for each individual unit (based on stratigraphic unit number) were then assessed to determine whether the unit in question had a dominantly high character.

For many geochemical criteria, data distribution is variable. This is especially the case with fluorine analyses. To address occurrences of no data associated with some units, A and C values were averaged for felsic units containing data and the value assigned to units lacking data. The I value was not attributed, as this is set for each mappable criterion. This step ensured that the assessment was not biased unduly toward data-rich regions and is especially applicable when considering igneous rocks buried under cover. Values of zero were substituted for a nominal value of 0.001 during this assessment.

3.5.3.1 Sources

The primary sources of uranium in magmatic-related uranium systems are the igneous rocks themselves. Primary mantle melts have very low uranium contents and, as a result, are unsuitable as targets for magmatic-related uranium mineralisation. For example, mid-ocean ridge basalts have a uranium content of 0.047 ppm (Sun and McDonough, 1989). As a result, magmas which have not undergone at least one episode of uranium concentration are unsuitable as potential targets for magmatic-related uranium mineralisation. These are mapped by the distribution of broadly felsic igneous rocks (Figure 3.5.3), which was determined using unit descriptions contained within the solid geology dataset. Uranium-rich igneous rocks (Figure 3.5.4) were identified from geochemical data. High uranium was defined as greater than the 75th percentile value for intrusive and volcanic rocks (10 and 8 ppm respectively).

Progressive remelting of crustal rocks which have already undergone a prior episode of uranium concentration will generally allow for more uranium enriched melts. However, it is important that available uranium is released into the melt during this melting. Consequently, high-temperature melts are used as a criterion for both intrusive-related (Figure 3.5.5) and volcanic-related (Figure 3.5.6) uranium systems, although they are treated separately. Temperatures are based on the zircon saturation temperature and calculated according to Watson and Harrison (1983). High temperatures are defined as greater than the 75th percentile for intrusive and volcanic rocks (831° and 883°C respectively).

For the intrusive-related system, high-temperature melts have been used to map the breakdown of uranium-bearing mineralogy in the magma source region. This allows for the melt to be enriched in uranium, and results in the generation of restite-poor granites, which permits further uranium

concentration with fractional crystallisation. The volcanic-related system utilises high-temperature melts to map volcanic rocks with uranium available to leaching by hydrothermal fluids because rocks which erupted at high temperatures are more likely to be glassy, and so more susceptible to leaching by hydrothermal fluids.

At the magmatic stage, fractional crystallisation is the most suitable mechanism for concentrating uranium in the melt. As mentioned above, the host rocks to the Kvanefjeld and Ross Adams deposits show evidence of very strong fractional crystallisation having taken place. Fractionated igneous rocks (Figure 3.5.7) were identified using the rubidium-strontium-barium triangular plot of El Bouseily and El Sokkary (1975) and high rubidium-strontium values, following a similar method to Champion and Heinemann (1994).

From the key deposit features described above, it is apparent that magmas with high uranium solubilities (to the result of peralkalinity or high halogen concentrations) are important in the mineral system (e.g., Thompson *et al.*, 1982; Peiffert *et al.*, 1996; Bailey *et al.*, 2001; Chabiron *et al.*, 2001). In the case of intrusive-related uranium systems, high uranium solubility allows uranium to be concentrated with progressive fractionation. This process is applicable also to volcanic-related uranium systems. However, it is critical also for generating a readily leachable uranium source because it allows uranium to be partitioned into the final melt components, which may then crystallise into a fine-grained or glassy matrix.

The identification of igneous rocks with high uranium solubility (Figure 3.5.8) is primarily based on fluorine concentration, as determined from geochemical data. Peralkaline igneous rocks are more favourable, but none were identified in the study area. The 75th percentile threshold for high fluorine is 1754 ppm for intrusive igneous rocks and 1800 ppm for volcanic rocks. Since fluorine is rarely analysed for, the presence of fluorite has been used to infer high fluorine concentrations. It was not possible to distinguish primary fluorite from secondary products, which has been reflected in the low C value. Similarly, A-type granites are commonly high in fluorine (Loiselle and Wones, 1979) and these have been used also to infer high fluorine contents in the absence of data. Note that this does not conflict with A-type rocks included in the criterion for favourable magma types (see below) because it has been used only as a proxy for high fluorine in the absence of other, more reliable data.

Favourable magma types are a criterion specific to intrusive-related systems (Figure 3.5.9). Magma types (i.e., A-type, I-type and S-type granites) have been determined from geological unit descriptions, Geoscience Australia's Stratigraphic Units Database (http://www.ga.gov.au/products-services/data-applications/reference-databases/stratigraphic-units.html), Drexel *et al.* (1993), Drexel and Preiss (1995), and geochemical characteristics.

The final weighting for the source systems component is shown in Figure 3.5.10.

Table 3.5.1. Theoretical and mappable criteria for magmatic-related uranium systems

MINERAL SYSTEM COMPONENT	TARGETED SYSTEM	CRITERIA		DATASET	IMPOR-TANCE	APPLIC-ABILITY	CONFI-DENCE	WEIGHT
		THEORETICAL	MAPPABLE					
1. Source of uranium	Intrusive and volcanic	Distribution of broadly felsic igneous rocks	Felsic igneous rocks	Solid Geology of South Australia (Cowley, 2006)	0.75	1.00	1.00	0.750
			Rocks with a felsic igneous component		0.75	0.50	1.00	0.375
	Intrusive	Distribution of favourable magma types	I- or A-type rocks	Solid Geology of South Australia (Cowley, 2006); literature review; geochemical data	0.5	0.75	0.75	0.281
			S-type rocks		0.5	0.25	0.75	0.094
	Intrusive and volcanic	Presence of U-enriched igneous rocks	Igneous rocks with high U contents	Solid Geology of South Australia (Cowley, 2006); geochemical data	0.75	0.75	0.25 – 1.00	0.141 – 0.563
	Intrusive and volcanic	Magmatic-stage U concentration via fractional crystallisation	Geochemical indicators suggesting fractionation	Solid Geology of South Australia (Cowley, 2006); geochemical data	0.75	0.75	0.25 – 1.00	0.141 – 0.563
			Uncertain degree of fractionation		0.75	0.50	0.25 – 1.00	0.094 – 0.375
	Intrusive	Breakdown of U-bearing minerals in magma source region	Intrusive igneous rocks with high zircon saturation temperatures	Solid Geology of South Australia (Cowley, 2006); geochemical data	0.50	0.50	0.25 – 1.00	0.063 – 0.250
	Volcanic	Volcanic rocks with U available to leaching by hydrothermal fluids	Volcanic rocks with high zircon saturation temperatures	Solid Geology of South Australia (Cowley, 2006); geochemical data	1.00	0.50	0.25 – 1.00	0.125 – 0.500
	Intrusive and volcanic	Igneous rocks with high U solubility	Igneous rocks with high F	Solid Geology of South Australia (Cowley, 2006); geochemical data	0.75	0.75	0.25 – 1.00	0.141 – 0.563
			Igneous rocks with fluorite		0.75	0.50	0.50	0.188
			A-type igneous rocks		0.75	0.25	0.75	0.141
2. Drivers	Intrusive	Fluid exsolution and volatile release	Presence of textural features indicating fluid exsolution (e.g., miarolitic cavities)	Solid Geology of South Australia (Cowley, 2006); literature review	0.75	1.00	0.75	0.5625
			Units with good evidence for high-level intrusion		0.75	0.75	0.75	0.422
			Units with moderate evidence for high-level intrusion		0.75	0.50	0.75	0.281
			Units with poor evidence for high-level intrusion		0.75	0.25	0.75	0.141
			Units with evidence for volatile release (breccias, greisens and veins)		0.75	0.75	0.75	0.422
	Volcanic	Thermally-driven hydrothermal fluid circulation	Intrusive igneous rocks co-magmatic with volcanic units	Solid Geology of South Australia (Cowley, 2006)	0.75	0.50	0.50	0.188
3. Pathways and architecture	Intrusive and volcanic	Fluid flow along permeable structures	2.5 km buffer around well-constrained faults	Solid Geology of South Australia (Cowley, 2006)	0.75	0.50	0.75	0.281
			2.5 km buffer around poorly-constrained faults		0.75	0.25	0.75	0.141
4. Depositional Mechanisms	Intrusive and volcanic	Direct evidence of elevated U	U^2/Th values one standard deviation above the mean for each unique geological unit	1:1 000 000 scale Surface Geology of Australia (Whitiker *et al.*, 2008); Radiometric Map of Australia (Minty *et al*., 2010)	0.50	0.75	1.00	0.375
			U^2/Th values two standard deviation above the mean for each unique geological unit		0.50	0.50	1.00	0.25
	Intrusive and volcanic	Chemical depositional sites	Reactive host rocks dominant	Solid Geology of South Australia (Cowley, 2006)	0.50	0.75	0.75	0.28125
			Reactive host rocks present		0.50	0.50	0.75	0.1875

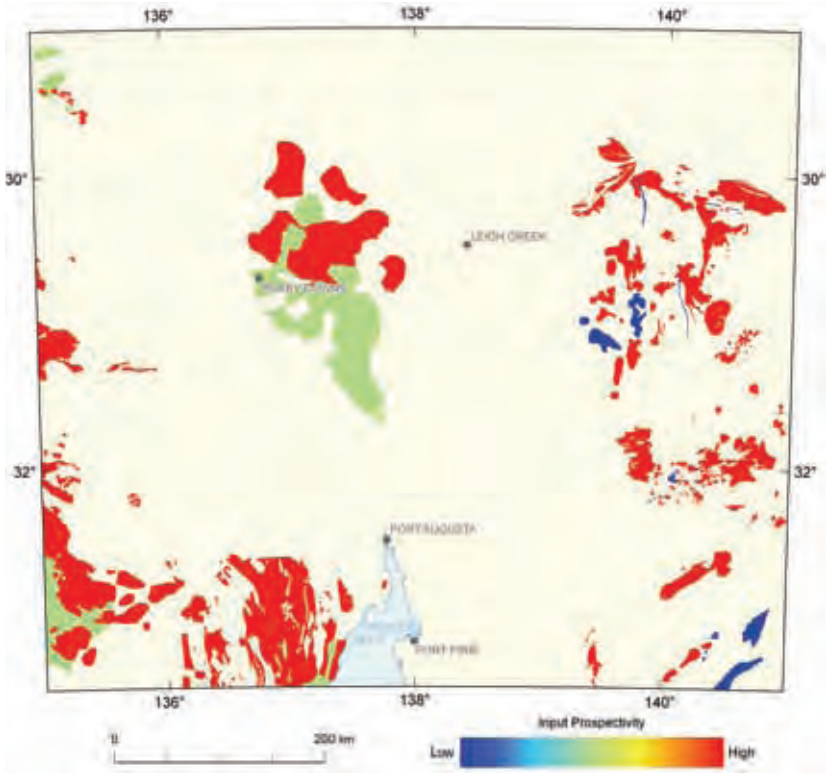

Figure 3.5.3a: *Variation in weighting for the distribution of broadly felsic igneous rocks criterion used in the assessment for intrusive-related uranium systems.*

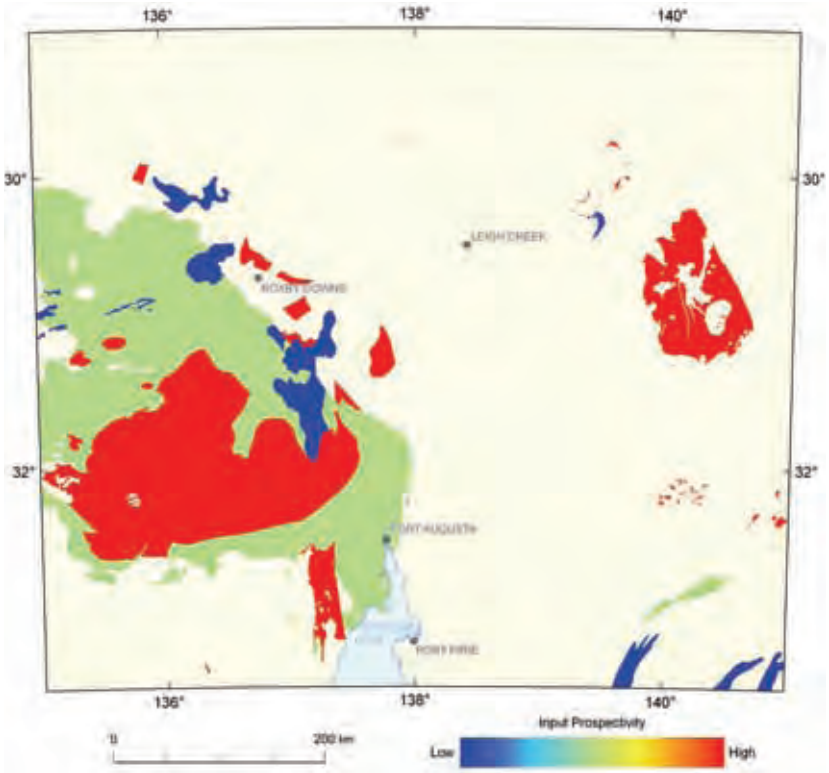

Figure 3.5.3b: *Variation in weighting for the distribution of broadly felsic igneous rocks criterion used in the assessment for volcanic-related uranium systems.*

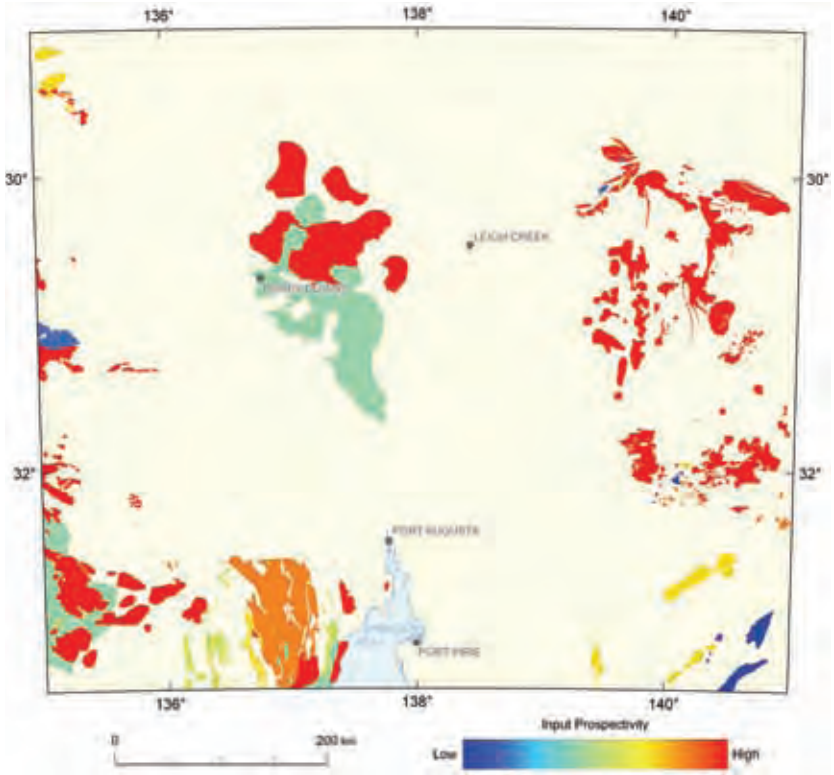

Figure 3.5.4a: *Variation in weighting for the distribution of uranium-enriched igneous rocks criterion used in the assessment for intrusive-related uranium systems.*

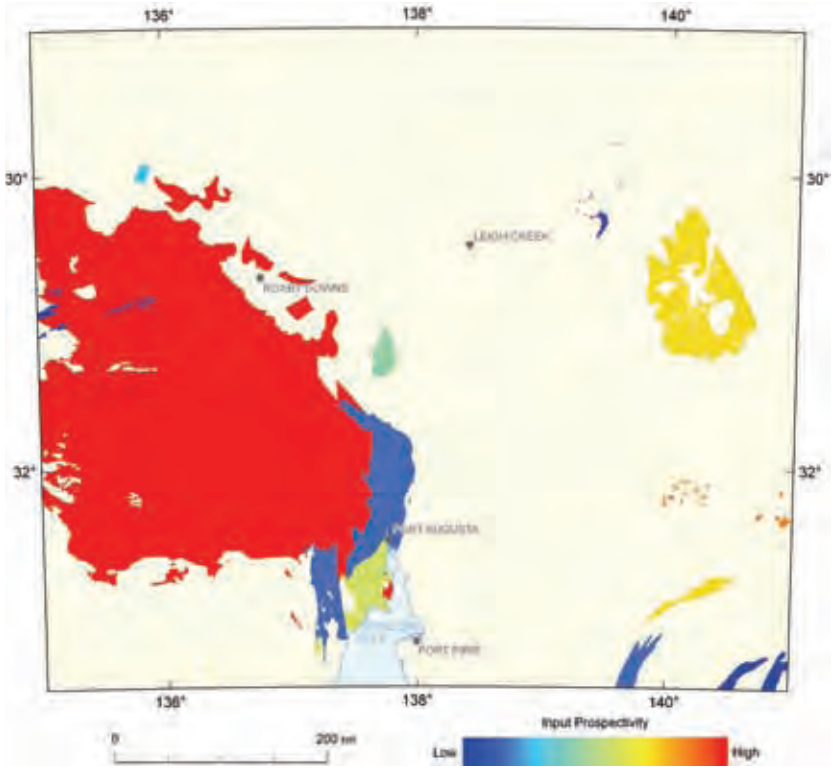

Figure 3.5.4b: *Variation in weighting for the distribution of uranium-enriched igneous rocks criterion used in the assessment for volcanic-related uranium systems.*

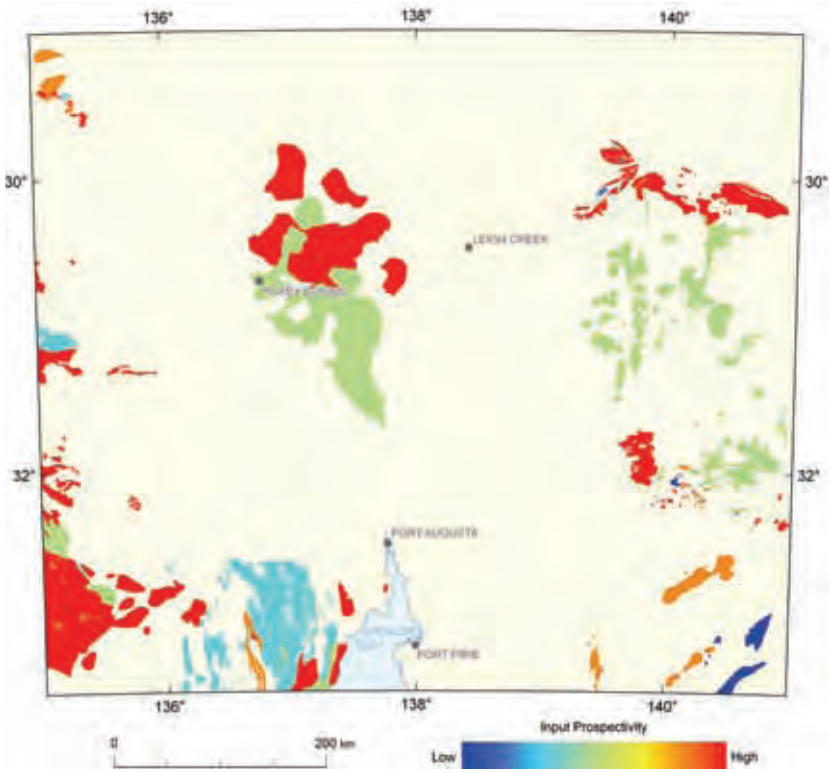

Figure 3.5.5: *Variation in weighting for the distribution of high-temperature intrusives criterion.*

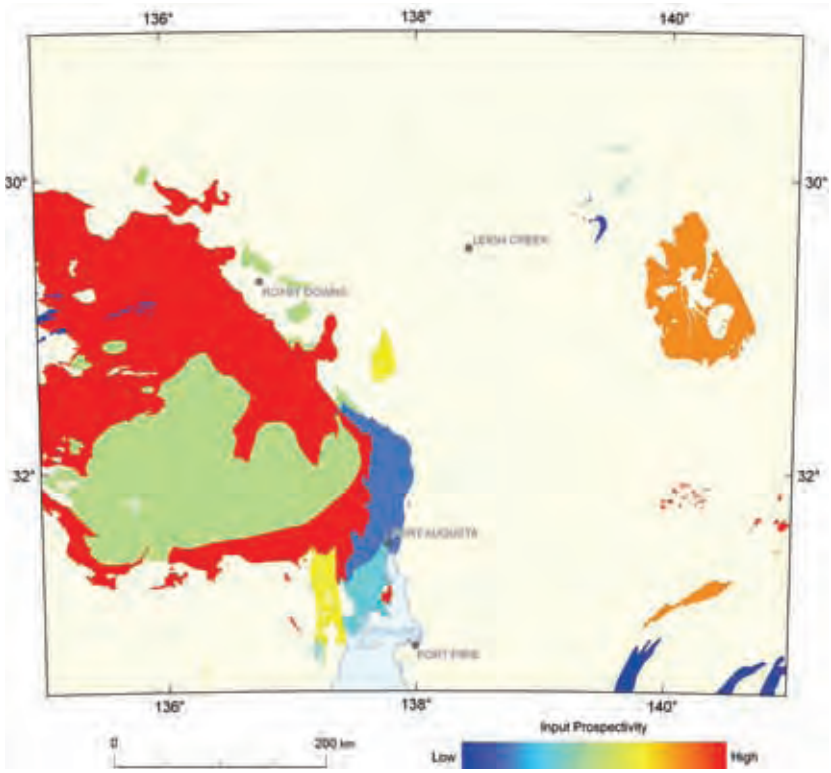

Figure 3.5.6: *Variation in weighting for the distribution of high-temperature volcanics criterion.*

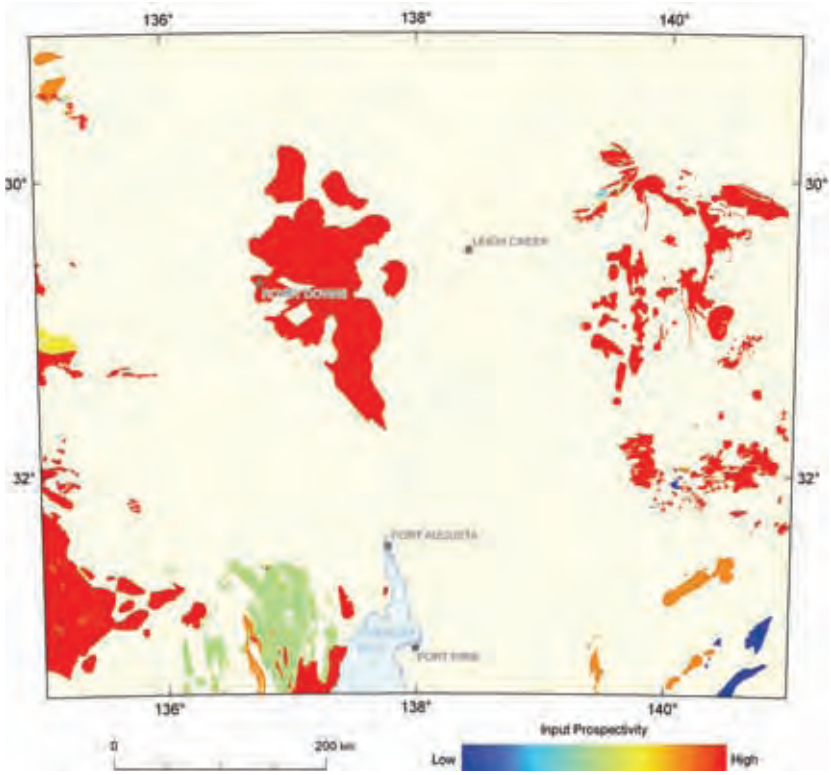

Figure 3.5.7a: *Variation in weighting for the distribution of fractionated igneous rocks criterion used in the assessment for intrusive-related uranium systems.*

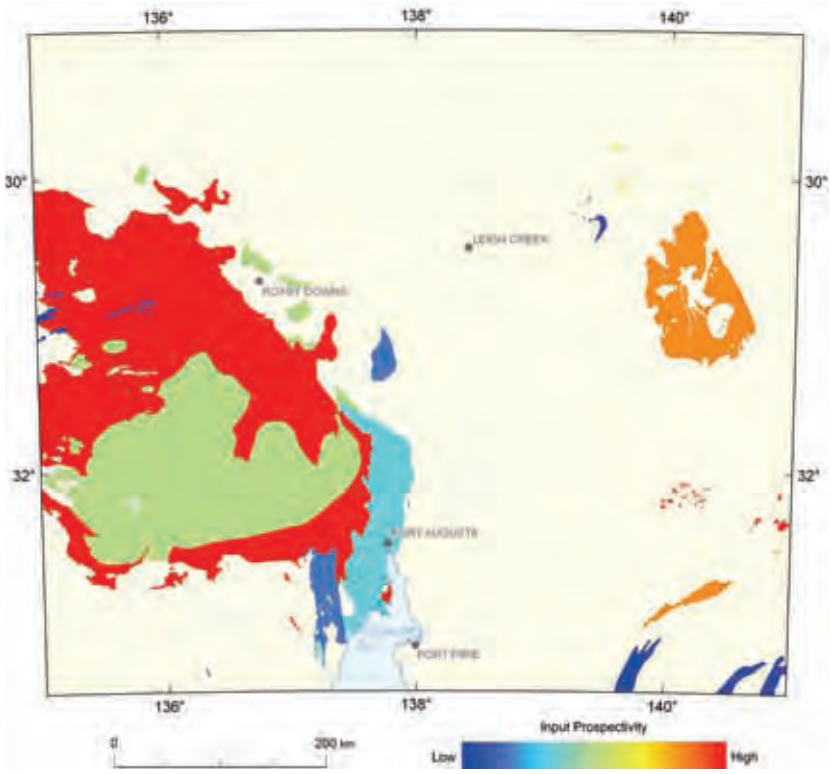

Figure 3.5.7b: *Variation in weighting for the distribution of fractionated igneous rocks criterion used in the assessment for volcanic-related uranium systems.*

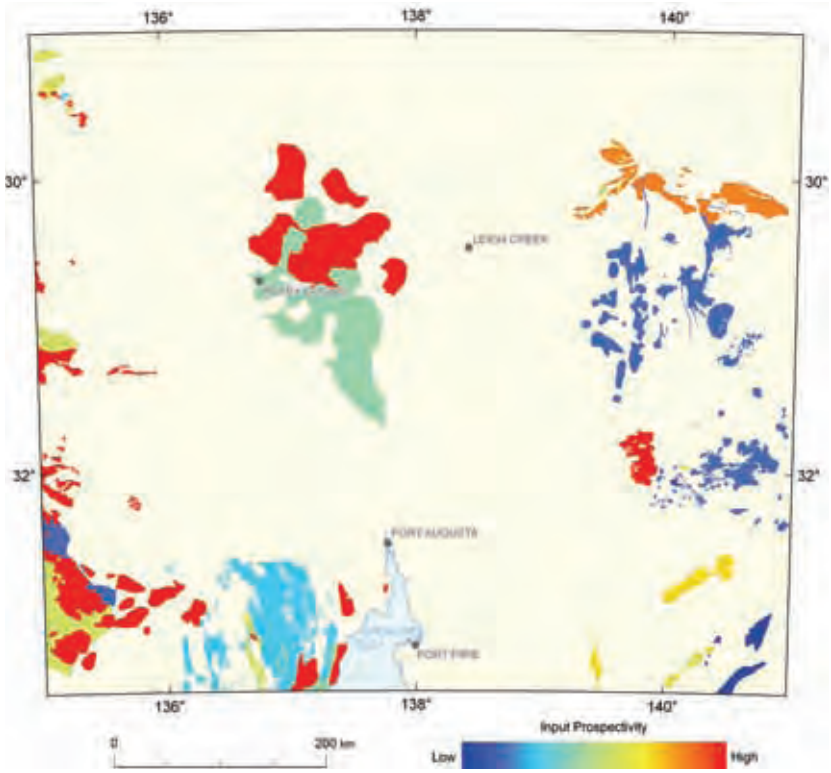

Figure 3.5.8a: *Variation in weighting for the distribution of igneous rocks with high uranium solubility criterion used in the assessment for intrusive-related uranium systems.*

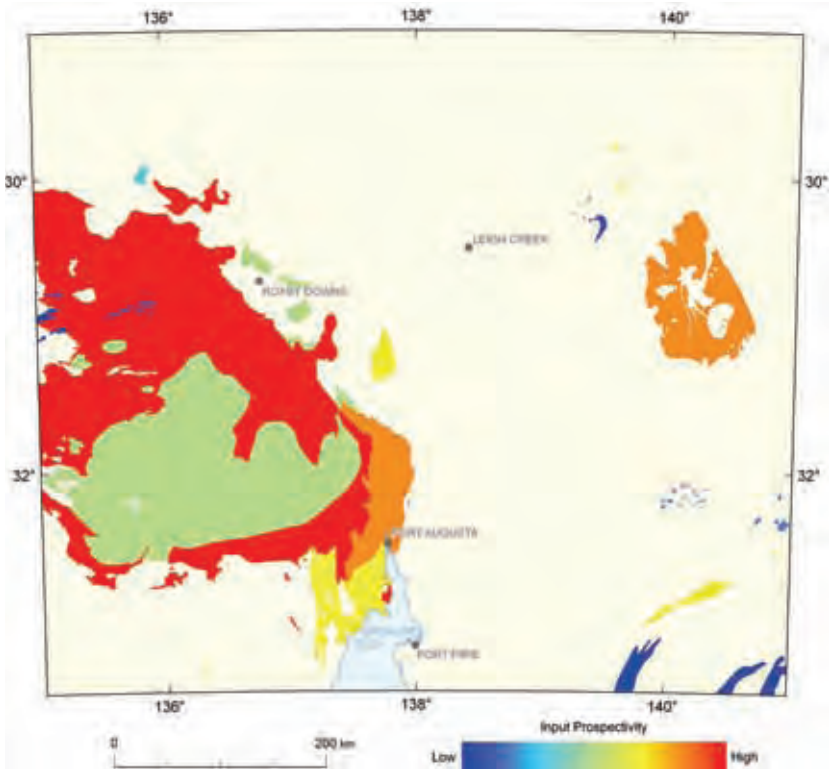

Figure 3.5.8b: *Variation in weighting for the distribution of igneous rocks with high uranium solubility criterion used in the assessment for volcanic-related uranium systems.*

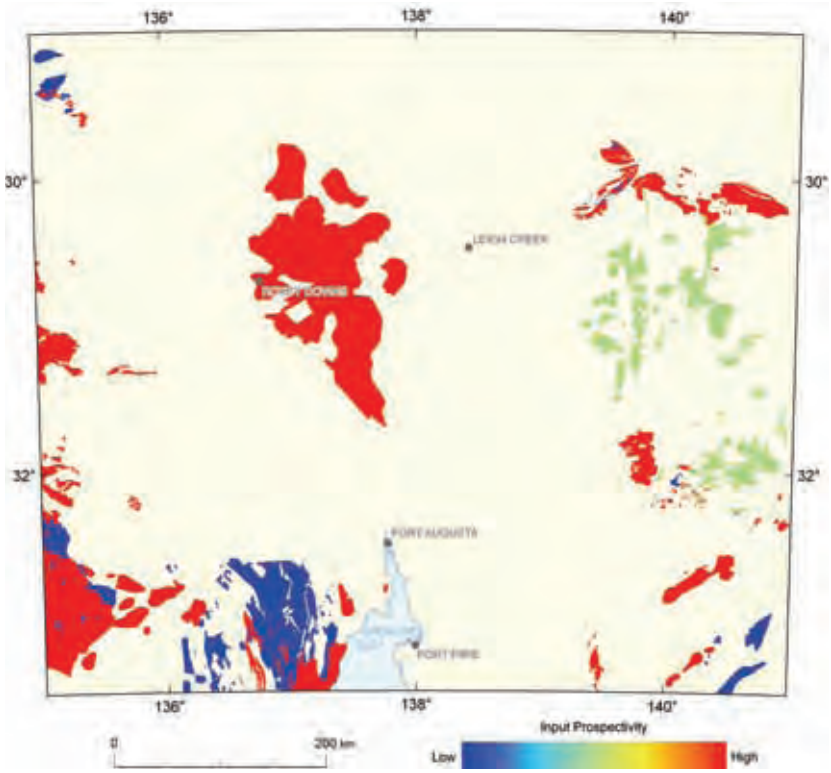

Figure 3.5.9: *Variation in weighting for the distribution of favourable magma types criterion for intrusive-related uranium systems.*

3.5.3.2 Drivers

Fluids in magmatic-related uranium mineral systems are primarily derived from the igneous rocks themselves (magmatic-hydrothermal). As a result, the fluid flow driver is related to exsolution processes. The intrusive-related and volcanic-related assessments each employ one criterion for the driver mineral systems component.

For intrusive-related uranium systems, this is driven by first boiling, or depressurisation of the magma either as a result of magma ascent or mechanical failure of the magma chamber (Candela, 1997). Three strands of evidence have been employed to map this criterion (Figure 3.5.11):

- Direct evidence for fluid exsolution, as represented by the presence of miarolitic cavities;
- Inferred evidence of fluid exsolution, as indicated by high-level granites, which are most likely to exsolve a magmatic fluid. Evidence for high-level intrusion has been rated as good (high-level or subvolcanic unit description), moderate (porphyritic granites), or poor (weakly porphyritic or uncertain evidence for high-level intrusion); and
- Evidence for volatile release, as indicated by the presence of breccias, greisens and veins.

Evidence for fluid exsolution and volatile release was determined from geological descriptions contained in digital geological layers and data from Budd *et al.* (2001).

In volcanic-related systems, fluid flow drivers may be more diverse because the fluid may be magmatic in origin, or may be derived from different sources (Figure 3.0.1). For example, meteoric water infiltration is suggested at Streltsovka in Russia by Chabiron *et al.* (2003). Fluids derived externally to the volcanic rock are driven by thermal gradients, likely from intrusions at depth (Nash, 2010).

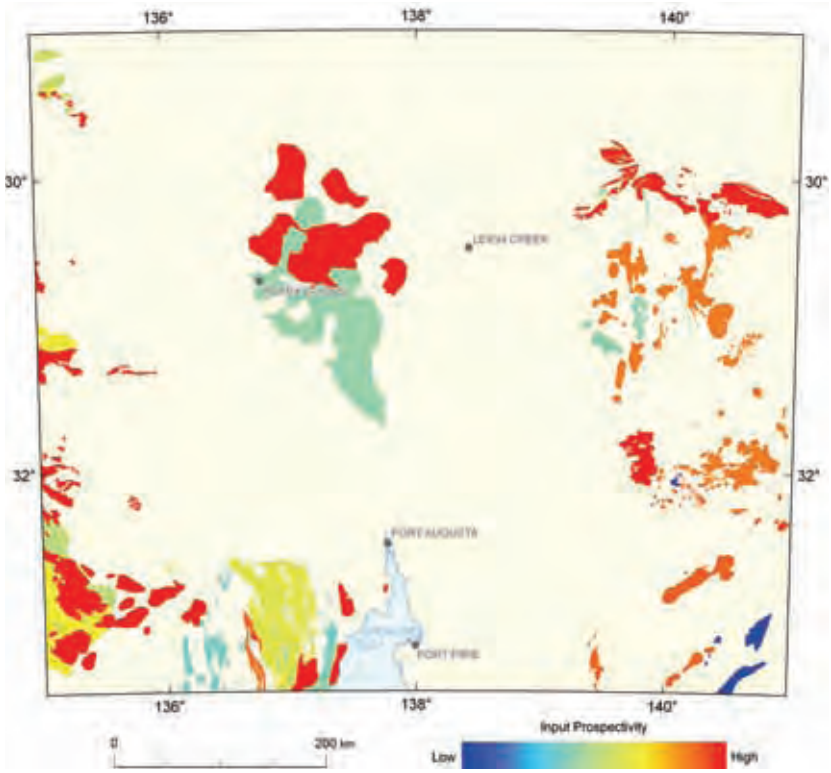

Figure 3.5.10a: *Variation in weighting for the source systems component for intrusive-related uranium systems.*

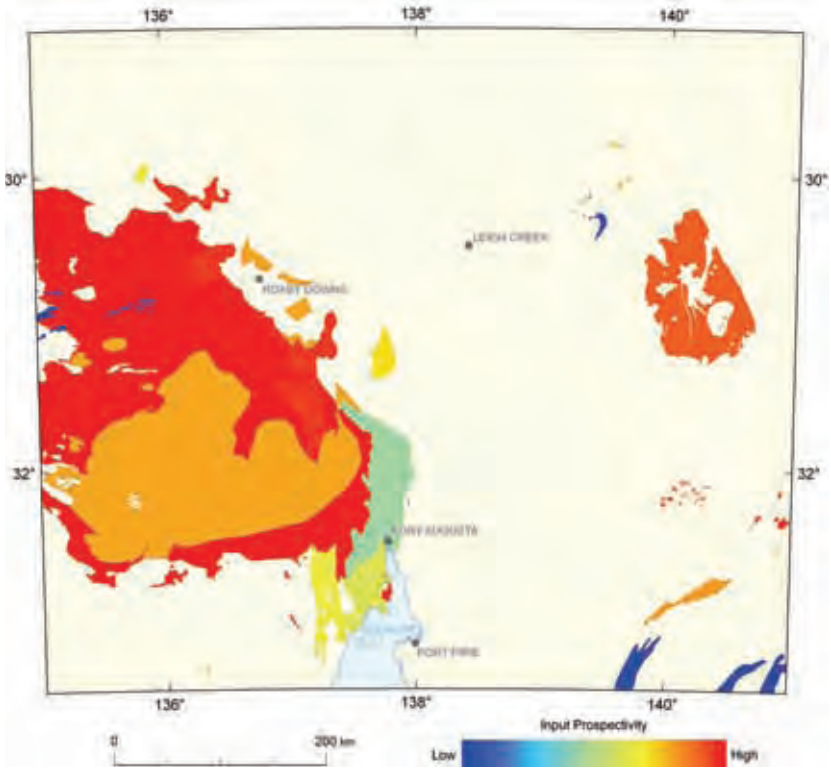

Figure 3.5.10b: *Variation in weighting for the source systems component for volcanic-related uranium systems.*

Co-magmatic intrusive igneous rocks were used to map the fluid flow driver for the volcanic-related uranium system (Figure 3.5.12). Co-magmatic intrusive and volcanic units were determined from time-space plots in Kositcin (2010). Intrusive units identified as potential drivers were extracted from the solid geology and buffered to 20 km. This distance was subjectively chosen after trialling several distance thresholds to allow the intrusive rocks to interact with their corresponding co-magmatic volcanic unit while not completely enveloping the unit. Because this criterion is time dependant, the generated buffers were only assigned I, A and C values where they overlap with co-magmatic volcanic rocks. Where this condition was not satisfied, a nominal value of 0.001 was assigned for A and C.

3.5.3.3 Fluid pathways and architecture

A structural control on ore formation has been observed at Crocker Well, Ross Adams and Streltsovka (King, 1954; Campana and King, 1958; Thompson, 1988; Chabiron *et al.*, 2003; Wilson and Fairclough, 2009). This suggests that these structures are important fluid flow pathways for uranium-bearing hydrothermal fluids.

Fluid flow pathways were mapped using faults extracted from the solid geology (Figure 3.5.13). These were categorised based on confidence in the spatial accuracy of the faults and buffered to a subjectively selected distance of 2.5 km. This distance was selected after testing several distance thresholds to permit a reasonably broad, but not unrealistic, zone of potential. Faults were filtered on the basis of interpreted age and were clipped to geological units corresponding to that age interval.

Lithological contacts may also act as fluid flow pathways. These have not been included in the assessment because of uncertainty in the precise location of lithological contacts in the solid geology data used. Although not used as a criterion in this assessment, the most apical parts of intrusions are the most favourable for concentrating magmatic fluids.

3.5.3.4 Deposition

The depositional mechanism for uranium in magmatic-related systems is poorly understood at present. Uranium-rich igneous rocks may crystallise uranium minerals directly from the melt as a magmatic mineral phase. However, these will most likely be in concentrations insufficient for economic exploitation. Uranium deposited from hydrothermal fluids represents a more attractive exploration target. Suggestions for depositional mechanisms include fluid mixing, boiling, pH change, decrease in ligand activity (e.g., via fluorite crystallisation), reduction and cooling (Skirrow *et al.*, 2009).

Two separate mappable criteria were used to generate the depositional mechanism systems component for both the intrusive-related and volcanic-related systems. The first, direct evidence of elevated uranium (Figure 3.5.14), was mapped using radiometric data from Minty *et al.* (2010). Radiometric data were processed to generate the U^2/Th product, which is useful for highlighting areas of anomalous uranium enrichment. Since radiometric data are limited to the Earth's surface, the data were clipped to the extent of igneous rocks derived from Geoscience Australia's 1:1 000 000 scale surface geology dataset. Statistics (mean and standard deviation) were calculated for each surface geology unit based on its stratigraphic unit number, and regions of one and two standard deviations above the mean were extracted for each unique unit as a mappable criterion.

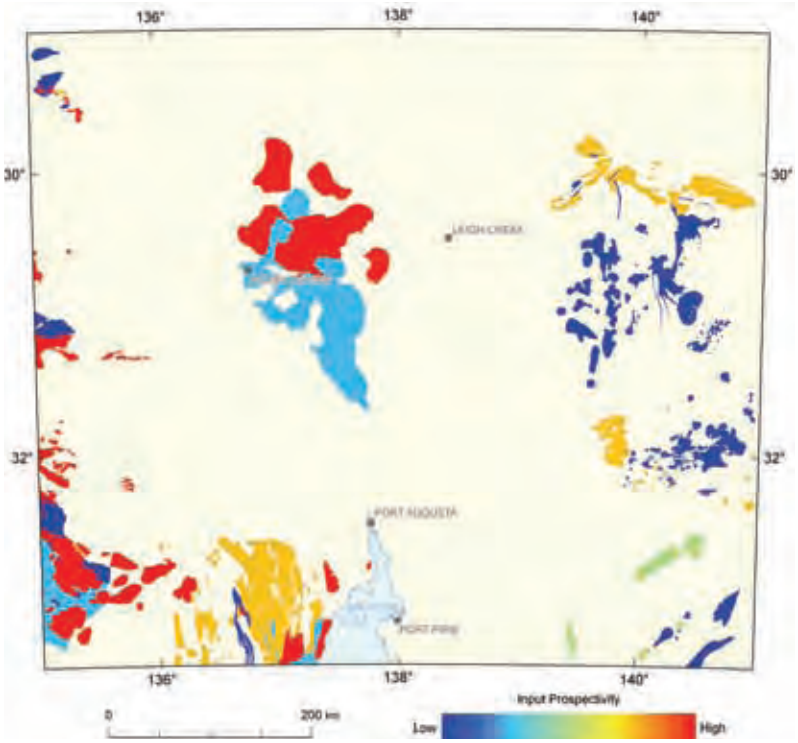

Figure 3.5.11: *Variation in weighting for the fluid exsolution and volatile release criterion used in the assessment for intrusive-related uranium systems. This also corresponds to the driver systems component for the intrusive-related system.*

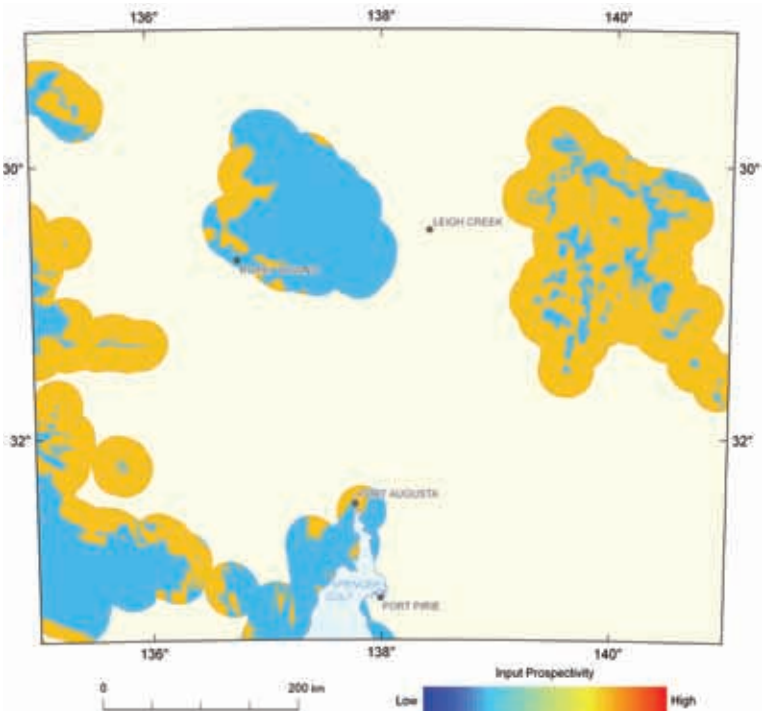

Figure 3.5.12: *Variation in weighting for the thermally-driven hydrothermal fluid circulation criterion used in the assessment for volcanic-related uranium systems. This also corresponds to the driver systems component for the volcanic-related system.*

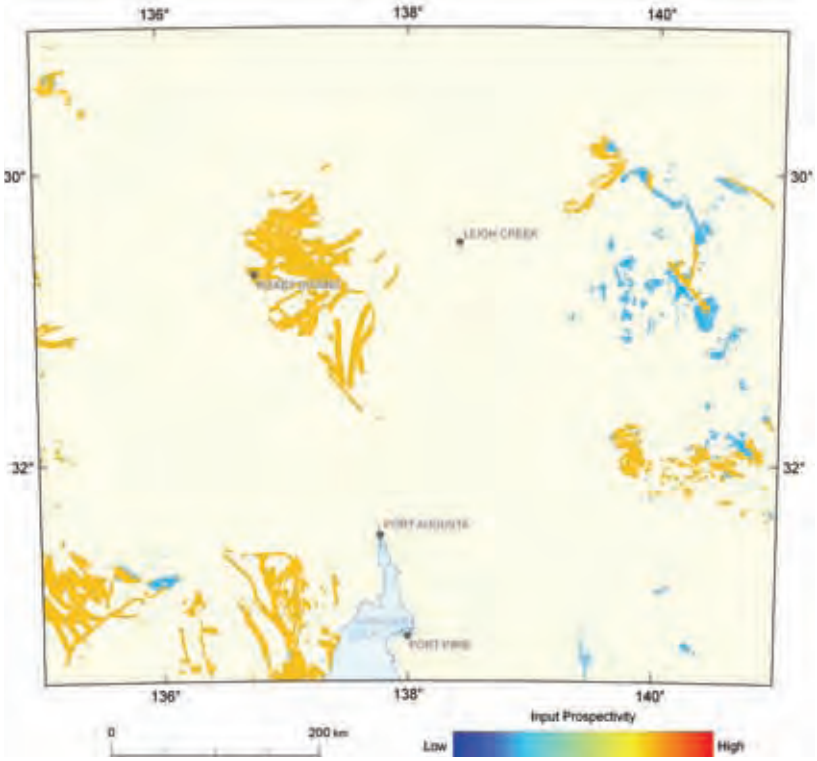

Figure 3.5.13a: *Variation in weighting for the fluid flow pathways criterion used in the assessment for intrusive-related uranium systems. This also corresponds to the fluid pathways and architecture systems component for the intrusive-related system.*

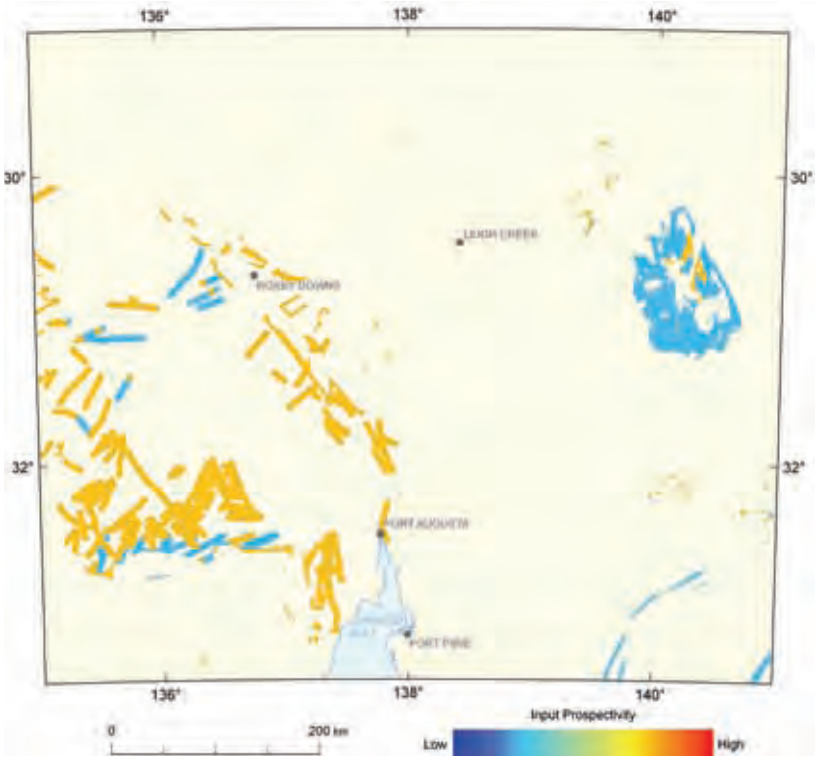

Figure 3.5.13b: *Variation in weighting for the fluid flow pathways criterion used in the assessment for volcanic-related uranium systems. This also corresponds to the fluid pathways and architecture systems component for the volcanic-related system.*

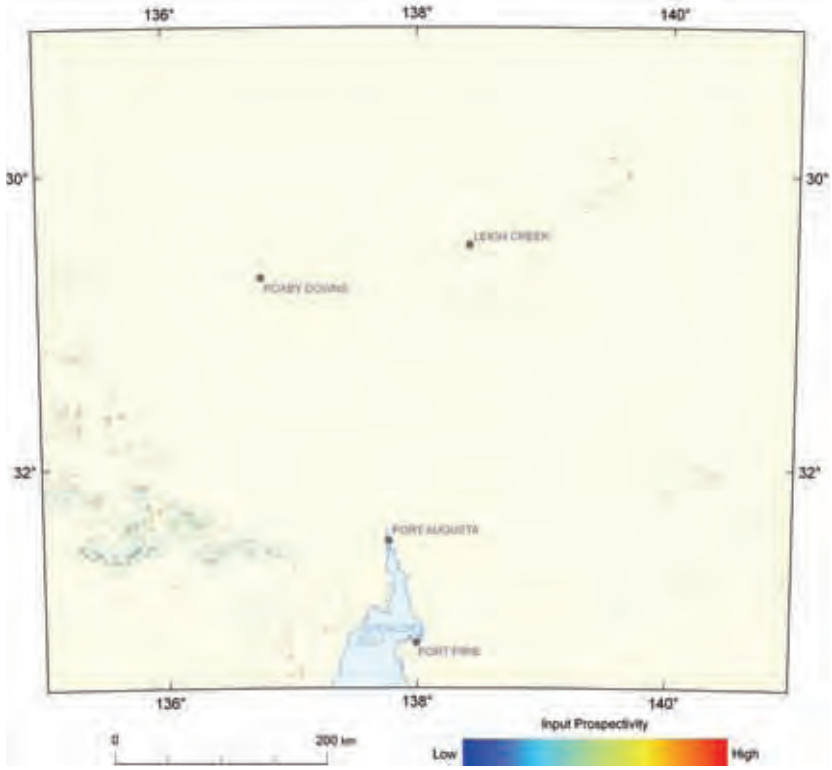

Figure 3.5.14: *Variation in weighting for the direct evidence of elevated uranium criterion.*

The second criterion used to generate the depositional mechanism systems component was the presence of chemical depositional sites (Figure 3.5.15). These were mapped as potentially reactive host rock units adjacent to the mapped igneous bodies. Reactive host rocks were taken to include carbonates, calcareous sediments and iron rich rocks (e.g., banded iron formation). These were determined using geological descriptions contained within the solid geology data used. For units identified as potentially reactive, the reactive component within the unit was classified as either dominant (reactive constituent comprises most of, or the entire unit) or present (reactive constituent is a minor fraction of the total unit). The identified units were buffered to a subjectively selected distance of 2.5 km to interact with the margin of the mapped igneous polygons and allow for a degree of spatial uncertainty in the location of the contact between the igneous unit and the host rock. Because this criterion is time-dependant, care was taken to filter the data to eliminate host rock units younger than the igneous body they interact with because these are unable to act as potential depositional sites.

The final weighting for the deposition systems component is shown in Figure 3.5.16.

3.5.4 Results

This investigation has identified several areas in South Australia which are potentially prospective for magmatic-related uranium systems. These are shown in Plates 3.6 (intrusive-related) and 3.7 (volcanic-related), and in Figures 3.5.17 and 3.5.18 below.

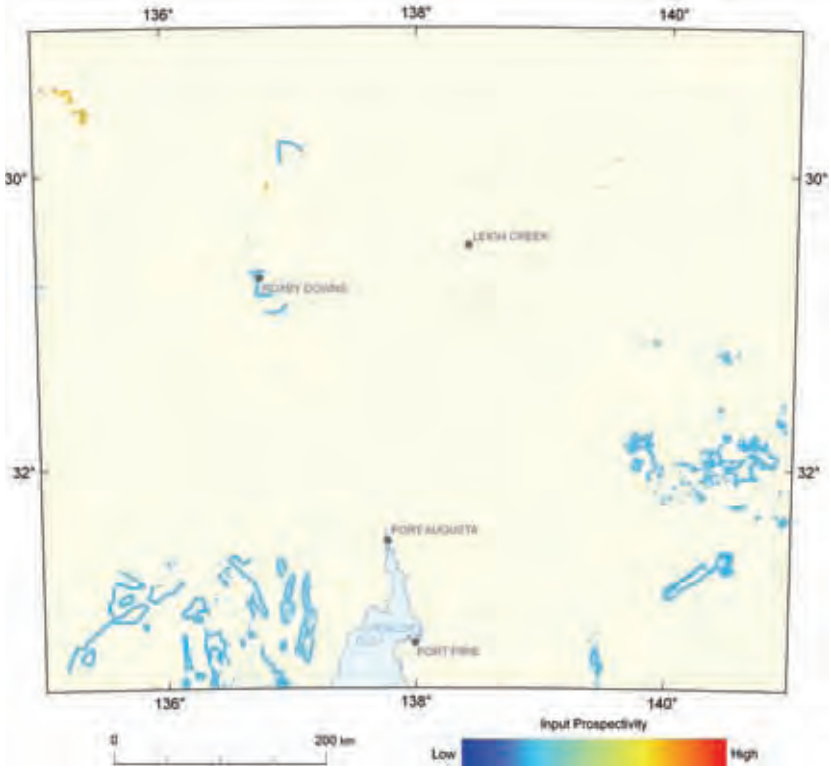

Figure 3.5.15a: *Variation in weighting for the reactive host rocks criterion used in the assessment for intrusive-related uranium systems.*

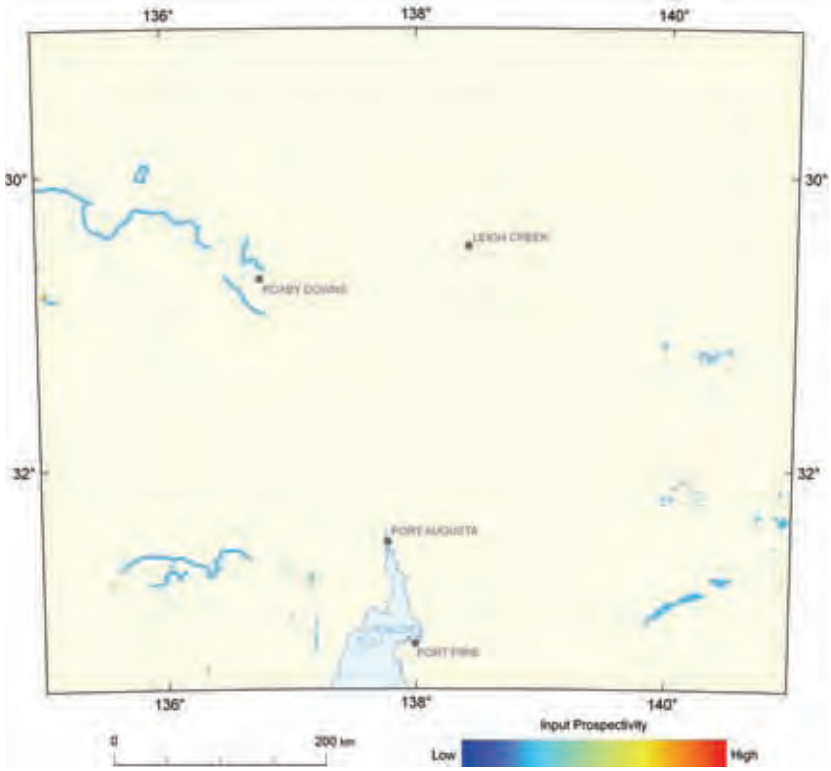

Figure 3.5.15b: *Variation in weighting for the reactive host rocks criterion used in the assessment for volcanic-related uranium systems.*

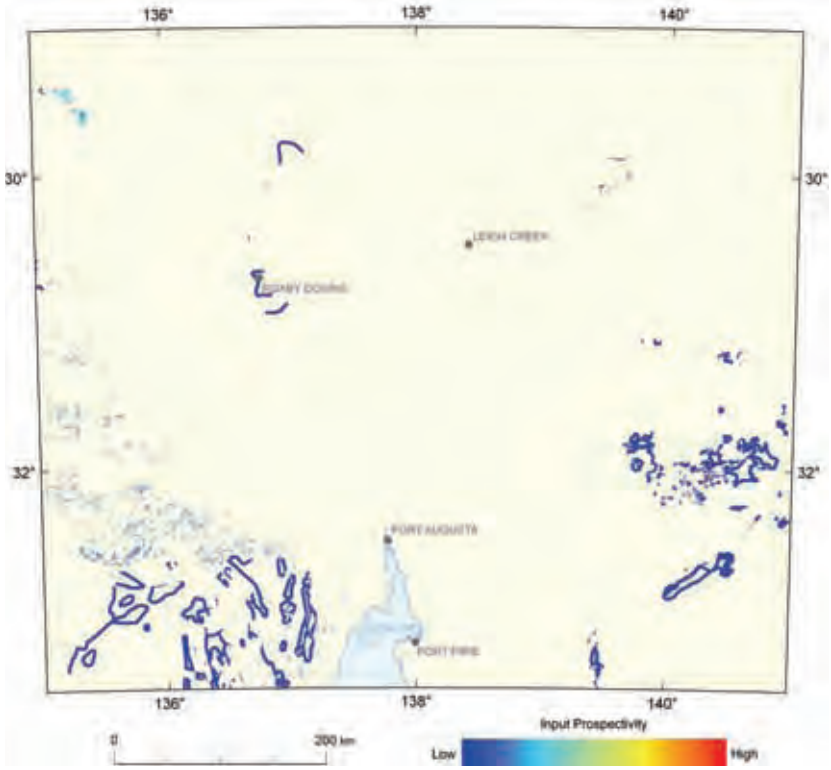

Figure 3.5.16a: *Variation in weighting for the deposition systems component for intrusive-related uranium systems.*

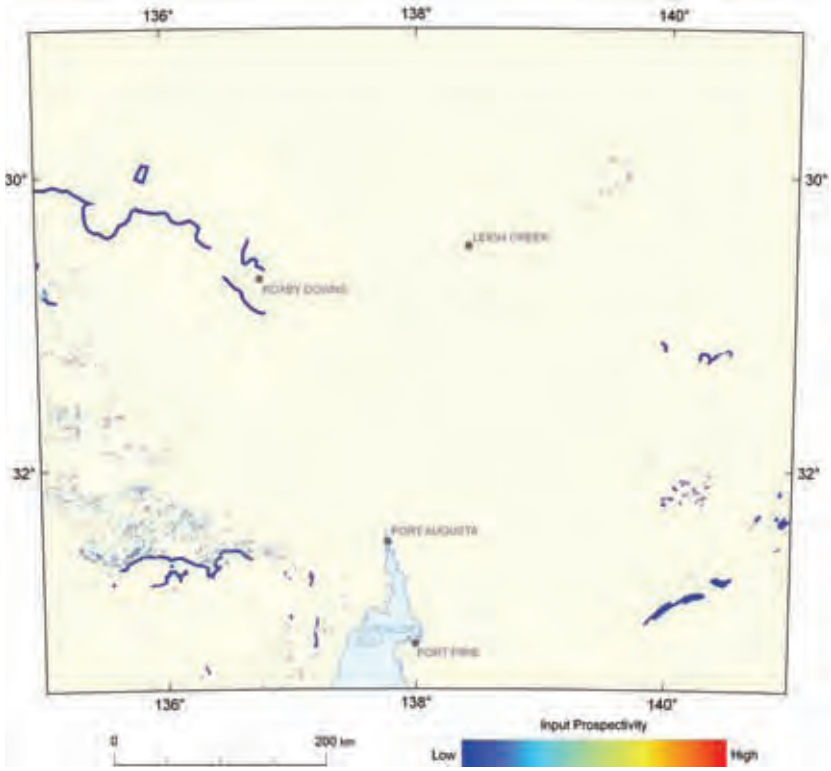

Figure 3.5.16b: *Variation in weighting for the deposition systems component for volcanic-related uranium systems.*

Potential for intrusive-related uranium mineralisation occurs most notably in the Olary Domain of the Curnamona Province, the Mount Painter Inlier, the region around Olympic Dam, the northwest of the study area, and the northern Eyre Peninsula, and is shown in Figure 3.5.17. The following regions of interest are highlighted:

A) In the Olary Domain, the highest potential is identified in the Crocker Well Suite, where known magmatic-related uranium mineralisation is present. Both the Crocker Well area itself and the Mount Victoria area to the north are highlighted in the assessment.
B) To the southeast of the Crocker Well area, the Basso Suite also shows high potential.
C) The entire Mount Painter Inlier, with the exception of Phanerozoic units, shows high potential for magmatic-related uranium systems. Notably, extensions of the Mount Painter Inlier occurring undercover to the northeast also show elevated potential.
D) High potential is associated with Hiltaba Suite granites in both the Olympic Dam and northern Eyre Peninsula. Many of these regions of high potential occur undercover.
E) One notable area highlighted occurs in the Curnamona Province, in the Benagerie Ridge region. Generally, granites in this region have been identified as Bimbowrie Suite, which is largely unprospective according to the results of this study. The recognition of moderate potential in the small granite body differentiated from the rest of the Bimbowrie Suite by Schofield (2010a) suggests that potential for magmatic-related uranium systems may occur undercover in the Curnamona Province, and further work is required to determine the character of the buried granites in the region.

The assessment for volcanic-related uranium systems also has highlighted a number of regions showing potential for magmatic-related uranium systems (Figure 3.5.18). In many cases, the identified regions are noted as being prospective also for intrusive-related uranium systems. The following regions of interest are highlighted:

A) Volcanic units in the Mount Painter Inlier.
B) I- to A-type volcanics of the Benagerie Ridge.
C) Volcanic units in the Olary Domain of the Curnamona Province.
D) Felsic units of the lower Gawler Range Volcanics. The highest potential, as identified in this study, occurs in the west, southwest and southeast of the unit.

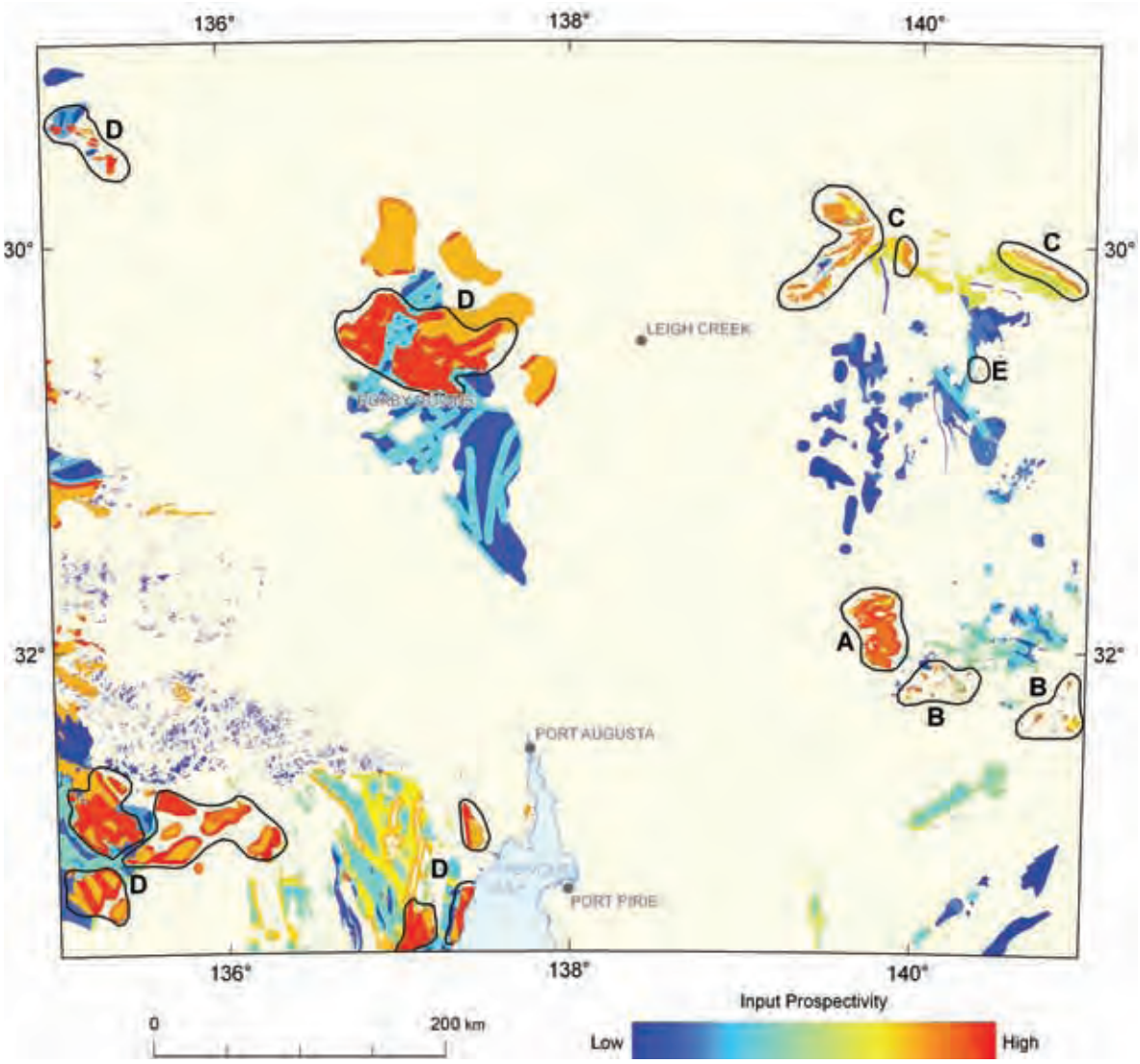

Figure 3.5.17: *Final modelled potential for intrusive-related uranium systems.*

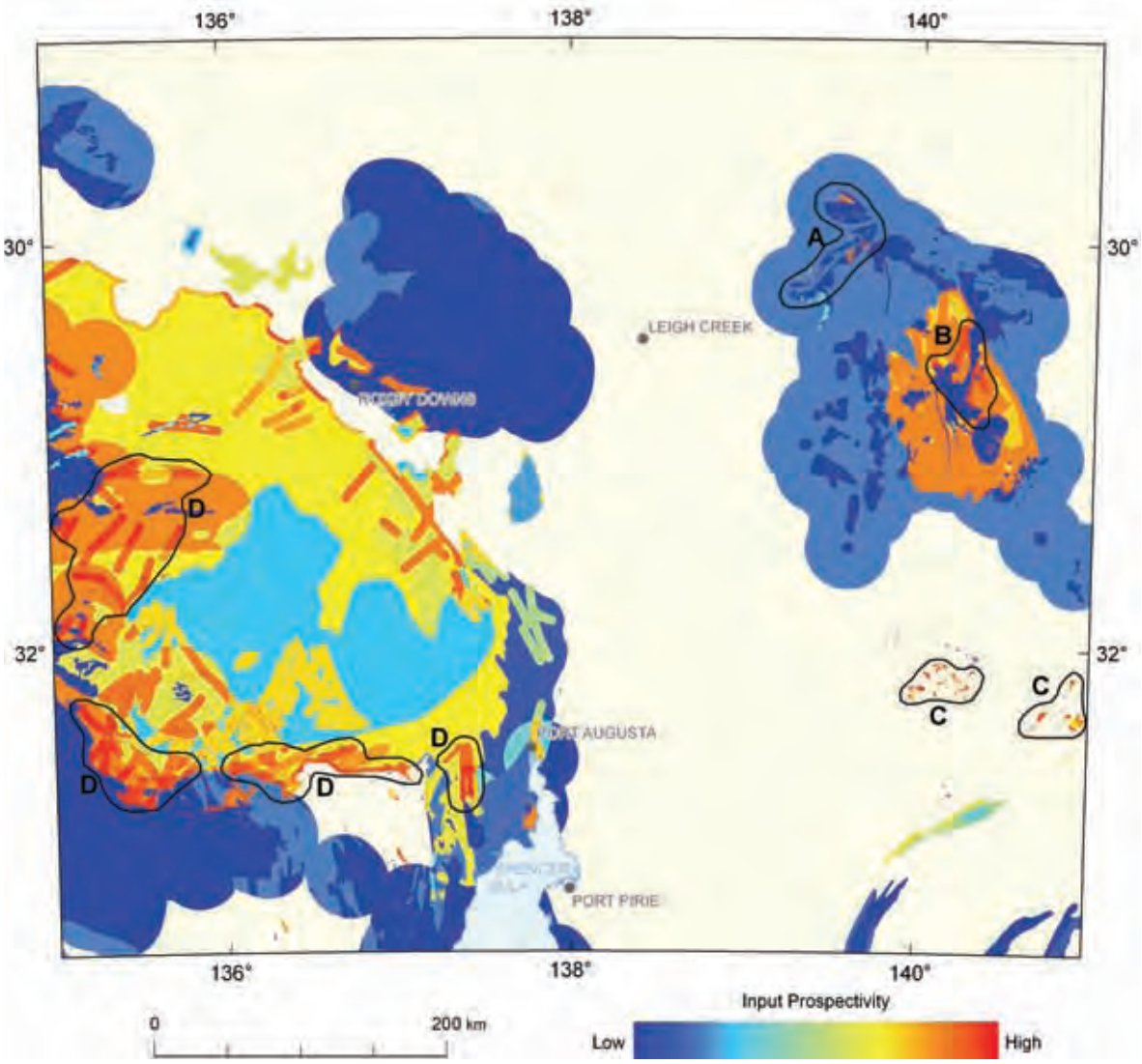

Figure 3.5.18: *Final modelled potential for volcanic-related uranium systems.*

3.6 URANIUM-COPPER MINERAL SYSTEMS RELATED TO THE ADELAIDE RIFT COMPLEX

D. L. HUSTON AND D. CONNOLLY

The Neoproterozoic was a major period of copper mineralisation globally (e.g., Hitzman *et al.*, 2005). During this period, ~820 Ma, the Zambian Copper Belt and its extensions into Zaire formed (Selley *et al.*, 2005). More recently, this copper epoch has been recognised in Australia with the discovery of the Nifty and Maroochydore deposits in the Yeneena Basin of Western Australia, which formed at a similar time (Huston *et al.*, 2007, 2009). In Zambia, recent discoveries (e.g., Lumwana) indicate that uranium deposits can be spatially related to copper deposits (www.equinoxminerals.com). Similarly, uranium mineralisation has been identified, though not quantified, at the Nifty deposit and unconformity-related uranium deposits at Kintyre have a broadly similar age to the Nifty deposit (~840 versus ~810 Ma, respectively: Cross *et al.*, 2011; Huston *et al*, 2007). These data, along with the presence of small-sized to moderate-sized copper deposits and occurrences in both the Amadeus Basin (Freeman *et al.*, 1990), which is part of the Centralian Superbasin (Walter *et al.*, 1995), and in the Adelaide Rift Complex (Preiss and Robertson, 2006) indicate that Neoproterozoic basins in Australia may also have potential for copper and uranium mineralisation. The purpose of this section is to assess the prospectivity of the Adelaide Rift Complex and underlying basement for Cryogenian-aged (i.e., 850 to 650 Ma) unconformity-related uranium and sediment-hosted copper±uranium deposits.

3.6.1 Uranium and copper deposits associated with the Adelaide Rift Complex

Although the Adelaide Rift Complex is not known as a uranium province, a number of uranium occurrences have been identified within this succession and in immediately underlying basement rocks commonly associated with copper (Figure 3.6.1). As Wilson and Fairclough (2009) have documented these occurrences in a moderate amount of detail, only their general characteristics are discussed here; details of more important uranium occurrences are summarised in Table 3.6.1. All of the uranium occurrences hosted in the Adelaide Rift Complex were classified as metamorphic-related by Wilson and Fairclough (2009). Figure 3.6.1 shows the spatial distribution of uranium and copper deposits in the Adelaide Rift Complex and immediate basement.

Table 3.6.1: Uranium occurrences associated with the Adelaide Rift Complex (summarised from Wilson and Fairclough, 2009; Wülser, 2009; Noble *et al.*, 1983; Coats, 1973; www.mindat.org)

NAME	LOCATION (LATITUDE, LONGITUDE)	PIRSA MINDEP NUMBER	DESCRIPTION
Shamrock copper	-30.1483, 139.3689	2046	Uranium is hosted in actinolite and quartz-actinolite-magnetite veins along minor faults and shears and along schistosity. The host shear zone strikes west-northwest and dips 80°N. The best drill intersection was 3.05 m grading 0.9 lb/ton U_3O_8 (0.04% U_3O_8), although dump samples yielded between 2 and 26 lb/ton U_3O_8 (0.08-1.1% U_3O_8). The veins are hosted by the Wooltana Volcanics, which consists dominantly of mafic volcanic rocks and forms the uppermost unit of the Arkaroola Subgroup. At the prospect, the Wooltana Volcanics consist of spotted mica-amphibolite-scapolite schist and scapolitic hornfels. This prospect occurs to the northwest of the Mount Painter Inlier.

NAME	LOCATION (LATITUDE, LONGITUDE)	PIRSA MINDEP NUMBER	DESCRIPTION
Valley-Shaft	139.3684, -30.1465	4418	The Valley prospect consists of a small (12 m × 0.6 m), pitchblende-bearing quartz lode. The Shaft prospect, to the east, also consists of a small (12 m × 0.9 m) quartz lode, in this case with disseminated meta-torbernite and uranophane. The total length of the Valley-Shaft system is 42 m; it is hosted by metasomatised calc-silicate rock and actinolite marble, probably of the Wywyana Formation. Like the nearby Shamrock prospect, this prospect is hosted by actinolite and quartz-actinolite-magnetite veins in the footwall to a fault. The best intersection was 0.46 m grading 76.7 lb/ton U_3O_8 (3.2% U_3O_8).
Pine Ridge	138.927, -34.766	8828	The Pine Ridge occurrence is hosted by an arenaceous unit within the Woolshead Flat Shale near a quartz-albite-sericite pegmatite. The mineralised zone is associated with a quartz-iron oxide-rich zone. The extent of the system, as determined from radiometric data is ~40 m. The best assay was 177 ppm U.
Fairview phosphate	139.1261, -33.8464	3861	The Fairview phosphate deposit is hosted by sheared and strongly altered metasedimentary rocks of the Skillogalee Dolomite. Previous production totalled 100 t grading ~25% P_2O_5 in 1903. Scintillometer readings indicate that, at surface, the mineralised zone extends over 375 m along strike and 5-30 m in width. Rock chip samples returned assays up to 0.3% U_3O_8 along with highly anomalous lanthanum and cerium. The deposit is also characterised by copper carbonate minerals.
Nichols Nob-Ogilvie	138.7035, -30.2990	3166, 4330	The Nichols Nob and Mount Ogilvie prospects are hosted in the Tapley Hill Formation adjacent to the Burr Diapir. These deposits are vein hosted. At both prospects uranium is associated with gold and nickel. Uranium is present both as uraninite and brannerite. At Nichols Nob, copper is also present; sulphide minerals include chalcopyrite, bornite, chalcocite (?), gersdorffite and skutterudite. Secondary minerals include oxides and carbonates of copper, nickel and cobalt.

The Adelaide Rift Complex is a well known copper province, with hundreds of copper occurrences and several historic and operating mines (Table 3.6.2). Three broad stratigraphic successions are known to host copper and uranium deposits/prospects (Tables 3.6.2 and 3.6.3):

- the Callanna Group, including the Arkaroola and Curdimurka subgroups;
- the Mundallio Subgroup of the Burra Group; and
- the Nepouie, Upalinna and basal Yerelina Subgroups of the Umberatana Group.

Table 3.6.4 summarises the production and resources of deposits with insufficient geological data to be included in Table 3.6.2. Of the mineralised successions, the Nepouie/Yerelina succession is the most prolific, with global (i.e. production and in-ground resources) copper resources amounting to just under 900 kt, or about 91% of the total for the Adelaide Rift Complex. The Mundallio Subgroup has global resouces of 82 kt, mostly from the historic Burra mine and the Callanna Group

has global resources of 11 kt. Uranium has not been produced and no resources have been established in the Adelaide Rift Complex.

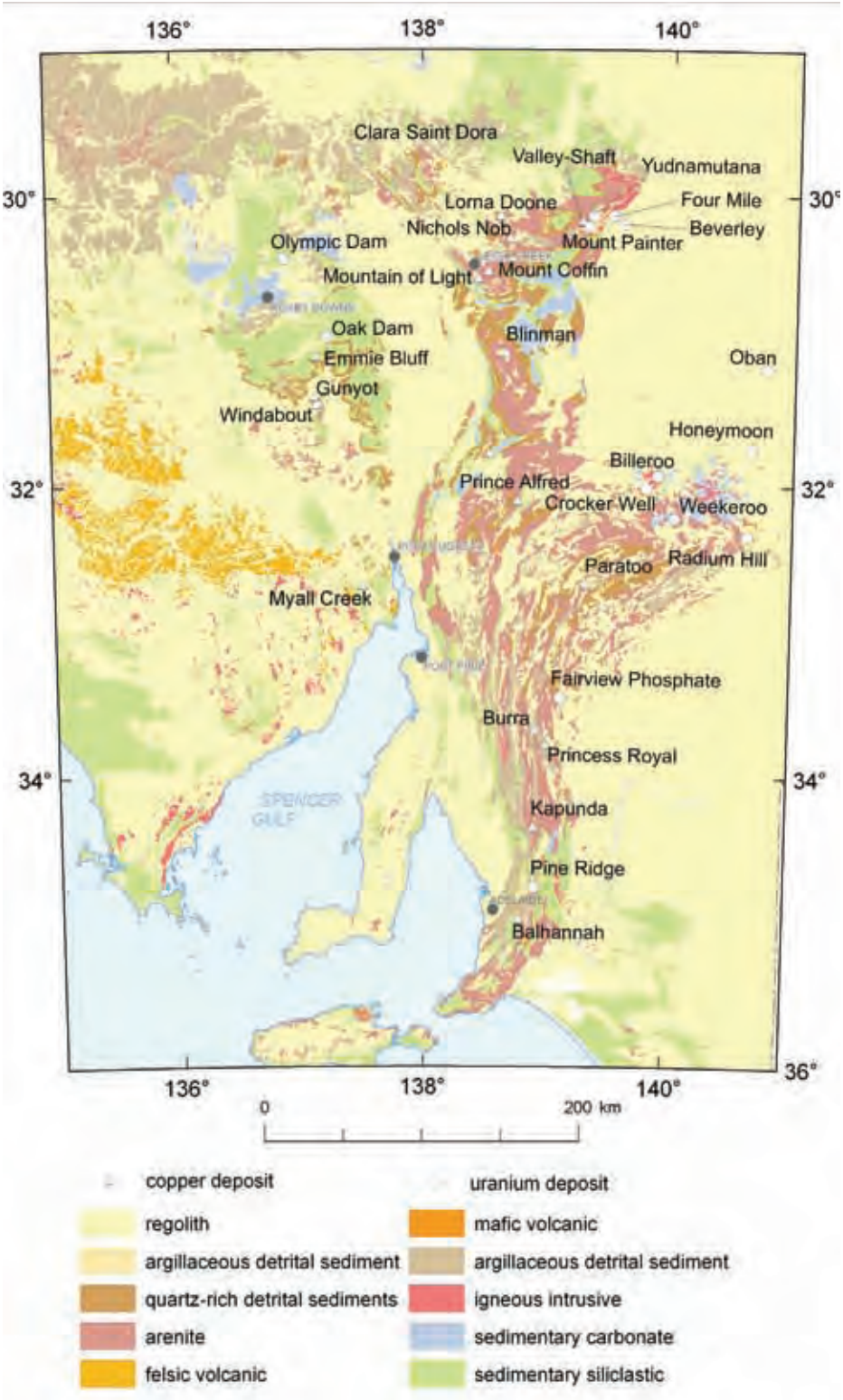

Figure 3.6.1: *Geology of the Adelaide Rift Complex (after Whitaker et al., 2008) showing the location of major copper deposits, and uranium-bearing prospects.*

Table 3.6.2: Major copper deposits in the Adelaide Rift Complex

NAME	LOCATION	PIRSA MINDEP NUMBER	PRODUCTION AND RESOURCES	HOST UNIT	DESCRIPTION	REFERENCES
Umberatana Group						
Mount Gunson Sandstone-hosted deposits				Whyalla Sandstone and Pandurra Formation	In the Mount Gunson district, sandstone-hosted deposits are hosted along an unconformity between the Mesoproterozoic Pandurra Formation and the lowermost part of the late-Neoproterozoic Whyalla Sandstone, which forms the base of the Yerelina Subgroup on the Stuart Shelf. Both units host copper, which is present as hypogene chalcopyrite, bornite and chalcocite within a network of fracture veins that form the matrix to hydrothermal breccias. The mineralised zones follow the unconformity; at Cattlegrid the sub-horizontal ore lens averaged 4.5 m in thickness, with an areal extent of 1400 × 600 m. The ore lenses are localised along the Pernatty Culmination, an inlier of Mesoproterozoic Pandurra Formation within the Stuart Shelf.	Knutson *et al.* (1983); Lambert *et al.* (1987); Tonkin and Creelman (1990); www.gunson.com.au
Cattlegrid	137.1472, -31.4438	3051	7.5 Mt @ 1.9% Cu & 8.3 g/t Ag[1]			
Cattlegrid South	137.1342, -31.4532	9479	0.7Mt @ 1.7% Cu & 10 g/t Ag[2]			
Main Open Cut, House and Gunyot	137.1651, -31.4331	3072	0.032 Mt @ 3.5% Cu and 12 g/t Ag, and 0.27 Mt at unspecified grade[1]			
East and West Lagoon	137.1886, -31.4272	3057	0.234 Mt @ 0.79% Cu and 12 g/t Ag[1]			
Tailings			7.2 Mt @ 0.14% Cu & 0.01% Co[2,3]			
Mount Gunson Black shale-hosted deposits				Tapley Hill Formation	Transgressive black shale of the Tapley Hill Formation hosts copper deposits in the Mount Gunson district, commonly where the host unit pinches out against the Pernatty Culmination. An important exception is the upper lens of the Emmie Bluff deposit, which is hosted in the Tapley Hill Formation, hundreds of metres above the unconformity with the Pandurra Formation. Mineralised zones commonly underlie the Whyalla Sandstone and consist largely of disseminated pyrite, chalcopyrite, bornite and chacocite in mudstone-dolostone.	Knutson *et al.* (1983); Lambert *et al.* (1987); Tonkin and Creelman (1990); www.gunson.com.au
MG14	137.1541, -314342	3090	1.1 Mt @ 1.7% Cu, 17 g/t Ag & 0.04% Co[2]			
Windabout	137.1314, -31.4148	3140	18.7 Mt @ 1.0% Cu, 10 g/t Ag & 0.05% Co[2]			
Emmie Bluff	137.1589, -31.1147	3035	24.0 Mt @ 1.7% Cu, 17 g/t Ag & 0.04% Co[2]			
Sweet Nell	137.2171, -31.6819	3125	0.35 Mt @ 1.2% Cu & 12 g/t Ag[2]			

NAME	LOCATION	PIRSA MINDEP NUMBER	PRODUCTION AND RESOURCES	HOST UNIT	DESCRIPTION	REFERENCES
Umberatana Group						
Kapunda	138.9180, -34.3466	4856	69kt @ 29.9% Cu[1] 4.3 Mt @ 1.1% Cu[4]	Tapley Hill Formation	Near-surface, oxidised copper-bearing veins provided copper production from the Kapunda deposit, mostly from 1844 to 1879. The deposit is stratabound in two coarser-grained dolomitic siltstone units in the Tapley Hill Formation. The copper is mostly vein-hosted, with veins filling fractures on the western limb of an anticline. The mineralised units contain disseminated to bedded Cu-Fe sulfides. Geochemical analyses indicate that mineralised dolomitic siltstone units are characterised by sodium and CO_2 enrichment, reflecting albite and dolomite enrichment. The mineralised units are also locally U-rich, assaying up to 150 ppm. The dominant sulfide assemblage is chalcopyrite-pyrite-pyrrhotite, with trace bornite, chalcocite, sphalerite and galena.	Dickinson (1953a); Lambert *et al.* (1980); Robertson (1995); Bampton (2003)
Mountain of Light Paltridge North Rossmann East	 138.4524, -30.5743 138.4441, -30.5700	 4370 4207	600 t[1] 0.89 Mt @ 0.83% Cu[2] 0.18 Mt @ 0.8% Cu[2]	Copley Diapir; Tapley Hill Formation	Copper orebodies at Mountain of Light are either hosted as blocks within (e.g., Paltridge North, in a block of Callana Group rocks) or in country rock (Tapley Hill Formation) along the margins (e.g., Rossman East) of the Copley Diapir. The ores are largely secondary copper carbonates, and are thought to be derived by weathering of primary chalcopyrite in quartz-carbonate veins.	Coats (1973); Bampton (2003); www.phoenixcopper.com.au
Lyndhust Diapir Lynda Lorna Doone	 138.6216, -30.1350 138.6245, -30.1394	 9482 4296	 1.00 Mt @ 0.72% Cu[2] 350[1] 0.84 Mt @ 0.75% Cu[2]	Tapley Hill Formation	Shallow orebodies, adjacent to the Lyndhurst Diapir, are characterised by malachite and copper oxides within the Tindelpina Shale Member of the Tapley Hill Formation and underlying tillite.	Coats (1973); Robertson (1995); Brampton (2003); www.phoenixcopper.com.au

NAME	LOCATION	PIRSA MINDEP NUMBER	PRODUCTION AND RESOURCES	HOST UNIT	DESCRIPTION	REFERENCES
Umberatana Group						
Mount Coffin Elise Adair West Jubilee	 138.5395, -30.5245 138.5469, -30.5211	 4232 8282	 2.0 Mt @ 0.9% Cu[4] 0.12 Mt @ 0.97% Cu[4]	Tapley Hill Formation	Secondary malachite, chalcocite and cuprite are associated with cross-cutting veins in Tindelpina Shale Member of the Tapley Hill Formation and in underlying tillite. The deposits are located adjacent to Mount Coffin diapir. The mineralised zones are steeply-dipping and patchy.	Coats (1973); Robertson (1995); www.phoenixcopper.com.au
Burra Group						
Burra	138.9262, -33.6783	3807	0.7 Mt @ 7.1% Cu[1] (1845-1877) 1.89 Mt @ 1.71% Cu[1] (1970-1981)	Skillogalee Dolomite	The Burra deposit is associated with felsic volcanic rocks and an intrusive rhyolite, which was dated at 797 ± 5 Ma. The deposit consists of three stratabound lenses within the Kooringa Member of the Skillogalee Dolomite adjacent to the north-northwest trending Kingston Shear. This shear juxtaposes the host against unmineralised diapiric breccia. In detail, the ores comprise jigsaw-fit breccias with angular blocks of Skillogalee Dolomite infilled by secondary copper minerals including malachite, azurite and chrysocolla, with minor chalcocite, cuprite and native copper. Although not directly observed, the hypogene sulfide assemblage is inferred as pyrite-chalcopyrite. The southern ore lens is associated with a complex alteration paragenesis involving early kaolinite accompanied by dolomite removal, which was following by microcline metasomatism that accompanied copper mineralisation. A chlorite-quartz assemblage developed along fractures, but has an uncertain relationship to copper mineralisation.	Drexel and McCallum (1986); Robertson (1995); Drexel (2008), Preiss *et al.* (2010)

NAME	LOCATION	PIRSA MINDEP NUMBER	PRODUCTION AND RESOURCES	HOST UNIT	DESCRIPTION	REFERENCES
Burra Group						
Princess Royal-Utica	139.0093, -33.7705	631	Not reported	Skillogalee Dolomite	Princess Royal contains two north-northwest trending mineralised zones. In the eastern zone, the ore is hosted by quartz-veined, silicified and brecciated dolomite, whereas in the western zone, copper is hosted by quartz-veined, hematitic gossan in silty dolomite. The copper is present as malachite, azurite and chalcocite in the veins/breccias and along fractures in the host. Gold (to 4.3 g/t; typically 0.2-0.7 g/t) is located either within or adjacent to the copper zones.	www.phoenixcopper.com.au
Paratoo	139.3287, -32.6791	1927	327 t Cu[1]	Upper Burra Group (Kadlunga Slate?); alternatively a xenoclast in a diapir	The Paratoo deposit is located within shales and dolomites of the upper Burra Group (Kadlunga Slate?), adjacent to the Paratoo diapir and along an anticlinal hinge. At surface, copper is hosted by four vein sets that define two zones parallel to the strike of the anticlinal crest. The veins are characterised by the assemblage quartz-pyrite-chalcopyrite-magnetite, with the sulfides weathered near surface. Copper is also present as secondary copper minerals (malchite, chrysocolla, tenorite and cuprite) along fractures and within the host rock in the oxide zone. In addition, secondary Cu-REE minerals are present near surface. At depth the host shale contains disseminated magnetite (to 3 mm porphyroblasts), pyrite, chalcopyrite, digenite (?) and native copper. It has been altered to a K-feldspar-quartz assemblage. In addition to LREE enrichment, mineralised veins are characterised by uranium (to 34 ppm) and gold (to 0.93 g/t) enrichment.	Brugger *et al.* (2006)

NAME	LOCATION	PIRSA MINDEP NUMBER	PRODUCTION AND RESOURCES	HOST UNIT	DESCRIPTION	REFERENCES
Burra Group						
Copper Claim	138.4817, -32.5271	5969	Not reported	Skillogalee Dolomite	Copper Claim consists of a stratabound zone located in an anticlinal core and has a lateral extent of 2.5 km × 1.0 km. In the supergene and weathered zones the dominant copper minerals are malachite and azurite with subordinate chalcocite and native copper. The host of copper in the hypogene zone is dominantly chalcopyrite with trace bornite. The dominant sulfide is pyrite; other iron sulfide minerals include marcasite, pyrrhotite and mackinawite. All sulfide minerals occur as disseminated grains in the host rocks, whereas chalcopyrite and pyrite also are present in concordant and discordant calcite-quartz veins, some of which pre-date dewatering features in the host unit. Copper mineralisation is associated with anomalous gold (to 0.38 g/t).	Rowlands *et al.* (1978); Robertson (1995)
Callana Group						
Blinman	138.6737, -31.0877	3206	0.207 Mt @ 4.8% Cu[1]	Recovery Formation	The Blinman deposit comprises a conformable, tabular body hosted by a large raft of dolomite and siltstone in the Blinman diapir. The body was 180 m long and up to 15 m wide. Three styles of copper mineralisation were recognised: (1) narrow veins in tensional fractures, (2) open-space filling, and (3) disseminations in the host dolomite (which made up the bulk of the ore). Oxidised ores were dominated by cuprite and malachite, whereas the hypogene assemblage was chalcopyrite-bornite-chalcocite with minor pyrite. Gangue minerals included barite, calcite, quartz and dolomite.	Dickinson (1953b); Robertson (1995)

NAME	LOCATION	PIRSA MINDEP NUMBER	PRODUCTION AND RESOURCES	HOST UNIT	DESCRIPTION	REFERENCES
Callana Group						
Yudnamutana	139.2794, -30.1768	2103	370 t Cu[1]	Wywyana Formation	The Yudnamutana field consists of a number of small mines, the largest of which was Yudnamutana, which were discovered in 1862 and produced until 1920. Three discrete styles of mineralisation were recognised: (1) fissure veins (e.g., Yudnamutana), (2) stockworks (e.g., Daly), and (3) replacement (e.g., Pinnacles). These deposits are hosted mostly by actinolitic marbles of the Wywyana Formation and by andalusite and mica schist. Although the ores were largely secondary in nature, the Pinnacles prospect contained disseminated to massive pyrite-chalcopyrite, and the lower parts of the fissure vein lodes are characterised by a hypogene assemblage of hematite-siderite-quartz-pyrite-chalcopyrite. The mines also produced minor bismuth, and trace molybdenite has been reported.	Ward and Jack (1916); Dickinson (1953b); Rowlands *et al.* (1978); Robertson (1995); Brampton (2003)

[1]Production
[2]Resource compliant with Joint Ore Reserves Committee (JORC) code
[3]Remnant, JORC-compliant resource present in tailings from previous mining activities
[4]Resouce not compliant (pre-dating) with JORC code

Table 3.6.3: Stratigraphy of the Adelaide Rift Complex (based on Preiss [1987, 1993, 2000] and Geoscience Australia stratigraphic database).

GROUP	SUBGROUP	FORMATION	MAXIMUM THICKNESS (M)	TYPE ZONE	SEQUENCE	DESCRIPTION	CORRELATES
Wilpena	Pound	Rawnsley Quartzite	410	Central Flinders Zone	M4.6-M4.5	Mature, medium- to coarse-grained sandstone and quartzite with local calcareous beds. Interpreted to have been deposited in a tidal shelf environment with intervals of trough cross bedding and wavy lamination.	Not present in Mount Lofty ranges and Stuart Shelf
		Bonney Sandstone	1200	Central Flinders Zone	M4.4	Fine to medium grained, flaggy to medium bedded, silty and feldspathic sandstone; locally hematitic. Interpreted to have been deposited in a *shallow-water, oxidising environment.*	Not present in Mount Lofty Ranges and Stuart Shelf
		Wonoka Formation	1000	Central Flinders Zone	M4.3-M4.2	Dominantly grey limestone, with lesser (decreasing up-section) shale and siltstone. Upper part of unit contains *ooid* grainstone, *stromatolitic bioherms* and (interpreted) shallow-water sandstone. Basal part of unit interpreted to have been deposited in a relatively deep water shelf slope, with upper part deposited during shallowing in a lagoonal environment.	Not present in Mount Lofty Ranges and Stuart Shelf
		Bunyeroo Formation	1630	Central Flinders Zone	M4.1	Partly *calcareous* shale and siltstone, with local *dolomite* and *limestone* beds, particularly in the upper part (e.g., Wearing Dolomite Member), and with minor phosphatic chert and black *carbonaceous* shale. A persistent thin unit of felsic detritus is interpreted as a debris layer derived from a bolide impact (Gostin *et al.*, 1986). The Bunyeroo Formation is interpreted to have been deposited in a relatively deep water marine basin, with probable shallower environments at higher stratigraphic levels. *The Wearing Dolomite Member hosts several copper prospects in the Beltana area.*	Yarloo Shale (Stuart Shelf)

GROUP	SUBGROUP	FORMATION	MAXIMUM THICKNESS (M)	TYPE ZONE	SEQUENCE	DESCRIPTION	CORRELATES
Wilpena	Sandison	ABC Range Quartzite	2000 (mainly <500)	Central Flinders Zone	M3.2	Slightly feldspathic, fine- to medium-grained *quartzite*, with minor siltstone. Interpreted to have been deposited in a prograding deltaic environment.	Uppermost Ulupa Sandstone (North Flinders Zone, Nackara Arc); uppermost Tent Hill Formation (Stuart Shelf)
		Brachina Formation	5800 (in correlate Ulupa Formation)	Central Flinders Zone	M3.2-M3.1	Alternating laminated siltstone and fine-grained sandstone. Interpreted to have been deposited in an upwardly shallowing marine environment. *Malachite-stained shale is present near base along type section at Brachina Creek.*	
		Nuccaleena Formation	700 (mostly <50)	Central Flinders Zone	M3.1	Purple shale with minor dolomite bands overlying basal bedded dolomite. This unit interfingers laterally with the Seacliff Sandstone, medium- to thick-bedded feldspathic quartzite and sandstone interbedded with silstone and impersistent dolomite layers. Interpreted to have been deposited in shallow water environments (deltaic environment for Seacliff Sandstone).	Seacliff Sandstone (Mount Lofty Ranges)
Umberatana	Yerelina	Ketchowia Siltstone	530	Nackara Arc	M2.3	Sandy, pyritic and rarely pebbly siltstone with interbedded calcareous and pyritic sandstone. Interpreted to have been deposited in marine, periglacial environment.	Uppermost Elatina Formation (Mount Lofty Ranges, South Flinders Zone)
		Grampus Quartzite	60	Nackara Arc	M2.3-M2.2	Medium- to coarse-grained feldspathic *quartzite*.	Upper Wyalla Sandstone (Stuart Shelf); Balparana Sandstone (North Flinders Zone); Upper Elatina Formation (Mount Lofty Ranges, South Flinders Zone)

GROUP	SUBGROUP	FORMATION	MAXIMUM THICKNESS (M)	TYPE ZONE	SEQUENCE	DESCRIPTION	CORRELATES
Umberatana	Yerelina	Pepuarta Tillite	200	Nackara Arc	M2.3-M2.2	Massive to bedded siltstone to sandy siltstone containing sparse granule- to boulder-sized erratics. Minor interbeds and lenses of *calcareous* sandy siltstone and sandstone. Interpreted to have been deposited in glaciomarine environment.	Mount Curtis Tillite (North Flinders Zone); central Elatina Formation (Mount Lofty Ranges, South Flinders Zone); lower Elatina Formation (Central Flinders Zone); central Whyalla Sandstone (Stuart Shelf)
		Gumbowie Arkose	90	Nackara Arc	M2.2	Arkosic sandstone with interbedded sandy siltsone, minor quartzite and pebbly sandstone.	Lower Elatina Formation (Mount Lofty Ranges and South Flinders Zone)
		Fortress Hill Formation	1830	Nackara Arc	M2.1	Grey-green, finely laminated and pyritic siltstone, with minor quartzite and lenses of gritty *limestone*. Interpreted to have been deposited in a glaciomarine environment in a relatively deep basin. *The correlative lower Wyalla Sandstone hosts a significant copper deposit at the Cattlegrid mine.*	Lowermost Elatina Formation (Mount Lofty Ranges, South Flinders Zone); lowermost Whyalla Sandstone (Stuart Shelf); equivalent missing in Central Flinders Zone
	Upalinna	Yaltipena Formation		Central Flinders Zone	M1.2	*Limeston*e with sandy beds, *calcareous* siltstone.	Restricted to Central Flinders Zone
		Trezona Formation	250	Central Flinders Zone	M1.2	Cycles of laminated greenish grey *calcareous* shale and siltstone grading to fine grained *stromatolitic, oolitic* and intraclastic hash breccia *limeston*e. Interpreted to have been deposited in a shallow lagoon environment.	

GROUP	SUBGROUP	FORMATION	MAXIMUM THICKNESS (M)	TYPE ZONE	SEQUENCE	DESCRIPTION	CORRELATES
Umberatana	Upalinna	Enorama Shale	450	Central Flinders Zone	M1.2	Mostly grey-green *dolomitic* shale and silty shale with minor red shale and fine sandstone. Equivalent Wilmington Formation consists of red-brown micaceous siltstone with fine sandstone interbeds. The Marino Arkose Member of Wilmington Formation yielded a SHRIMP zircon spectrum with a youngest age of ~657 Ma, interpreted as maximum depositional age.	Wilmington Formation (South Flinders Zone, Mount Lofty Ranges)
		Angepena Formation	1330	Mount Lofty Ranges	M1.1	Finely laminated red-brown to purple siltstone with mudcracks and with dolomitic interbeds. Correlate Etina Formation contains *stromatolitic limestone*. Interpreted to have been deposited in oxidised, shallow water to emergent environments. *At Warrahimbo homestead, the correlative Etina Formation hosts copper mineralisation along cross-cutting faults.*	Etina Formation (Central Flinders Zone); Tarcowie Siltstone and Waukaringa Siltstone (Nackara Arc); lower Yudnapinna beds (Stuart Shelf)
	Nepouie	Brighton Limestone	60	Mount Lofty Ranges	S3.2	Dominantly ooid grainstone interfingering with *stromatolite* bioherms. Interpreted to have been deposited in upwardly-shallowing marine conditions, possibly into supra-tidal mudflats (*sabkhas*) or very shallow lagoons.	Balcanoona Formation (North Flinders Zone); basal Etina Formation (Central Flinders Zone)
		Tapley Hill Formation	3500	Mount Lofty Ranges	S3.1	*Calcareous or dolomitic, carbonaceous* and pyritic siltstone with local lenticular conglomerate interbeds. Oldest unit of Adelaide Rift Complex to transgress onto Stuart Shelf. Includes local dolomite, shaly arkose and greywacke members. Locally the unit is stromatolitic. Interpreted to have been deposited in open marine environment with localised shallow water facies. *This unit hosts copper deposits at Kapunda and Mount Gunson.*	Same unit name throughout Adelaide Rift Complex.

GROUP	SUBGROUP	FORMATION	MAXIMUM THICKNESS (M)	TYPE ZONE	SEQUENCE	DESCRIPTION	CORRELATES
Umberatana	Yudnamu-tana	Wilyerpa Formation	2700	Nackara Arc	S2.2	Mostly siltstone, shale and mudstone, with lesser sandstone, quartzite and greywacke, and with minor tillite and pebbly mudstone. Includes *Warcowie Dolomite* Member at base.	Upper Sturt (Mount Lofty Ranges) and Appila Tillites (South Flinders Zone); Serle Conglomerate (North Flinders Zone)
		Brenda Siltstone	260	Nackara Arc	S2.1	Mostly thinly laminated iron-rich (hematite) siltstone, with lesser medium to coarse grained gritty sandstone, glacially derived pebbly siltstone and *carbonate (limestone and dolomite)*. Includes *iron-rich Braemar ironstone facies*, which consists of hematitic siltstone with occasional lenses of tillite. Interpreted to have been deposited in a deep marine periglacial environment.	Holowilenia Ironstone (Central Filnders Zone) Lyndhurst Formation (North Finders Zone)
		Pualco Tillite	3300	Nackara Arc	S2.1	Gritty, *dolomitic* or *calcareous* siltstone and minor thin sandstone with pebble to boulder sized glacial clasts; matrix supported diamictite. Includes quartzite, and minor siltstone, pebbly quartzite and conglomerate interbeds.	Basal Sturt (Mount Lofty Ranges) and Appila Tillites (South Flinders Zone); Meringa Tillite (Central Flinders Zone); Fitton Formation and Bolla Bollana Tillite (North Flinders Zone)
Burra	Belair	Kadlunga Slate		South Flinders Zone	S1.2	Sericitic and *graphitic* slate	
		Gilbert Range Quartzite	75	South Flinders Zone	S1.2-S1.1	Partly laminated feldspathic *quartzite* to arkose	

GROUP	SUBGROUP	FORMATION	MAXIMUM THICKNESS (M)	TYPE ZONE	SEQUENCE	DESCRIPTION	CORRELATES
Burra	Belair	Mintaro Shale	1200	South Flinders Zone	S1.1	Laminated siltstone or slate with minor *dolomitic* siltstone, sandstone and *dolomite*. Includes Leasingham Quartzite Member at base. Interpreted to have been deposited in permanently submerged marine environment, possibly in a pro-delta slope.	Mitcham Quartzite (Adelaide area; with Leasingham Quartzite Member)
	Unnamed	Saddleworth Formation	1350	South Flinders Zone	T3.3-T3.2	Dominantly laminted shale, slate and siltstone with *dolomite* (upper and lower Auburn Dolomite and Beauford Dolomite), sandstone (Watervale Sandstone Member: between upper and lower *Auburn Dolomite*), and shale (Bethel Shale) members. The *Auburn Dolomite Member* and the Bethel Shale are *carbonaceous*. Interpreted to have been deposited in an offshore marine environment that represents the deepest marine conditions for the Burra Group.	Myrtle Springs Formation (North Flinders Zone); Glen Osmond Slate (Mount Lofty Ranges)
	Unnamed	Undalya Quartzite	1500	South Flinders Zone	T3.2-T3.1	Medium-grained feldspathic *quartzite* interbedded sandy, *carbonaceous* and pyritic shale; locally *stromatolitic*. Interpreted to have been deposited in lagoonal or tidal flat environment.	Stonyfell Quartzite (Mount Lofty Ranges)
	Mundallio	Woolshed Flat Shale	200	Nackara Arc	T3.1	Sandstone and siltstone passing upwards into laminated silstone with silty *dolomite* interbeds. The Balhannah shale Member is *carbonaceous*. Interpreted to have been deposited in an offshore marine environment.	
		Skillogalee Dolomite	4000	Nackara Arc	T2.2-T2.1	D*olomite* and dark grey, c*arbonaceous dolomit*e with *magnesite* and chert. This unit contains *stromatolite* bioherms, and *shortite* and *halite* molds. *Total organic carbon contents are up to 1.58%*. Interpreted to have been deposited in shallow-marine to peritidal environment.	Castambul Formation and Montacute Dolomite (Mount Lofty ranges)

GROUP	SUBGROUP	FORMATION	MAXIMUM THICKNESS (M)	TYPE ZONE	SEQUENCE	DESCRIPTION	CORRELATES
Burra	Mundallio	Skillogalee Dolomite (continued)	4000	Nackara Arc	T2.2-T2.1	At Burra this unit contains felsic volcanic units and has been intruded by felsic dykes (Drexel, 2008). Laser ablation zircon U-Pb analyses from the dykes indicate an age of 797 ± 5 Ma (A Reid, in Drexel, 2008; Priess *et al.*, 2010). *The Burra mine is one of the most significant copper deposits in the Adelaide Rift Complex.*	Castambul Formation and Montacute Dolomite (Mount Lofty ranges)
	Emeroo	Bungaree Quartzite	500	Nackara Arc	T1.3	Fine- to coarse-grained feldspathic *quartzite* or arkose, siltstone and minor *dolomite*; mainly light-coloured. Interpreted to have been deposited in a flood-plain or tidal flat environment, possibly in a delta.	Witchelina Quartzite (North Flinders Zone); Wortupa Quartzite (Central Flinders Zone); uppermost Aldgate Sandstone (Mount Lofty Ranges)
		River Wakefield Formation	780	Nackara Arc	T1.3-T1.2	Complex unit with four members previously defined as separate formations. The upper Benbournie Member consists of partly silty *dolomite* containing dolomite pebbles and with interbedded siltstone and sandstone. This unit is underlain by the Stradbrooke Member, which consists of phyllitic, laminated and *dolomitic* fine sandy siltstone with minor interbedded dolomite beds and a black, *carbonaceous* siltstone at base. The Stradbroke Member is underlain by the Ingomar Memnber, which consists of micaceous and feldspathic, fine- to medium-grained quartzite with minor sandy siltstone. The basal unit is the Boconnor Member, which consists of Sandy phyllite, *quartzite* and minor lenticular *dolomite*.	Willawalpa Formation (North Flinders Zone); Opaminda Formation (Central Flinders Zone); Aldgate Sandstone (Mount Lofty Ranges)

GROUP	SUBGROUP	FORMATION	MAXIMUM THICKNESS (M)	TYPE ZONE	SEQUENCE	DESCRIPTION	CORRELATES
Burra	Emeroo	Blyth Dolomite	130	Nackara Arc	T1.1	Basal unit of sandstone, siltstone and minor *dolomite* overlain by upper unit of *dolomite marble*, fine-grained *dolomite*, grey to black chert, sandstone and minor siltstone.	Lower Blue Mine Conglomerate (Central and North Flinders Zones); Wirreanda Dolomite (1300-m-thick; Central Flinders Zone); upper Top Mount sandstone beds (North Flinders Zone)
		Rhynie Sandstone	1500	Nackara Arc	T1.1	Medium- to coarse-grained arkose and shaly *quartzite* with hematite laminae. Contains local conglomerate, *magnesite*-bearing *dolomite* interbeds and local altered and amygdaloidal *basalt*. *Halite* casts in correlative Humanity Seat Formation. Interpreted to have been deposited in a dominantly fluvial environment with peritidal-marine influence.	Humanity Seat Formation and lower Top Mount sandstone beds (North Flinders Zone); Woodnamoka Phyllite (Central Flinders Zone); Arbury Park Sandstone Member of Aldgate Sandstone (Mount Lofty Ranges)
Burra	Emeroo	Boucat Volcanics		South Flinders Zone	T1.1	Rhyolite, porphyritic dacite, *basalt*, and lesser porphyritic *andesite*. Deformation along shear zones produced quartz-muscovite and biotite schist. SHRIMP U-Pb zircon data from rhyolite gave age of 777 ± 7 Ma (M Fanning, in Preiss, 2000), inconsistent with ~797 Ma age from rhyolite intruding younger Skillogalee Dolomite (A Reid, in Drexel, 2008). *The Boucat Volcanics hosts malachite-bearing quartz-magnetite shear zones at Mutooroo Ridge prospect.*	Restricted to South Flinders Zone

GROUP	SUBGROUP	FORMATION	MAXIMUM THICKNESS (M)	TYPE ZONE	SEQUENCE	DESCRIPTION	CORRELATES
Callanna	Curdimurka	Boorloo Siltstone	520	North Flinders Zone	W2.3	Mostly black, *carbonaceous* and shaly siltstone with *dolomite* near base, a fine sandstone/ *quartzite* near the middle and a series of *dolomite* interbeds at top. The upper dolomite beds contain abundant *gypsum pseudomorphs* and *cauliflower chert*. Interpreted to have been deposited in fluvial, restricted marginal marine or lacustrine environments. *Minor copper present in correlative Kirwan Siltstone near Worumba homestead. Quartz-carbonate-hematite veins with secondary copper minerals at Broughton and Wheal Sarah deposits near Spalding in correlative River Broughton beds.*	Kirwan Siltstone, Waraco Limestone (Central Flinders Zone); River Broughton beds (South Flinders Zone).
		Cooranna Formation	780	North Flinders Zone	W2.3	Siltstone, sandstone, *carbonate* and pyritic siltstone and sandstone (uppermost). This unit contains *halite casts* and pits *after gypsum*, and *shortite* and *cauliflower chert*. Interpreted to have been deposited in fluvial, restricted marginal marine or lacustrine environments.	Upper Arkaba Hill beds (Central Flinders Zone); lowermost River Broughton beds (South Flinders Zone).
		Hogan Dolomite	645	North Flinders Zone	W2.3	*Dolomite*, *dolomitic* siltstone and sandstone, with abundant *halite casts*, *cauliflower chert*, and *stromatolites* near the base. Interpreted to have been deposited in fluvial, restricted marginal marine or lacustrine environments.	Lower Arkaba Hill beds (Central Flinders Zone)
		Recovery Formation	2220	North Flinders Zone	W2.2	Grey sandstone with shaly partings, laminate siltstone, *dolomite* and *calcareous* siltstone, and with *halite casts, gypsum pseudomorphs* and *stromatolites*. Interpreted to have been deposited in a hypersaline tidal flat environment. *Correlative Niggly Gap beds contain copper at Blinman mine and near Worumba homestead.*	Niggly Gap beds (Central and South Flinders Zones)

GROUP	SUBGROUP	FORMATION	MAXIMUM THICKNESS (M)	TYPE ZONE	SEQUENCE	DESCRIPTION	CORRELATES
Callana	Curdimurka	Dunns Mine Limestone	335	North Flinders Zone	W2.2	*Carbonaceous limestone*, sandy *limestone* and *dolomite* interbedded with *calcareous* siltstone and sandstone. This unit contains *shortite pseudomorphs, cauliflower chert*, authigenic microcline, *scapolite* and *stromatolites*. Interpreted to have been deposited in coastal sabhka and playa lake environments. *This unit contains copper-bearing quartz-carbonate veins at the Callanna, Dunns and Rook workings.*	Wirrawilka beds (Central Flinders Zone)
		Rook Tuff	60	North Flinders Zone	W2.1	Partly laminated, flaggy siltstone with tuffaceous shale and silstone, and with a lenticular, 3-m-thick porphyryic crystal tuff of dacitic composition near base. TIMS U-Pb analysis of zircon indicates an age for the crystal tuff of 802 ± 10 Ma (Fanning *et al.*, 1986).	Restricted to Willouran Ranges
		Dome Sandstone	1480	North Flinders Zone	W2.1	Dominantly coarse-grained feldspathic sandstone with minor pebble conglomerate, *calcareous* sandstone, sandy *dolomite* and immature arkose, and with thin green siltstone interlayered throughout. This unit contains locally abundant *halite* clasts and, where in stratigraphic contact, grades into the underlying Noranda Volcanics. Interpreted to have been deposited in fluvial to shallow-marine, intertidal environments.	Restricted to Willouran Ranges
	Arkaroola	Wooltana Volcanics	2400	Central Flinders Zone	W1.2	Mostly *basalt* flows, with minor trachyte, *andesite* and rhyolite, and with interflow tuff, shale and siltstone. Variably altered by *epidote, hematite*, chlorite, calcite, antigorite and tremolite. Amygdales filled by microcline, albite, calcite and quartz. Veins also contain microcline. *Basaltic* rocks interpreted as extrusive equivalents to Gairdner dyke swarm,	Noranda Volcanics (North Flinders Zone); Cadlareena Volcanics (Peake and Denison Inlier); Wilangee Basalt (Barrier Ranges)

GROUP	SUBGROUP	FORMATION	MAXIMUM THICKNESS (M)	TYPE ZONE	SEQUENCE	DESCRIPTION	CORRELATES
Callana	Arkaroola	Wooltana Volcanics (continued)				which yielded a baddeleyite SHRIMP U-Pb age of 827 ± 6 Ma (Wingate *et al.*, 1998). *Basaltic rocks of the Wooltana Volcanics and correlates host minor copper prospects and occurrences.*	
		Wywyana Formation	460	Central Flinders Zone	W1.1	Dolomitic and actinolitic *marbles*; *calc-silicate* and *para-amphibolite*. *Stromatolites* recognised in low-metamorphic-grade correlates (Cooma-ree Dolomite). *Evaporitic minerals shortite and loughlinite* recognised near Yudnamutana. Interpreted to have been deposited in hyper-saline, alkaline, lacustrine environment. Alternatively, the correlative Coominaree Dolomite was interpreted to have been deposited on a shallow water shelf by Ambrose *et al.* (1981). *The Wywyana Formation hosts copper deposits at Clara St Dora and in the vicinity of Yudnamulana Hill.*	Black Knob Marble (North Flinders Zone); Coomaree Dolomite (Peake and Denison Inlier); Boco Formation (Barrier Ranges)
		Paralana Quartzite	1220	Central Flinders Zone	W1.1	Pink *quartzite* overlain by impure grey sand-stone; *stromatolites* present in upper part. Interpreted to have been deposited in fluviatile to shallow marine environment. Upper contact transitions into Wywyana Formation with presence of actinolitic *quartzite* and para-amphibolite.	Cutana beds (South Flinders Zone); Younghusband Conglomerate (Peake and Denison Inlier)

Italics indicate features important in mineral systems analysis or the location of copper deposits and occurrences.

Table 3.6.4: Copper production of poorly described deposits in the Adelaide Rift Complex

CALLANNA GROUP		BURRA GROUP		UMBERATANA GROUP	
Deposit	Cu (kt)	Deposit	Cu (kt)	Deposit	Cu (kt)
Clara St Dora	300	Montacute	300	Paull Consolidated	1000
				Prince Alfred	2000

Data from Bampton (2003)

3.6.1.1 Deposits hosted by the Callana Group

The Callanna Group, which consists of the basal Arkaroola Subgroup and the overlying Curdimurka Subgroup (Table 3.6.3), was deposited between ~830 and ~800 Ma. The age range is based on the correlation of the Wooltana Volcanics in the Arkaroola Subgroup with the 827 ± 6 Ma (Wingate *et al.*, 1998) Gairdner Dyke Swarm and ages of 802 ± 10 Ma (Fanning *et al.*, 1986) for the Rook Tuff in the Curdimurka Subgroup.

The Arkaroola Subgroup consists of a basal quartzite which is overlain by a carbonate-dominated unit that, in turn, is overlain by dominantly basaltic volcanics. These rocks, which are interpreted to have been deposited in variably shallow marine, fluviatile and lacustrine environments (Ambrose *et al.*, 1981; Preiss, 1993, 2000), host epigenetic copper±uranium deposits in carbonate-dominated and basaltic units (Tables 3.6.1-3.6.3). The most significant deposits include those in the Yudnamuntana field, which are located along the northwest margin of the Mount Painter Inlier and were worked between 1862 and 1867 (Table 3.6.2; Figure 3.6.1; Bampton, 2003). Minor copper deposits and occurrences are numerous, including the Clara St Dora deposit (Table 3.6.4). There are several minor uranium-bearing occurrences also in the Yudnamuntana field, hosted both by the Wywyana Formation (Valley-Shaft) and the Wooltana Volcanics (Shamrock copper). Both of these deposits are epigenetic, the former in pitchblende-bearing quartz lodes and the latter in actinolite-bearing veins along shears (Table 3.6.1).

The Curdimurka Subgroup contains the Blinman deposit, which is interpreted to be hosted by a raft of Recovery Formation equivalent within the Blinman diapir (Tables 3.6.2 and 3.6.3). Because the ores were restricted to a megaclast, it is possible that they formed prior to emplacement of the clast within the diapir. The Dunns Mine Limestone contains a number of small copper working at Callana, Dunns and Rook workings (Table 3.6.3; Preiss, 1993).

3.6.1.2 Deposits hosted by the Burra Group

The Burra Group, which overlies the Callanna Group, consists mostly of siliciclastic and carbonate rocks with minor mafic to felsic volcanic units. The Boucaut Volcanics, inferred to lie near the base of the Burra Group, comprises both coherent and highly sheared bimodal volcanic rocks (basalt and rhyolitic) (Preiss, 1993; Table 3.6.3). At Burra, felsic volcanic rocks and intrusive dykes occur in the Kooringa Member, Skillogalee Dolomite, Mundallio Subgroup. Drexel (2008) and Preiss *et al.* (2010) indicate an age of ~790 Ma for both dykes and extrusives. This age, combined with the ~802 Ma age of the Rook Tuff in the Curdimurka Subgroup indicates that the lower and middle part of the Burra Group was deposited rapidly ~800 to ~790 Ma.

The Burra Group hosts copper deposits, prospects and occurrences at two, or possibly three, stratigraphic levels, the Boucat Volcanics and the Mundallio Subgroup. The third possible level is the upper Burra Group (Kadlunga Slate: Brugger *et al.*, 2006). Of these stratigraphic levels, the

uppermost and lowermost are relatively minor, with the most significant deposits in the Mundallio Subgroup.

Deposits hosted by the Boucat Volcanics include the Mutooroo Ridge prospect, which is characterised by malachite within quartz-magnetite shear zones (Table 3.6.3). The Paratoo prospect is hosted by shale and dolomite that Brugger *et al.* (2006) interpreted to be within the upper Burra Group, possibly Kadlunga Slate equivalents. However, W Preiss (*pers. comm.*, 2011) suggests that the host to the Paratoo prospect could be a xenoclast of Callana Group within the Paratoo diapir.

In the vicinity of Burra, the Mundallio Subgroup hosts a number of deposits and prospects, the most significant of which is the historic Burra mine (Table 3.6.2). This deposit, which produced 82 kt of copper up to 1981 when the mine closed (Drexel, 2008), is hosted by the Kooringa Member of the Skillogalee Dolomite. The Kooringa Member consists of a distinctive package of siltstone, limestone and dolomite, with a tuffaceous component identified in siltstone (Drexel, 2008). The succession is intruded by felsic porphyrytic dykes which cut stratigraphy very obliquely. These dykes provided the ~790 Ma age, and, if the inference of a genetic link between copper mineralisation and dyke emplacement (Drexel, 2008) is correct, this age corresponds to the age of mineralisation. The deposit is in sheared contact with unaltered and generally unmineralised breccias of the Burra diapir (Drexel, 2008).

Because the Burra mine was developed within the oxide zone, the ore mineralogy is dominated by secondary copper minerals (Drexel, 2008), with very minimal indication of the primary mineralogy. These limited indications include an observation by Nixon and Townend (1966) of chalcopyrite with inclusions of bornite. The porphyry also contains disseminated pyrite euhedra completely replaced by chalcocite. Limonite pseudomorphs after pyrite are also disseminated in the Kooringa Member (Drexel, 2008).

Texturally, the ores commonly consist of breccias of all host rock types, dolomite, siltstone and porphyry, infilled by secondary copper minerals. Alteration assemblages associated with hypogene mineralisation are dominated by microcline and affect clasts within the breccias. Other alteration minerals include tourmaline, which is spatially associated with the felsic dykes and crystalline dolomite. The latter is developed in a massive body of recrystallised dolomitic marble that is laced with secondary copper sulfide, oxide and carbonate veins (Drexel, 2008).

Other than the Burra deposit, the Skillogalee Dolomite contains a number of other prospects and occurrences, the most important being Copper Claim and Princess Royal. Both of these deposits are strataform, with the Copper Claim prospect extending over an area of 1.0 × 2.5 km (Rowlands *et al.*, 1978). At this deposit, chalcopyrite and trace bornite are present as disseminated grains and in calcite-quartz veins (Rowlands *et al.*, 1978). Low level gold has also been identified at this prospect. At Princess Royal, copper is present as secondary minerals in veins and breccias. This prospect also contains low grade gold zones which overlap, or are adjacent to the copper zones.

Uranium is present at the Fairview phosphate mine, which is hosted by the Skillogallee Dolomite. This prospect also contains secondary copper minerals, and is enriched in the light rare-earth-elements lanthanum and cerium (Table 3.6.1; Wilson and Fairclough, 2009). Uranium is also anomalous at the Pine Ridge prospect, which is hosted by a quartz-iron oxide-rich zone in the Woolshed Flat Shale adjacent to a pegmatite (Table 3.6.1; Wilson and Fairclough, 2009). Uranium, along with light rare-earth-elements and gold values, are also present at the Paratoo deposit (Brugger *et al.*, 2006) in carbonaceous siltstone of uncertain stratigraphic position.

As discussed above, many copper deposits in the Burra Group are known to contain uranium, gold and light rare-earth-elements. It is possible that these elements may be present at deposits such as Burra where they have not been assayed for in sufficient detail. Evidence from deposits which contain these elements suggest that their enrichment may be offset from copper enrichment.

3.6.1.3 Deposits hosted by the Umbertana Group

The Umbertana Group, particularly the Tapley Hill Formation, has by far the largest concentration of copper in the Adelaide Rift Complex. This group consists predominantly of siliciclastic rocks, mostly silstone and shale, with lesser carbonate units, although some of the siliciclastic rocks are dolomitic or calcareous (Table 3.6.3; Preiss, 1993). Unlike the Burra and Callanna Groups, the Umbertana Group does not contain significant volcanic units. The Umbertana Group also records two periods of glaciation as indicated by the Pualco and Pepuarta tillites and their correlates (Table 3.6.3; Preiss, 1993).

The main copper host in the Umbertana Group is the Tapley Hill Formation, a unit characterised by calcareous or dolomitic carbonaceous siltstone. It is the oldest unit of the Adelaide Rift Complex to transgress onto the Stuart Shelf. The largest deposits hosted by the Tapley Hill Formation are shale-hosted deposits in the Mount Gunson area (Knutson *et al.*, 1983: 617.9 kt copper), and at Kapunda (67.9 kt copper). Other smaller deposits hosted by this unit include deposits adjacent to the Copley (Mountain of Light), Lyndhurst (Lynda and Lorna Doone) and Mount Coffin (Elsie Adair) diapirs (Table 3.6.2). In the Mount Gunson area, copper is present also along the unconformity between the Adelaide Rift Complex and basement (167.4 kt copper). In these sandstone-hosted deposits, copper is hosted both by the Whyalla Sandstone and by the unconformably underlying Mesoproterozoic Pandurra Formation (Knutson *et al.*, 1983: Table 3.6.2).

Although deposits hosted by the Umbertana Group are broadly stratabound, in detail the copper is mostly present as veins or as the infill to breccias, although some is present as disseminated grains in the host. In hypogene zones at Mount Gunson and Kapunda, significant copper is present as bornite and chalcocite, although the dominant copper mineral is mostly chalcopyrite (Table 3.6.2). At Mount Gunson, copper minerals are distinctly zoned, with chalcopyrite grading into bornite and then into chalcocite from northwest to southeast (Tonkin and Creelman, 1990). Mount Gunson and Kapunda also contain abundant pyrite as well as minor to trace sphalerite, galena. The Mount Gunson deposits also carry minor to trace carrolite, witichenite and native bismuth (Tonkin and Creelman, 1990). Pyrrhotite is reported at Kapunda (Lambert *et al.*, 1980).

Lambert *et al.* (1980) describe albite and dolomite alteration of the host siltstone at Kapunda. In addition, they note that the mineralised zones can also be uranium-rich, with assays of up to 150 ppm. The Mount Gunson deposit carries significant cobalt and silver, hosted by carrolite and bornite-chalcocite, respectively. The assemblage copper-silver-cobalt±uranium noted for deposits in the Umbertana Group is similar to that seen in the Zambian Copper Belt (Hitzman *et al.*, 2005) and differs from the assemblages present in lower stratigraphic units in the Adelaide Rift Complex.

3.6.2 Diapirs and their relationship to mineralisation

The Adelaide Rift Complex is characterised by a large number of breccia zones. These breccia zones, which are commonly, but not exclusively, coincident with the cores of domes and anticlines, generally contain clasts interpreted as having been derived from the Callanna Group at the base of the Neoproterozoic succession (Webb, 1961; Coats, 1964; Dyson, 2001). Individual megaclasts within the breccia bodies can have dimensions of several hundreds of metres. Webb (1960) initially

interpreted the breccia bodies as diapirs, although other processes, including slumping, tectonic breciation and sedimentary brecciation, have also been proposed for their origin (see discussion in Preiss, 1985).

Despite the controversy over their origin, there is a close spatial association between many of the copper deposits of the Adelaide Rift Complex with these breccia zones. Of the 12 districts/deposits listed in Table 3.6.2, seven are spatially associated with the breccia zones, either within megaclasts (e.g., Blinman) or in country rock adjacent to the breccia bodies. Dyson (2001) suggested that the breccia zones, which he interpreted as diapirs, acted as fluid pathways. However, the largest district in the study area, at Mount Gunson, is not spatially associated with breccia bodies, suggesting that other fluid pathways may have been used by cupriferous fluids in this case.

3.6.3 Mineral system model for uranium and copper deposits associated with the Adelaide Rift Complex

As described in Section 3.1, a weighted fuzzy index overlay approach has been used to assess the potential for copper and uranium in the Adelaide Rift Complex. This method used a mineral system approach that has been divided into four components:

- sources of metals, fluid and salinity;
- drivers for fluid flow;
- fluid pathways and architecture; and
- depositional mechanisms and sites.

This model (Figure 3.6.2) was kept very general as the evidence described above (e.g., multiple stratigraphic hosts, multiple metal assemblages, variable alteration assemblages) suggests that there may have been more than one mineral system operating during the evolution of the Adelaide Rift Complex. Table 3.6.5 summarises the characteristics of, and source data for, the mappable criteria used to assign potential for each mineral system components. This analysis differs from other analysis in that it extended south from the study area to cover the entire Adelaide Rift Complex.

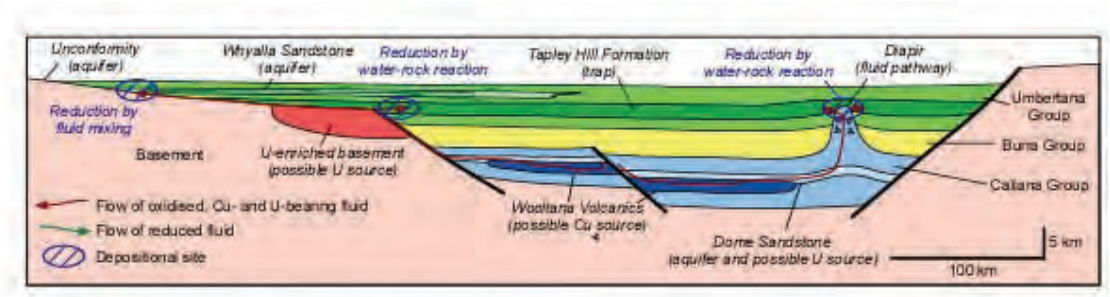

Figure 3.6.2: *Schematic model for Cu±U mineral systems in the Adelaide Rift Complex*

3.6.3.1 Sources

The most fundamental component of a mineral system is a source for the commodities ultimately concentrated in a mineral deposit. For the mineral system under consideration, the main commodity to consider is copper, although by-product commodities produced in the Adelaide Rift Complex include cobalt and silver. The other commodity important in this analysis is uranium. These commodities are inferred to be leached by evaporative, hypersaline basinal fluids, formed under shallow water marine conditions as they circulate through the rift basin and basement (Figure 3.6.2).

The distribution of mafic to intermediate volcanic rocks is considered as a proxy for copper sources because these are generally elevated in copper (Wedepohl, 1974). Regions containing mafic rocks were determined from Figure 12 of Coats and Preiss (1987). These regions were generalised from this figure to include both the distributions of mapped mafic volcanic rocks and bodies identified as xenoclasts in diapirs. Figure 3.6.3 shows variations in the weighting of the copper source derived using these data and the weights given in Table 3.6.5.

The distribution of potential uranium sources was mapped using two criteria:

- the distribution of uranium-rich rocks within the basement as determined from radiometric data; and
- the distribution of felsic volcanic rocks within the Adelaide Rift Complex.

These rocks can be enriched in uranium (Roger and Adams, 1969) and their glassy nature can aid in leaching by basinal fluids. Figures 3.6.4 and 3.6.5 show variations in the weighting of the uranium source derived using these data and the weights given in Table 3.6.5.

The most likely mineralising fluid in the Adelaide Rift copper±uranium mineral system was an oxidised basinal brine (Lambert *et al.*, 1980). If mineralisation was syngenetic or early diagenetic, brine factories within the host succession are likely fluid sources. If mineralisation was epigenetic, shallow water sedimentary successions, particularly where halite or other indications of evaporative conditions are present, represent good potential sources for mineralising brines. In analagous systems elsewhere, for instance the Zambian Copper Belt or the Kupferschiefer deposits in north-central Europe, basinal brines are generally invoked as the ore fluid (Hitzman *et al.*, 2005). To map the distribution of potential sources of brines, the presence of halite or other mineralogical indications of evaporative fluids were used. In addition, the presence of stromatolites was used to indicate shallow depositional conditions, which may be conducive also to the formation evaporative brines. Mineralogical evidence of evaporative processes was given a higher weight than the presence of stromatolites. These characteristics were extracted from Preiss (1987) and Preiss *et al.* (2000) and are summarised in Table 3.6.3. Figure 3.6.6 shows variations in the weighting for fluid source using these data and the weights given in Table 3.6.5. Assigning of weights was done at the subgroup level.

The normalised, cumulative (additive) weighting for the sources of metals and fluids is shown as inserts in Plates 3.8 and 3.9. Inspection of these insets and Figures 3.6.3, 3.6.4 and 3.6.6 indicates that the strongest control on high values for this mineral system component is the inferred availability of basinal brines, which is mapped on a subgroup basis and, therefore, relatively restricted. The inferred availability of source rocks for both copper and uranium is more widespread and this is enhanced by buffering around the source rocks. It must be stressed that uranium source constitutes about 40% of the cumulative weighting. Consequently, the distribution of potential uranium sources (Figure 3.6.4) should be given additional weight in targetting uranium-bearing systems.

3.6.3.2 Drivers

Mechanisms proposed to drive fluid flow in major sediment-hosted copper provinces around the world are quite varied (cf., Hitzman *et al.*, 2005) and broadly include compaction (of basinal sediments), gravitation (through differential topography) and convection (if a heat source is present). All of these mechanisms may have driven fluid flow in the Adelaide Rift Complex at different times.

Table 3.6.5. Mappable criteria and weights used for mineral potential analysis of the Adelaide Rift Complex for copper±uranium deposits.

MINERAL SYSTEM COMPONENT	CRITERIA		DATASET	IMPOR-TANCE	APPLIC-ABILITY	CONFI-DENCE	WEIGHT	COMMENTS
	THEORETICAL	MAPPABLE						
1. Source of uranium	Distribution of U-enriched rocks in the basement	10 km buffer around U-enriched basement rocks 30 km buffer around U-enriched basement rocks 100 km buffer around U-enriched basement rocks	Radiometric Map of Australia (Minty *et al*., 2010)	1.00 1.00 1.00	0.75 0.50 0.25	1.00 1.00 1.00	0.750 0.500 0.250	Uranium values greater than or equal to 10 ppm were extracted from the filtered uranium band and converted to a polygon shape file. A spatial query was used to select values for crystalline basement only. Buffers were allowed to extend into Adelaide Rift Complex.
	Distribution of felsic volcanic rocks within Adelaide Rift Complex	30 km buffer including and around mapped felsic volcanic rocks within the Adelaide Rift Complex	1:100 000 scale geology GIS; Preiss (1987)	0.50	0.50	1.00	0.250	Compositional classification taken from geological unit descriptions.
1. Source of copper	Distribution of mafic volcanic rocks within Adelaide Rift Complex	Regions containing mapped mafic volcanic rocks 30 km buffer around regions with mapped mafic rocks 100 km buffer around regions with mapped mafic rocks	Coats and Preiss (1987)	1.00 1.00 1.00	0.75 0.50 0.25	0.50 0.50 0.50	0.375 0.250 0.125	Interpreted distribution of mafic rocks based on Figure 12 of Coats and Preiss (1987).
1. Source of fluids and ligands	Distribution of evaporite minerals or other evidence of shallow water environments conducive to production of basinal brines	Subgroup with evidence (e.g., minerals or casts) of evaporative minerals (halite or shortite)	Preiss (1987, 2000); Geoscience Australia stratigraphic database (see table 3.6.3)	1.00	1.00	1.00	1.000	
		Subgroup with stromatolites (evidence of shallow water environment)		1.00	0.50	1.00	0.500	
3. Architecture of potential fluid pathways	Distribution of basal unconformity between Adelaide Rift Complex and basement	1 km buffer of unconformity 5 km buffer of unconformity 10 km buffer of unconformity	1:100 000 scale geology GIS; Preiss (1987); Tonkin and Creelman (1990)	0.50 0.50 0.50	1.00 0.75 0.50	1.00 1.00 1.00	0.500 0.375 0.250	Unconformity interpreted from solid geology map.
	Distribution of mapped faults	2 km buffer of fault 5 km buffer of fault	Surface Geology of Australia 1: 1 000 000 scale (Whitaker et al., 2008)	1.00 1.00	1.00 0.50	0.75 0.75	0.750 0.375	
	Distribution of interpreted faults	2 km buffer of fault 5 km buffer of fault	Magnetic and Gravity Maps of Australia; 1:100 000 scale geology GIS	0.50 0.50	1.00 0.50	0.75 0.75	0.375 0.188	Faults interpreted from aeromagnetic and gravity data taking into account mapped faults.
	Potential sedimentary aquifers	One formational unit above or below potential aquifer Two formational units above or below potential aquifer	PIRSA 1:100 000 scale geology GIS; Preiss (1987)	0.75 0.75	1.00 0.50	1.00 1.00	0.750 0.375	Aquifer itself was assigned a weight of zero.
	Distribution of diapirs	2 km buffer of diapir (includes diapir) 5 km buffer of diapir	Preiss (1987)	0.50 0.50	1.00 0.50	1.00 1.00	0.500 0.250	
4. Depositional mechanisms and environment	Evidence of uranium deposition	U^2/Th radiometric maps - 1σ above mean U^2/Th radiometric maps - 2σ above mean	Radiometric Map of Australia (Minty *et al*., 2010)	0.75 0.75	0.50 0.75	0.50 1.00	0.188 0.563	
	Thorium enrichment that may indicate uranium deposition at depth	Th enrichment - 1σ above mean Th enrichment - 2σ above mean	Radiometric Map of Australia (Minty *et al*., 2010)	0.25 0.50	0.25 0.25	0.50 0.50	0.031 0.063	
	Redox gradients - carbonaceous rocks	Formations containing carbonaceous rocks 2 km buffer around formations containing carbonaceous rocks	PIRSA 1:100 000 scale geology GIS; Preiss (1987)	1.00 1.00	0.75 0.50	1.00 1.00	0.750 0.500	Distribution of carbonaceous units, based on descriptions in Preiss *et al.* (1987), as determined from GIS.
	Redox gradients - Fe^{2+}-rich rocks	Formations containing Fe^{2+}-rich rocks 2 km buffer around formations containing Fe^{2+}-rich rocks	PIRSA 1:100 000 scale geology GIS; Preiss (1987)	0.75 0.75	0.75 0.50	1.00 1.00	0.563 0.375	Distribution of Fe^{2+}-rich units, based on descriptions in Preiss (1987), as determined from GIS.
	Chemical gradients - carbonate-rich rocks	Formations containing carbonate-rich rocks 2 km buffer around formations containing carbonate-rich rocks	PIRSA 1:100 000 scale geology GIS; Preiss (1987)	0.50 0.50	0.75 0.50	1.00 1.00	0.375 0.250	Distribution of carbonate-rich units, based on descriptions in Preiss (1987), as determined from GIS.

However, they are not mappable using currently available data, so fluid flow drivers were excluded from this analysis.

3.6.3.3 Fluid pathways and architecture

As shown in Figure 3.6.2, there are a number of pathways which mineralising fluids could follow from source to trap, including stratigraphic pathways, such as unconformities or sedimentary aquifers, and structural pathways, such as faults and diapiric breccias. All four of the potential fluid pathways were considered in this analysis. Weights for each are summarised in Table 3.6.5.

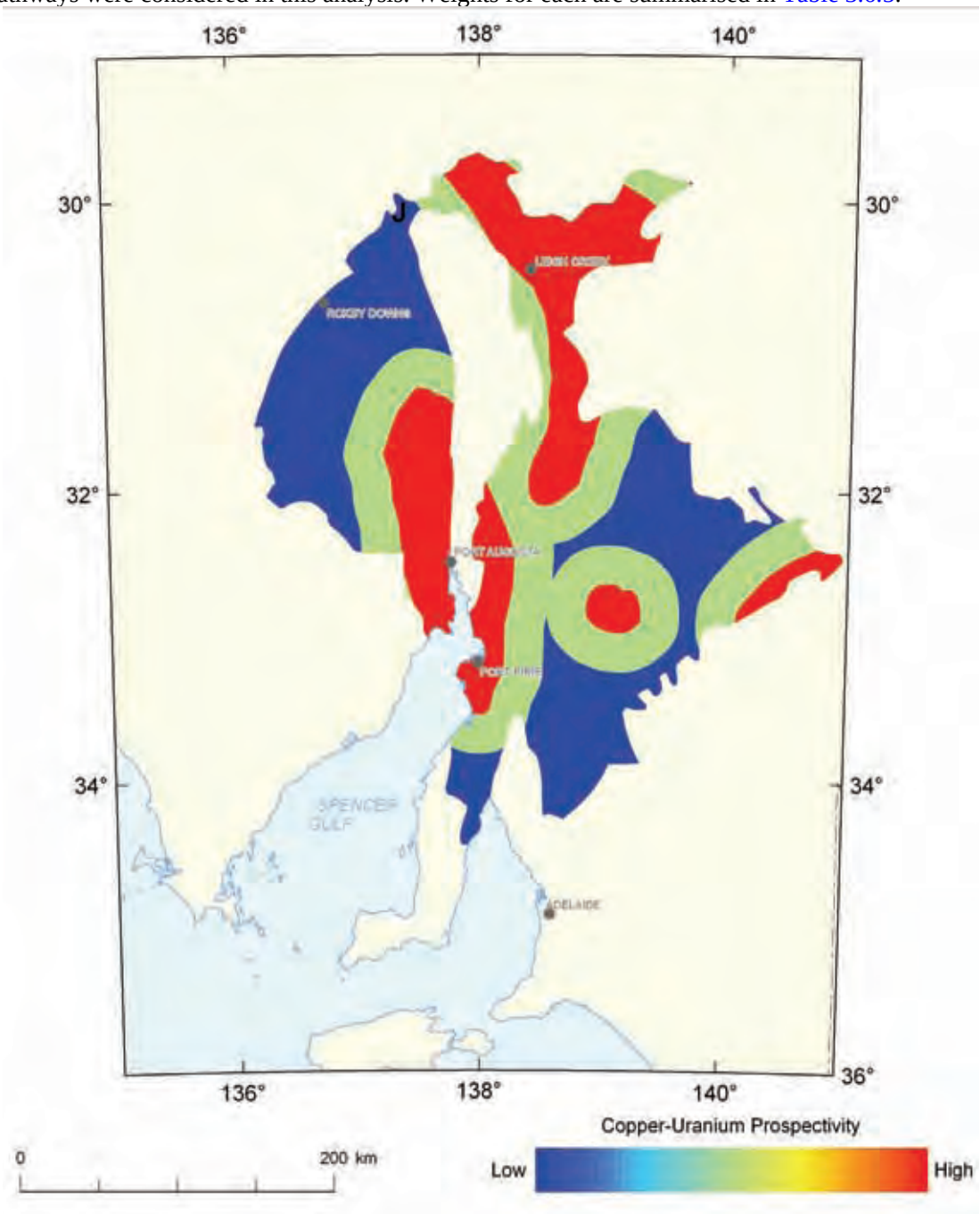

Figure 3.6.3: *Variations in the weighting of copper source, Adelaide Rift Complex mineral system.*

Faults in effect were given a double weighting because two different datasets were used as mappable ingredients. The first was the distribution of mapped faults, which was given a higher weight than the second dataset, the distribution of faults inferred from potential field data. Although this second dataset should identify through-going faults more effectively, there is greater uncertainty in the interpretation, resulting in the lower weight. Because deposition of many types of mineral deposits (e.g., lode gold systems) occurs on second, or lower order structures, the faults were buffered in the analysis.

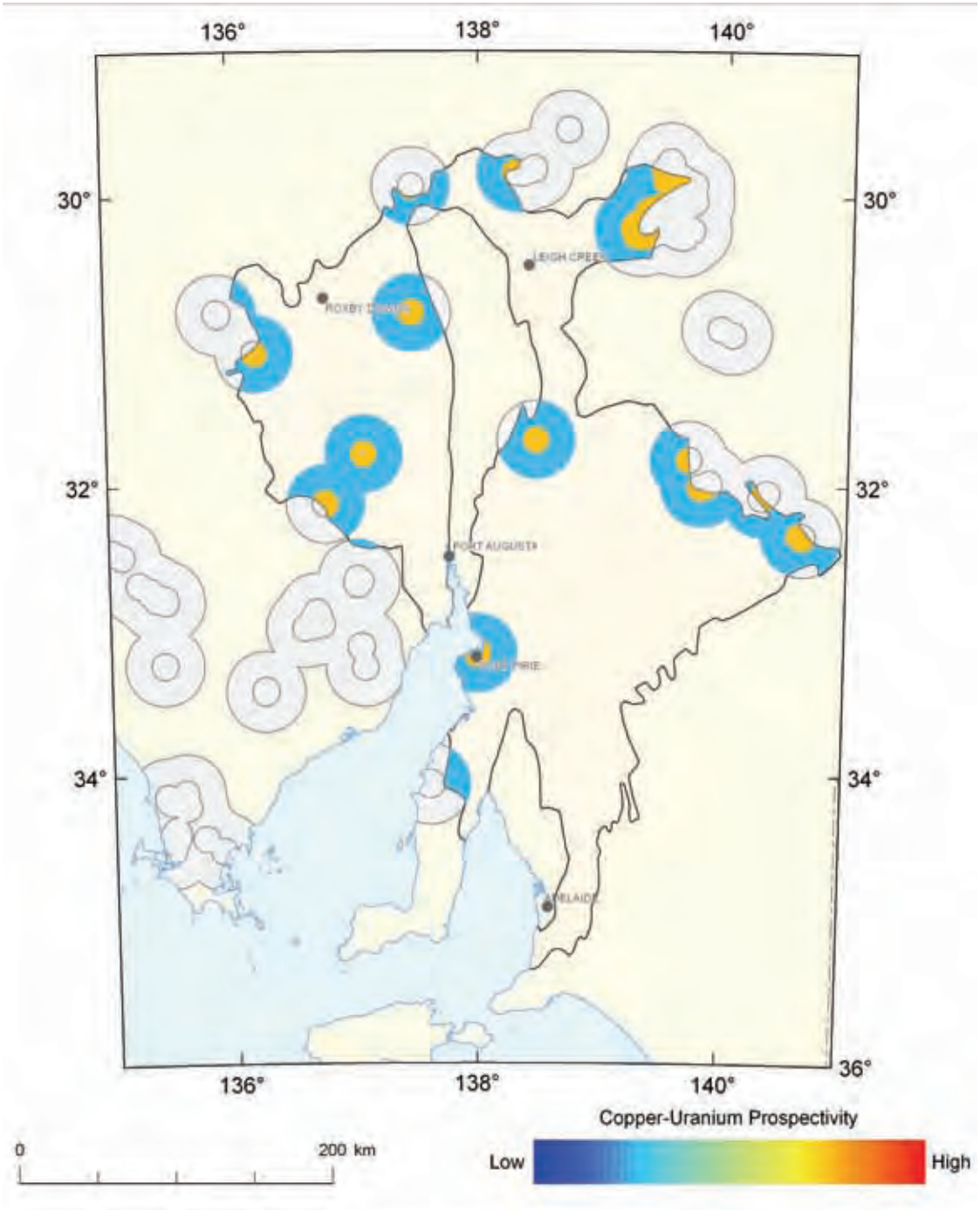

Figure 3.6.4: *Variations in the weighting of uranium source as determined from radiometric data, Adelaide Rift Complex mineral system.*

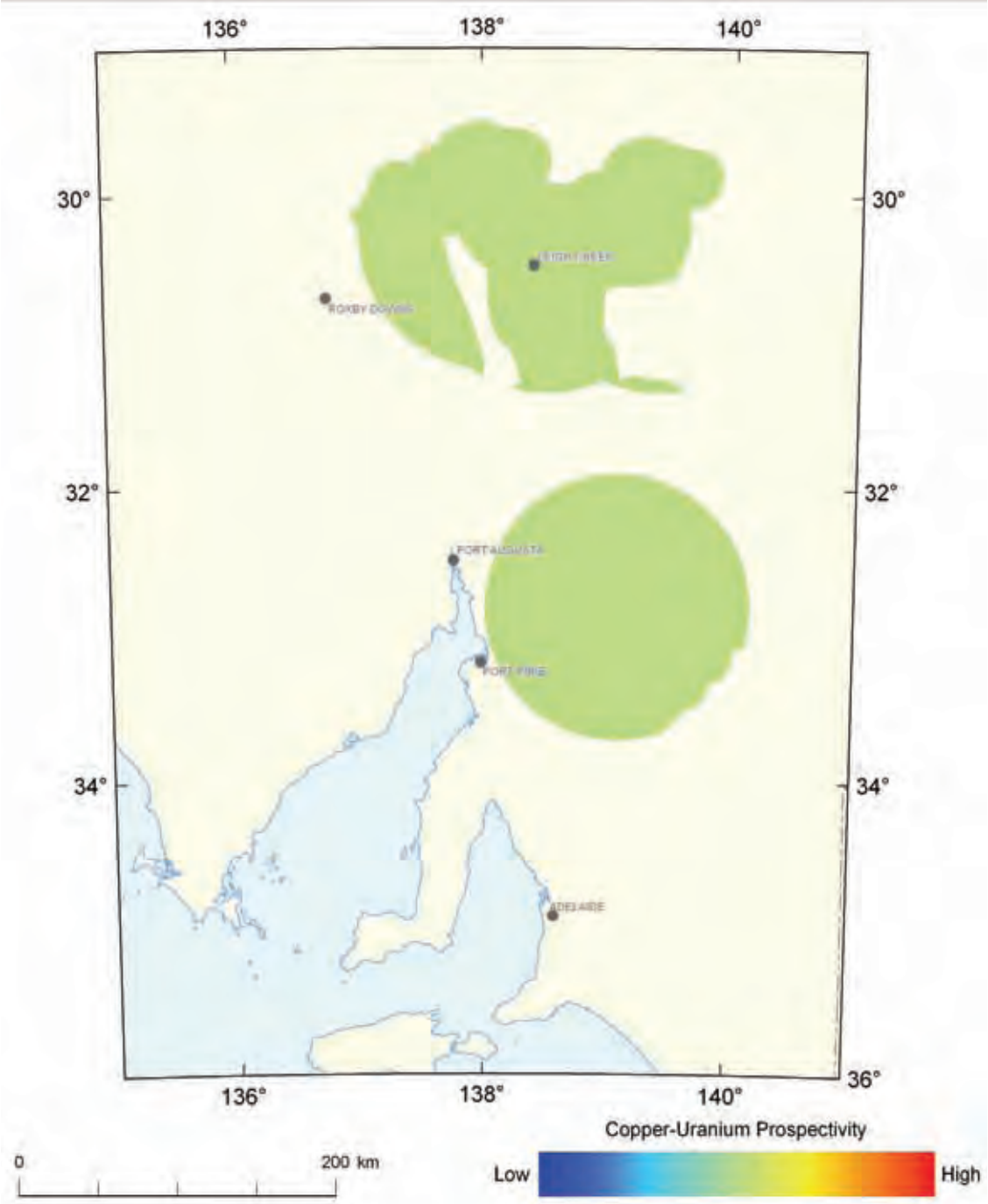

Figure 3.6.5: *Variations in the weighting of uranium source as determined from the distribution of felsic volcanic rocks, Adelaide Rift Complex mineral system.*

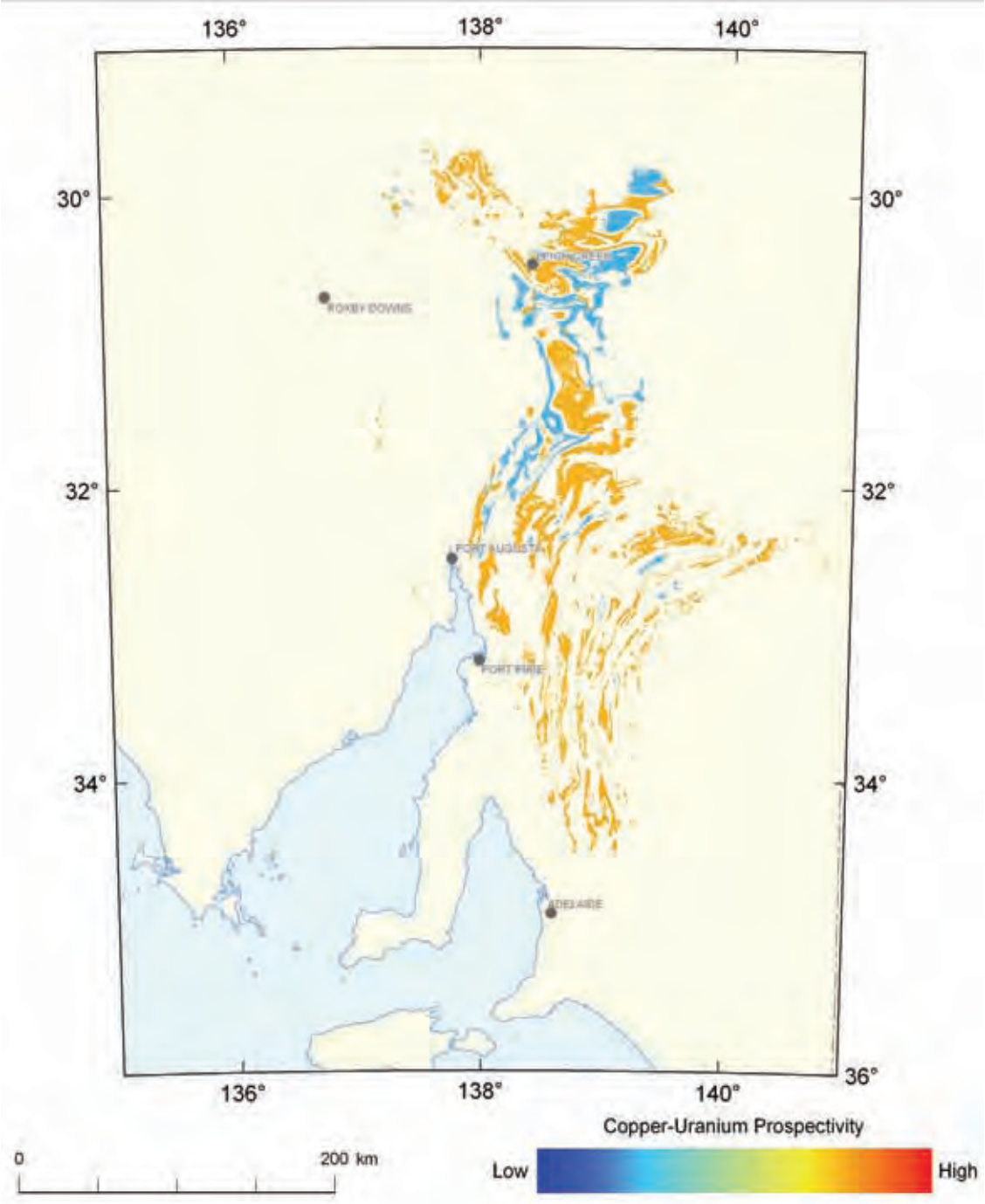

Figure 3.6.6: *Variations in the weighting of brine source, Adelaide Rift Complex mineral system.*

Figures 3.6.7 and 3.6.8 show variations in the combined weighting for faults using the weights given in Table 3.6.5.

As discussed in Section 3.6.2 there is an empirical relationship between many of the known copper deposits and diapiric breccias. This is interpreted to indicate that these features acted as fluid pathways from the lower parts of the stratigraphy into the upper parts of the stratigraphy (Figure 3.6.2). For this analysis, the distribution of diapirs was taken from Coats and Preiss (1987) and buffered (Table 3.6.5). Figure 3.6.9 shows variations in the weighting for diapiric breccias using the weights given in Table 3.6.5.

Sedimentary aquifers were interpreted to include clean quartzites identified from summary descriptions of the lithology by Preiss (1987, 2000: Table 3.6.3). It is important to note that the quartzites themselves were given no weight in the analysis. Weights were given to stratigraphic units (at the formation level) above and below the potential aquifer (Table 3.6.5). This was done because the aquifers are generally chemically inactive and unlikely to cause deposition. Figure 3.6.10 shows variations in the weighting for sedimentary aquifers as described above and using the weights given in Table 3.6.5.

In some models for unconformity-related uranium deposits (see Section 3.3), unconformities which define the base of the basin also have acted as fluid pathways (Figure 3.6.2). Consequently, the basal unconformity of the Adelaide Rift Complex was inferred as a potential fluid pathway, though given a relatively low weighting, with buffers of up to 10 km (Table 3.6.5). Unconformities can be difficult to treat in this analysis because they are generally only identified from surface mapping. In relatively flat dipping areas, such as the Stuart Shelf, the unconformity can be relatively extensive in the shallow subsurface, yet be mapped and given weight only along the basin margins. This shortcoming of the analysis must be borne in mind when considering the results (see Section 3.6.4.1). Figure 3.6.11 shows variations in the weighting for the basal unconformity of the Adelaide Rift Complex as described above and using the weights given in Table 3.6.5.

The normalised, cumulative (additive) weighting for fluid pathways is shown as insets in Plates 3.8 and 3.9. Inspection of these insets and Figures 3.6.6 to 3.6.11 indicates a complex interplay between stratigraphic and structural features that define fluid pathways. The highest values are coincidences between diapiric breccias, faults and favourable stratigraphy. The importance of the basal unconformity is restricted. Importantly, the Stuart Shelf has relatively low potential as identified from this mineral system component, partly because of a lack of data and because of the flat-lying character of large parts of this area. The very southern part of the study area lacked some data sets (i.e., 1:100 000 scale faults), so its true potential is probably higher than assessed.

3.6.3.4 Deposition

The analysis of sediment-hosted copper-uranium deposits in the Adelaide Rift Succession has used two types of data to identify depositional sites;

- direct evidence of uranium deposition; and
- the composition of potential host rocks.

The first data type was extracted from radiometric data. Uranium anomalism at the surface (Table 3.6.5; measured as U^2/Th: Mernagh *et al.*, 1998) is taken as possible evidence of uranium mineralisation at or near the surface (Figure 3.6.12), and thorium anomalism is taken as possible evidence of uranium mineralisation at depth (Table 3.6.5; Figure 3.6.13). These parameters are more-or-less empirical and apply to most, if not all, uranium systems.

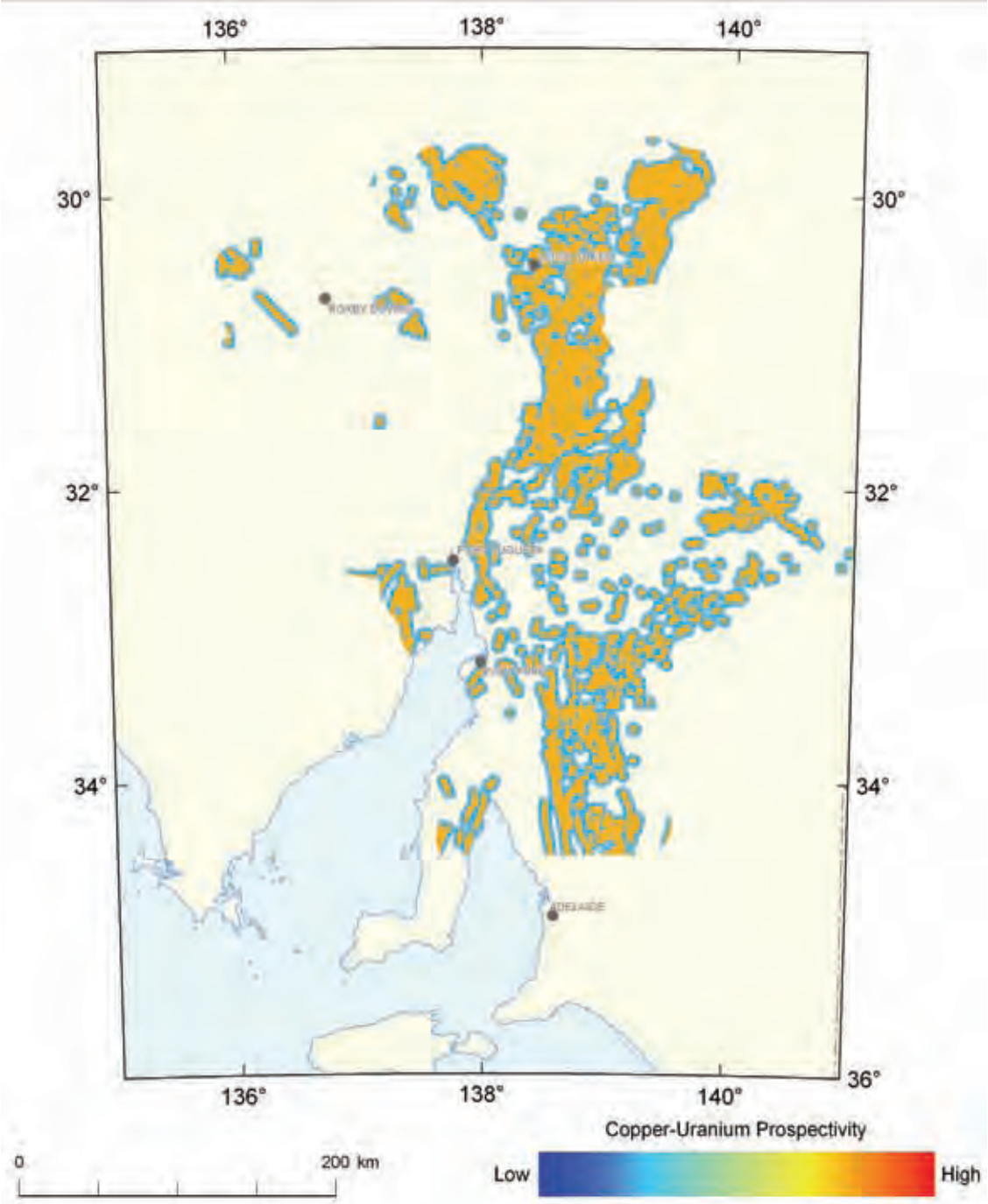

Figure 3.6.7: *Variations in the weighting of fluid pathways - mapped faults, Adelaide Rift Complex mineral system.*

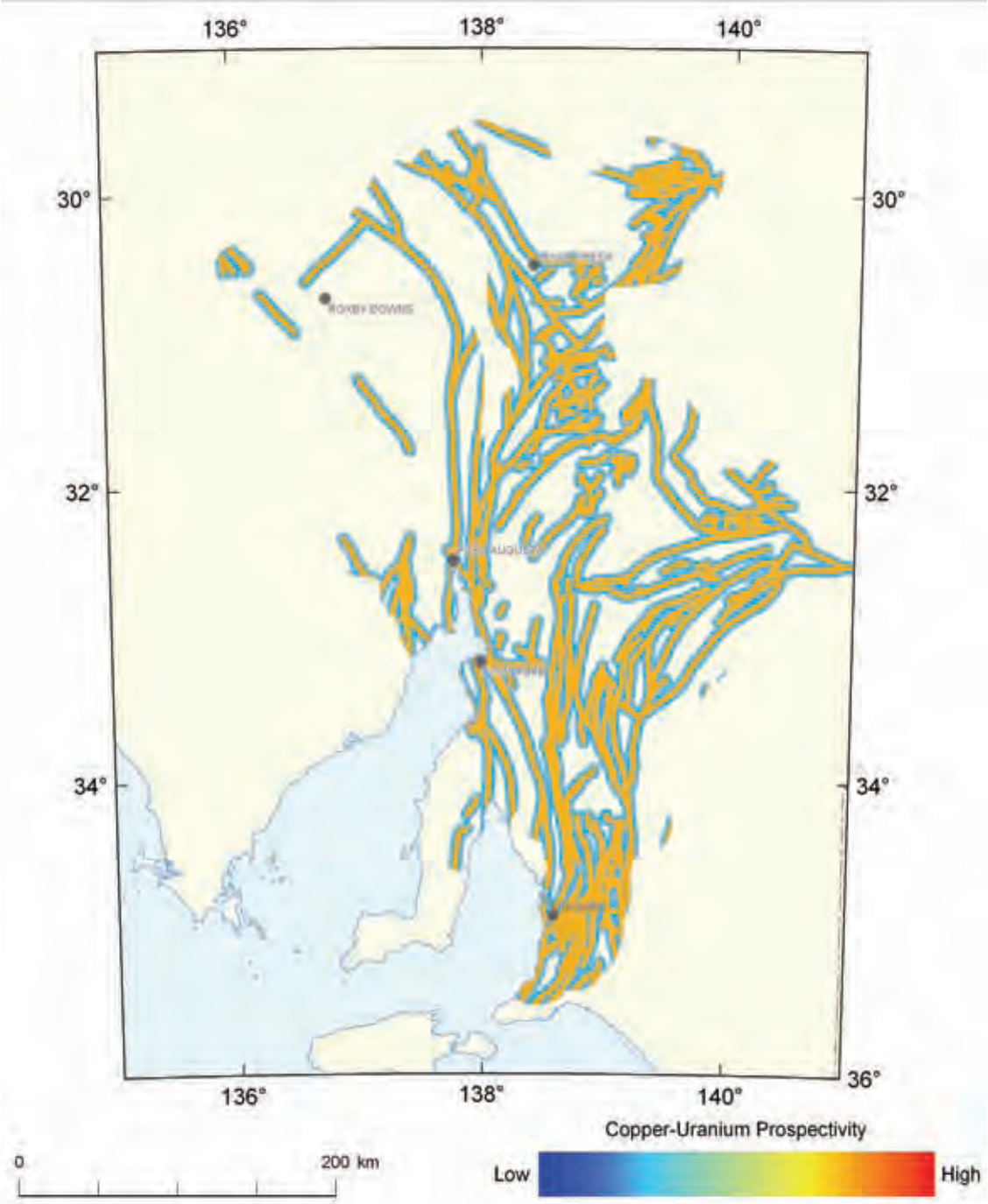

Figure 3.6.8: *Variations in the weighting of fluid pathways - interpreted faults, Adelaide Rift Complex mineral system.*

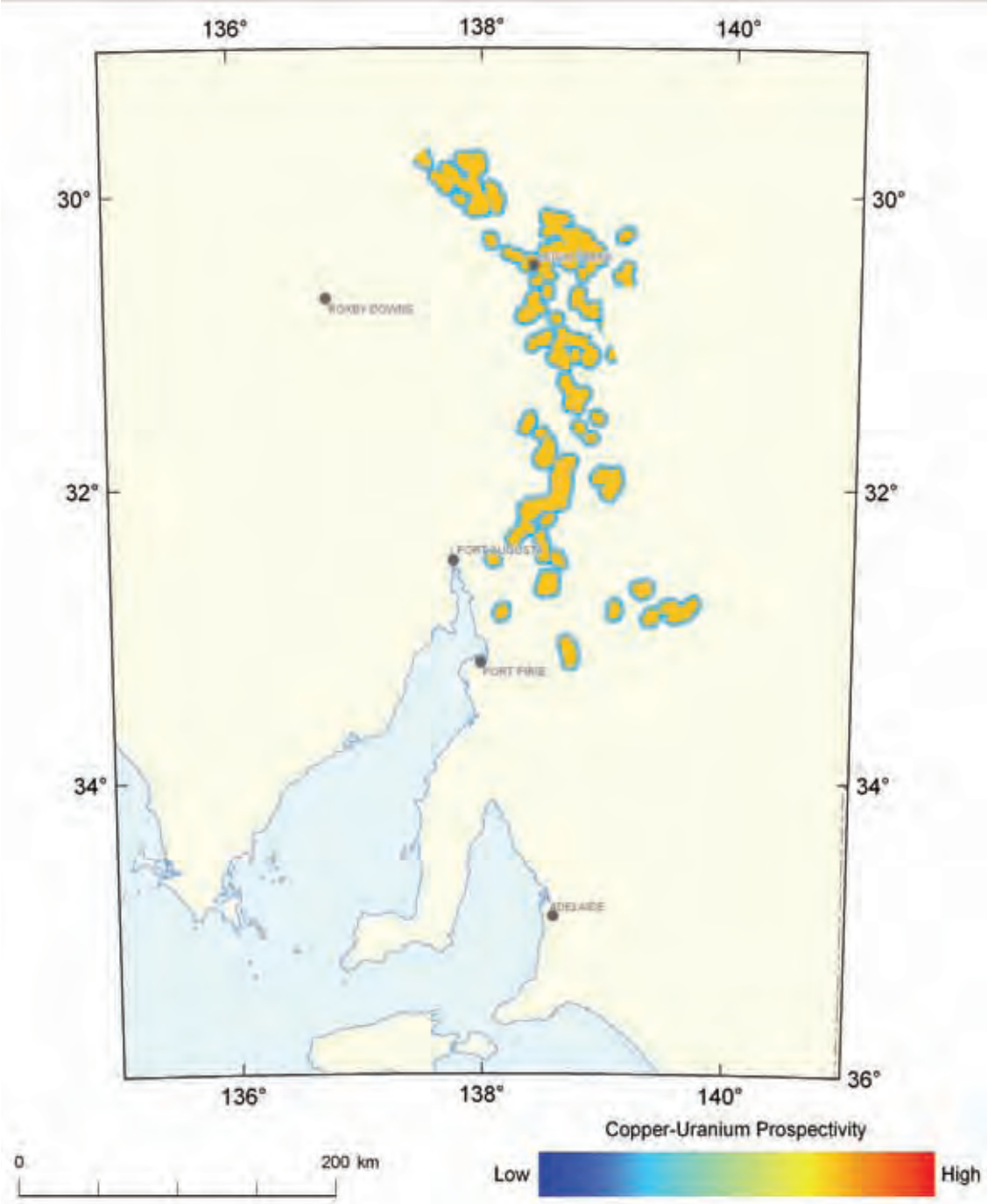

Figure 3.6.9: *Variations in the weighting of fluid pathways - diapiric breccias, Adelaide Rift Complex mineral system.*

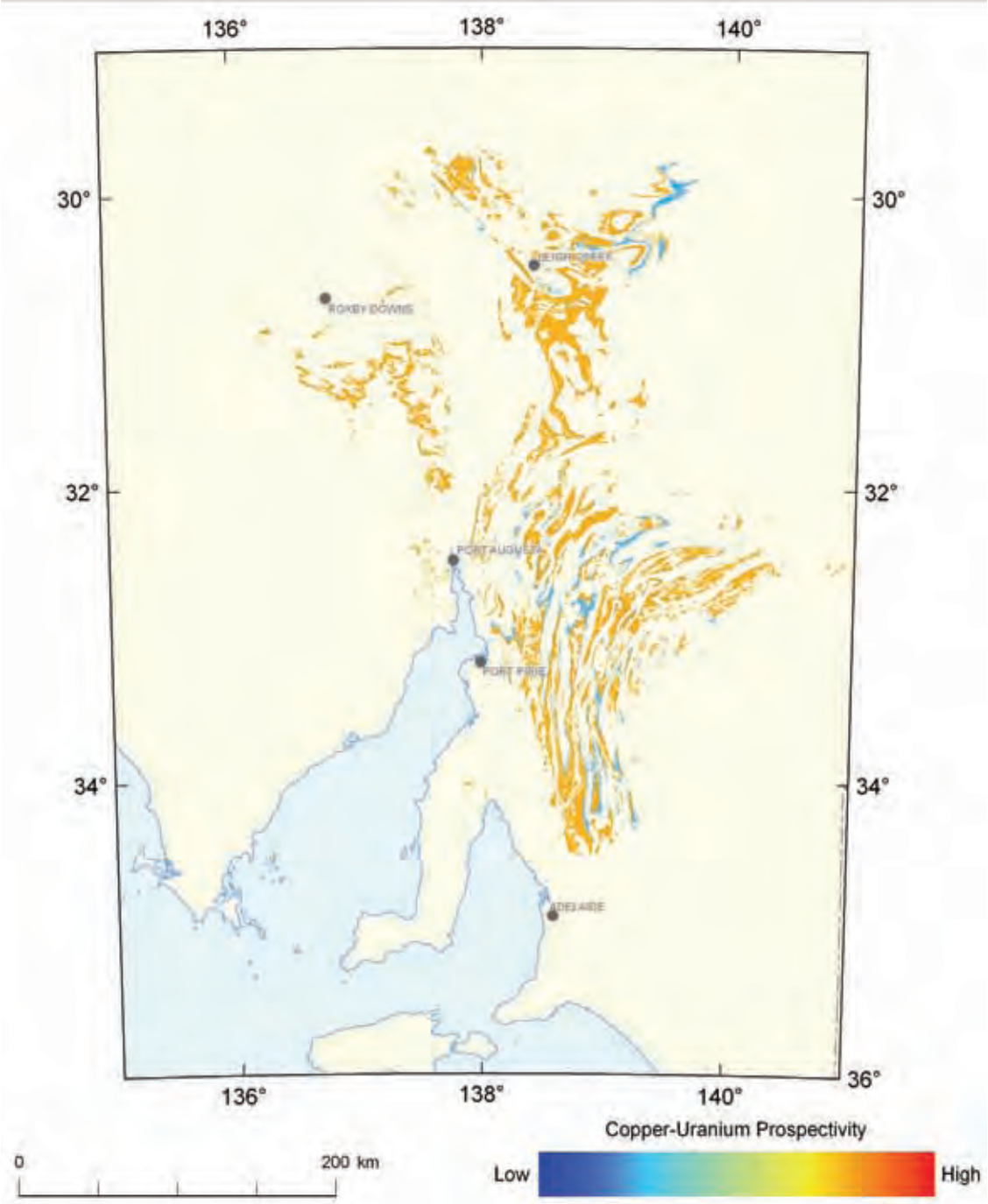

Figure 3.6.10: *Variations in the weighting of fluid pathways - sedimentary aquifers, Adelaide Rift Complex mineral system. Note that prospective areas are not the pathways themselves, but stratigraphic units above and below the aquifers.*

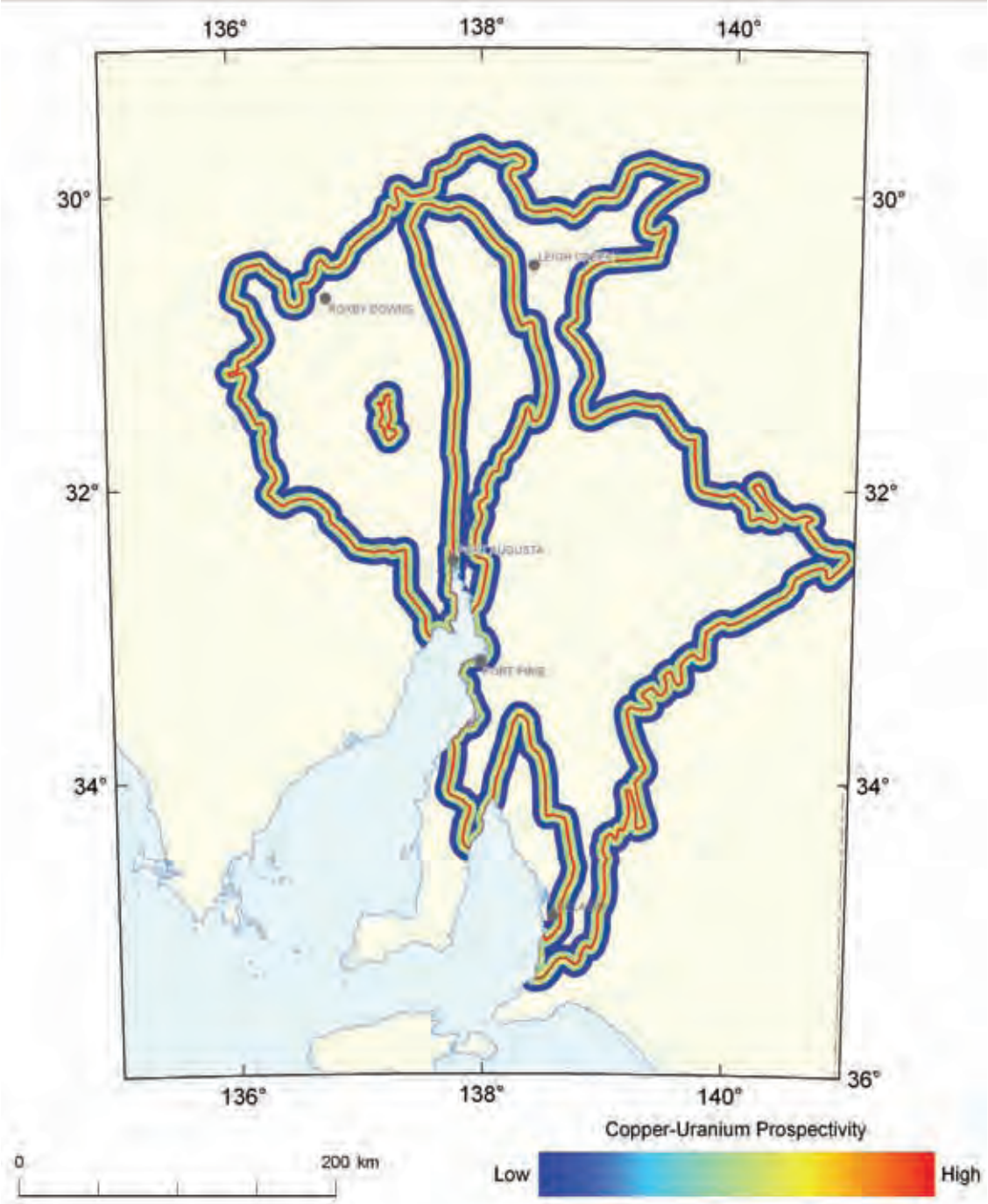

Figure 3.6.11: *Variations in the weighting of fluid pathways-basal unconformity, Adelaide Rift Complex mineral system.*

Depositional mechanisms in sediment-hosted copper deposits are generally thought to be chemical. Oxidised, hydrogen sulfide-poor, basinal brines, which can carry high concentrations of both copper and uranium (Lambert *et al.*, 1980; Hitzman *et al.*, 2005), interact with reduced rock units or fluids, reducing the ore fluid and causing ore deposition. This mechanism, which can occur at or near surface, or at depth within the sedimentary pile (Figure 3.6.2), requires interaction of the ore fluid with a reduced rock package, a reduced sedimentary environment or fluids equilibrated with such rocks and environments. Because ambient fluids in the rock package are likely to be in chemical equilibrium with the host rock, the characteristics of the rock package also acts as a proxy for these fluids.

Based on the lithologies described by Preiss (1987), potential reducing rock units that could act as traps for copper and uranium include carbonaceous rocks and Fe^{2+}-rich rocks, including mafic volcanic rocks and banded iron formation. These rocks were identified at the formation level and buffered (Table 3.6.5) as potential depositional sites (Figure 3.6.14 and 3.6.15). In addition, carbonate rocks (limestone, dolomite and magnesite) were identified and included in the analysis because these rocks can also be highly chemically reactive. However, carbonate rocks were given a lower weighting than either carbonaceous or Fe^{2+}-rich rocks (Table 3.6.5). Figure 3.6.16 shows the weighting assigned to carbonate rocks.

As might be expected from the criteria used for construction, the deposition component of the mineral system is dominated by the distribution of lithological units at the formational level (insets to Plates 3.8 and 3.9). This is consistent with the observation from the distribution of known deposits that there is a strong stratigraphic control on the distribution of deposits.

3.6.4 Results

After combining the three mineral systems components discussed above and using the methods described in Section 3.6.1, Plates 3.8 and 3.9 illustrate the final results of this analysis. Figure 3.6.17 summarises the potential of the entire area. The distribution of deposits, prospects and occurrences have been overlaid in all of these diagrams. Overall, there is a reasonably good correlation of known deposits and assessed potential. This relationship is an independent check of the analysis method because the distribution of known deposits was not used in the analysis. With the exception of the Mount Gunson deposits (see below) and the Paratoo prospect, all copper deposits in Table 3.6.2 are associated spatially with anomalies identified by the analysis. The few uranium-bearing prospects summarised in Table 3.6.1 mostly correspond to areas of enhanced copper-uranium potential identified in this study, as do the copper deposits with anomalous uranium discussed in the text. These results give some confidence to the analysis presented herein, and give credence to areas of higher potential identified outside of known districts.

In addition to the known deposits and districts, the analysis has highlighted a nunber of other areas of interest. These are shown in Figure 3.6.17 and include the following (keyed to the figure):

A) An area to the south of Leigh Creek. This area is along the eastern margin of the Torrens Hinge Zone and contains several prospects and occurrences.
B) An area to the west of Lake Frome. This area is along the eastern margin of the Adelaide Rift Complex and includes several small prospects and occurrences.
C) An area to the west of Blinman. This area is also along the eastern margin of the Torrens Hinge Zone and contains several prospects and occurrences.
D) A series of three areas to the northeast of Hawker. The westernmost area is one of the most intense high areas identified in the analysis. Two of these areas appear to be associated with diapiric breccia, with the westernmost associated with the Upalinna Diapir.

E) A north-south trending area to the east of Port Augusta. This area is along the eastern margin of the Torrens Hinge Zone and contains several prospects and occurrences
F) A small area to the east of Port Pirie. This area contains no known prospects and occurrences.
G) A north-south trending area further to the east of Port Pirie. This area contains no known prospects and occurrences.
H) A north-south trending area to the southeast of Port Pirie. This area is parallel to the belt which contains the Burra and Utica deposits. It has a few prospects and occurrences.
I) An area to the southeast of Paratoo. This area contains a few prospects and occurrences.
J) An area in the northern tip of the Stuart Shelf, halfway between Olympic Dam and Maree. This area is the most intense high areas in the Stuart Shelf, but contains no known deposits, prospects of occurrences.
K) The area around Mount Gunson, particularly to the south. Mount Gunson is the most significant district in the study area and the area to the south contains a number of deposits with small-scale production.

These areas should be considered to have potential for both copper and uranium. Other areas not highlighted in Figure 3.6.17 also may have potential. It must be noted that the very southernmost part of the assessed area (south of 34.5° south latitude) has lower apparent potential because some data sets (1:100 000 scale geology and derived features) used elsewhere in the study area were not available here. Areas of known copper mineralisation should be assessed for uranium potential through analyses of mineralised rocks associated with known deposits and prospects. It is important to bear in mind that uranium and copper (and gold) enrichment is not necessarily coincident, both from a theoretical standpoint and from observations at some deposits.

3.6.4.1 Mount Gunson and the copper-uranium potential of the Stuart Shelf

Although the analysis has highlighted areas of known mineralisation and identified additional areas of interest to the east of the Torrens Hinge Zone, the Stuart Shelf to the west of the Torrens Hinge Zone has apparently lower potential, despite hosting the most significant Neoproterozoic copper district at Mount Gunson. The Mount Gunson area is the most highly mineralised zone within the Adelaide Rift Complex, but the analysis gave it only moderate potential. The district is located along the western margin of the northern part of this moderate level anomaly.

The Stuart Shelf differs from rocks to the east of the Torrens Hinge Zone in the intensity of deformation and the preserved stratigraphy. In the Stuart Shelf, a relatively flat-lying Neoproterozoic cover sequence overlies Mesoproterozoic basement. Only the upper part (Tapley Hill Formation of Nepouie Subgroup and above) of the Adelaide Rift Complex succession transgresses onto the shelf.

The moderate level potential associated with Mount Gunson contains contributions from all three mineral system components assessed in this study. The main contribution stems from exposure of the Tapley Hill Formation, which contributes to the final weighting, both as a source of brine and a depositional site (carbonaceous, carbonate rock). Smaller contributions come from the presence of anomalous U^2/Th (depositional site), the spatial association of the anomaly with a regional structure inferred from potential field data (fluid pathway), an association with an unconformity between the Neoproterozoic rocks and underlying Mesoproterozoic rocks (fluid pathway) and a location in the outer buffer for copper source as established from the distribution of mafic igneous rocks inferred from potential field data.

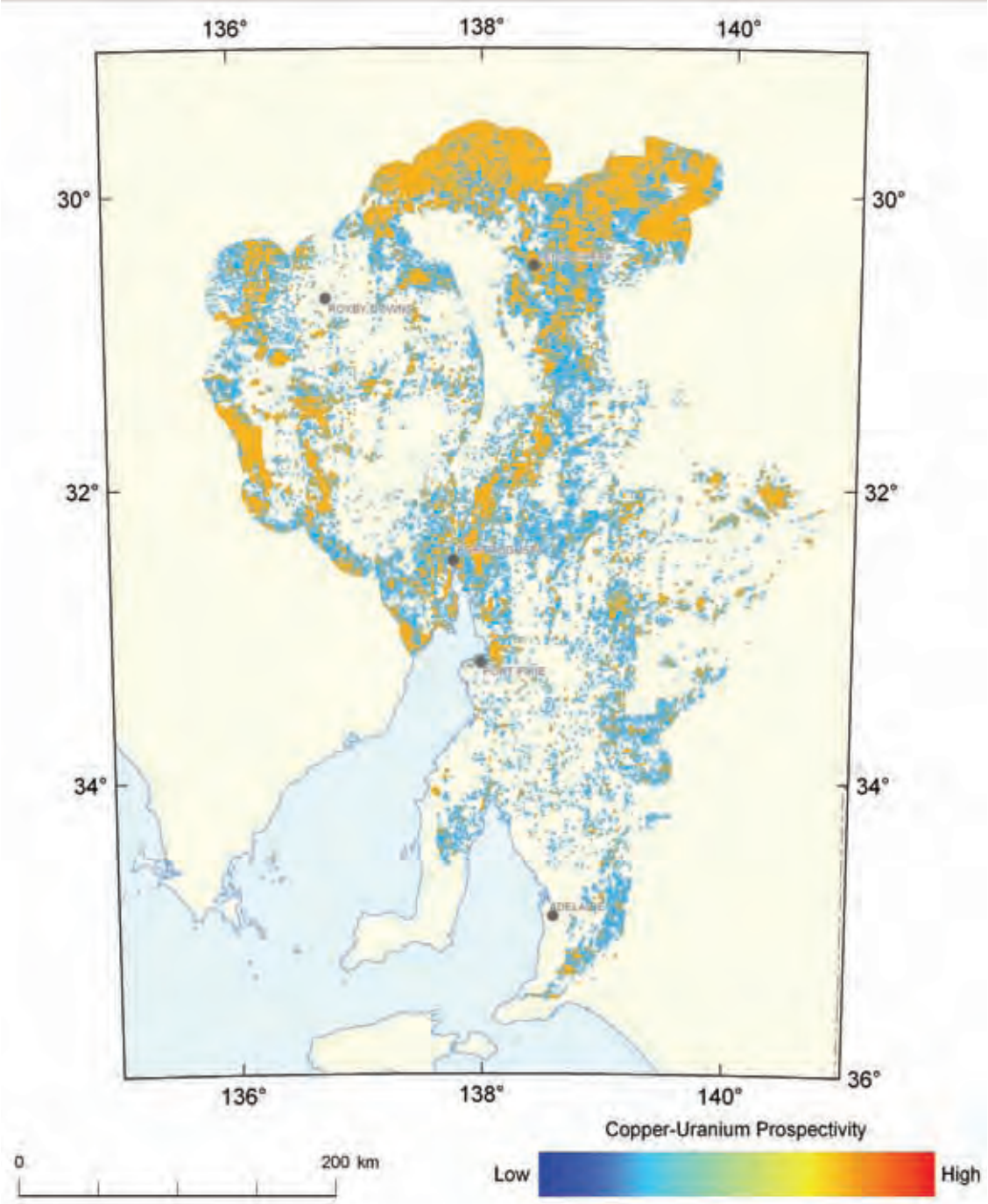

Figure 3.6.12: *Variations in the weighting of depositional site - U^2/Th, Adelaide Rift Complex mineral system.*

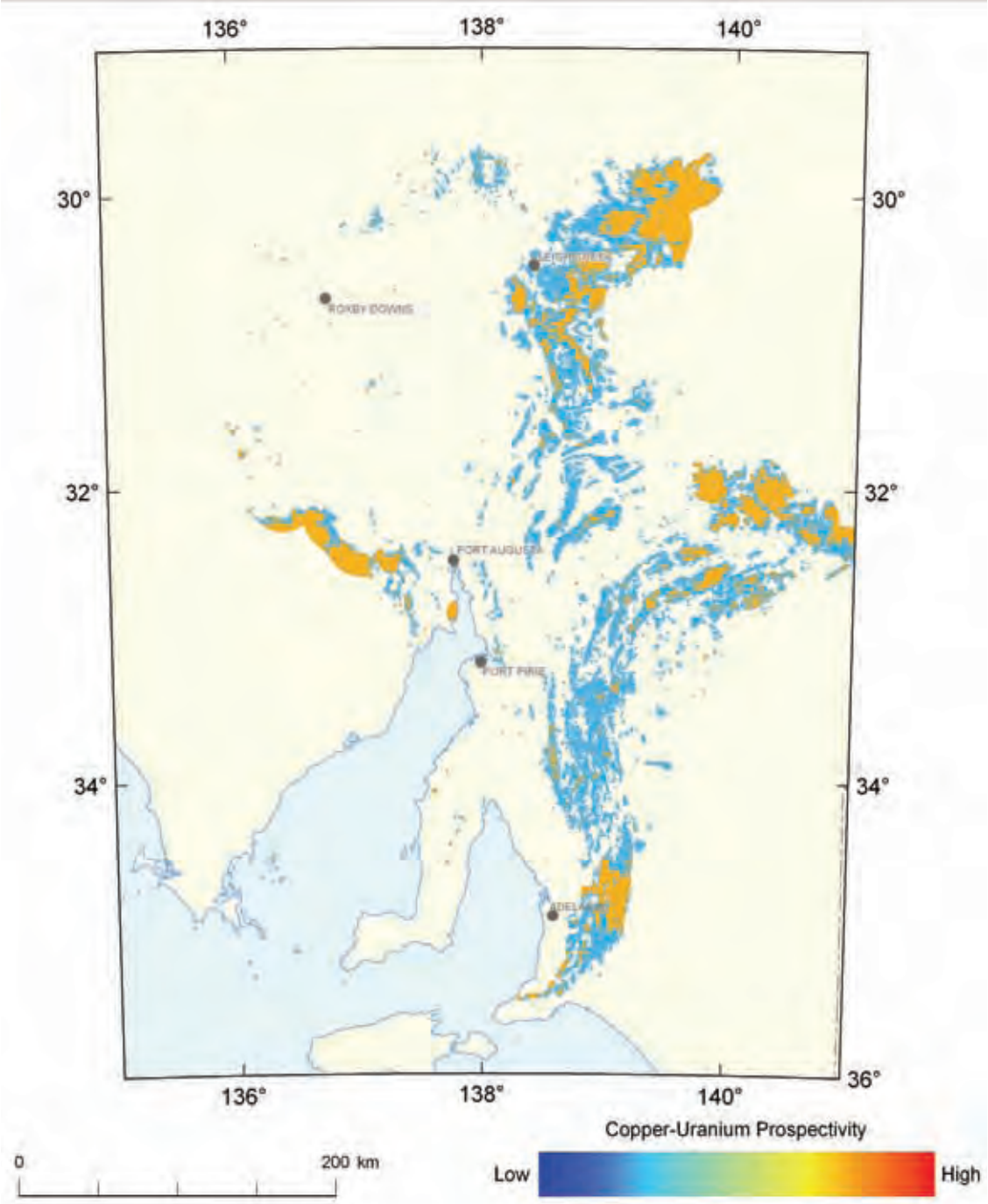

Figure 3.6.13: *Variations in the weighting of depositional site - Th, Adelaide Rift Complex mineral system.*

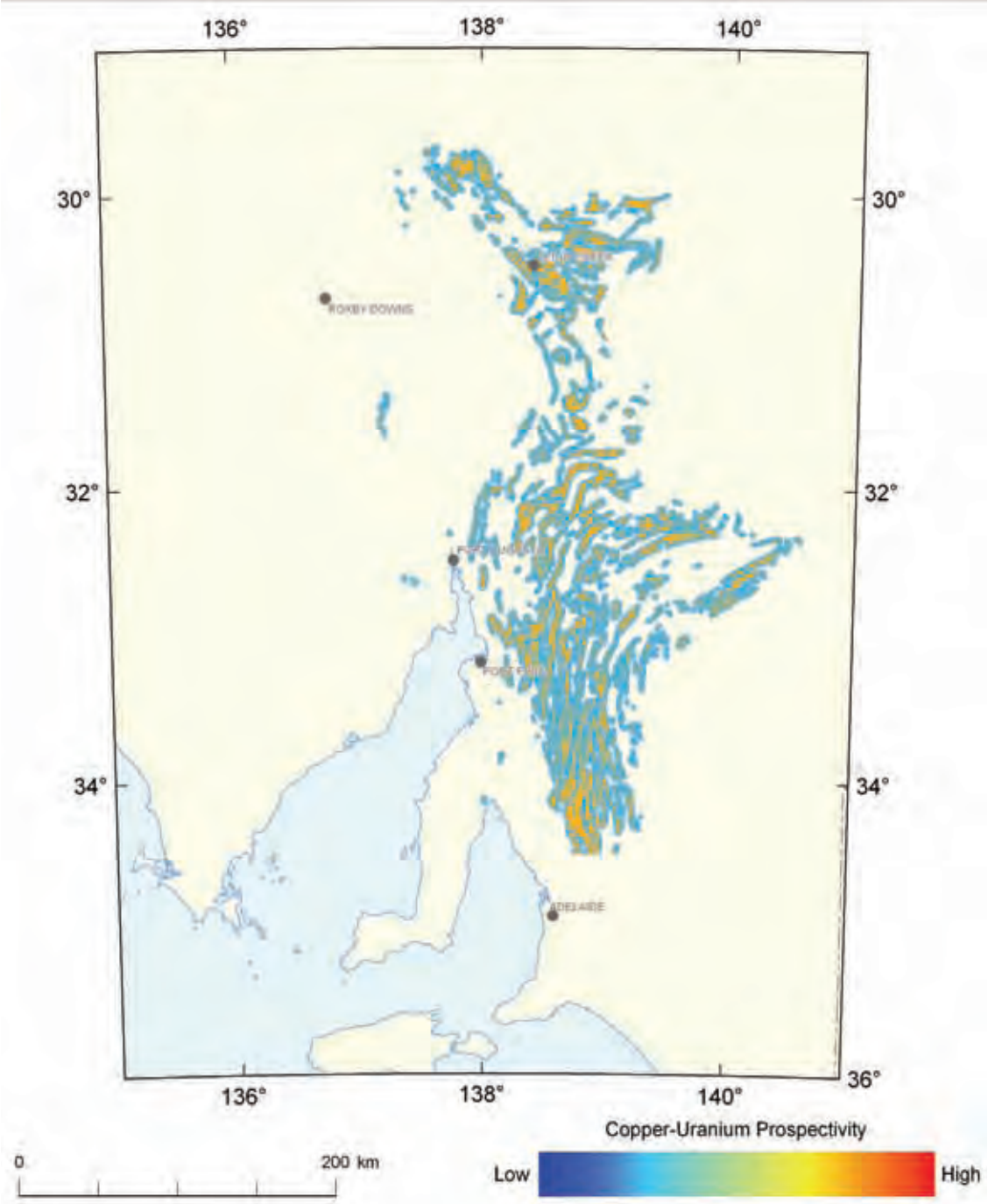

Figure 3.6.14: *Variations in the weighting of depositional site-carbonaceous rocks, Adelaide Rift Complex mineral system.*

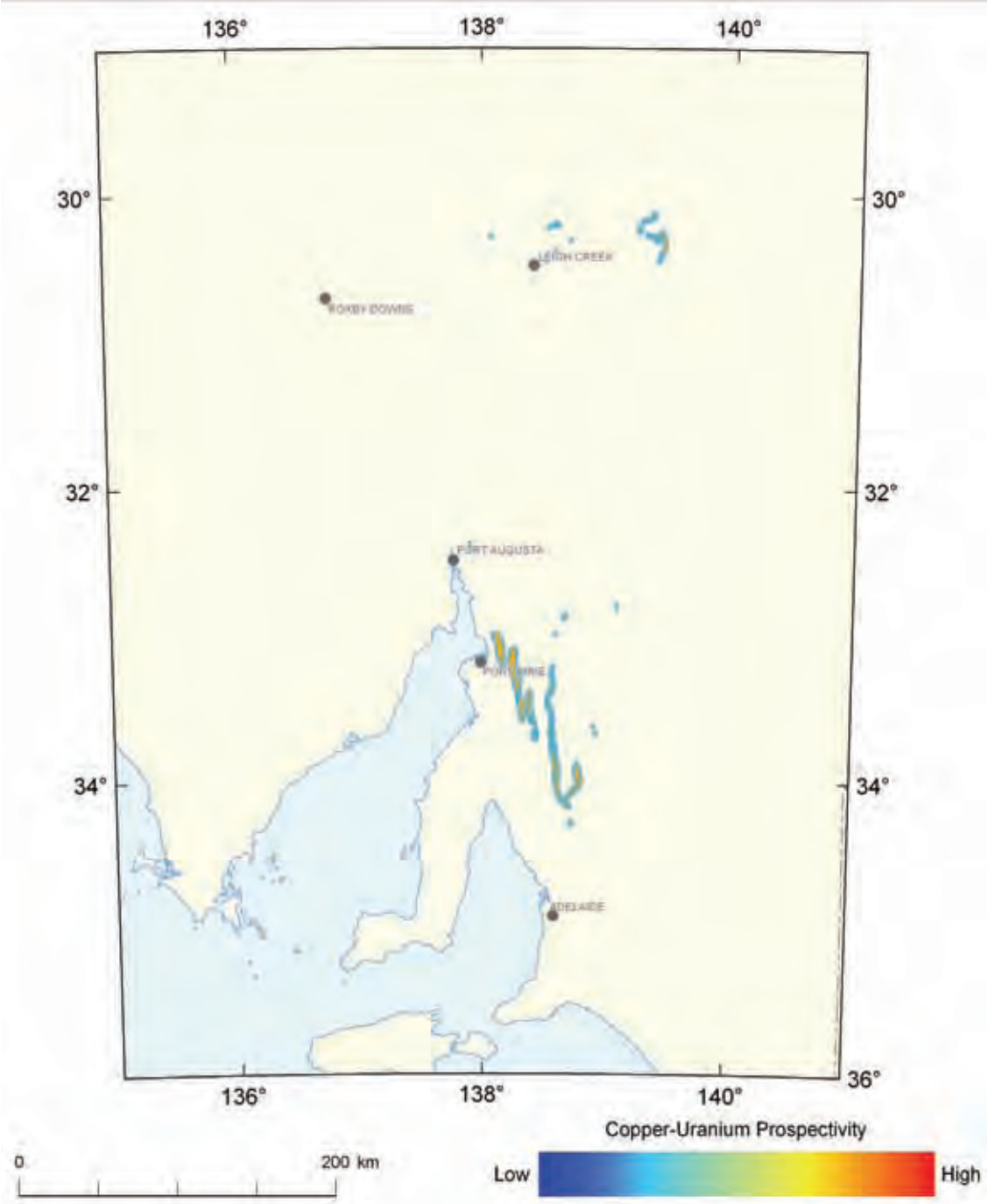

Figure 3.6.15: *Variations in the weighting of depositional site-Fe^{2+}-rich rock, Adelaide Rift Complex mineral system.*

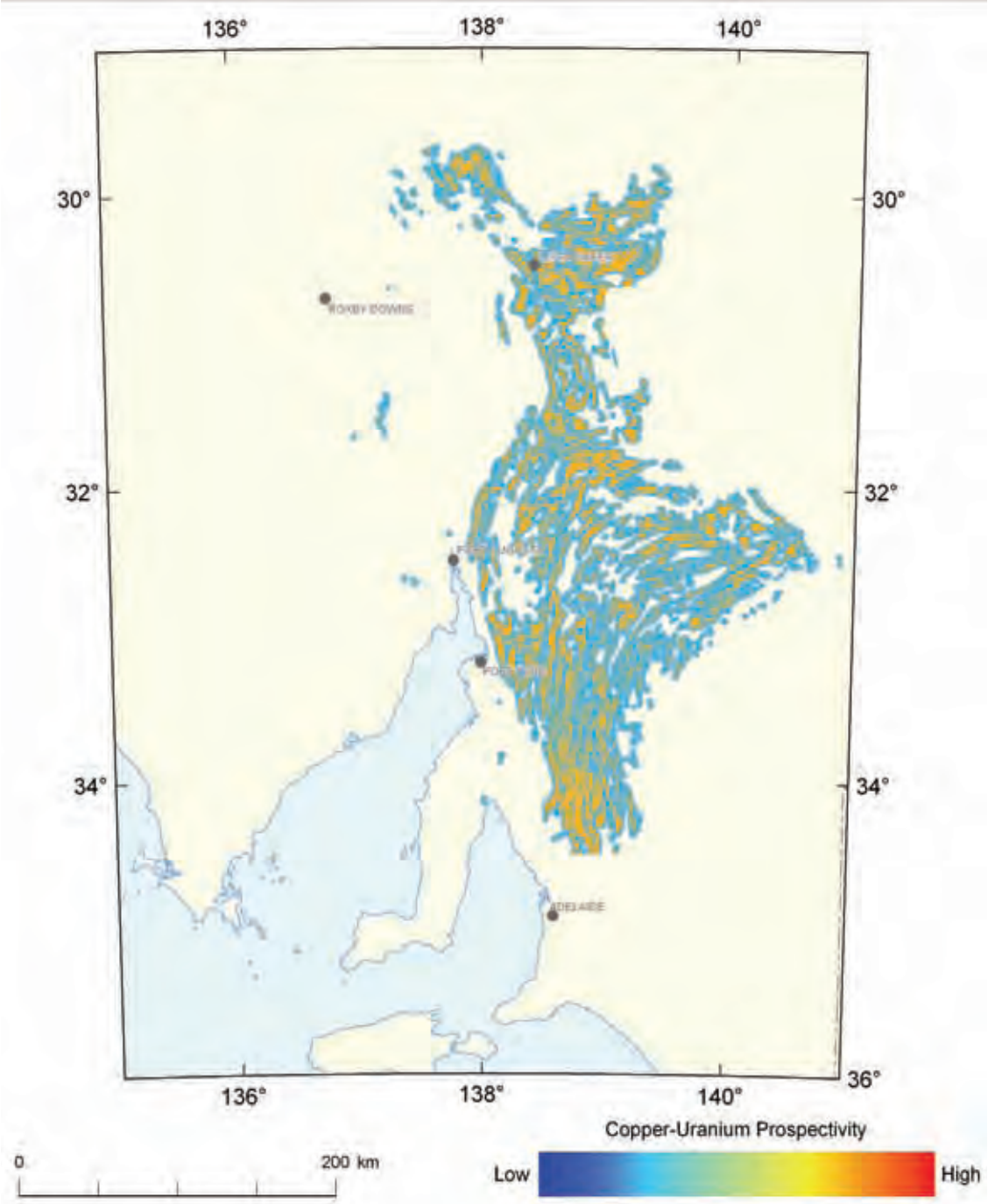

Figure 3.6.16: *Variations in the weighting of depositional site - carbonates, Adelaide Rift Complex mineral system.*

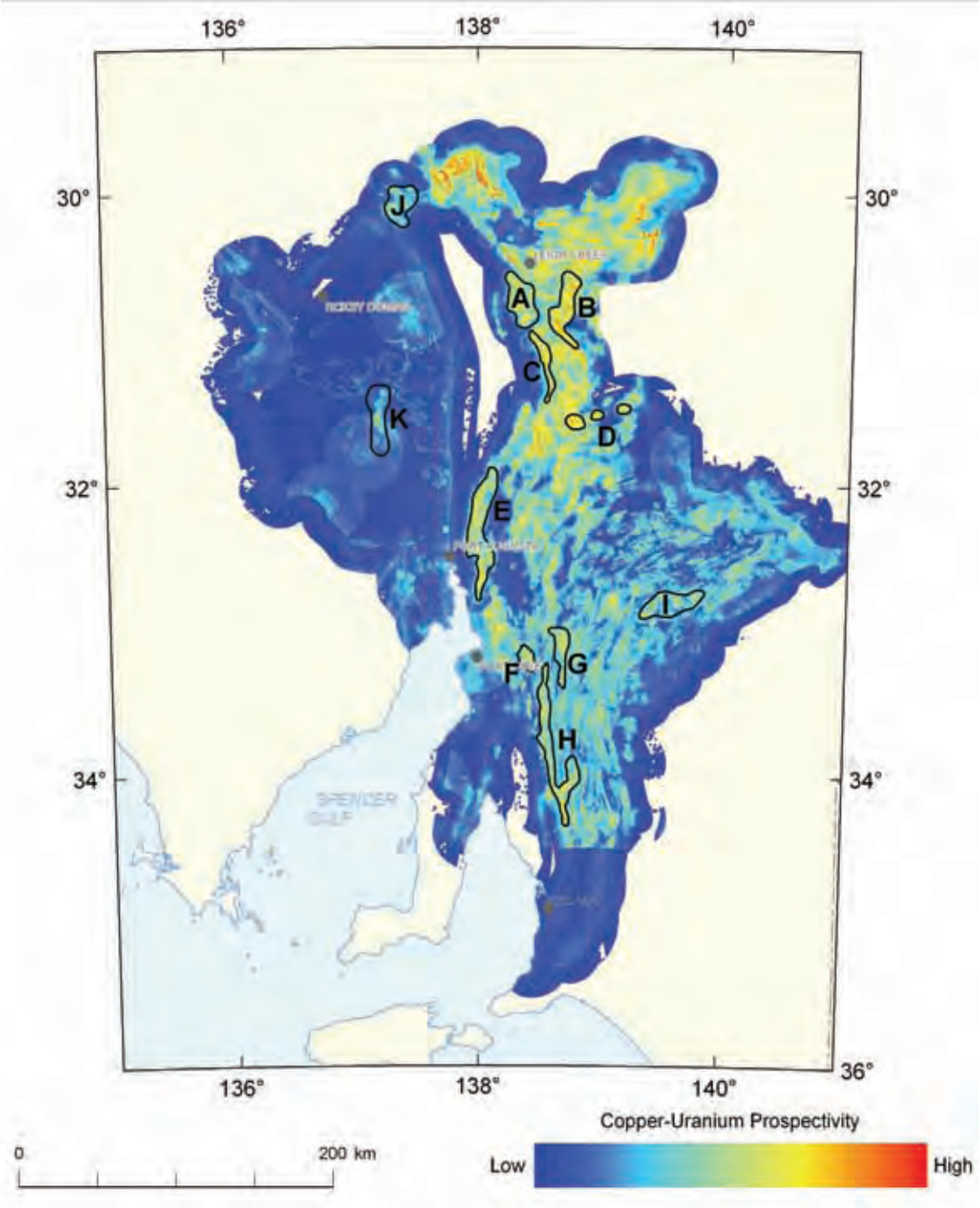

Figure 3.6.17: *Copper-uranium prospectivity of the Adelaide Rift Complex.*

The deposits are associated with the Pernatty Culmination, an inlier of Mesoproterozoic Pandurra Formation unconformably overlain by Neoproterozoic rocks. Approximately 21% (167 kt) of the global resource at Mount Gunson is localised directly on this unconformity, which may have acted as a fluid pathway or, less convincingly, as a redox boundary. These prospects also may be localised where the Whyalla Sandstone onlaps and pinches out on the Pernatty Culmination (cf. Figure 3 of Tonkin and Creelman, 1990). The copper-uranium potential assessment does not account for these geological relationships very well. Although unconformities were considered as fluid pathways in the analysis, the analysis only considered them where they are exposed at surface (with a 10 km buffer). Because of the shallow dip of Neoproterozoic rocks, this unconformity is likely to be at relatively shallow depth through much of the Stuart Shelf, a factor not considered in the analysis. The distribution of culminations was not considered at all in the analysis. However, these culminations may be mapped from variations in depth to basement maps (see discussion of 3D model in Chapter 4) or, possibly, using airborne electromagnetic data. A further mappable ingredient which might be given higher weighting on the Stuart Shelf is faults inferred from geophysical data sets. This brief discussion indicates that incorporation of additional data or a change in the weight assigned to current data may provide a better analysis of mineral potential in Neoproterozoic successions in the Stuart Shelf. This discussion also suggests that the potential of the Stuart Shelf may be under-estimated in this analysis.

4 Geothermal systems

A. J. MEIXNER, A. KIRKBY, D. C. CHAMPION, R. WEBER, D. CONNOLLY, AND E. GERNER

A geothermal energy system comprises three key components, a heat source, a fluid to transport the heat and sufficient permeability to enable the fluid to circulate through the rock. Conventional, or hydrothermal geothermal systems are associated with active volcanism. In these systems, the three components of a geothermal energy system generally exist naturally. In areas distal to active volcanism it is possible to artificially create a geothermal energy system. Of the three components listed above, a heat source is the only one required to occur naturally; fluids can be artificially injected into hot rocks and permeability can be chemically or hydraulically created.

Geothermal energy systems in Australia are generally either hot rock systems (also known as Engineered or Enhanced Geothermal Systems, EGS) or hot sedimentary aquifer systems (Figure 4.1). The heat sources for either geothermal system are most commonly thought to be basement rocks (typically granites) or sediments which are enriched in the radioactive elements uranium, thorium and potassium. The decay of these three elements over time generates heat, and, if these high-heat-producing rocks are buried beneath a sufficient thickness of insulating units (typically sediments), the heat is trapped and temperatures as high as 250°C can be found at less than 5 km depth. Only basement heat sources are considered in this geothermal assessment. The requirement for insulation (in the case of hot rock systems) and permeable stratigraphic formations (in the case of hot sedimentary aquifer resources) means that geothermal systems in Australia are more likely to be associated with sedimentary basins than areas of outcropping basement.

In areas where high-heat-producing basement rocks are not known to be present, geothermal systems can still be present as temperature in any location generally increases with crustal depth. In addition, hot fluid can migrate away from the area in which it was initially heated, forming hot sedimentary aquifer systems with no immediately obvious heat source. However, geothermal systems remote from local sources of enhanced heat production are likely to be relatively low temperature systems.

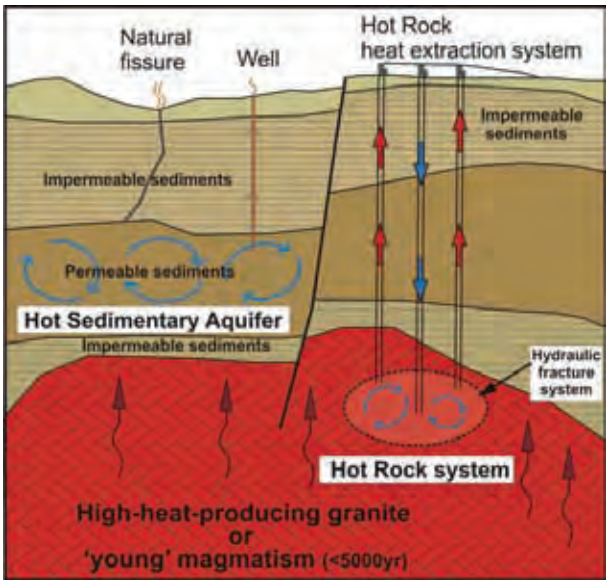

Figure 4.1: *Schematic diagram of styles of geothermal systems found in Australia.*

There are a variety of applications for a geothermal resource, dependant on the temperature and volume of the available fluid. Higher temperature resources (more than 200°C) are ideal for generating electricity, although much lower temperatures can be suitable in the right circumstances. High temperature resources (e.g., 300°C) can have cycle conversion efficiencies up to 20% (Tester, 1982). In off-grid areas dependant on fuel-oil for on-site power generation, lower temperatures may be used to economically generate power. Although possible, electricity generation from lower temperature resources is thermodynamically less efficient with only about 6% of the thermal energy being converted into electrical energy. Low temperature geothermal resources (less than 150°C) can be used to provide heat for industrial or domestic processes. For these lower temperature resources, direct use is a more thermodynamically-efficient use of the geothermal resource. Examples of potential applications where geothermal heat can be used directly are displayed in Figure 4.2.

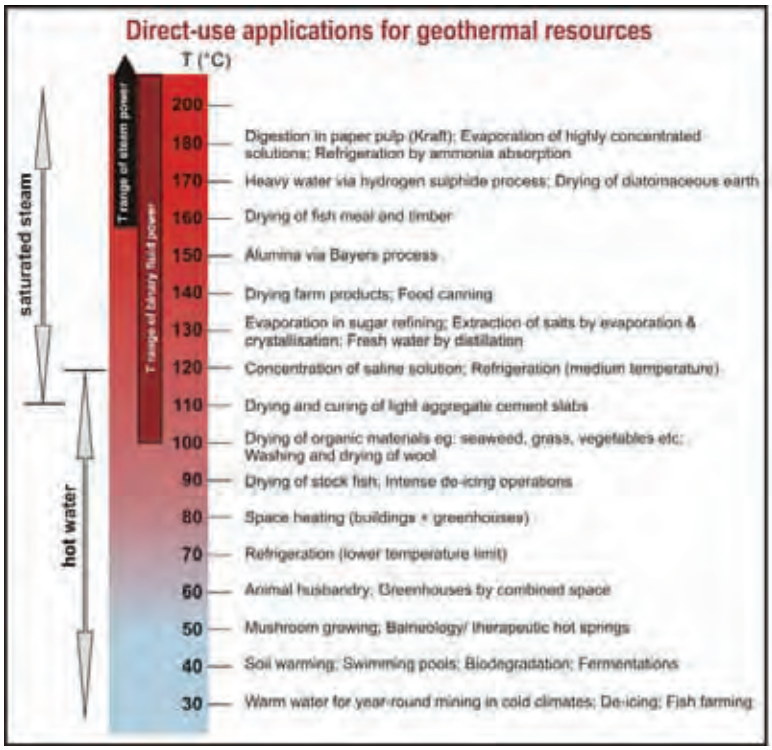

Figure 4.2: *The variety of applications for direct-use of geothermal heat, as a function of the resource temperature (modified from Lindal, 1973).*

Although Australia is yet to generate electricity from a hot rock geothermal system, a small binary power plant in Birdsville, southwest Queensland, has been generating electricity from a low temperature (about 100°C) hot sedimentary aquifer system in the Great Artesian Basin. The plant has been operating since the early 1990s and is currently generating about 80 kW nett.

An assessment of hot rock and hot sedimentary aquifer geothermal prospectivity in north Queensland has previously been produced as part of the Australian Government's Energy Security Initiative. The north Queensland study (Ayling and Lewis, 2010) used a GIS based approach similar to that used elsewhere to identify potential regional-scale geothermal resources (e.g., Noorollahi *et al.*, 2007). For this geothermal prospectivity analysis of east-central South Australia, a different approach has been adopted. The hot rock and hot sedimentary aquifer geothermal prospectivity is based on the results of 3D thermal modelling which was conducted on a 3D geological map constructed as part of this study.

4.1 PREDICTING TEMPERATURE AT DEPTH

Exploration for geothermal resources ultimately aims to locate commercially exploitable temperatures at economically-drillable depths. Ideally, this could be achieved by measuring temperature in deep drillholes distributed in a grid-like manner. On a continental scale, however, this is not economically or logistically feasible and, as result, other data and methods must be used to predict temperature at depth.

To predict temperature at depth the transfer of heat in the crust must be considered. Heat flows in the earth by conduction or advection of fluids (Stüwe, 2007). Heat can be produced in the crust by radiogenic, chemical and mechanical heat sources. Gibson *et al.* (2008) propose that as the Australian continent is not subjected to active tectonism, there is minimal chemical or mechanical heat production and at depths of interest for geothermal electricity generation the dominant mode of heat transfer is conduction.

The heat transfer process is described in the following equation (modified after Stüwe, 2007):

$$\frac{dT}{dt} = \kappa\left(\frac{d^2T}{dz^2}\right) + u\left(\frac{dT}{dz}\right) + (A)/(\rho c_p) \qquad (1)$$

Where κ = the thermal diffusivity and is given by $k/(\rho c_p)$, k = thermal conductivity, ρ = density, c_p = heat capacity, A = the heat production because of radiogenic heat sources and u is the advection rate vector. This equation assumes a constant thermal conductivity.

Gibson *et al.* (2008) also proposed that, for the Australian crust, it is sufficient to consider only the case of the thermal steady state based on the assumption that the crust has attained thermal equilibrium since the last period of tectonic or magmatic disturbance. For steady state $\frac{dT}{dt} = 0$.

The steady state equation for conductive heat flow can be expressed as:

$$Q_0 = Q_d + \int A(z)\partial z \qquad (2)$$

Where Q_0 = surface heat flow, Q_d = heat flow at depth d, $\int A(z)\partial z$ = the integral of volumetric heat generation from the surface to d, A = heat production and z = depth.

The heat flow at depth d can be calculated from the following relationship:

$$Q_d = \lambda_d \cdot \left[\frac{\Delta T}{\Delta z}\right]_d \qquad (3)$$

Where: λ_d = thermal conductivity at depth d and T = temperature

From equations (2) and (3), it can be seen that the key datasets for calculating temperature at depth are: heat flow, thermal conductivity, and heat production. The relationship between these variables is diagrammatically illustrated in Figure 4.3.

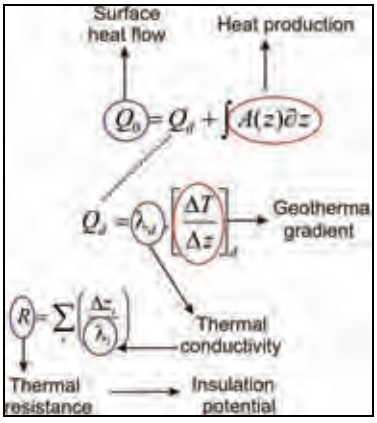

Figure 4.3: *Relationship between key physical parameters useful for geothermal resource exploration.*

4.2 3D THERMAL MODELLING USING GEOMODELLER

For this study, 3D temperature prediction was achieved by performing thermal modelling on a 3D geological map using the 3D GeoModeller[1] software package. GeoModeller explicitly solves the following steady state equation for 3D temperature prediction (Stüwe, 2007):

$$\left(\frac{d\left(-k\frac{dT}{dx}\right)}{dx} + \frac{d\left(-k\frac{dT}{dy}\right)}{dy} + \frac{d\left(-k\frac{dT}{dz}\right)}{dz} \right) + \rho c_p \left(u_x \frac{dT}{dx} + u_y \frac{dT}{dy} + u_z \frac{dT}{dz} \right) = -A \qquad (4)$$

The above equation combines conduction and heat production terms as well as considering spatially varying thermal conductivity. The equation is discretised with an explicit finite difference scheme within GeoModeller utilising a voxelised grid. This finite difference approximation is iteratively solved with a Gauss-Seidel iteration scheme until the sum of the residual errors fall below a given threshold (Gibson *et al.*, 2008).

Boundary conditions were applied to the derived equation for 3D temperature prediction as follows:

- for the four vertical sides, Neumann type boundary conditions where all lithologies and temperatures are mirrored beyond the model boundaries, thereby implying that no heat flows through the model boundaries;
- for the bottom boundary, either a constant heat flow or temperature; and
- for the top boundary, a constant temperature, such as the mean annual surface temperature (Gibson *et al.*, 2008).

The effects of topography are dealt with by applying the top boundary condition via a topographic surface, such as a digital elevation model (Gibson *et al.*, 2008).

Once the boundary conditions and topography are set, further inputs are required in order to compute the temperature in 3D. These inputs consist of a voxelised 3D geological model with thermal conductivity and heat production values assigned to each lithology within the model (Gibson *et al.*, 2010). The number of iterations must be specified also and should be large enough for the model to

[1] http://www.geomodeller.com/geo/index.php?lang=EN&menu=homepage

reach thermal equilibrium. The solver then populates a 3D grid with modelled outputs. The outputs are summarised in Table 4.1.

Table 4.1: Summary of outputs solved in 3D by the thermal modelling component of GeoModeller (from Gibson *et al.* 2010).

3D temperature and other outputs from GeoModeller	
Temperature	(°C) Solved for every cell/voxel centre by Finite Difference.
Vertical Heat Flow	(mW/m^2) Flow of heat measured in energy per time per unit area. Solved for each cell/voxel centre with respect to the centre of the cell immediately above.
Vertical Temperature Gradient	(°C/km) Change of temperature over a distance. Solved for each cell/voxel centre with respect to the centre of the cell immediately above.
Total Horizontal Temperature Gradient	(°C/km) Change of temperature over a distance of one cell to 4 neighbours in the horizontal plane. Equal to the square root of the sum of the squares of the horizontal temperature gradients in the x and y directions. (An expression of gradient strength with no expression of direction within the horizontal plane.)

4.3 TEMPERATURE AND HEAT FLOW DATA

The OZTemp[2] database is an updated and improved version of the AUSTHERM05 borehole temperature database previously described by Chopra and Holgate (2005). OZTemp stores temperature and geothermal gradients collected from drillholes around Australia. Using measured and estimated thermal gradients, surface temperature estimates and depth to basement information, these temperatures have been vertically extrapolated to 5 km depth. The interpreted temperatures at 5 km were gridded to produce a map of crustal temperature at 5 km across the Australian continent. An image of the temperature at 5 km, covering the energy assessment area, is shown in Figure 4.4 and highlights the paucity of downhole temperature measurements in the region. The interpolation required to produce a continuous grid spanning large spatial data gaps results in unreliable temperature predictions within these gaps.

Although caution must be used when viewing the temperature at 5 km map (Figure 4.4), it is a valuable tool in predicting temperatures at depth near data locations. The map shows a general north-south trending temperature anomaly, although it is not well constrained to the north because of a lack of data points. Two distinct temperature anomalies are located to the east. Both of these anomalies are located where Curnamona Province occurs at depth.

Neumann *et al.* (2000) identified a zone of elevated heat flow within South Australia which they called the South Australian heat flow anomaly. A large portion of the assessment area occurs within this zone, which overlaps the boundary between the eastern Gawler Craton and sediments of the Adelaide Rift Complex (Figure 2.1). McLaren *et al.* (2003) also recognised elevated heat flow in the region, which forms part of the continental-scale Central Australian heat flow province. This province, which includes the energy assessment area, was formed mostly during the Proterozoic including the Archean portions of the Gawler Craton. The average surface heat flow in the province is 82 ± 25 mW/m^2, which is well above average global values of 49-54 mW/m^2 (Chapman and Furlong, 1977; Morgan, 1984). Figure 4.5 shows the heat flow determinations in the assessment area which have been used to validate the thermal modelling. All of the heat flow determinations shown in Figure 4.5 are above the global average value.

[2] https://www.ga.gov.au/products/servlet/controller?event=GEOCAT_DETAILS&catno=70604

Within the study area, heat flow determinations (Figure 4.5) show considerable variation over short distances (e.g., 40 mW/m^2 variation over about 12 km distance). Housemann *et al.* (1989) made heat flow determinations in several drill-holes in the Olympic Dam area and recognised that heat flow varies by a factor of more than two. Matthews and Bearsdmore (2007), who compiled heat flow data which included a portion of the energy assessment area, concluded that it is unlikely heat flow varies in a gradual fashion between current heat flow data points but is more likely to vary over short wavelengths and be dependant on basement geology. The high lateral variation of heat flow means that the data density of existing heat flow measurements (Figure 4.5), although useful in the immediate vicinity of the measurement location, is not adequate to make heat flow predictions across large regions where no heat flow data exist.

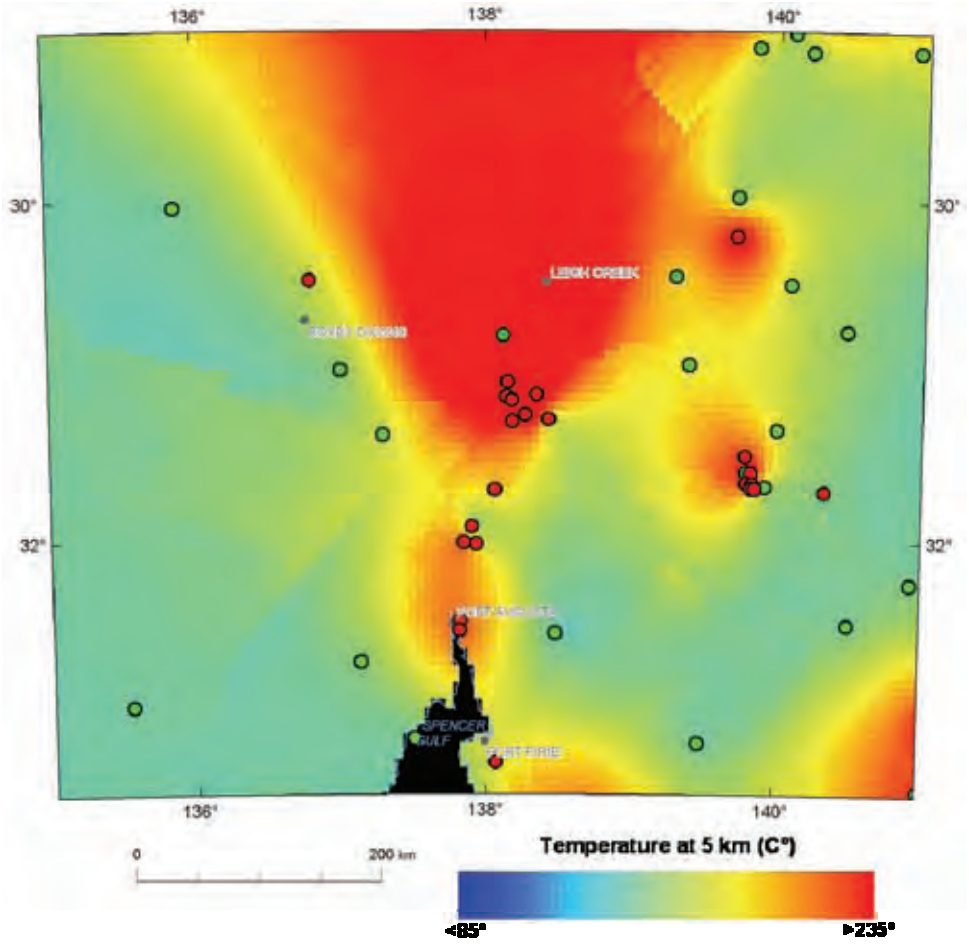

Figure 4.4: *Image of temperature at 5 km depth map generated from the OZTemp database. The locations of down-hole temperature measurements are shown (green – open file; red – confidential). These down-hole temperature measurements were used to constrain the thermal properties of the 3D geological map during thermal modelling.*

It is possible using 3D thermal modelling techniques to produce continuous predictions of heat flow at the surface. These predictions, however, are only as good the input 3D geological map, thermal properties and boundary conditions assigned to compute the thermal model. The major factor controlling the heat flow at the surface is the lateral and vertical distribution of heat production as evident from equation (2). Although the lateral and vertical distribution of thermal conductivity

influences the refraction of heat flow from the vertical, based on the thermal modelling, compared to the vertical heat flow this refraction is small, generally less than 10% .

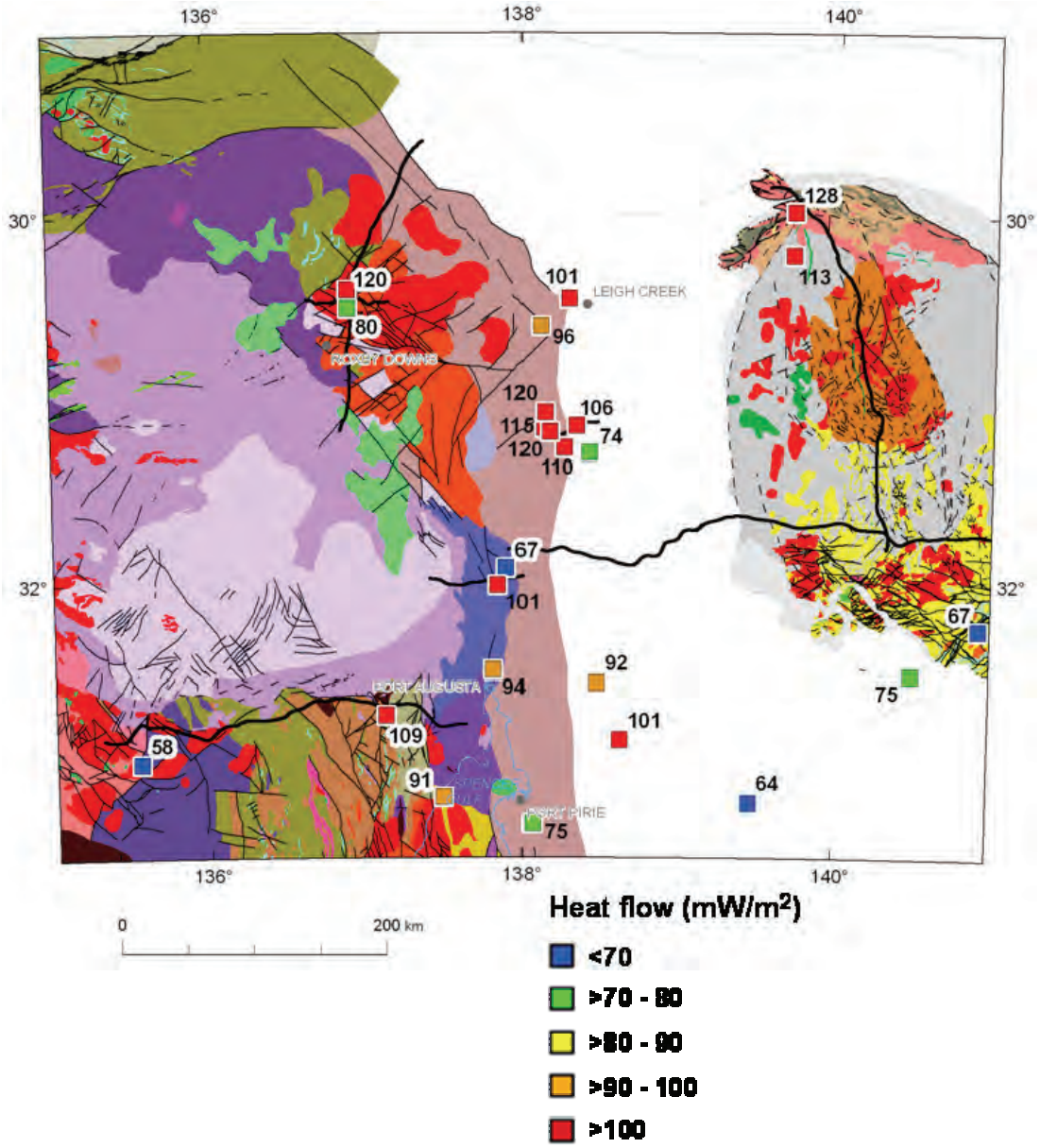

Figure 4.5: *Measured surface heat flow in the assessment area which were used to constrain the thermal properties of the 3D geological map during thermal modelling. The solid geology map showing only the Mesoproterozoic and older units (Cowley, 2006) is shown as, are the locations of deep seismic lines.*

After excluding recent tectonism, magmatic activity, hydrological activity and abnormal mantle heat flow, Neumann *et al.* (2000) concluded that the elevated heat flow in the South Australian heat flow anomaly was to the result of enrichment of uranium, thorium and potassium in granitic and volcanic lithologies from the Gawler Craton and Mount Painter Inlier. Regression of the heat flow data in the South Australian heat flow anomaly by Neumann *et al.* (2000) gave a characteristic length-scale of 9.7 km and a reduced heat flow of 29.5 mW/m^2, although these results are poorly constrained. The characteristic length scale is a measure of the thickness of the enriched upper crustal layer that

accounts for the observed spatial variations of surface heat flow, while the reduced heat flow is a measure of the constant component of heat flow from the mantle (Lachenbruch, 1968; Birch, *et al.*, 1968). The characteristic length scale and reduced heat flow value are similar to the values calculated by McLaren *et al.* (2003) for the central Australian heat flow province of 10 km and 40 mW/m^2 respectively. McLaren *et al.* (2003) give a corrected reduced heat flow of 25 mW/m^2 as a best estimated for the central Australian heat flow province. This corrected reduced heat flow takes into account the lateral heat transfer associated with lateral variations in heat production (Jaupart, 1983). The above values suggest that all but about 30 to 40 mW/m^2 of the observed heat flow in the energy assessment area originates from heat production in the top approximate 10 km of the crust.

Neumann *et al.* (2000) produced heat production values from geochemical analyses of uranium, thorium and potassium concentrations for South Australian Archean to Mesoproterozoic lithologies. These heat production values are plotted against longitude in Figure 4.6. The upper bound of the shaded region is the binned average while the lower bound is the binned median. The gap in the data is the result of the covering of the Precambrian basement by the Neoproterozoic Adelaide Rift Complex sediments. Based these data, Neumann *et al.* (2000) calculated median surface heat production values of about 3 µW/m^3 for the western Gawler Craton, about 5 µW/m^3 for the eastern Gawler Craton, about 6 µW/m^3 for the Mount Painter Inlier and about 2.5 µW/m^3 for the Willyama Inliers. These heat production values do not take into account the spatial variation of each rock type because outcrop of the Precambrian basement is generally poor. However, Sandiford *et al.*, (1998) gave an area-integrated heat production for the Mount Painter and Mount Babbage Inliers of 9.9 µW/m^3, a higher value than the approximate 6 µW/m^3 produced by Neumann *et al.* (2000). All of these values for surface heat production are significantly in excess of averaged upper continental crustal heat production values of 1.7 µW/m^3 (Rudnick and Gao, 2003), strengthening the argument that the elevated measured heat flow values are from enriched upper crustal sources.

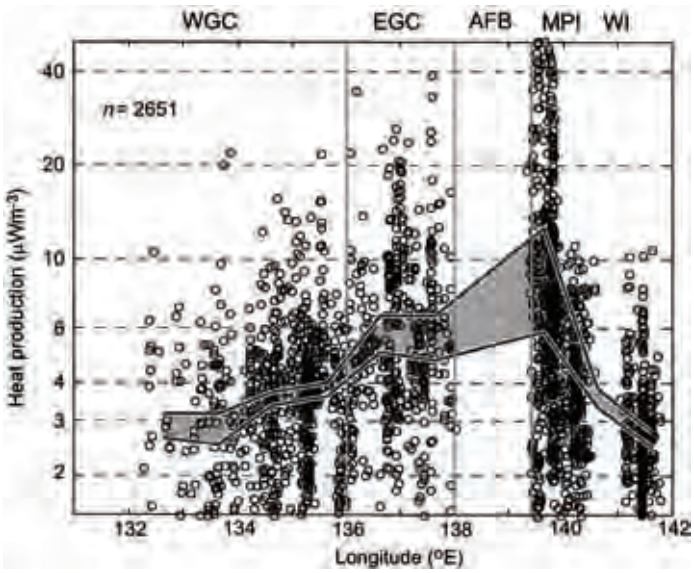

Figure 4.6: *Surface heat production values for South Australian Archean to Mesoproterozoic lithologies plotted as a function of longitude. WGC – Western Gawler Craton, EGC – Eastern Gawler Craton, AFB – Adelaide Fold Belt (Adelaide Rift Complex), MPI – Mount Painter Inlier, WI – Willyama Inliers. From Neumann et al., (2000).*

4.4 THERMAL CONDUCTIVITY DATA

Thermal conductivity is the measure of how well a rock conducts heat energy. For a geothermal resource, a low thermal conductivity is desirable because the insulating effect is greater, improving the potential for trapping heat (or elevating temperature) at depth. Thermal conductivity data is very sparse in Australia and there are only a handful of publicly available values for samples within South Australia. Therefore, thermal conductivity values needed to be estimated for formations based on averages for rock-type in the study area in order for the assessment to be undertaken.

For the purposes of thermal modelling, thermal conductivity values were assigned to each basin in the assessment area. Thermal conductivity values also were assigned separately to granites and the different basement terranes. Basin thermal conductivity values were determined by assigning a value to each unit in a basin. Where thermal conductivity data were available for specific formations these values were used. There were several basins which contained significant published data such as the Cooper and the Eromanga basins (Beardsmore, 2004).

For formations where no published data exist, the thermal conductivity values were estimated. This was done by obtaining literature information on lithology and estimating the percentage of each rock present. For example, if the literature stated the formation was composed of majority sandstone and minor siltstone, it was assumed that the formation was 80% sandstone and 20% siltstone (as done by Beardsmore, 2004). The thermal conductivity values assigned to each lithology are based on a compilation of published literature values, which are summarised in Table 4.2.

The final thermal conductivity for each basin was determined by applying a weighted harmonic mean of each of the formation values, using the relative proportions of each formation. In basins such as the Cooper Basin, where detailed stratigraphic information exists and the stratigraphy varies from one region to another, the thermal conductivity was estimated for more than one region in the basin. The values which were assigned to each basin in the model are shown in Table 4.3.

4.5 HEAT PRODUCTION DATA

4.5.1 Heat Production data for Neoproterozoic and younger basins.

Heat production values were calculated for the same basins as those for which thermal conductivity values were calculated (Table 4.3). Heat production averages were calculated for each basin based on heat production data for individual units (formations, subgroups or groups) within the basin and weighted for unit thicknesses (based on compiled idealised cross-sections as used for thermal conductivity calculations). Standard deviation values were calculated by a weighting system based on the relative thickness of each unit. For the Adelaide Rift Complex, a number of idealised cross sections were compiled with the final heat production value used (Table 4.7) representing an average of the heat production values from each section.

4.5.1.1 Methodology

Heat Production data for individual basin units were taken from values calculated by Goodwin and van der Wielen (in prep). These values were obtained from potassium, thorium and uranium concentration grids from the Australia-wide, levelled and back-calibrated gamma-ray data set (Minty, 2010). Each grid was intersected with the 1:1 000 000 scale Surface Geology of Australia map (Raymond and Retter, 2010), allowing average potassium, thorium and uranium concentration data to be assigned to each geological unit. Using these concentrations, heat production values were calculated for each geological unit. As the calculation of heat production requires a volume-mass

conversion, density values were also required. Density values were applied to all geological units within the Surface Geology of Australia map coverage, based on lithology descriptions or actual measured values (about 5% of all units), heat production values were calculated for each grid unit and statistical distributions (especially average and standard deviation) compiled for each unit.

Table 4.2: Common lithologies and thermal conductivity values (Tc).

LITHOLOGY	Tc (W/mK)	ERROR (W/mK)	# SAMPLES	REFERENCES
Alluvium	1.3	0.1	3	Southern Methodist University (SMU)
Andesite	2.25	0.05	29	Norden and Forster, 2006; Cermak *et al.*, 1982
Argillite	3.7	0.5	5	Davis *et al.*, 2007
Basalt	2.17	0.17	65	Norden and Forster, 2006; Skvarla *et al.*, 1981, in Beach *et al.*, 1987; Raznjevic, 1976; Cermak *et al.*, 1982; Sass, 1964
Chert	2.3	0.4	14	GA, Skvarla *et al.*, 1981, in Beach *et al.*, 1987; Cermak *et al.*, 1982
Claystone	1.58	0.10	307	GA[1], SMU[2], Cermak *et al.*, 1982
Coal	0.29	0.09	98	Raznjevic, 1976; Cermak *et al.*,1982
Conglomerate	2.67	0.19	119	GA, Cermak *et al.*, 1982
Dacite	2.3	0.1	4	Norden and Forster, 2006
Diorite	2.93	0.08	180	SMU, Cermak *et al.*, 1982
Dolerite	2.49	0.14	55	Sass, 1964; Norden and Forster, 2006; Cermak, 1982
Dolomite	3.31	0.10	385	Beach, 1985, in Beach *et al.*, 1987; Carter *et al.*, 1998; Cermak *et al.*, 1982
Dunite	4.4	0.1	7	Cermak *et al.*, 1982
Gabbro	2.69	0.08	55	Sass, 1964; Cermak *et al.*, 1982
Granite	3.00	0.15	316	GA, Galson *et al.*, 1987; Cermak *et al.*, 1982
Granodiorite	2.86	0.10	158	Davis *et al.*, 2007;Cermak *et al.*,1982
Halite	3.92	0.17	67	Cermak *et al.*,1982
Limestone	2.39	0.57	1221	Beardsmore, 1996; Davis *et al.*, 2007; Beach, 1985, in Beach *et al.*, 1987; Cermak *et al.*, 1982
Marble	2.98			SMU
Marl	2.24	0.18	175	Hurtig and Schlosser, 1979; Kappelmeyer and Haenel, 1974, in Beach *et al.*, 1987; Cermak *et al.*, 1982
Mudstone	1.9	0.3	6	GA
Quartz Monzonite	2.76	0.04	17	Davis *et al.*, 2007
Quartzite	4.60	0.30	189	Davis *et al.*, 2007; Cermak *et al.*,1982
Rhyolite	4.00	0.23	182	Norden and Forster, 2006; Cermak *et al.*, 1982
Sandstone	3.60	0.10	450	GA; Davis *et al.*, 2007; Beach, 1985, in Beach *et al.*, 1987; Carter *et al.*, 1998
Schist	2.80	0.208	135	GA; Cermak *et al.*,1982
Shale	1.92	0.19	469	GA; Beach, 1985, in Beach *et al.*, 1987; Carter *et al.*, 1998;Cermak *et al.*,1982
Siltstone	2.83	0.19	35	GA, Beardsmore, 1996
Trachyte	2.5	0.5	2	Norden and Forster, 2006
Tuff	2.01	1.14	47	SMU[5], Cermak *et al.*,1982
Unconsolidated Sediment	1.45	0.27	25	Raznjevic, 1976; Cermak *et al.*, 1982

[1]Unpublished Geoscience Australia thermal conductivity database
[2]Southern Methodist University geothermal database, http://www.smu.edu/geothermal/georesou/alldata.csv

Table 4.3: Thermal conductivity values (Tc) assigned to each basin in the study area.

BASIN	REGION	Tc (W/mK)	ERROR (W/mK)	Basin Tc (W/mK)	Basin Tc Error (W/mK)
Aelaide Rift Complex	*Stuart Shelf*	2.7		2.7	0.3
	Mount Lofty	2.6			
	South Flinders Zone	2.9			
	Nackara Arc	2.7			
	Central Finders Zone	2.5			
	North Flinders Zone	2.9			
Arckaringa		1.8	0.2	1.8	0.2
Arrowie	*North Central Trough*	2.7	0.3	2.7	0.3
	Eastern Platform	2.7	0.3		
	South Central Platform	2.7	0.3		
Carieweloo		3.0	0.3	3.0	0.3
Cooper	*Patchawarra*	1.9	0.3	2.1	0.2
	Elsewhere	2.0	0.3		
Eromanga	*Southwest*	2.4	0.4	2.4	0.4
	Cooper Region	2.5	0.3		
Eucla	*Bunda Plateau*	1.7	0.5	1.9	0.5
	Ooldea Range	2.1	0.3		
Lake Eyre	*Tirari Sub Basin*	2.8	0.4	2.3	0.3
	NE Lake Eyre	2.4	0.2		
	Callabonna Sub Basin	2.3	0.3		
Murray	*West*	1.7	0.1	1.6	
	East (Winnambool)	1.8	0.1		0.1
	East (Geera)	1.5	0.1		
Pirie		1.9	0.3	1.9	0.3
Torrens		1.8	0.4	1.8	0.4
Walloway		1.5	0.1	1.5	0.1
Warburton		3.2	0.2	3.2	0.2
Willochra		1.9	0.1	1.9	0.1

This methodology provides a relatively non-biased approach to calculating heat production for outcropping geological units. There are, however, a number of potential deficiencies in this approach. These and, where applicable, corrections to address the deficiencies are described below:

- Gamma ray data under-estimation of uranium concentration because of radon loss. This can be corrected for by utilising an empirical 1.4 factor, such that corrected U (Uc) = U * 1.4. Uc values were used in the calculation of heat production.
- Surficial effects, such as actual area of outcrop of each unit and degree of weathering. The intersection of the gamma-ray data (grid cell size 100 m) with the 1:1 000 000 scale Surface Geology of Australia map creates two problems. Firstly, the pixelation of the gamma-ray grid means there is not a precise match between unit boundaries and gamma-ray data. Secondly, and more importantly, units as defined by the Surface Geology of Australia map comprise a mixture of actual outcrop and subcrop, as well as residual and transported regolith material, all with a variably weathered overprint. The result is that the element concentrations as determined by this methodology may not be truly representative of the unit and vary based on both percentage of outcrop and degree of weathering. This is especially true for uranium and potassium, which are more mobile in the landscape than thorium. To overcome this deficiency, the data have been partly corrected by assuming the concentration of thorium is fixed and the concentrations of uranium and potassium, are

related to that of thorium by empirical relationship. Uranium concentration was recalculated as Th/4, based on the common thorium-uranium ratio of 4 (Taylor and McLennan, 1985; Rudnick and Gao, 2003), while potassum concentration (in %) was recalculated as thorium x 0.2667 (based on an empirical curve defining the dominant upper limit of potassium on a potassium versus thorium plot of all Australian units). The resultant regression of original heat production versus recalculated heat production gave a correction factor of 1.24 (Figure 4.7). All heat production values for basins (Table 4.7) were revised using this correction factor.

- Unit heat production values are based only on outcrop potassium, thorium and uranium concentration data. Therefore units with little outcrop may be misrepresented. For those units (in the basins) with no outcrop, heat production values were assigned based on similar outcropping units within the basin. For non-outcropping basins such as the Cooper, heat production values used were based on an average value for all of the sedimentary basins.
- Assigned densities may be inaccurate. Given the small range in densities of most crustal rocks (2.6-3.0), however, resultant errors in heat production from this are probably <10%.

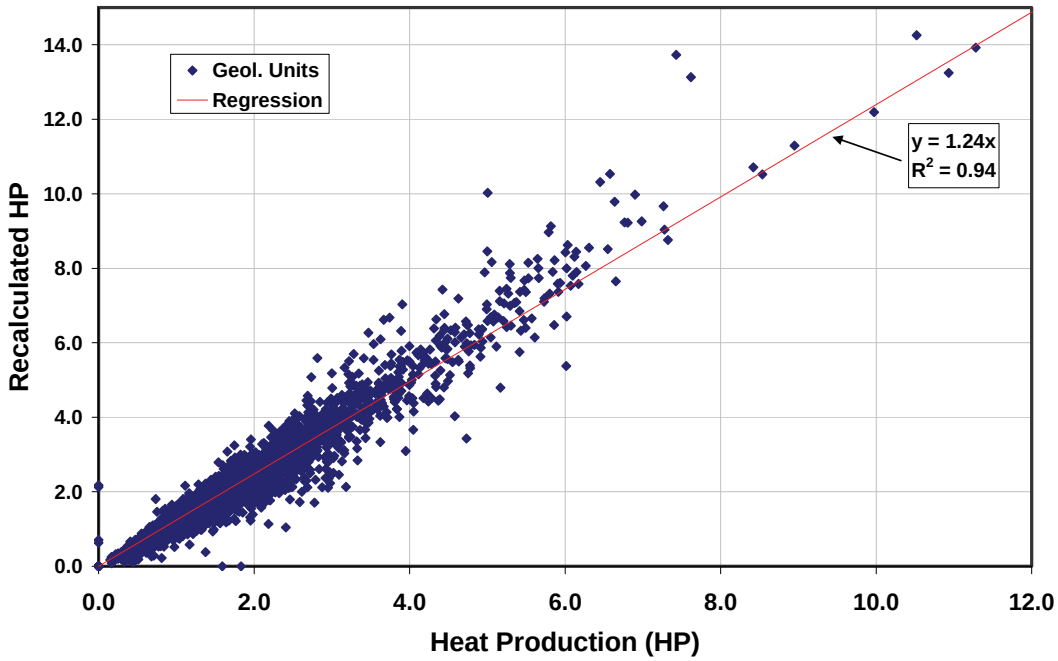

Figure 4.7: *Heat production (HP) data for Australian geological units (calculated from airborne gamma-ray data) versus recalculated HP values (based on adjusting uranium and potassium concentrations). Regression gives a correction factor of 1.24. Refer to text for further discussion.*

4.5.2 Heat production data for intrusive units and basement rocks

Heat production values were calculated also for felsic intrusive and selected extrusive igneous rock units (Table 4.4). The units were named largely following the usage of Cowley (2006), with selected units being subdivided where significant geographic heat production variations were evident. Unlike heat production data for sedimentary basins, calculations for igneous units were based largely on available geochemical data and supplemented with the gamma-ray data for units with little or no available geochemical data. Upper crust average heat production values (calculated from Rudnick and Gao, 2003) also were utilised for a number of basement units, including the west Gawler Craton.

Table 4.4. Median and standard deviation heat production (HP) values for felsic igneous and other units of the Gawler and Curnamona provinces. Data calculated from available geochemistry. Refer to text for further information. SD = standard deviation. Median (trim) = calculated median once samples of uncertain affinity (including analyses <58% SiO_2), samples with thorium and/or uranium below detection, and outliers removed. Average heat production values from Neumann *et al.* (2000) also shown for comparison.

	Number of samples	Median HP (μWm^{-3})	SD	Trimmed Median HP (no. of samples)	Average HP from Neumann *et al*. (2000) (no. of samples)	Comments
Gawler Craton						
Donnington Suite	31	1.1	1.8	1.7 (21)	3.7 (40)	
Myola Volcanics				3.8 (1)	4.0 (3)	Very little data
McGregor Volcanics	8	4.0	2.8	5.4 (6)	5.8 (10)	Little data
Unit L36 (formerly Lincoln Complex)	55	4.0	3.0	4.3 (45)		
Moody Suite	15	4.3	2.5		4.8 (27)	
Tunkilia Suite	64	2.1	1.5	2.1 (63)		
St Peter Suite	73	1.6	1.3	2.0 (57)		
Gawler Range Volcanics	313	3.5	2.0	4.0 (215)		
Hiltaba: all	520	4.3	5.2			
Hiltaba west	340	3.6	2.4	3.6 (335)		west of 136.5º
Hiltaba east	180	7.5	4.2	8.0 (170)		east of 136.5º
Curnamona region						
Basso Suite	24	4.4	2.9	4.2 (23)		
Poodla Hill Suite	10	1.8	1.0	1.6 (9)		
Bimbowrie Suite	221	5.6	3.1	5.9 (152)		
Moolatawana Suite (All units) *Includes Petermorra Volcanics*	134	7.8	26.2	9.4 (114)		
Moolatawana Suite (normal Th-U) *Includes Petermorra Volcanics*	75	5.1	2.6	5.8 (55)	4.5-7.2 *(Wattleowie Granite, Terrapinna Granite and Petermorra Volcanics)*	
Moolatawana Suite (high Th-U)	59	25.4	30.7	22.7 (34)	11.3-61.6 *(Mt Neill Granite, Hot Springs Gneiss, Box Bore Granite, Yerila Granite)*	

4.5.2.1 Methodology

Heat production values were calculated based on uranium, potassium and thorium concentrations from available whole-rock data sourced from Geoscience Australia's OZCHEM database, Primary Industries and Resources South Australia (PIRSA) geochemical database and, where available, published data. Only those units containing felsic igneous material were considered. Geochemical data were assigned to respective geological units based on unit names (where specified), or on a combination of location and age (as specified for each sample), or, where unit name and age information was absent, on location (unit name assigned on polygon sample fell in) and comparison

with known samples from the unit in question. The resulting classified data set was then filtered, removing geochemical data where:

- sample locations could not be confidently placed within geological units;
- samples were known to be anomalously altered or to represent extreme outliers;
- samples did not have potassium, thorium and uranium data; and
- samples did not belong to targeted solid geology units (in particular mafic units).

The resulting geochemical data for each geological unit were checked to ascertain coherence of the data and test for any identifiable subgroupings. For a number of solid geology units, e.g., Hiltaba Suite in the Gawler Craton, and felsic igneous rocks in the Mount Painter and Mount Babbage inliers (largely Moolawatana Suite), it was evident that:

- there is significant variation in heat production; and
- that natural subgroupings were evident within the geochemical data. Budd (2006) recognised four major subgroups within the Hiltaba Suite.

Although the new data confirmed the subdivision of Budd (2006), the overlapping spatial association of the subgroups made subdivision of the Hiltaba Suite (into these subgroups) an unviable process for the 3D model. However, it was evident that the subgroups with the highest heat production are more common in the east. Accordingly, the Hiltaba Suite was subdivided on the basis of geography into the east and west Hiltaba Suite. Similarly, it was evident from the geochemistry of Moolawatana Suite granites in the Mount Painter and Mount Babbage inliers that two clear heat production subgroups are present. It was apparent also that these two subgroups are spatially localised and could be represented by a number of minor adjustments to the 3D model.

Prior to calculating heat production for each geological unit, statistics were compiled for potassium, thorium and uranium concentrations. Outliers were removed to better quantify standard deviation (which is adversely affected by skewed data distributions). Median values and standard deviations were then calculated for use in 3D thermal modelling (see Table 4.4). For the units without any geochemical data, heat production values were calculated based on similar units. For example, the Benagerie Ridge Volcanics were assumed to have a similar heat production value to the Gawler Range Volcanics (Table 4.4).

4.6 3D GEOLOGICAL MAP CONSTRUCTION

4.6.1 Map construction

A 3D geological map of the energy assessment region was constructed using Gocad[3] software. The map incorporates the two major components required for a geothermal play:

- the cover sequence, providing the thermal insulation; and
- the basement, the source of the high-heat-producing units.

The cover sequence consists of a series of stacked sedimentary basins and volcanic units ranging in age from the Mesoproterozoic to the Cenozoic. The basal interfaces of the basins and volcanic units were constructed as surfaces in Gocad. The surfaces were constrained using a range of data sources of varying degrees of reliability. The lateral extent of each basin and volcanic unit was determined using shapefiles from GIS datasets and solid geology maps. The absolute depths of basal surfaces, or

[3] http://www.gocad.org/

relative depths of basal surfaces provided by sediment/volcanic thickness information, were sourced from, in approximate order of decreasing reliability:

- drill-holes; seismic interpretations;
- published drill-hole constrained sections;
- depth to magnetic source estimations;
- published isopach maps;
- published cross-sections; and
- published descriptions of sediment/volcanic thicknesses.

Existing 3D models and a depth to magnetic basement map, constrained by the above data, were also incorporated into the 3D geological map. The basal surfaces of the stacked basins were constructed from the top of the model, the topographic surface, down to the basement, (i.e. from the most recent basins to the oldest). The topography was defined by the digital elevation model which was sourced from Geoscience Australia's Geophysical Archive Data Delivery System (GADDS, 2010)[4]. The basins were constrained with data which delineates the thickness of sediments, as well as data that delineates the absolute depths to a basal surface. Where thickness constraints were used, it was necessary for the surface above the basin (i.e. the digital elevation model or the base of an overlying basin) to have been constructed already. A comprehensive description of data sources for all cover sequences is provided below. Figure 4.8 shows an oblique view of the top of basement surface, which separates the cover from the basement.

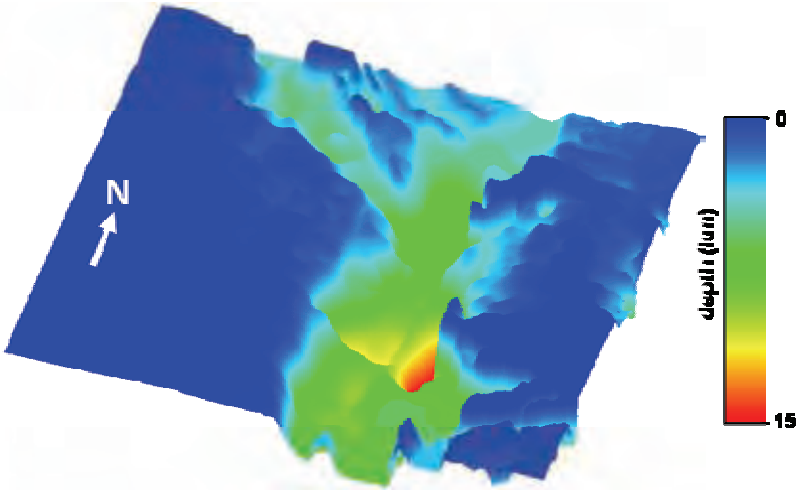

Figure 4.8: *Oblique view of the top of basement surface which separates the cover sequences (Mesoproterozoic Gawler Range and Benagerie Ridge volcanics and overlying younger sediments) from the basement.*

The basement portion of the 3D geological map consists of a series of basement blocks separated by surfaces. These surfaces, modified from Henson (2010), correspond to sub-vertical and sub-horizontal crustal structures identified from recently acquired deep seismic reflection surveys in the assessment area (Korsch and Kositcin, 2010a,b). The sub-vertical structures delineate the interfaces between the east Gawler Craton, west Gawler Carton and Curnamona Province in the upper crustal region, while the sub-horizontal surfaces separate the upper and lower crust. See section 4.6.2.16 below for a comprehensive description of basement surface construction.

[4] http://www.geoscience.gov.au/bin/mapserv36?map=/public/http/www/geoportal/gadds/gadds.map&mode=browse

The model space was then voxelised. Regions within the 3D volumes were created using the above watertight surfaces. The voxel cell dimensions were assigned a vertical cell size of 100 m and a horizontal size of 2 km over a 3D volume of 590 km by 508 km and a 16 km vertical extent (15 km below sea level and 1 km above sea level to include topography).

High-heat-producing bodies were incorporated into the 3D geological map as regions within the upper basement blocks. Granite suites with a heat production of greater than 3.0 µW/m^3 (Table 4.4) were considered high-heat-producing and included as separate bodies in the 3D map (Figure 4.9). A simplified polygon GIS layer was created which incorporated high-heat-producing granites from the Solid Geology of South Australia map (Cowley, 2006), as well as two extra polygons which were created for this study and were based on information provided by geothermal exploration companies. The simplified polygons were imported into Gocad to delineate the horizontal extents of the high-heat-producing bodies with the tops of all but one of the bodies located at the top of the basement. The depth extents of the high-heat-producing bodies were set at 1, 2, 3, 4 or 5 km below the basement cover interface (Figure 4.9) and were determined from interpretations of seismic data, or the lateral extent of the bodies (see below for details).

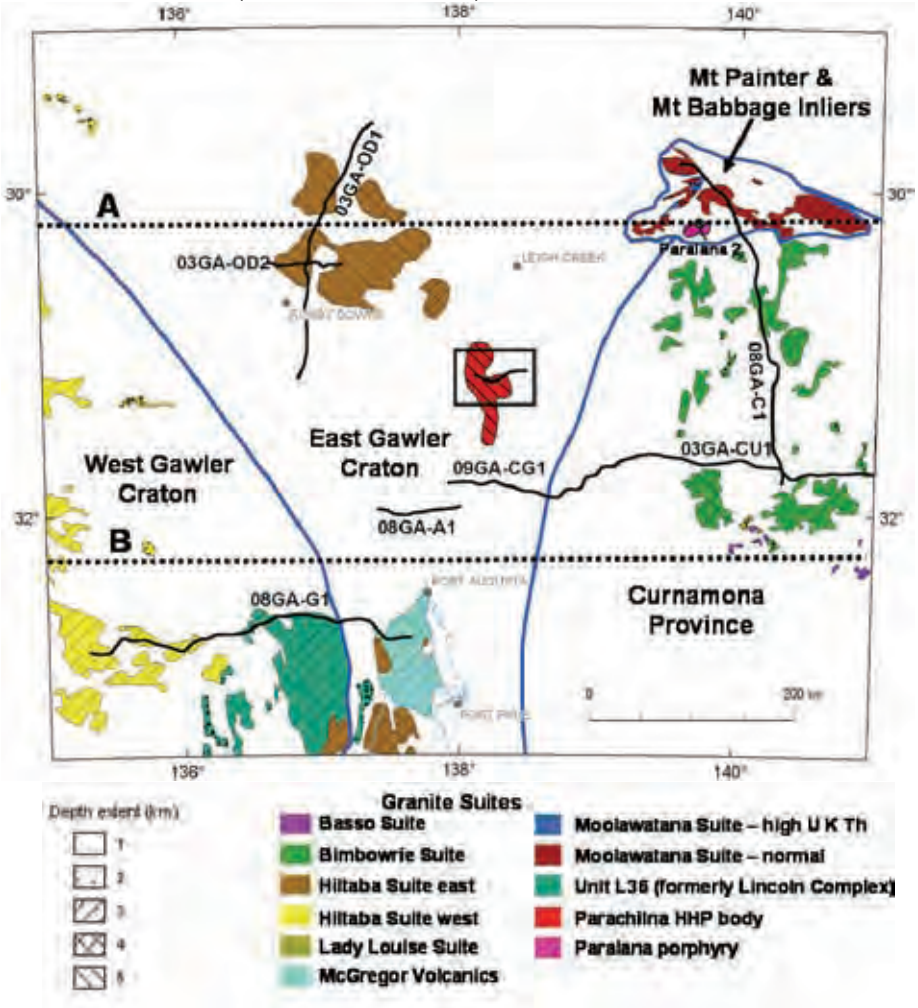

Figure 4.9: *Map of basement features incorporated into the 3D geological map. The blue lines show the boundaries between the different heat-producing basement blocks. The coloured polygons show the high heat-producing bodies (> 3.0 µW/m^3) and their depth extent. The black box shows the location of the Torrens Energy 3D model. The locations of Paralana 2 well, the deep crustal seismic lines (black lines) and the locations of cross sections (dashed lines) in Figure 4.10 are also shown.*

4.6.2 Detailed descriptions of map elements

The following section lists each element of the 3D geological map and the data used to constrain their 3D geometries. Figure 4.10 shows sections through the 3D geological map and the major basement blocks as well as a number of the high-heat-producing granitic bodies. The cover sequence is dominated by sediments of the Adelaide Rift Complex which onlap onto Cariewerloo Basin sediments (blue) and Gawler Range Volcanics (dark blue) in the west. Younger sedimentary basins (light blue, green and yellow) onlap onto the Adelaide Rift Complex and older units.

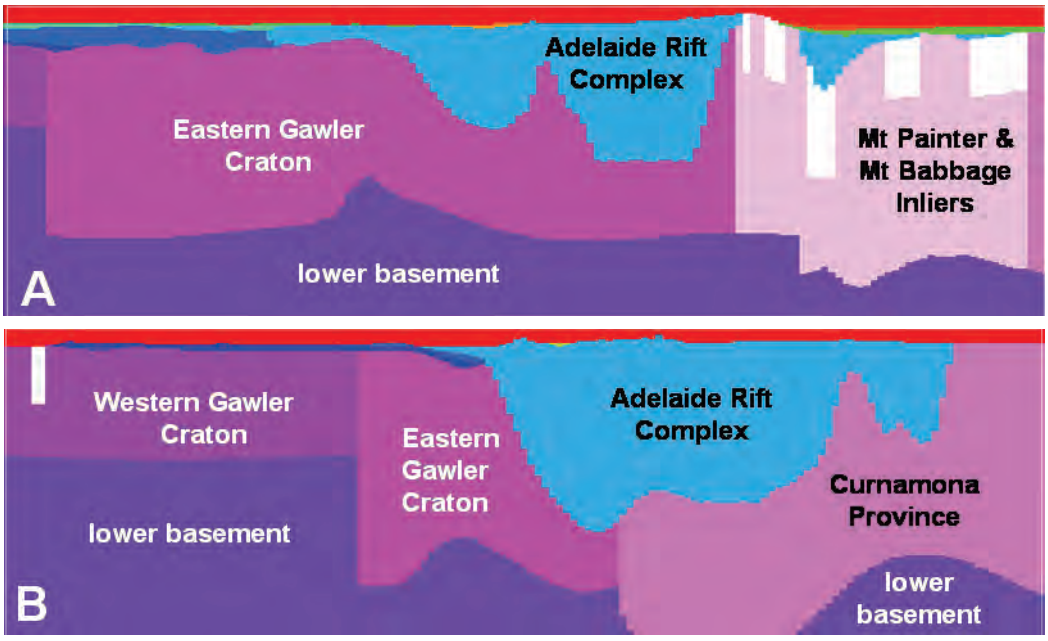

Figure 4.10: *Cross sections A and B through the 3D geological map (see Figure 4.9 for location of the sections). White polygons are high heat-producing granitic bodies. The red polygons are the region above the topography.*

4.6.2.1 Eucla Basin

The Eucla Basin is a Cenozoic marine-terrestrial basin located in the southwestern corner of the assessment area and ranging in thickness from about 25 to100 m in the assessment area (Benbow *et al.*, 1995). The lateral extent of the Eucla Basin was constrained using PIRSA's mineral geological provinces GIS dataset (PIRSA, 2006a). The Eucla Basin was assigned a thickness of 75 m, tapering to zero at the edges of the basin. The surface was constructed by subtracting the thickness from the digital elevation model.

4.6.2.2 Lake Eyre Basin

The Lake Eyre Basin is a Late Paleocene basin located in the northeastern corner of the assessment area. The basin has a thickness of up to 250 m within the assessment area (Callen *et al.*, 1995; PIRSA, 2010a). The lateral extent of the Lake Eyre Basin was constrained using PIRSA's mineral geological provinces GIS dataset (PIRSA, 2006a). In the Curnamona region, its depth was constrained using the Cenozoic layer of PIRSA's Curnamona cover model. Elsewhere, it was

assigned a thickness of 150 m (tapering to zero at the edges of the basin) with the surface constructed by subtracting this value from the digital elevation model.

4.6.2.3 Torrens Basin

The Torrens Basin is a structural depression coincident with the Torrens Hinge Zone, immediately west of the Flinders Ranges. Its thickness ranges from 800 m in the south to less than 100 m in the northwest. The lateral extent of the Torrens Basin was constrained using PIRSA's mineral geological provinces GIS dataset (PIRSA, 2006a). In the southern part of the basin its thickness was constrained using a confidential 3D model supplied by Torrens Energy (Jerome Randabel, *pers. comm.*). In the northern part of the basin, the thickness was constrained to approximately 100 to 150 m in the west and about 200 m in the east in accordance with drillhole-constrained cross sections drawn by Alley and Benbow (1995).

4.6.2.4 Pirie Basin

The Late Eocene to Quaternary Pirie Basin is located directly south of the Torrens Basin. Only its northern half is located in the assessment area. The lateral extent of the Pirie Basin was constrained using PIRSA's mineral geological provinces GIS dataset (PIRSA, 2006a). In the assessment area, the Pirie Basin was assigned a thickness of 240 m in accordance with two drillhole-constrained seismic lines located on the western side of the basin, in the far south of the assessment area.

4.6.2.5 Willochra and Walloway Basins

The Willochra and Walloway Basins are similar sized basins covering small regions immediately northeast of the Pirie Basin. Drillhole-constrained cross sections (Alley and Lindsay, 1995a, b; Kwitko, 1982) show that the Walloway Basin is thicker, reaching a maximum depth of about 380 m in the west, gradually decreasing towards the east. In comparison, the Willochra Basin is approximately 200 m thick in the north, 150 m in the south, and only about 80 m in the centre (Alley and Lindsay, 1995b, c; Kwitko, 1982). The lateral extents of the Willochra and Walloway basins were constrained using PIRSA's mineral geological provinces GIS dataset (PIRSA, 2006a). The basin depths were constrained using the total thickness estimates described above.

4.6.2.6 Murray Basin

The Paleocene to Quaternary Murray Basin is located in the southeastern corner of the assessment area (Rogers *et al.*, 1995) and attains a thickness of up to 350 m. The lateral extent of the Murray Basin was constrained using PIRSA's mineral geological provinces GIS dataset (PIRSA, 2006a). The depth extent of the Murray Basin was constrained in the assessment area using two cross sections which traverse the area of interest within the basin from east to west and from north to south.

4.6.2.7 Eromanga Basin

The Eromanga Basin is a Jurassic to Cretaceous basin covering a large area over South Australia, the Northern Territory, Queensland and New South Wales. The lateral extent of the Eromanga Basin was constrained using PIRSA's mineral geological provinces GIS dataset (PIRSA, 2006a). The depth of the basin in the assessment area was constrained using three 3D models of varying scale and complexity. In the Curnamona region, the Mesozoic surface of PIRSA's Curnamona sedimentary basin model (PIRSA, 2010a) was used. The Z-horizon surface from PIRSA (2006b)

defines the base of late Carboniferous sediments in the Cooper Basin region. Outside the extent of the Cooper Basin, the Z-horizon delineates the base of the Eromanga Basin. In areas where the Z-horizon is not available, a surface defining the base of the Eromanga Basin was used from the regional scale 3D model of van der Wielen *et al.* (2011).

4.6.2.8 Cooper Basin

The Cooper Basin is late Carboniferous to early Triassic in age (PIRSA, 2010b). Only a small portion of the basin, with thicknesses of up to 1600 m, is located in the northeast of the study area. The rest extends further northeast into northern South Australia and Queensland. The lateral and vertical extent of the basin and composition is well defined from petroleum exploration drilling and seismic data. The lateral extent of the Cooper Basin was constrained using PIRSA's mineral geological provinces GIS dataset (PIRSA, 2006a). The Z-horizon surface from PIRSA (2006b) was used to define the base of the Cooper Basin.

4.6.2.9 Arckaringa Basin

The Arckaringa Basin is Permo-Carboniferous in age and is located in the northwestern corner of the study area. It attains a thickness of up to 1300 m in the assessment area. The basin contains a number of accumulations of coal and, as a result, has a lower thermal conductivity than many of the other basins in the area. The lateral extent of the Arckaringa Basin was constrained using PIRSA's petroleum basins dataset (PIRSA, 2002). Two sets of constraints were used to define the base of the basal surface. Where the Arckaringa directly overlies basement, depth to basement constraints were used (Henson, 2010; Meixner and Roy, 2010) while thickness contours digitised from PIRSA (2010b) were used elsewhere.

4.6.2.10 Warburton Basin

The Warburton Basin underlies the Cooper Basin in the northeast of the assessment area. It extends north and east of the assessment area, with only a small proportion in the south of the basin occurring within the assessment area. The lateral extent of the basin was constrained using PIRSA's minerals provinces GIS dataset (PIRSA, 2006a). The depth of the basin was constrained using Geoscience Australia's depth to magnetic basement map of the Gawler-Curnamona region (Henson, 2010; Meixner and Roy, 2010) where the Warburton Basin directly overlies basement. Elsewhere, the depth to the base of the basin was assumed to be half way between the base of the Eromanga Basin, and the base of the Adelaide Rift Complex and Arrowie Basin sequences.

4.6.2.11 Neoproterozoic/Arrowie Basin Succession

The Neoproterozoic sequences of the Adelaide Rift Complex and the Cambrian Arrowie Basin form part of one semi-continuous succession, although with several internal unconformities. The thermal conductivity estimates for the Adelaide Rift Complex and Arrowie Basin are within 0.1 W/mK (Table 4.3), a value which is less than either of the thermal conductivity errors (0.3 W/mK for both sequences). The Adelaide Rift Complex and Arrowie Basin have been grouped together for the thermal modelling because they will provide the same degree of thermal insulation.

The Adelaide Rift Complex and Arrowie Basin occur across more than half of the assessment area. The sequence is thickest (up to 17 km) in the Adelaide Fold Belt region, which runs north-south in the centre of the assessment area (Figure 4.8). Elsewhere, the sequence is thinner, around 1 to 2 km thick in the Stuart Shelf region and up to about 5 km thick (thinning to the east) in the Curnamona

Province. The depth extent of the Adelaide Rift Complex and Arrowie Basin were constrained using the following:

- A portion of the basal surface of the Adelaide Rift Complex and Arrowie Basin was constrained by Geoscience Australia's depth to magnetic basement map of the Gawler-Curnamona region (Figure 4.11) (Henson, 2010; Meixner and Roy, 2010). The magnetic character of the Adelaide Rift Complex changes in the assessment area. In the Stuart shelf and Cunamona Province regions (Figure 2.1) the Adelaide Rift Complex is relatively thin and does not contain significant magnetic material and, as a result, the depth to basement map is delineating the base of the Adelaide Rift Complex. Within the Adelaide Fold Belt region, the Adelaide Rift Complex is relatively thick, deformed and contains significant magnetic material and, as a result, the depth to basement map does not delineate the base of the Adelaide Rift Complex;
- In the Adelaide Fold Belt region where no other constraints were available, the Proterozoic Seebase surface (de Vries *et al.*, 2006);
- In the southern Torrens Basin region, a confidential 3D model over the Parachilna Play, supplied by Torrens Energy and based on seismic and drillhole data (Figure 4.9) (Jerome Randabel, *pers. comm.*);
- Interpretation of depth to the base of the Neoproterozoic sequences from seismic line 09GA-CG1 (Figure 4.9) (Henson, 2010; Preiss *et al.*, 2010);
- Drillhole data for a small portion overlying the Cariewerloo Basin; a single drillhole interception (Paralana 2, Figure 4.9) (Reid *et al.*, 2010); and
- A fault which was defined by Henson (2010) running along the eastern side of the Adelaide Fold Belt.

4.6.2.12 Cariewerloo Basin

The Mesoproterozoic Pandurra Formation of the Cariewerloo Basin is deposited onto the northeastern portion of the Gawler Craton (Cowley, 1991). The lateral extent of the Pandurra Formation was constrained using the Solid Geology of South Australia map (Cowley, 2006). Its depth extent was constrained by drill-hole data (Cowley, W.M, PIRSA, *pers.com*., 2010) and by a digitised isopach contour map of Cariewerloo Basin sediment thickness (Cowley, 1991).

4.6.2.13 Gawler Range Volcanics

The extensive Mesoproterozoic Gawler Range Volcanics is divided into upper and lower units on the Solid Geology of South Australia map (Figure 4.5) (Cowley, 2006). The Gawler Range Volcanics attain a maximum thickness of about 600 m, based on selected drillholes on the eastern margin of the Gawler Craton (Blissett *et al.*, 1993). The lateral extent of the Gawler Range Volcanics was defined by the solid geology map. The basal surface was constrained using a total thickness of 600 m where the upper Gawler Range Volcanics is present on the solid geology map. A value of 300 m for the thickness was used where the lower Gawler Range Volcanics is present on the solid geology map. In the region of the seismic line 03GA-OD1 (Figure 4.9) thickness interpretations after Goleby *et al.* (2003), which range from a few hundred to about 2000 m, were used to constrain the basal surface.

4.6.2.14 Benagerie Ridge Volcanics

The Mesoproterozoic felsic and mafic Benagerie Ridge Volcanics do not outcrop and are located in the east of the assessment area within the northwestern Curnamona Province. They are equivalent in age to the Gawler Range Volcanics and achieve a maximum thickness of about 1500 m based on

seismic interpretation (Korsch *et al.*, 2010). The Solid Geology of South Australia map (Cowley, 2006) provided the Benagerie Ridge Volcanics lateral extent, while the depth extent was set based on a thickness of 1500 m, tapering to zero towards the edge of the Benagerie Ridge Volcanics.

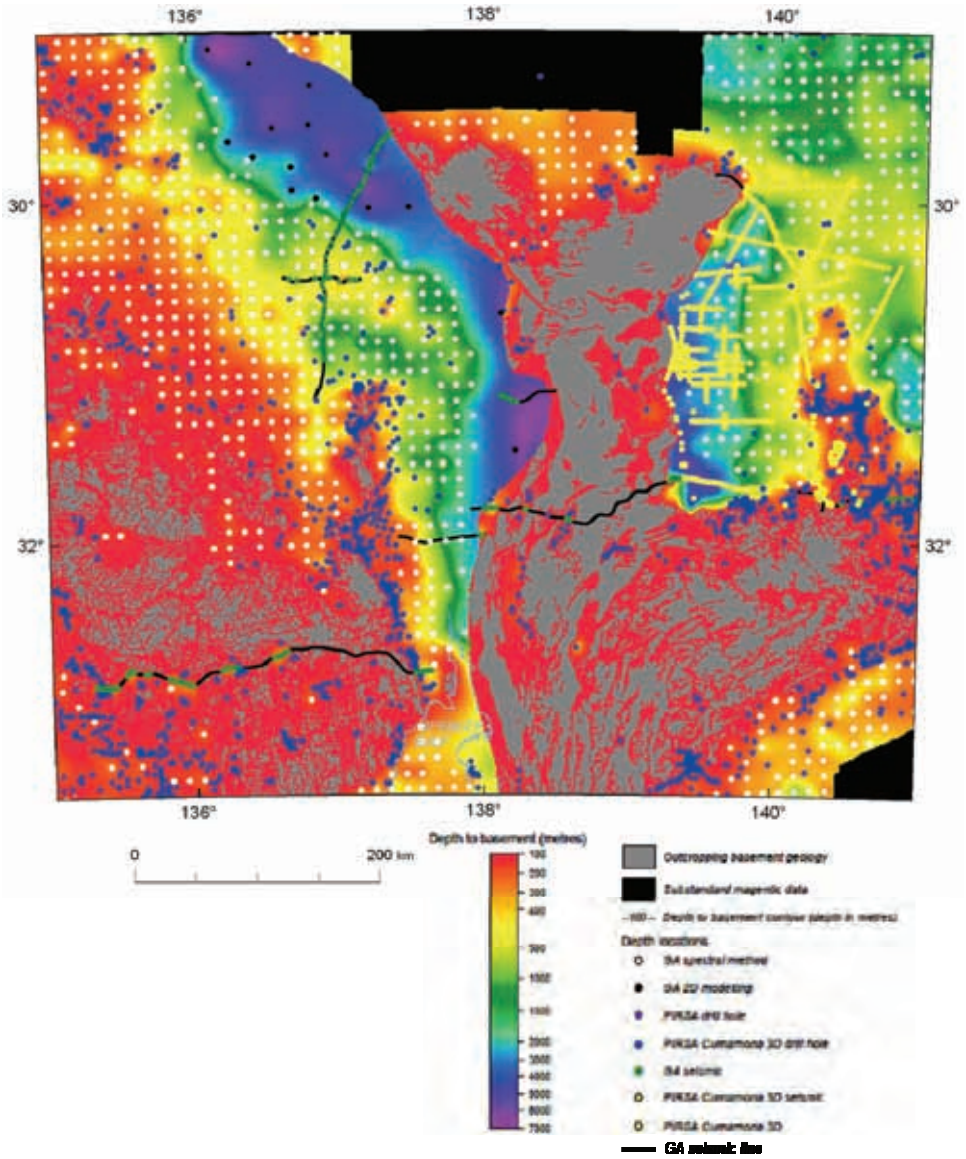

Figure 4.11: *Depth to magnetic basement map of assessment area (modified from Meixner and Roy, 2010). The depth to magnetic basement surface provided constraints for constructing the base of the Adelaide Rift Complex and Arrowie Basin sequence..*

4.6.2.15 Basement high-heat-producing bodies

A GIS polygon layer was created representing high-heat-producing bodies within the study area (Table 4.4). Because of the large number of individual polygons and the density of polygon vertices in the Solid Geology of South Australia map (Cowley, 2006), it was not possible to import the polygon layer directly into the model. Simplification of the polygons was achieved by excluding high-heat-producing granitic bodies with diameters less than about 5000 m, as well as grouping a

number of closely spaced small polygons (less than 5000 m) into larger polygons. The new polygons vertex spacing was also restricted to be greater than about 2000 m providing additional simplification. The individual high-heat-producing polygons were grouped into granite suites based on heat production values (Table 4.4; Figure 4.9). The new polygon layer was then used to define 3D regions within the 3D geological map.

The tops of the high-heat-producing bodies were assumed to coincide with the top of the basement in the 3D geological model (Figure 4.8). The depth extents of a number of the bodies were determined based on interpretations of seismic lines where the basal contacts of the granites were imaged (Figure 4.9). These bodies include the McGregor Volcanics, unit L 36 (formerly Lincoln Complex), the Hiltaba Suite east, all of which are approximately 3 km thick on seismic line 08GA-G1 (Fraser *et al.*, 2010b) and the Burgoyne Batholith, part of the Hiltaba Suite east, which are about 5 km thick on seismic line 03GA-OD1 (Lyons and Goleby, 2005). For bodies where the basal contact was not imaged on seismic, the thickness was defined based on a ratio of lateral to vertical extent of 4:1. While it is clear that there is no simple or universal relationship between a granite body's horizontal versus vertical extent, there is a general consensus that individual plutons are wider than deeper (e.g. see review by Petford *et al.*, 2000). A somewhat arbitrary ratio of 4:1 (lateral to vertical extent) was used to determine depth of granites in the 3D map.

An issue encountered when applying this ratio is that only a small number of the high-heat-producing bodies exhibit circular shapes in their lateral extent. Where bodies were elongated, the short axis of the ellipse was used to determine the vertical extent. Where the shapes of bodies were highly irregular a lateral extent was estimated to reflect the overall size of the body. The above depth extents were rounded to whole numbers (1, 2, 3, 4 and 5 km) as a means to simplifying the process of importing the polygon layer into Gocad and constructing the regions within the 3D geological map.

Heat flow determinations (Figure 4.5) and down-hole temperatures from the Paralana Geothermal Play (Petratherm Limited) and Parachilna Play (Torrens Limited) suggest anomalously high-heat flows and temperatures at depth. Preliminary thermal modelling indicates that to reproduce these values, a large amount of heat production is required in the crust in these regions, most likely sourced from within the basement. Therefore, to match the heat flow data, two additional bodies were added to the polygon layer, delineating high-heat-producing bodies in the basement. These bodies, the Paralana porphyry and the interpreted Parachilna high-heat-producing body (Figure 4.9), were added based on information supplied by Petratherm Limited and Torrens Energy Limited as described below.

4.6.2.15.1. Paralana Porphyry

Recent drilling at Paralana 2 well by Petratherm Limited encountered a felsic porphyry intrusive at 3910 m within the basement (Reid, 2010), 513 m below the base of sediments of the Adelaide Rift Complex. The heat production values calculated for the intrusive body of 10 to 12 $\mu W/m^3$ (Reid, 2010) was based on geochemical data (Mathieu Messeiller, *pers. comm.*). Although the drill-hole provides a depth to the top of the high-heat-producing body, it does not provide a lateral extent. Images of first vertical derivative of the total magnetic intensity, reduced to pole data, show the Paralana 2 well to be located within a broad, but subtle, magnetic anomaly. The long wavelength of the anomaly suggests that the magnetic source is deeply buried and may be associated with the high-heat-producing felsic intrusive. This interpretation is supported by outcropping high-heat-producing Moolawatana suite granites in the Mount Painter and Mount Babbage inliers to the northwest which are highly magnetic. The polygon defining the lateral extent of the Paralana porphyry was digitised

around the edge of the magnetic anomaly located on the Paralana 2 well. The depth extent assigned to the body of 3 km was based on the 4:1 lateral to depth ratio, rounded to the nearest whole number.

4.6.2.15.2. Parachilna high-heat-producing body

Thermal modelling on a 3D model over the Parachilna Play (Figure 4.9) in the southern Torrens Basin region, supplied by Torrens Energy (Jerome Randabel, *pers. comm.*), indicates the need to have high-heat production values in the basement in order to match heat flow measurements and down hole temperatures. In thermal modelling performed by Torrens Energy, the heat production rate in the basement was not differentiated and a single value of 10 $\mu W/m^3$ was used based on correlations with Hiltaba Suite granites. The high-heat production value used for the basement was necessary for the thermal model to match the measured heat flow (Jerome Randabel, *pers. comm.*). For the regional thermal modelling of this study it was necessary to differentiate a high-heat-producing body from the surrounding basement. Images of the first vertical derivative and the total magnetic intensity, reduced to pole data, show a strong north-south trending magnetic anomaly located in the Torrens Energy 3D model region. The long wavelength of the magnetic anomaly suggests that the top of the source of the magnetic anomaly is deeply buried. This is consistent with Torrens Energy's interpretation, where the interpreted top of this source ranges from about 3000 m in the northwest to more than 8000 m in the southeast of the Torrens Energy 3D model region. Portions of the buried Hiltaba Suite granites to the northwest, identified from the Solid Geology of South Australia map (Cowley, 2006) also correlate with strong magnetic anomalies. As a result, the magnetic anomaly was interpreted to delineate the high-heat-producing body and a polygon defining the lateral extent of the Parachilna high-heat-producing body was been digitised based on this anomaly. The thickness of the body was assumed to be 5 km, based on the 4:1 lateral to depth ratio described in Section 4.6.2.15, rounded to the nearest whole number.

4.6.2.16. Basement

Initial thermal model runs were conducted on a homogeneous basement, using a single heat production value (see below). Basement includes all lithologies in the assessment area which are Mesoproterozoic and older, excluding the younger high-heat-producing bodies that have intruded the basement. A comparison of the modelled and measured heat flow values indicated that a heterogeneous basement with regions of different heat production was required to match the surface heat flow data. To achieve this, the basement was divided into a series of separate terrains with different thermal properties (Figures 4.9 and 4.10). A number of these terrains have been delineated from a series of sub-vertical and sub-horizontal 3D surfaces modified from Henson (2010). The sub-vertical surfaces correspond to major crustal penetrating structures identified from recently acquired deep seismic reflection surveys in the assessment area (Korsch and Kositcin, 2010a,b). The structures separate three crustal blocks, the eastern and western Gawler cratons and the Curnamona Province. The sub-horizontal surfaces delineate upper and lower crustal layers, identified from the seismic data based on differing seismic reflectivity (Korsch and Kositcin, 2010a,b). These crustal layers were incorporated into the 3D geological map in order to provide depth constraints to the upper thermal property blocks. Although the lower crustal layer was subdivided by Henson (2010), the lower crust for the final thermal models was left undivided because there is no evidence for different lower crustal thermal properties between the three regions.

Subsequent forward modelling runs indicated that a further subdivision was required to separate the Mount Babbage and Mount Painter inliers from the Gawler and Curnamona provinces (Figures 4.9 and 4.10). The separation of the Mount Babbage and Mount Painter inliers allowed elevated heat production values to be assigned to the basement blocks in this region in order to match the

measured heat flow values. To achieve this separation, two surfaces were added to the model which extend vertically upward from the undivided lower crust to either the digital elevation model, or the basement/cover interface where the Mount Painter and Mount Babbage Inliers are under cover.

The surface separating the northern and western extents of the Mount Painter and Mount Babbage Inliers from the east Gawler Craton was constructed using a combination of the Solid Geology of South Australia map (Cowley, 2006), the total magnetic intensity map (reduced to the pole) and Bouguer gravity data. The magnetic and gravity images were used to interpret the extent of the westerly extension of the two inliers beneath the sediments of the Adelaide Rift Complex and Arrowie Basin. The nature of the magnetisation and density distribution of both the cover (Adelaide Rift Complex and Arrowie Basin) and basement (Mount Painter and Mount Babbage Inliers) are such that the inferred boundary is tenuous and is considered to represent a conservative estimation of basement extension to the west.

The surface separating the southern extents of the Mount Painter and Mount Babbage Inliers from the Curnamona Province was located using the Solid Geology of South Australia map (Cowley, 2006) as well as images of the Bouguer gravity data. The southerly basement extension is delineated by either the southerly extent of the Moolawatana Suite, where the suite is interpreted to subcrop beneath Adelaide Rift Complex and Arrowie Basin, or by an approximate east-west trending change in the magnitude of the gravity data.

4.7 GEOTHERMAL PROSPECTIVITY CONFIDENCE MAPS

Three additional 3D models have been constructed to provide an indication of the distribution of reliability in the geothermal assessment. The first incorporates the distribution of data uncertainty used to construct the 3D geological map while the second and third models incorporate the distribution of the thermal property data uncertainty (thermal conductivity and heat production). To visualise these 3D data uncertainty models, the data uncertainty values were summed vertically up to the top layer to provide a 2D representation of the data uncertainty as a series of confidence maps. The three confidence maps were then combined to give an overall confidence map. As the hot rock and hot sedimentary aquifer prospectivity are derived from the thermal model and as the combined confidence map highlight regions of higher and lower confidence in the thermal model, the confidence maps, therefore, highlight regions of higher and lower confidence in the hot rock and hot sedimentary aquifer prospectivity maps.

4.7.1 3D geology confidence map

The voxelised 3D geological map was used as the base to construct the 3D data uncertainty model. A map of the 3D geology confidence is shown in Figure 4.12. To produce this uncertainty model all of the input data to the 3D geological map was assigned an uncertainty rating. The data uncertainty values (Table 4.5) are an interpretation of the ability of that data to define a geological contact or assign a particular lithology to a region within the 3D geological map. For example, the uncertainty value applied to a lithological contact derived from a drillhole is lower than that for a lithological contact derived from a published cross-section.

For the cover sequence, each stacked sedimentary basin and volcanic unit was given a combined uncertainty value which was assigned to the uncertainty model. Where multiple geological data were used to construct that basin unit (but could not be placed accurately on a map) the final uncertainty value assigned was an estimated average of all the input data uncertainty. For some basins accurately located drillhole, seismic or other data were used to construct their base. In these cases the basins

were assigned a background uncertainty value, with the intention that where located data exists it would be used to update the uncertainty model at a later step (described below). Table 4.6 lists the background uncertainty values applied to each basin.

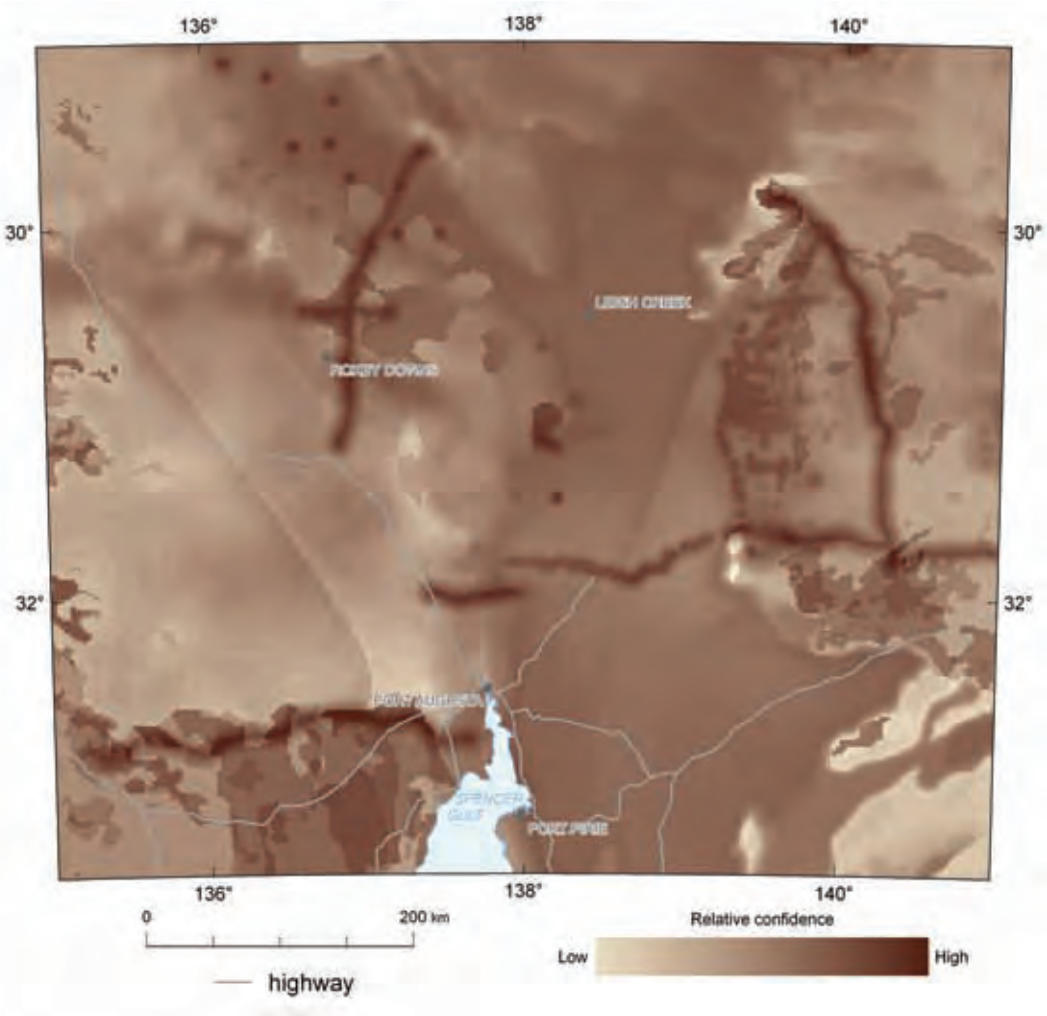

Figure 4.12: *3D geology confidence map. Two dimensional representation of the reliability and uncertainty in the data hat has been used to produce the 3D geological map.*

Table 4.5: The data types used to produce the 3D geological map and the uncertainty value (low number – low uncertainty; high number – high uncertainty) assigned to that data type.

GEOLOGICAL DATA	UNCERTAINTY VALUE
Outcropping Palaeoproterozoic and older basement	1
Drill holes	2
Seismic interpretations in the cover	3
Existing 3D model (constructed from drill hole data)	3
Published cross-section (based on drill hole data)	3
Palaeoproterozoic and older basement under cover	3
Magnetic depth estimates	4
Seismic interpretations in the basement	4
Published contours defining basin thickness	4
Single published value for basin thickness	5

Table 4.6: Combined uncertainty data values (low number – low uncertainty; high number – high uncertainty) assigned to the uncertainty model for the sedimentary basins and volcanic units.

BASINS AND VOLC. UNITS	COMBINED UNCERTAINTY VALUE
Eucla Basin	2
Lake Eyre Basin	2
Torrens Basin	3
Pirie Basin	2
Willochra Basin	4
Walloway Basin	3
Murray Basin	3
Eromanga Basin	4
Cooper Basin	4
Arckaringa Basin	3
Warburton Basin	2
Adelaide Rift Complex + Arrowie Basin	2
Cariewerloo Basin	4
Gawler Range Volcanics	2
Benagerie Ridge Volcanics	2

For the basement portion of the 3D geological map uncertainty model, new regions were constructed. These regions were mapped onto the top of basement surface and projected vertically downwards. The regions and their assigned uncertainty values include:

- where basement geology is delineated by outcropping mapped geology from a modified version of the Surface Geology of Australia 1 :1 000 000 scale map (Whitaker *et al.*, 2008) uncertainty equals one;
- where basement is undercover but has been interpreted on the Solid Geology of South Australia map (Cowley, 2006) uncertainty equals three; and
- where basement is unknown (blank regions in Figure 4.5) uncertainty equals six.

Confidence in the model will decrease with depth. A value of 2000 m was selected as the depth value beyond which the cells were assigned an uncertainty value of six. A linear interpolation was applied between the previously assigned surface uncertainty values (for the cover) and the top of basement uncertainty value (for the basement). The combined uncertainty values for the sedimentary basins and volcanic units (Table 4.6) were then incorporated into the uncertainty model. If the uncertainty values for the sedimentary basins and volcanic units were higher than the values in the 3D uncertainty model, then the uncertainty values in the uncertainty model were re-assigned these values.

Where depth delineating data exists (drill-holes, seismic and magnetic depth estimates), the cells in the uncertainty model were re-assigned a new value based on their ability to resolve geology at depth (Table 4.5). The cells enclosing the depth location point (i.e. depth to the base of a sedimentary basin defined by a drill-hole intersection, and all cells vertically above that cell to the topographic surface) were assigned an uncertainty value reflecting the data type. The uncertainty values were then interpolated linearly in an outward direction, increasing from the value assigned to that data type at the data point location, to the existing uncertainty value at a radius of 10 km from the data point.

4.7.2 Thermal property confidence maps

The thermal modelling results, which form the basis of the geothermal assessment, are fundamentally influenced by the values of heat production and thermal conductivity assigned to the thermal model. The 3D distribution of heat production and thermal conductivity control the vertical heat flow at the surface, as well as the geothermal gradients. Uncertainty in the assigned values results in uncertainty in the surface heat flow and temperature at depth. To gauge the level of confidence in the thermal modelling results, heat production and thermal conductivity confidence maps were generated.

Uncertainty ratios for the heat production and thermal conductivities were assigned to each unit in the 3D thermal model to produce the heat production and thermal conductivity 3D uncertainty models. The uncertainty values assigned to the thermal model are shown in Table 4.7. The ratios mostly consist of the first standard deviation of the property uncertainty calculated during the thermal property data compilation, divided by the thermal property used in the final forward model run. Where no standard deviations exist the uncertainty ratios were estimated.

To produce the thermal property confidence maps, the thermal property uncertainties were summed vertically, up to the topographic surface. The heat production uncertainties were summed from the base of the model (15 km), while the thermal conductivity uncertainty was summed from 5 km depth. The heat production and thermal conductivity confidence maps are shown in Figure 4.13.

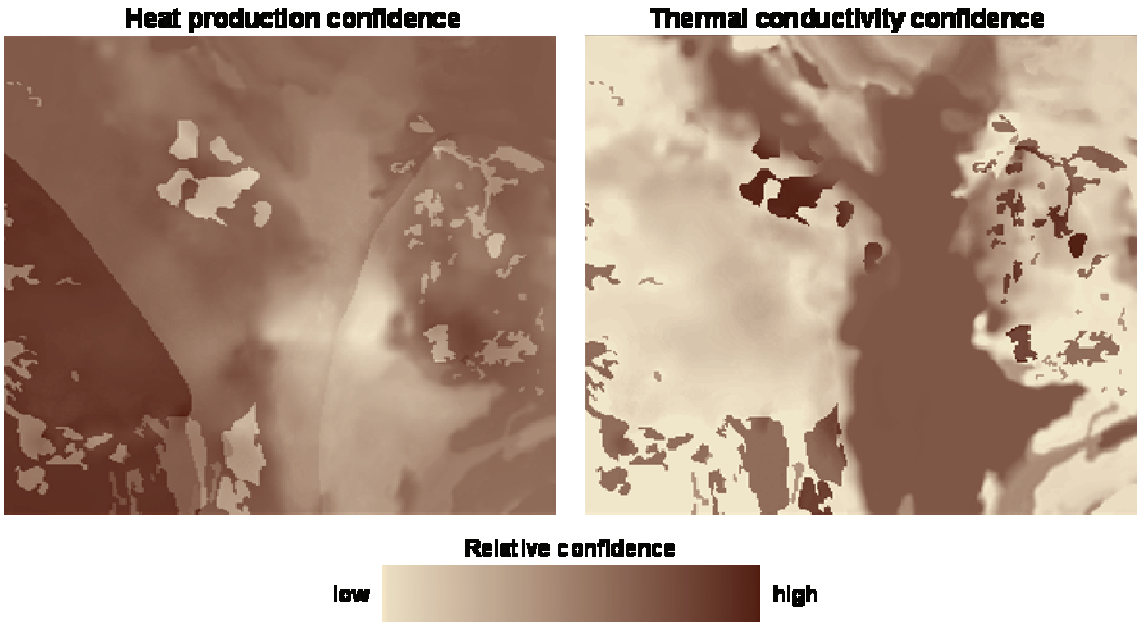

Figure 4.13: *Images of the thermal property confidence maps.*

4.7.3 Combined confidence map

The combined confidence map (Figure 4.14) incorporates the confidence values of the 3D geological map, heat production and thermal conductivity confidence maps. The confidence values which made up these three maps were normalised and then combined using the following formula.

$$\text{Combined} = (\text{3Dmap} \times \text{HP}) + (\text{3Dmap} \times \text{Tc}) \quad (5)$$

Where: Combined = the combined confidence map; 3Dmap = the 3D geology confidence map; HP = the heat production confidence map; and Tc = the thermal conductivity confidence map.

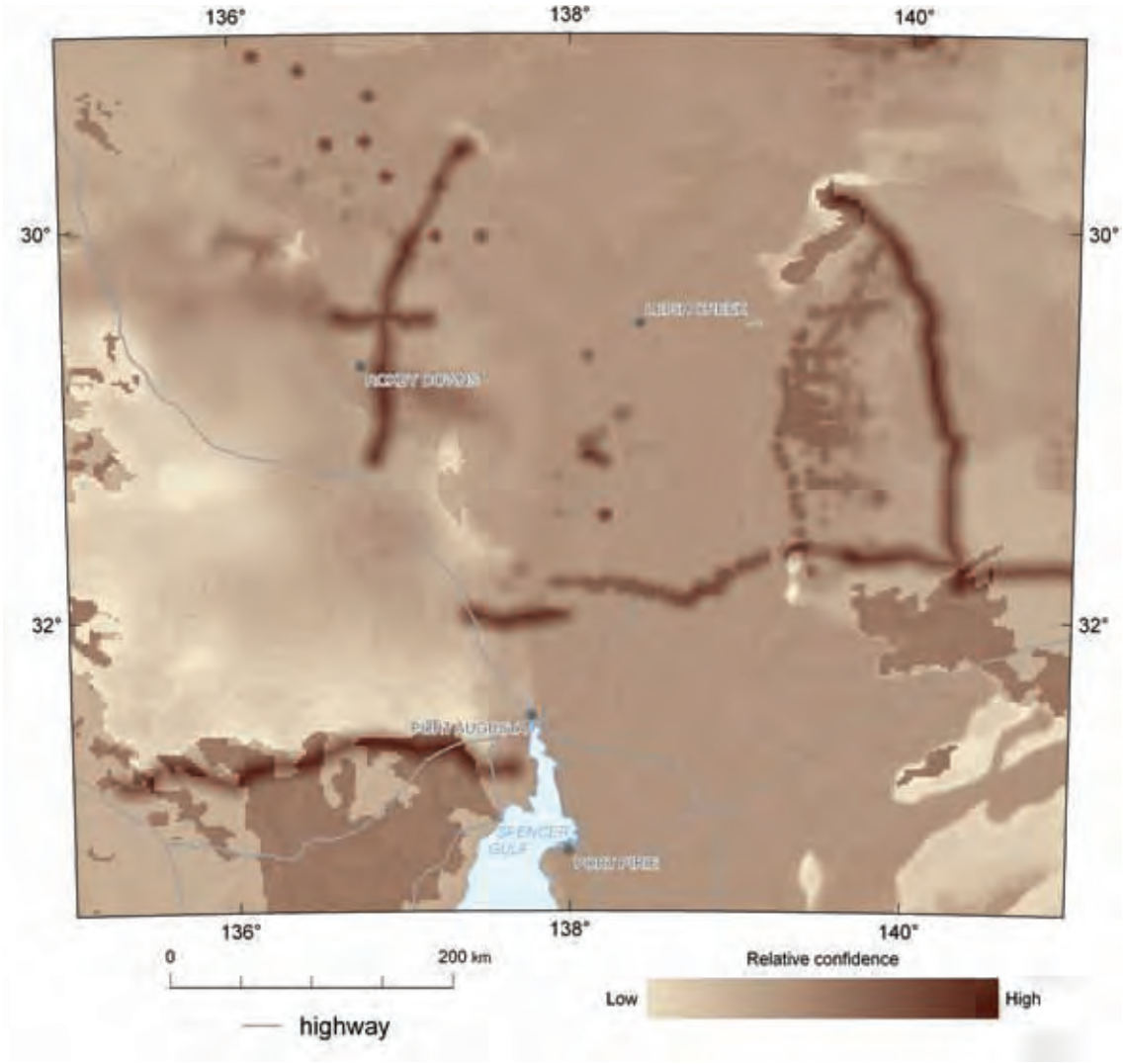

Figure 4.14: *Combined confidence map incorporates the data uncertainty that has produced the 3D geological map, as well as the uncertainty in the heat production and thermal conductivity data.*

4.8 THERMAL MODELLING

4.8.1 Work flow

A number of forward thermal model runs were performed using the thermal modelling component of the GeoModeller software. The individual elements of the voxelised 3D geological map were assigned initial thermal properties based on the thermal conductivity (Tables 4.2 and 4.3) and heat production (Table 4.4) data compilations as described in the previous sections.

The boundary conditions for all of the thermal model runs were set as follows. The cells in the 3D mesh that coincide with the topographic surface were assigned a constant temperature of 22°C. This

value was calculated based on the mean annual surface temperature of 19°C from the Bureau of Meteorology[5] at the location of 138° longitude and 21° latitude. The 22°C value assigned equates to the average soil temperature which is generally about 3°C higher than the average air temperature (Howard and Sass, 1964).

A constant heat flow of 36 mW/m^2 was applied to the base of the model at 15 km depth. This value was calculated by adding the heat flow contribution due to the heat produced between the base of the model and the base of the crust, to the heat flow at the base of the crust. Rudnick and Gao (2003) give estimates of the heat production of 1.0 µW/m^3 for mid crustal lithologies (13 to 23 km depth) and 0.19 µW/m^3 for lower crustal lithologies (more than 23 km depth). The MOHO depth in the region is 40 km (Korsch and Kositcin, 2010a,b). Based on these heat production values and depth extents, the heat flow contribution from the MOHO to the base of the model (15 km depth) is 11 mW/m^2. Adding 25 mW/m^2, the reduced heat flow calculated at the base of the crust from McLaren *et al.* (2003), results in 36 mW/m^2 heat flow at the base of the model.

After boundary conditions were assigned a forward thermal model was computed and the resulting 3D mesh of calculated temperatures and heat flows were compared initially to the available surface heat flow determinations, and then later to the down-hole temperatures. Where the difference, or residual between the measured and modelled surface heat flows and temperatures were considered large, the thermal properties in that region of the model were adjusted and the thermal model was rerun. This iterative process continued until no further improvements could be made due to the simplicity of the 3D geological map. The heat production and thermal conductivity values assigned to the initial and final thermal model run are shown in Table 4.7.

The thermal modelling was conducted using batch scripts. The batch script bypasses the GeoModeller GUI and allows the 3D geological model to be constructed in GoCad, rather than in GeoModeller. The first process in the batch script is to import the GoCad voxet into XML format, the format that GeoModeller uses to store 3D geological map information. The script then assigns the thermal property values to each element in the 3D geological map. The final section of the script sets the boundary conditions, the output voxet name, the maximum number of iterations and the temperature residual. This residual is the temperature difference for the model cells between the second last and last iteration. The modelling is complete once either the user specified maximum number of iterations is completed, or the temperature residual drops below the value specified in the script. The temperature residual should be of a value low enough and the iterations high enough so that the model will reach thermal equilibrium.

The initial forward model runs were conducted on the voxelised 3D geological model at a reduced resolution compared to the final model. The computation time for the full resolution model (cell size of 2 by 2 km lateral, 100 m vertical) was prohibitive (>20 days) on a high-end desk-top personal computer. The excessive computation times were due to the large number of cells (12.8 million) and the number of iterations (about 100 000) required for the model to reach thermal equilibrium. The reduced resolution model (cell size of 6 by 6 km lateral, 100 m vertical) allowed forward models to run in ~12 hours. The final forward model, from which the geothermal energy assessment is based, was run on a model with a cell size of 4 by 4 km lateral and 100 m vertical. This forward model run took approximately 4 days to compute 100 000 iterations with a final temperature residual of 4×10^{-5}°C.

[5] http://www.bom.gov.au/jsp/ncc/climate_averages/temperature/index.jsp?maptype=6&period=an

Table 4.7: Thermal properties used in initial and final thermal models, with uncertainties (1σ) from data compilations and ratios of this uncertainty to final modelled property value.

3D Geological map unit	HEAT PRODUCTION (μW/m^3)				THERMAL CONDUCTIVITY (W/mK)			
	Initial	Final	Uncer-tainty	Ratio	Initial	Final	Uncer-tainty	Ratio
Eucla Basin	1.0[1]	1.0	0.33	0.3	1.9	1.9	0.54	0.28
Lake Eyre Basin	1.3[1]	1.3	0.29	0.23	2.3	2.0	0.28	0.14
Torrens Basin	1.3[1]	1.3	0.32	0.25	1.8	1.8	0.38	0.21
Pirie Basin	1.1[1]	1.1	0.24	0.22	1.9	1.9	0.30	0.16
Willochra Basin	1.3[1]	1.3	0.32	0.25	1.9	1.9	0.14	0.07
Walloway Basin	1.3[1]	1.3	0.36	0.28	1.5	1.5	0.13	0.09
Murray Basin	1.2[1]	1.2	0.57	0.48	1.6	1.3	0.08	0.06
Eromanga Basin	1.4[1]	1.4	0.34	0.22	2.4[10]	2.4	0.40	0.17
Cooper Basin	1.2[7]	1.2		0.5*	1.4	1.4	0.20	0.14
Arckaringa Basin	1.3[1]	1.3	0.29	0.22	1.8	1.8	0.19	0.11
Warburton Basin	1.6[1]	1.6	0.50	0.31	3.2	3.2	0.19	0.06
Adelaide Rift Complex + Arrowie Basin	1.9[2]	2.4	0.86	0.36	2.7	3.2	0.34	0.13
Cariewerloo Basin	1.1[1]	1.1	0.28	0.25	3.0[11]	3.0[11]	0.34	0.11
Gawler Range Volcanics	3.5[3]	3.5		0.5*	3.0	3.0	0.18	0.06
Benagerie Ridge Volcanics	3.5[4]	3.5		0.5*	3.0	3.0	0.18	0.06
Lower basement	1.7[5]	1.7	0.2	0.12	2.0	2.0		0.25*
west Gawler Craton	1.7[5]	1.7		0.25*	3.0	3.0		0.33*
east Gawler Craton		4.0		0.25*	3.0	3.0		0.33*
Curnamona Province		2.2		0.25*	3.0	3.0		0.33*
Mt Painter & Mt Babbage		5.0		0.25*	3.0	3.0		0.33*
Basso Suite	4.4[3]	5.4	2.9	0.54	3.0	3.0	0.15	0.05
Binbowrie Suite	5.6[3]	5.6	3.1	0.55	3.0	3.0	0.15	0.05
Unit L36 (Lincoln Complex)	4.0[3]	6.0	3.0	0.50	3.0	3.0	0.15	0.05
Hiltaba Suite east	7.5[3]	7.5	4.2	0.56	3.0	3.0	0.15	0.05
Hiltaba Suite west	3.6[3]	3.6	2.4	0.67	3.0	3.0	0.15	0.05
Lady Louise Suite	4.4[9]	4.4	0.5	0.11	3.0	3.0	0.15	0.05
Moolawatana Suite normal	5.1[3]	5.1	2.6	0.51	3.0	3.0	0.15	0.05
Moolawatana Suite HHP	25[3]	40	14	0.31	3.0	3.0	0.15	0.05
McGregor Volcanics	4.0[3]	4.0	2.8	0.70	3.0	3.0	0.15	0.05
Paralana porphyry	11[8]	18		0.25*	3.0	3.0	0.15	0.05
Parachilna HHP body	7.5[6]	14		0.25*	3.0	3.0	0.15	0.05

* Estimated value, see text for explanation.

[1] calculated from corrected and weighted gamma-ray data

[2] average of HP values calculated from 6 basin sections

[3] calculated from geochemical data

[4] assumed same HP vale as the Gawler Range Volcanics

[5] assumed equivalent to average upper crust (Rudnick and Gao, 2003)

[6] assumed same HP as Hiltaba east

[7] average value of all basins

[8] published value (Reid, 2010)

[9] value assigned from Hiltaba Suite east

[10] published value (Gibson *et al.*, 2010)

[11] assumes Pandurra Formation is mostly sandstone with minor conglomerate, siltstone and shale

4.8.2 Improvements due to multiple forward model runs

Figure 4.15 shows the heat flow residuals (measured minus modelled) for the initial and final forward model runs. There is a marked improvement between the initial and final runs in the heat flow residuals, and hence the match between the measured and modelled heat flows. These improvements were achieved by altering the heat production in different basement blocks as described in Section 4.6.2.16.

The basement for the initial run was modelled as one unit with a heat production value of 1.7 $\mu W/m^3$ (average of upper crust; Rudnick and Gao, 2003). However this value was not sufficient to match the measured surface heat flow. At this stage the model was split into different basement terranes (as described in Section 4.6.2.16), and these were assigned different heat production values. The undivided lower basement (Figure 4.10) was assigned a heat production value of the 1.7 $\mu W/m^3$. To determine heat production values for the upper crustal blocks, a number of forward model runs were performed. The heat production values that produced the lowest residual for each basement region were determined and used in the final model. The values are: west Gawler Craton – 1.7 $\mu W/m^3$; east Gawler Craton – 4.0 $\mu W/m^3$; Mount Painter and Mount Babbage inliers – 5.0 $\mu W/m^3$; and Curnamona Province – 2.2 $\mu W/m^3$. In some instances the heat flow residuals were reduced further by adjusting the heat production of individual high-heat-producing bodies. The heat production values which were modified from the initial model run are shown in final column of Table 4.7.

After the heat flow data had been matched, the thermal conductivity values were altered over a series of forward model runs in order to match the down-hole temperature measurements. Figure 4.16 shows the improvements to the residual temperatures between the initial and final forward model runs, while Table 4.7 shows the initial and final thermal conductivity values used in these runs. Minor reductions in the thermal conductivities were made to the Lake Eyre and Murray basins during the modelling process, in order to increase the modelled down-hole temperatures located within the basins. Both these basins have a limited depth extent (< 350 m maximum) and so the changes to the modelled temperatures were small. A major modification of the thermal conductivity between the initial and final forward model runs was made to the values of the Adelaide Rift Complex and Arrowie Basin (Table 4.7) which were increased from 2.7 to 3.2 W/mK. Due to its large spatial coverage and depth extent, up to 15 km at its deepest, this increase in thermal conductivity resulted in significant reductions in modelled temperatures in and beneath thicker sequences of the unit.

The thermal modelling process resulted in significant improvements between the modelled and measured down-hole temperature and surface heat flow data. The median of the heat flow residuals for the final forward model run of 5.7 mW/m^2 is a marked improvement over the initial model run, with a residual of 40 mW/m^2. The improvement in the match with the temperature data is evident in Figure 4.17, and provides confidence that the thermal model is replicating the thermal structure at least in the region of data measurements.

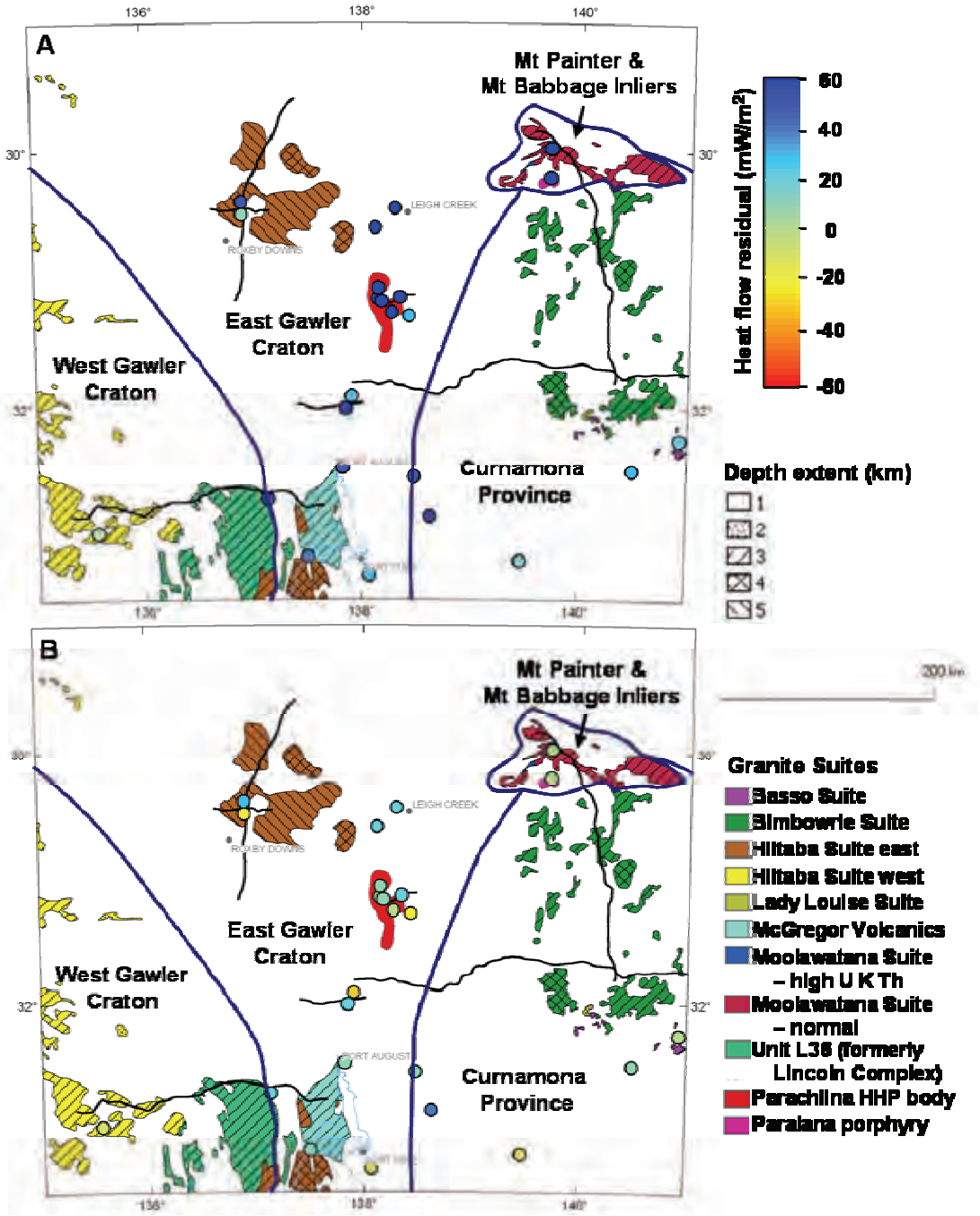

Figure 4.15: *Residual heat flow values (measured minus the modelled) for the initial forward model run (A) and the final forward model run (B). Low residuals indicate a good match between the measured and modelled heat flows. Positive numbers indicate the modelled heat flows are too low, while negative numbers indicate the modelled heat flows are too high. The high heat-producing granitic bodies and basement terrains are also shown.*

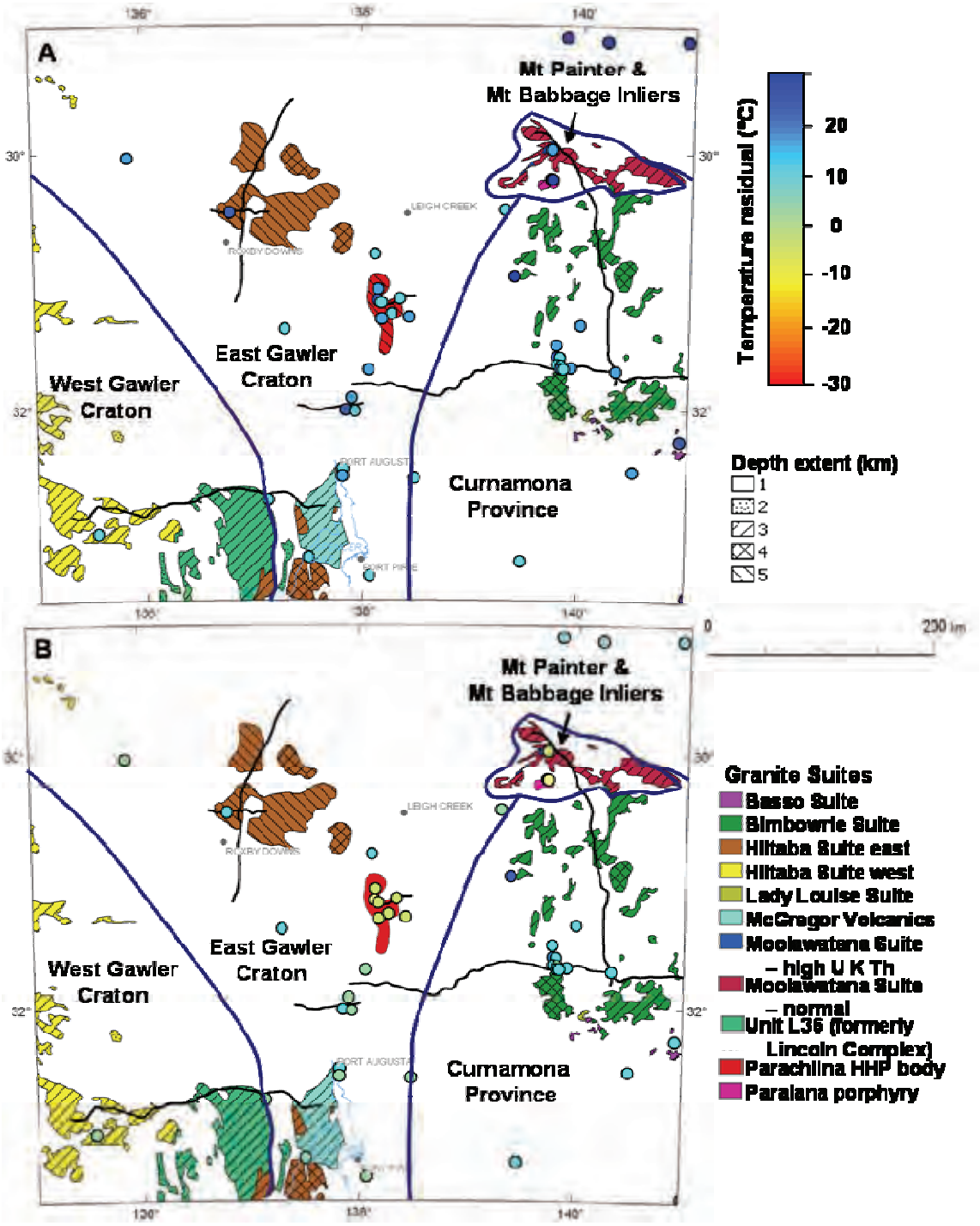

Figure 4.16: *Residual down-hole temperatures (measured minus the modelled) for the initial forward model run (A) and the final forward model run (B). Low residuals indicate a good match between the measured and modelled temperatures. Positive numbers indicate the modelled temperatures are too low, negative numbers indicate the modelled temperatures are too high. The high heat-producing granitic bodies and basement terrains are also shown.*

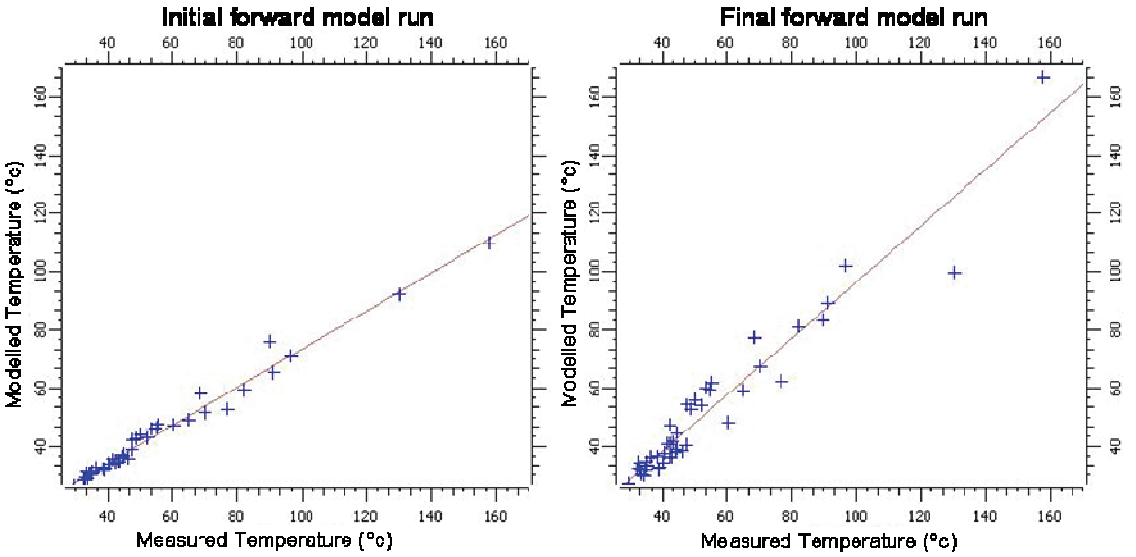

Figure 4.17: *Scattergrams showing the measured and modelled temperatures for the initial and final forward model runs at the down-hole measurement locations. Lines of best fit are also shown. The improved match between the measured and modelled temperatures for the final forward model run is evident by the line of best fit almost diagonally bisecting the plot space.*

4.8.3 Implications of thermal modelling

The heat flow residual for the final model run (5.7 mW/m^2) suggests that on average there is not enough heat production in the model to account for the measured heat flow. Although it would have been possible to reduce the heat flow residual further (ideally to zero) this was not attempted for the following reason. Figure 4.15 shows that the majority of the heat flow measurement locations with a negative residual do not coincide with known or interpreted high-heat-producing granites. There are large regions in the solid geology map, mostly corresponding to thick sequences of Adelaide Rift Complex, where basement features (such as granites) have not been interpreted (white regions, Figure 4.5). It is possible, therefore, that there is considerably more granite, some of which may be high-heat-producing, that has not been included in the Solid Geology of South Australia map (Cowley (2006), and therefore the model. It is also likely that a number of the higher heat flow measurements located under thick sequences of Adelaide Rift Complex (positive residuals in Figure 4.15), which do not coincide with modelled high-heat-producing granitic bodies, are the result of elevated heat flows due to unidentified buried high-heat-producing bodies.

The improvement in the match between the modelled and measured heat flow between the initial and final runs (Figure 4.15) is primarily due to increasing the heat production value assigned to the east Gawler Craton (4.0 µW/m^3) and to a lessor degree, the Mount Painter and Mount Babbage (5.0 µW/m^3) basement blocks. These elevated values would be considered unrealistic for Proterozoic/Archaean basement which is devoid of high-heat-producing granites when compared to an average upper crustal heat production value of 1.7 µW/m^3 (Rudnick and Gao, 2003). If, however, it is assumed that not all of the potential high-heat-producing granites have been identified in the basement, then these elevated basement heat production values could represent an averaged value of basement and unidentified high-heat-producing granitic bodies.

There are a limited number of heat flow measurements in the west Gawler Craton (one measurement) and the Mount Painter and Mount Babbage regions (two measurements).

Consequently, there are not many measured data points to compare the modelled results against, which restricts the degree of confidence in the heat production values assigned to the basement blocks being representative of the blocks as a whole. However, the larger number of heat flow measurements in the east Gawler Craton and Curnamona Province, the majority of which are located away from high-heat-producing bodies (Figure 4.15), provide a higher degree of confidence that the heat production values assigned to these basement blocks are representative of the basement blocks.

The predicted temperatures at depth, although influenced by low thermal conductivity cover, are more heavily influenced by the heat production values assigned to the basement blocks and the high-heat-producing granite bodies. This is evident in the similarities between the heat flow at the surface (Figure 4.18), and the temperature at 4 km depth slice (Figure 4.19). The main reason for this is the restricted depth extent of the effective insulation in the thermal model. The thermal conductivity assigned to the Adelaide Rift Complex and Arrowie Basin sediments of 3.2 W/mK is of a similar magnitude to that of all of the upper basement units (Table 4.7). As a result, the only insulating components in the assessment area are the younger basins, with the exception of the Warburton Basin which also has a reasonably high thermal conductivity (3.2 W/mK). An image of the depth extent of these basins is revealed in Plate 4.3 and shows that the insulating cover where it is present is generally thin compared to depths targeted by geothermal explorers. The exception is in the Cooper Basin in the northeast of the assessment area where the depths of thermally insulating cover is up to around 2700 m.

The modelled temperatures in the Curnamona Province are all lower than the measured temperatures (positive residuals, Figure 4.16). The two thermal properties which have the most influence on these modelled temperatures are the heat production assigned to the Curnamona Province basement and the thermal conductivity of the Adelaide Rift Complex and Arrowie Basin sequence. Increasing the basement heat production will result in an increase of the modelled temperatures, although this increasing heat production would have a detrimental impact in matching the heat flow measurements in this region. Decreasing the thermal conductivity of the cover would increase the modelled temperatures but would have a detrimental impact in matching the measured down-hole temperatures in the east Gawler Craton region because the Adelaide Rift Complex and Arrowie Basin have been modelled as one continuous and homogeneous unit. Ideally it would be beneficial to divide the unit into two, assigning lower thermal conductivities to the units in the Curnamona region.

During construction of the 3D geological map an attempt has been made to incorporate as much complexity as possible in order to accurately represent the highly complex geology of the region. , However, the complexity built into the model is limited by the nature of the data which has been used to construct the map. The limited basement outcrop has resulted in a heavy reliance on other data such as drill-holes, seismic and magnetic and gravity interpretations. As a result, the 3D geological map is limited by the quality and spatial coverage of these data and their interpretations. Thermal modelling allowed improvements to be made in the match between the measured and modelled down-hole temperature and heat flow data, primarily by dividing the basement into different heat production terrains. As a result, down-hole temperature and heat flow measurements are highly usefull in both validating and improving the results of the thermal modelling. More down-hole temperature and heat flow measurements would allow the complexity of the 3D model to be improved and, therefore, the reliability of the model in predicting temperatures away from temperature and heat flow data also would improve.

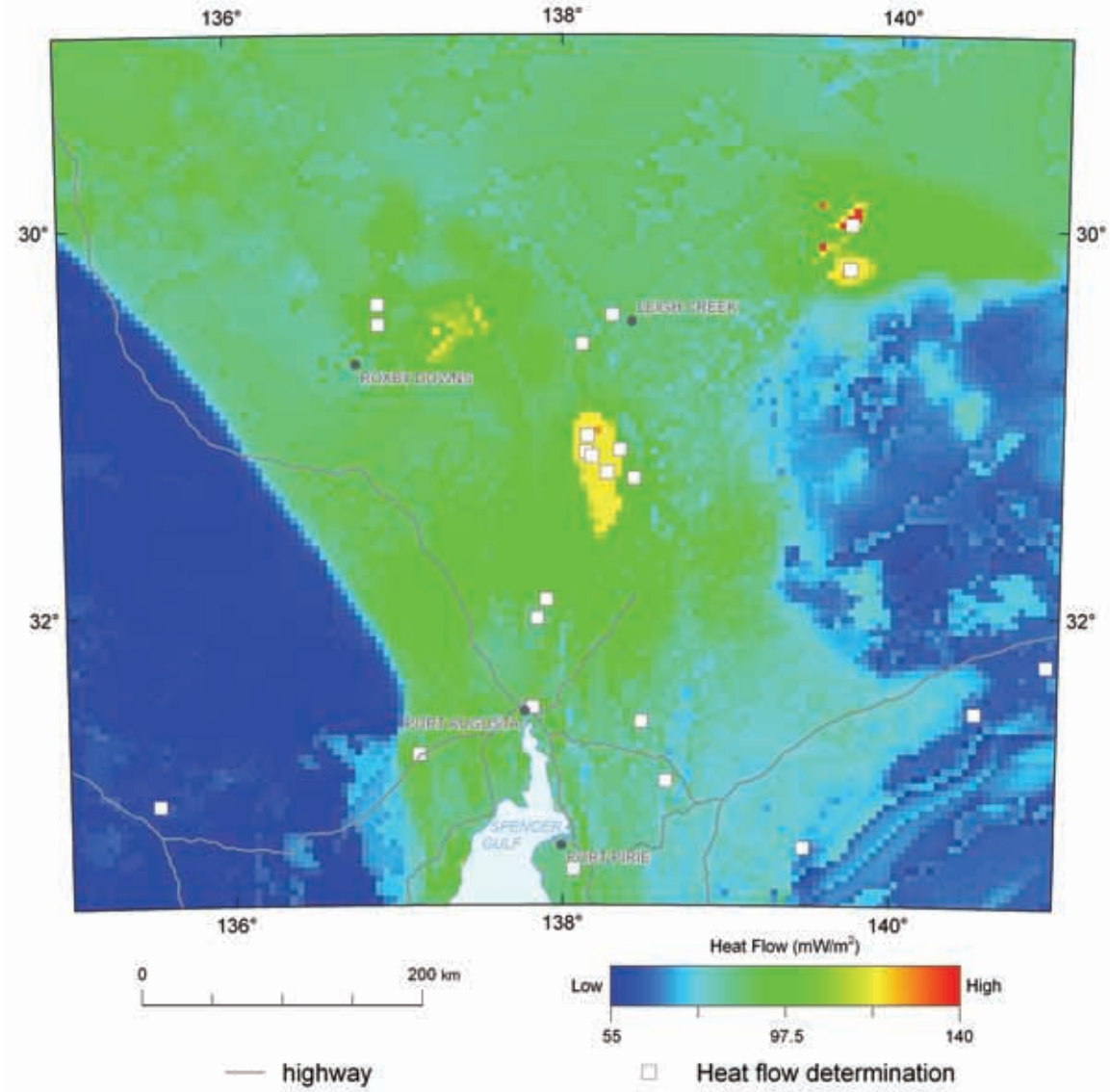

Figure 4.18: *Modelled heat flow at the topographic surface. The locations of the heat flow measurements, which were used to constrain the thermal model, are shown.*

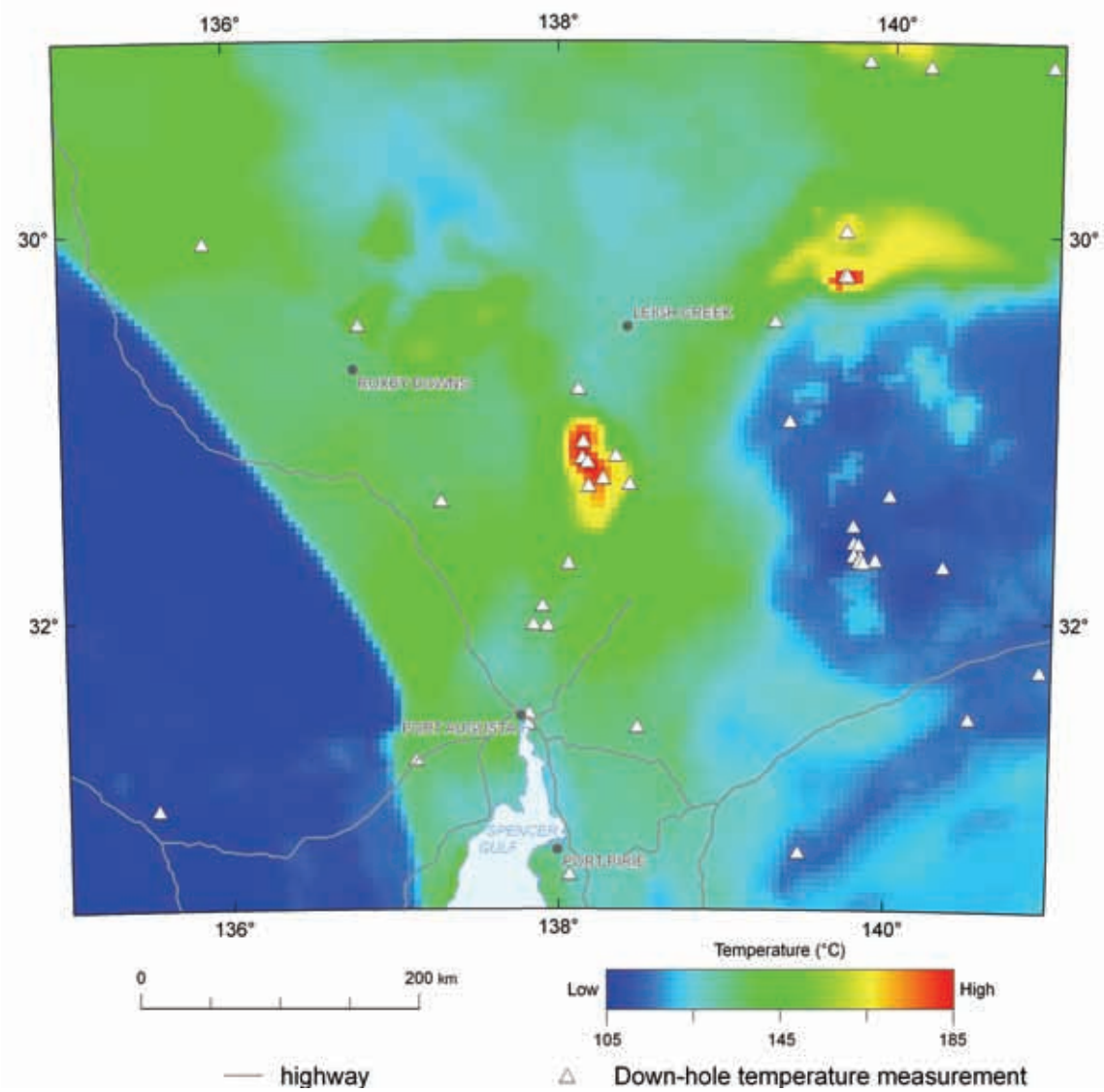

Figure 4.19: *Depth slice at four kilometres showing the calculated temperatures of the thermal model. The locations of the down-hole temperature measurements, which were used to constrain the thermal model, are shown.*

4.9 HOT ROCK GEOTHERMAL PROSPECTIVITY

The predicted temperatures at a 4 km depth slice through the thermal model (Figure 4.19) can be used to identify areas which have a higher hot rock geothermal potential. The 4 km depth slice image shows regions of high temperatures (up to 185°C) which have higher prospectivity, and regions of low temperature (as low as 104°C), which have lower prospectivity. There are three broad regions of differing hot rock prospectivity in the assessment area:

- low prospectivity in the southwest corresponding to the west Gawler Craton;
- moderate to high prospectivity in the centre (east Gawler Craton, the Adelaide Fold Belt, the Mount Painter and Mount Babbage inliers); and
- low to moderate prospectivity in the southeast (Curnamona Province).

The prospectivity of these three broad regions is influenced dominantly by the heat production assigned to the basement blocks:

- 1.7 µW/m^3 – west Gawler Craton;
- 4.0 µW/m^3 – east Gawler Craton; and
- 2.2 µW/m^3 – Curnamona Province.

The Mount Painter and Mount Babbage inliers coincide with high hot rock prospectivity because of the high-heat production assigned to the basement block (5.0 µW/m^3).

Within the central broad region of moderate to high hot rock prospectivity (Figure 4.19) are two smaller regions of lower prospectivity. One region occurs to the west of Marree and the other in the vicinity of Leigh Creek. These regions correspond to thick sequences of Adelaide Rift Complex and Arrowie Basin sediments (Figure 4.8). Thick sedimentary sequences are often associated with higher hot rock prospectivity. However, the thermal conductivity values of the Adelaide Rift Complex and Arrowie Basin sediments are relatively high compared to the other sedimentary basins in the region, and are similar to the basement units (Table 4.7). These older Neoproterozoic to Cambrian sediments are highly lithified and, in some portions of the assessment area, are deformed, which has increased the thermal conductivity and, therefore, are not acting as a thermal blanket. Additionally, the heat production of the Adelaide Rift Complex and Arrowie Basin sediments (2.4 µW/m^3) are lower than the east Gawler Craton basement (4.0 µW/m^3) that they are displacing in the 3D model. The lower heat production results in lower temperatures at depth and, as a result, lower hot rock prospectivity in regions containing thick sequences of the Adelaide Rift Complex and Arrowie Basin sediments.

Localised regions of higher hot rock prospectivity occur across the entire assessment area and correspond to high-heat-producing granite bodies which have intruded into the basement. The location, composition and depth extent of these high-heat-producing bodies are shown in Figure 4.9. The larger the volume of the granite body and the higher the heat production (Table 4.7), the greater the temperature at depth and, consequently, a greater hot rock prospectivity.

The highest temperatures at depth coincide with the Paralana Porphyry (east of Arkaroola, Figure 4.19) and Parachilna high-heat-producing body (northwest of Hawker, Figure 4.19). Both these bodies have been modelled using high-heat productions of 18 µW/m^3 and 14 µW/m^3, respectively, which resulted in the high hot rock prospectivity. Although both of these heat production values are higher than original estimates of 11 µW/m^3 for the Paralana Porphyry (published value; Reid, 2010) and 7.5 µW/m^3 for the Parachilna high-heat-producing body (correlation with Hiltaba Suite east), the modelled temperatures and heat flow values produce a good match with measured temperature values in the vicinity of these bodies (Figures 4.15 and 4.16).

Other regions which have higher hot rock prospectivity as a result of high-heat-producing granites include:

- buried Hiltaba Suite east granites to the northeast of Roxby Downs (7.5 µW/m^3);
- outcropping and shallow buried Moolawatana Suite high-heat-producing bodies to the north and northeast of Arkaroola (40 µW/m^3); and
- buried Moolawatana Suite normal heat-producing granites to the east-northeast of Arkaroola (5.1 µW/m^3).

Although the heat production for the Moolatawana Suite is very high (40 µW/m^3), their volume is relatively small with a limited spatial extent (Figure 4.9) and a modelled depth extent of 2 km. This small volume and lack of insulating sediments (Figure 4.20) has resulted in only a moderate hot rock prospectivity.

The thermal blanketing effect of the cover sediments generally has only a minor impact on the hot rock prospectivity because of the restricted depth extent and spatial distribution of the effective

insulation (Table 4.7; Figure 4.20). The regions which have elevated temperatures at depth because of the affect of insulating sediments are the northern edge of the assessment area where thick sequences of low thermal conductivity Eromanga Basin (2.4 W/mK; up to 1600 m thickness) and Cooper Basin (1.4 W/mK; up to 2760 m at the base) sediments occur and in the centre of the assessment area where there are thicker sequences of the north-south trending Torrens Basin (1.8 W/mK; up to 720 m thickness; Figure 4.20).

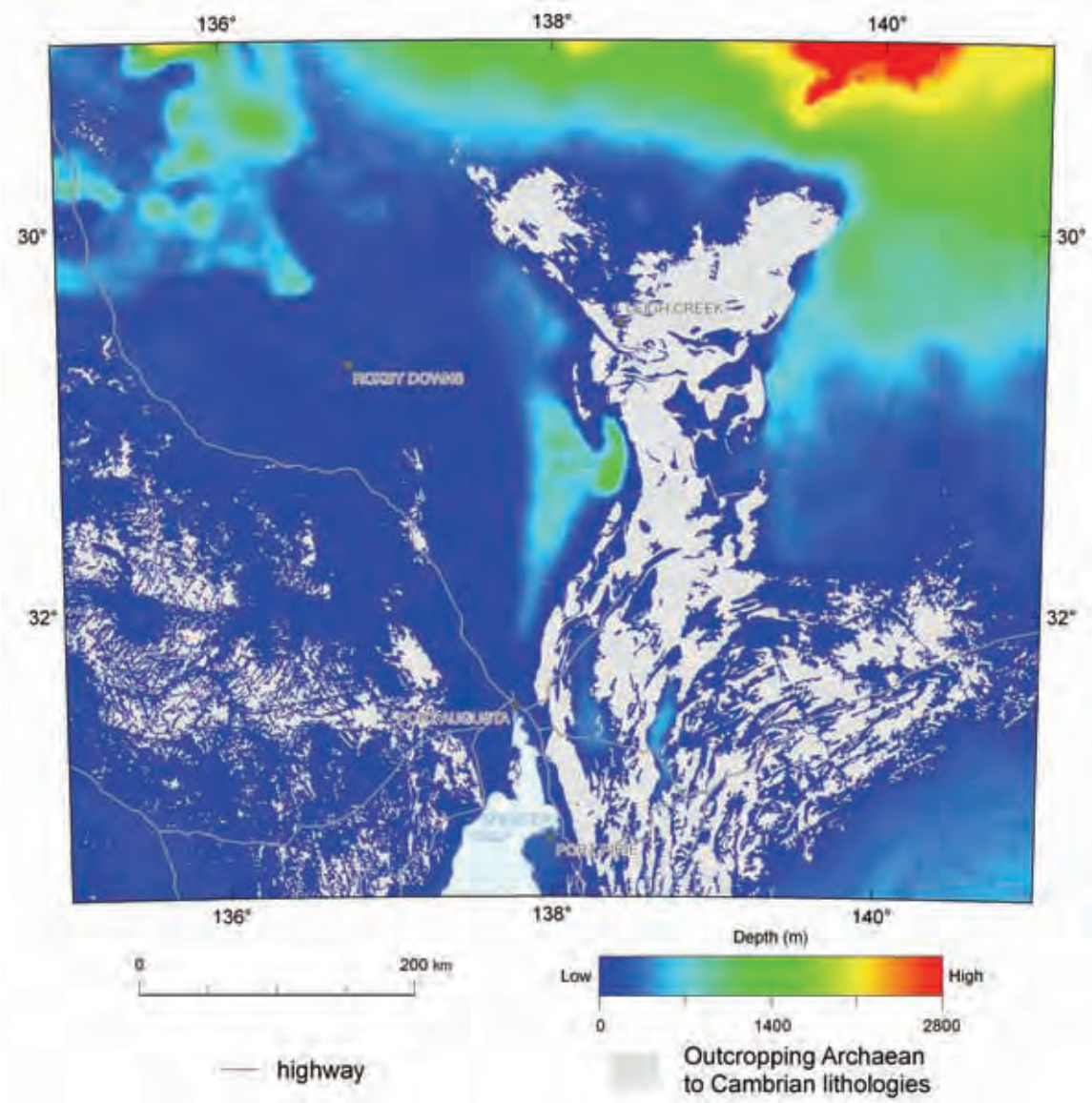

Figure 4.20: *Depth extent of thermally insulating sedimentary basins that have relatively low thermal conductivities (<2.5 W/mK).*

The hot rock prospectivity (Figure 4.19) should be viewed in conjunction with the combined confidence map (Figure 4.14). The construction of these maps is discussed below. The maps show the distribution of reliability of the hot rock prospectivity image based on the quality of the geological and thermal property data used in modelling. A comparison between the results of the thermal modelling and measured heat flow and temperature data (temperature residual – Figure 4.16; heat flow residual – Figure 4.15) can also be used as a measure of reliability of the hot rock prospectivity.

The Woomera Prohibited Area is situated in the northwest of this assessment area (Figure 4.21) and has previously been assessed for hot rock potential (Geoscience Australia, 2010). The hot rock prospectivity determined in this study is, in general, similar to the previous assessment in the Woomera Prohibited Area. The prospectivity for the Woomera Prohibited Area in both assessments ranges from low to moderate. Although the magnitude of the prospectivity is similar, there are differences in the spatial correlation between the assessments. The differences are due to two factors. Firstly, the two assessments considered the thickness of the sediments differently. The previous assessment of the Woomera Prohibited Area (Geoscience Australia, 2010) showed a small region of higher potential because of thick sedimentary cover, as defined by the Proterozoic Seebase surface (de Vries *et al.*, 2006). Most of the sediment thickness in this region is made up of the Pandurra Formation of the Mesoproterozoic Cariewerloo Basin, which is more than 2000 m thick in parts of the overlapping area. The geothermal assessment of Geoscience Australia (2010) was heavily influenced by sediment thickness and assumed that the Pandurra Formation would have thermal conductivity values consistent with typical thermally resistive younger basins. For the current assessment, the thermal conductivity value of the Cariewerloo Basin was estimated to be 3.0 W/mK based on its lithological composition (sandstone dominated with lesser conglomerate, siltstone and shale) and published thermal conductivites of rock types tabulated in Table 4.7. This relatively high thermal conductivity value means that this unit is a relatively poor insulator. This means that the higher thermal conductivities have resulted in a lower prospectivity in this assessment compared to the assessment shown in Geoscience Australia (2010) in regions containing thick sequences of the Cariewerloo Basin. In addition, the prospectivity for the current assessment was influenced by the magnitude of the basement heat production which, in the Woomera Prohibited Area, consisted of two separate basement blocks of differing values. In the previous Woomera Prohibited Area assessment (Geoscience Australia, 2010), the basement was considered as one homogenous heat-producing unit. These two differing inputs, as well as the differing methodology (Geoscience Australia, 2010, GIS approach; this current assessment, 3D thermal model), account for the observed differences.

4.10 HOT SEDIMENTARY AQUIFER GEOTHERMAL PROSPECTIVITY

The pre-requisite for a hot sedimentary aquifer resource is the presence of a suitably permeable aquifer at a sufficiently high temperature for utilisation. There is limited data available on the presence of aquifers in the study area. The available porosity and permeability data is summarised in Table 4.8. Where data is unavailable, general comments about basin lithologies from published sources have been included in the table. The basins which have permeability that may be suitable for hot sedimentary aquifer development are listed in Table 4.8. The Warburton Basin, although listed, is not considered to have hot sedimentary aquifer potential. Although the Pando Formation and Mooracoochie Volcanics have high porosities and the Mooracoochie Volcanics has fracture porosity, it is considered that both units would require additional fracturing to produce adequate permeability.

Figure 4.21 shows the temperatures derived from the thermal modelling at the basal contact of the basins which contain high permeability units. The maximum predicted temperatures at the base of the Murray Basin (41°C), Willochra Basin (37°C) and Walloway Basins (43°C) are too low for these basins to have potential for electricity development. The Eromanga Basin, which has a maximum basal temperature of 85°C in a small region in the northeast of the model, has moderate hot sedimentary aquifer prospectivity. The Cooper Basin, which is situated beneath the Eromanga Basin, has a higher hot sedimentary aquifer prospectivity with maximum temperatures at its base of 128°C (within the study area).

Table 4.8: Summary of basins in study area that have units potentially suitable for hot sedimentary aquifer resources.

BASIN	UNIT	LITHOLOGY	POROSITY	PERMEABILITY	REFERENCE
Eromanga Basin	Murta Formation			21.03mD in some places up to 661mD	PIRSA 2010c
	Namur Sandstone			601mD and in some places up to 4300mD	PIRSA 2010c
	Birkhead Formation			200mD and in some places up to 4950mD	PIRSA 2010c
	Hutton Sandstone			897mD and in some places up to 5130mD	PIRSA 2010c
	Poolowanna Formation		porosity 18%	364mD and in some places up to 1917mD	PIRSA 2010c
	Algebuckina Sandstone		Major artesian aquifer, porosity >20%		PIRSA 2010c
Cooper	Patchawarra Formation		10.5%, up to 25.3%	up to 2500mD	PIRSA 2010b
	Toolachee Formation		12.4% up to 25.3%,	up to 1995mD	PIRSA 2010b
	Tirrawarra Sandstone		11.1%, up to 18.8%	up to 329mD	PIRSA 2010b
Warburton Basin	Pando Formation		5-20%	Needs fractures for permeability	PIRSA 2010b
	Mooracoochie Volcanics	Fractured and weathered tuff and ignimbrite	Up to 17%	Needs fractures for permeability	PIRSA 2010b
Willochra Basin		Confined and unconfined aquifers			ANRA[6]
Walloway Basin		Confined and unconfined aquifers			ANRA
Murray Basin	3 aquifer units Renmark Group, Murray Group, Pliocene Sands Aquifer				MDBA[7]

There are large differences between the hot sedimentary aquifer prospectivity in this study and the hot sedimentary aquifer prospectivity undertaken previously in the Woomera Prohibited Area (Geoscience Australia, 2010). The previous assessment of the Woomera Prohibited Area (Geoscience Australia, 2010) indicates hot sedimentary aquifer prospectivity ranges from low/moderate to moderate/high but in this current assessment the prospectivity is all low. The Eromanga Basin, which is situated in the east of the Woomera Prohibited Area, has high permeability (Table 4.8), a pre-requisite for hot sedimentary aquifer prospectivity. In the previous assessment of the Woomera Prohibited Area (Geoscience Australia, 2010), the main criteria for a hot sedimentary aquifer was the presence of an aquifer, but that assessment did not take into account the

[6] Australian National Resources Atlas www.anra.gov.au
[7] Murray-Darling Basin Authority. www.mdba.gov.au

depth or thickness of the aquifer. This identification of an aquifer was then combined with the Woomera Prohibited Area hot rock assessment to obtain the overall hot sedimentary aquifer assessment. As a result, the presence of the permeable Eromanga Basin was assessed to have moderate to high hot sedimentary aquifer prospectivity. For this assessment, the prospectivity was based on the predicted temperature at the base of the basin, which contains the permeable sediments. As the Eromanga Basin is thin (less than 260 m) in the Woomera Prohibited Area (Figure 4.21) the temperatures are low (below 42°C) and, as a result, the hot sedimentary aquifer prospectivity is also low.

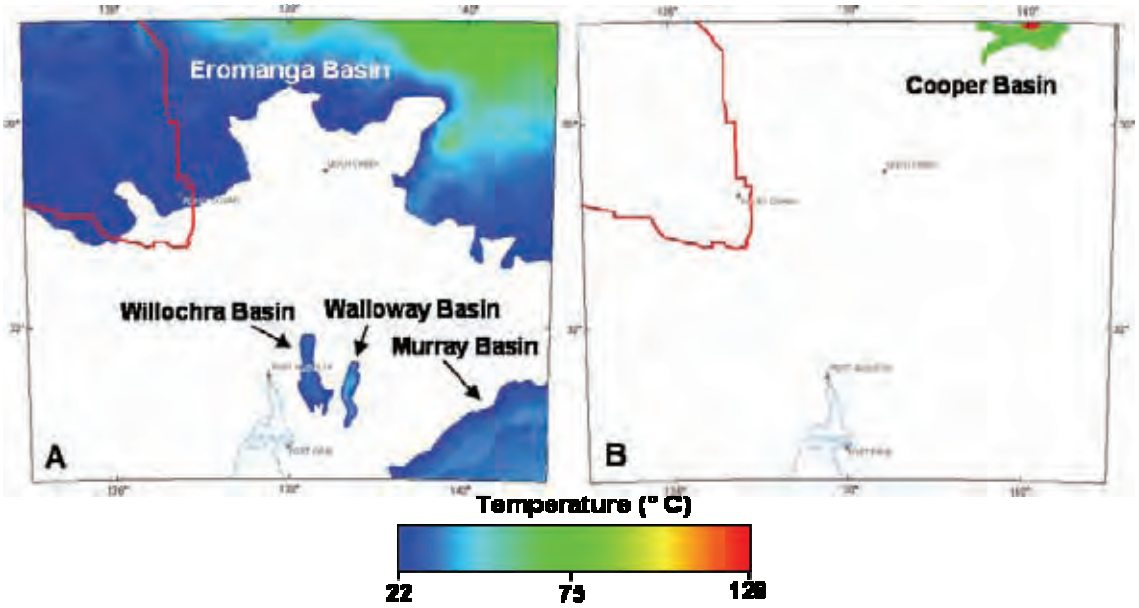

Figure 4.21: *Temperatures derived from the thermal model at the basal contact of the Murray, Willochra, Walloway and Eromanga Basins (A) and at the base of the Cooper Basin (B), which is situated beneath the Eromanga Basin. The location of the Woomera Prohibited Area is shown in red.*

5 Summary and conclusions

Assessments of the uranium and geothermal energy potential of east-central South Australia have been undertaken using a GIS-based geological systems approach. For uranium, sandstone-hosted (including both roll-front and paleochannel varieties), iron oxide-copper-gold-uranium, unconformity-related and sediment-hosted copper-uranium mineral systems were considered. For geothermal energy, both hot rock and hot sedimentary aquifer systems were considered.

5.1 METHODOLOGY — URANIUM

The mineral potential assessment methodology developed for the uranium systems analysis is knowledge-driven and develops mappable geological criteria from a mineral systems model. The mineral systems approach includes four key components:

- sources of metals and fluids;
- drivers of fluid flow;
- fluid pathways and architecture; and
- deposition sites.

Criteria weightings were assigned subjectively and are a product of the importance, applicability and confidence of the given criterion. The final assessment combined each of the mappable criteria under its relevant uranium systems components, which was then normalised to the number of inputs to avoid over-representation of any of the mineral system components. The final map was produced by adding together the individual component weightings.

5.2 SANDSTONE-HOSTED URANIUM

Prospectivity analysis for sandstone-hosted uranium deposits was carried out for both the paleochannel and roll-front sub-types. The analysis used the distribution and rock types within Mesozoic and Cenozoic basins, aquifer hydrogeochemistry and other features to assess prospectivity. Both analyses identified the highest prospectivity to be located to the east and northeast of the Mount Painter area. The area corresponds with an area of known mineralisation including the Beverley and Beverley North mines and the Four Mile and Honeymoon deposits. For the paleochannel sub-type, higher prospectivity is associated with paleochannels developed as part of the Lake Eyre Basin. For the roll-front sub-type, areas of higher prospectivity are associated with sandstone aquifers within the Eromanga Basin. Other areas identified in the analysis as having high to very high prospectivity include two areas in the far southwestern part of the study area (paleochannel sub-type) and an area to the north of Roxby Downs (roll-front sub-type).

5.3 IRON OXIDE-COPPER-GOLD-URANIUM

The prospectivity of the study area was assessed for iron oxide-copper-gold deposits, particularly for uranium-rich systems. The analysis highlighted areas of known deposits in the Olympic Dam and Prominent Hill districts in addition to areas which lack known deposits. The area surrounding the Carrapateena deposit was highlighted only at a moderate level, possibly because widely spaced gravity data did not allow resolution of zones of magnetite and hematite using geophysical inversion techniques. In addition to the two known districts, the analysis identified an area to the north and west of Spencer Gulf as having higher prospectivity. Although hematitic alteration assemblages have been reported in this area, no significant iron oxide-copper-gold deposits have been recognised. The

modelling also has identified as having prospectivity areas in the northern Curnamona Province which are under extensive and deep cover.

5.4 UNCONFORMITY-RELATED URANIUM

The prospectivity of the study area for unconformity-related uranium deposits has been carried out for two time periods, the Precambrian and the Phanerozoic. The Precambrian Eon accounts for the main period of unconformity-related mineralisation, while the Phanerozoic Eon has been assessed for the potential for unconformity- related mineralisation in younger successions. The assessment for the Precambrian Eon centres on the southern end and eastern margin of the Cariewerloo Basin. This is because of the presence of favourable aquifers such as the Cariewerloo Basin and the Corunna Conglomerate, as well as potential uranium-rich source rocks and carbonaceous units of the Hutchison Group. Another region in the southwest corner of the aessment area has high prospectivity because of the presence of possible uranium-rich source rocks, favourable structures and the Corunna Conglomerate. The assessment for the Phanerozoic Eon highlights the Mount Painter and Mount Babbage Inliers and the surrounding Callabona Sub-basin. The Callabona Sub-basin contains several unconformities between overlapping parts of the Arrowie, Eromanga and Lake Eyre basins. There is another area of moderate to high potential around Olympic Dam that has the potential for remobilisation of uranium in the Phanerozoic Eon, which could lead to unconformity-related uranium deposits in this region.

5.5 MAGMATIC-RELATED URANIUM

The assessment for magmatic-related uranium systems was subdivided into intrusive-related and volcanic-related sub-systems. The mineral systems model employed for each of the sub-systems is largely similar, although some important differences exist. Analysis for intrusive-related systems highlighted a number of regions in both the Curnamona Province and the Gawler Craton. In the Curnamona Province, the area in the vicinity of Crocker Well and the Basso Suite southeast of Crocker Well show potential. The Mount Painter Inlier in the northern Curnamona Province also shows high potential. In the Gawler Craton, potential is dominated by Hiltaba Suite granites, with the highest favourability occurring in the southwest and northwest of the study area as well as the region around Olympic Dam. In many cases, the same regions identified as having potential for intrusive-related systems also exhibit favourability for volcanic-related uranium. As a result, volcanics in the Mount Painter Inlier and in the Olary Domain of the Curnamona Province are highlighted, as along with the central Benagerie Ridge Volcanics. In the Gawler Craton, felsic components of the lower Gawler Range Volcanics are highlighted, with the greatest potential indicated in the western, southwestern and southeastern margins of the unit.

5.6 STRATABOUND COPPER-URANIUM IN THE ADELAIDE RIFT COMPLEX AND STUART SHELF

Neoproterozoic successions in the Adelaide Rift Complex and on the Stuart Shelf have been significant historical producers of copper, with some of these deposits containing significant, though sub-ore-grade concentrations of uranium. Given this observation and the fact that many sediment-hosted copper deposits around the world (e.g., Kupferschiefer in Poland and the Zambian Copper Belt) have associated uranium-bearing zones, Neoproterozoic rocks in the study area were assessed for copper-uranium prospectivity using a sediment-hosted mineral system model developed for the Adelaide Rift Complex. This analysis identified areas with known deposits, as well as areas without significant known deposits. The areas without significant known deposits included several to the south of Leigh Creek, three associated with diapirs to the northeast of Hawker, several others east of

Port Pirie and an area near the northern tip of the Stuart Shelf. These areas were highlighted because of the presence of coincident stratigraphic (fluid source, fluid pathway and depositional site) and structural (fluid pathway) features identified as important controls on mineralisation in the mineral system model.

5.7 METHODOLOGY — GEOTHERMAL

Hot rock and hot sedimentary aquifer geothermal prospectivity was mapped based on the results of 3D thermal modelling which was conducted from a 3D geological map. The 3D map was constructed from geological and geophysical data in the assessment area, including outcrop geology maps, solid geology interpretation maps, drill-hole data, seismic interpretations and depth to magnetic source modelling. The 3D map, which was constructed to 15 km depth, delineates the known and interpreted basement high-heat-producing granite suites as well as the thermally insulating cover sequences. The map also delineates the permeable units in the cover sequence. Thermal conductivity and heat production values were assigned to each unit of the 3D map and were sourced from measured datasets, or calculated from datasets such as geochemical data. Thermal forward models were computed and the modelled heat flow and temperature results compared to measured surface heat flow values and down-hole temperatures. Some heat production values of basement units and thermal conductivities of cover sequences were modified to minimise the difference between the modelled and measured data.

Confidence maps have been generated which provide an indication of the reliability of the 3D geological map and thermal modelling. The 3D geological confidence map incorporates the distribution of data uncertainty used to construct the 3D geological map, while the combined confidence map also incorporates the uncertainty in the thermal property data. These confidence maps highlight regions of higher and lower confidence in the prospectivity maps.

5.8 HOT ROCK GEOTHERMAL

Hot rock geothermal prospectivity was determined from a temperature at 4 km depth slice through the optimal thermal model. The estimated temperature at this depth ranges from 104° to 185°C. This modelling identified three broad regions with different prospectivity. Low prospectivity was determined in the southwest part of the study area, corresponding to the western part of the Gawler Craton. Moderate to high prospectivity was indicated in the centre (east Gawler Craton, the Adelaide Fold Belt, the Mount Painter and Mount Babbage Inliers) of the study area and low to moderate prospectivity was indicated in the southeast (Curnamona Province). The prospectivity of these three broad regions is influenced mainly by the heat production value assigned to the basement blocks. Localised regions of higher prospectivity occur across the entire assessment area and correspond to high-heat-producing granite bodies which have intruded into the basement. The thermal blanketing effect of the cover sediments generally has only a minor impact on the hot rock prospectivity. This is because of the restricted depth extent and spatial distribution of the effective insulation.

5.9 HOT SEDIMENTARY AQUIFER GEOTHERMAL

Hot sedimentary aquifer prospectivity was modelled as generally low. The sedimentary basins which have sufficient permeability are mostly at shallow depths and the estimated temperatures at the base of these basins (less than 45°C) equates to low prospectivity. The exception is a small region in the northeast of the assessment area where thick sequences of Cooper Basin sediments have estimated maximum temperatures of 128°C.

6 Acknowledgements

This contribution has benefited from the efforts of many during its production. Discussions with Cam McCuaig, Arianne Ford and Alok Porwal from the Centre for Exploration Targeting at the University of Western Australia were critical in refining the GIS methodology. Subhash Jaireth, Aden McKay and Yanis Miezitis also provided feedback about the methodology. The contribution was improved significantly from a full review by Arianne Ford and by reviews of sections by geologists from the Department of Primary Industry and Resources, South Australia (PIRSA), including Tim Baker, Betina Bendall, Wayne Cowley, Claire Fricke, Bernd Michaelsen and Tania Wilson. Leesa Carson, James Johnson, Narelle Neumann, Bill McKay, Daniel Rawson and Alan Reid assisted at various stages of production, while Lindsay Highet and Andrew Retter provided significant help in the cartographic design. Alan Reid provided final copy editing.

7 References

Ahmad, M. and Wygralak, A. S., 1990. Murphy Inlier and environs — regional geology and mineralisation. *Australasian Institute of Mining and Metallurgy Monograph,* **14**, 819-826.

Alley, N. F., and Benbow, M. C., 1995. Torrens Basin. In: Drexel, J. F. and Preiss, W. V. (eds), The geology of South Australia. Volume 2, The Phanerozoic. *Geological Survey of South Australia Bulletin,* **54(2)**, 187-188.

Alley, N. F., and Lindsay, J. M., 1995a. Willochra Basin. In: Drexel, J. F. and Preiss, W. V. (eds), The geology of South Australia. Volume 2, The Phanerozoic. *Geological Survey of South Australia Bulletin,* **54(2)**, 198.

Alley, N. F., and Lindsay, J. M., 1995b. Walloway Basin. In: Drexel, J. F. and Preiss, W. V. (eds), The geology of South Australia. Volume 2, The Phanerozoic. *Geological Survey of South Australia Bulletin,* **54(2)**, 198.

Ambrose, G. J., Flint, R. B. and Webb, A. W., 1981. Precambrian and Palaeozoic geology of the Peake and Denison Ranges. *Geological Survey of South Australia Bulletin,* **50**. 71pp.

Ashley, P. M., 1984. Sodic granitoids and felsic gneisses associated with uranium-thorium mineralisation, Crockers Well, South Australia. *Mineralium Deposita,* **19**, 7-18.

Ashley, P. M., 2000. Review of the geology and metallogenesis of the Olary Domain, South Australia. *AGSO Record,* **2000/10**, 4-7.

Ashley, P. M. and Plimer, I. R. 1998. Proterozoic Olary Domain, South Australia: Regional and local scale alteration and mineralisation. *Geological Society of Australia Abstracts,* **49**, 14.

Ashley, P. M., Lawie, D. C., Conor, C. H. H. and Plimer, I. R. 1997. Geology of the Olary Domain, Curnamona Province, South Australia, and Field Guide to 1997 Excursion Stops. *Geological Survey of South Australia Report Book,* **97/17**.

Ashley, P. M., Conor, C. H. H. and Skirrow, R. G. 1998. Geology of the Olary Domain, Curnamona Province, South Australia. Field guidebook to Broken Hill Exploration Initiative excursion, 13-15 October, 1998. *Primary Industries and Resources South Australia Report Book,* **99/12**, 53 pp.

Ayling B. and Lewis, B., 2010. Geothermal systems. In: Huston, D.L. (ed), An assessment of the uranium and geothermal potential of north Queensland. *Geoscience Australia Record*, **2010/14**, 68-91.

Bailey, J. C., Gwodz, R., Rose-Hansen, J. and Sørensen, H., 2001. Geochemical overview of the Ilímaussaq alkaline complex, South Greenland. *Geology of Greenland Survey Bulletin,* **190**, 35-53.

Barnett, S. R., 1989. The hydrogeology of the Murray Basin in South Australia. Unpublished M.Sc. thesis, Flinders University South Australia.

Barnicoat, A., 2009. The mineral systems approach of the pmd*CRC. *Geoscience Australia Record,* **2008/09**, 1-6.

Barovich, K. M. and Foden, J., 2002. Nd isotope constraints on the origin of 1580 Ma Curnamona Province granitoid magmatism. *Geological Society of Australia Abstracts,* **67**, 156.

Bastrakov, E., Jaireth, S. and Mernagh, T. P., 2010. Solubility of uranium in hydrothermal fluids at 25° to 300°C: Implication for the formation of uranium deposits. *Geoscience Australia Record,* **2010/29**, 91pp.

Bastrakov, E. N., Skirrow, R. G. and Davidson, G. J. 2007. Fluids in sub-economic Fe-oxide Cu-Au systems of the Olympic Cu-Au-(U) province. *Economic Geology,* **102**, 1415-1440.

Beach, R., 1985, Sedimentary heart flow in the $\Delta Q = 0$ region of Alberta, Unpublished M. Sc. Thesis, University of Alberta, Edmonton, Alberta.

Beach, R. D. W., Jones, F. W. and Majorwicz, J. A., 1987. Heat flow and heat generation estimates for the Churchill Basement of the Western Canadian Basin in Alberta, Canada. *Geothermics*, **16,** 1-16.

Beardsmore, G., 1996, Thermal history of the Browse Basin and its implications for petroleum exploration. Unpublished PhD thesis, Monash University.

Beardsmore, G., 2004. The influence of basement on surface heat flow in the Cooper Basin, *Exploration Geophysics*, **35**, 223-225.

Belperio, A., Flint, R. and Freeman, H. 2007. Prominent Hill: A hematite-dominated, iron oxide copper-gold system. *Economic Geology*, **102**, 1499-1510.

Benbow, M. C., Lindsay, J. M. and Alley, N. F., 1995. Eucla Basin and Paleodrainage. In: Drexel, J. F. and Preiss, W. V. (eds), The geology of South Australia. Volume 2, The Phanerozoic. *Geological Survey of South Australia Bulletin,* **54(2)**, 178-186.

Berning, J., Cooke, R., Hiemstra, S. A. and Hoffman, U., 1976. The Rössing uranium deposit, South West Africa. *Economic Geology,* **71**, 351-368.

Bierlein, F.P., Ashley, P.M. and Seccombe, P.K. 1996. Origin of hydrothermal Cu-Zn-Pb mineralisation in the Olary Block, South Australia: evidence from fluid inclusions and sulfur isotopes. *Precambrian Research,* **79**, 281-305.

Birch, A. F., Roy, R. F. and Decker, E. R., 1968. Heat flow and thermal history in New England and New York. In: E. Zen, White, W. S., Hadley, J. B. and Thompson, J. B. (eds), *Studies of Appalachian Geology: Northern and Maritime,* Interscience, New York (1968), 437-451.

Blissett, A. H., Creaser, S. J., Daly, S.J., Flint, R.B., and Parker, A.J., 1993. Mesoproterozoic. In: Drexel, J. F., Preiss, W. V. and Parker, A.J. (eds), The Geology of South Australia. Volume 1, The Precambrian. *Geological Survey of South Australia Bulletin,* **54(1)**, 107-127.

Bonham-Carter, G. F., 1994. Geographic information systems for geoscientists: modelling with GIS. Pergamum Press, New York, 398p.

Brampton, K F., 2003. Copper mining and treatment in South Australia. *MESA Journal,* **28**, 38-44.

Brugger, J., Ogierman, J., Pring, A., Waldron, H. and Kolitsch, U., 2006. Origin of the secondary REE-minerals at the the Paratoo copper deposit near Yunta, South Australia. *Mineralogical Magazine,* **70**, 609-627.

Budd, A. R., 2006. The Tarcoola goldfield of the Central Gawler Gold Province, and the Hiltaba Association granites, Gawler Craton, South Australia. Unpublished PhD, Australian National University.

Budd, A. R. and Fraser, G. L. 2004. Geological relationships and Ar/Ar constraints on gold mineralisation at Tarcoola, central Gawler gold province, South Australia. *Australian Journal of Earth Sciences,* **51**, 685-699.

Budd, A. R., Skirrow, R. G., 2007. The nature and origin of gold deposits of the Tarcoola goldfield and implications for the Central Gawler Gold Province, South Australia. *Economic Geology*, **102**, 1541-1563.

Budd, A. R., Wyborn, L. A. I. and Bastrakova, I. V. 2001. The metallogenic potential of Australian Proterozoic granites. *Geoscience Australia Record,* **2001/12**, 152pp.

Callen, R. A., Alley, N. F. and Greenwood, D. R., 1995. Lake Eyre Basin. In: Drexel, J. F. and Preiss, W. V. (eds), The geology of South Australia. Volume 2, The Phanerozoic. *Geological Survey of South Australia Bulletin,* **54(2)**, 188-194.

Campana, B. and King, D., 1958. Regional geology and mineral resources of the Olary Province. *Geological Survey of South Australia Bulletin*, **34**, 133pp**.**

Campbell, I. H., Compston, D. M., Richards, J. P., Johnson, J. P. and Kent, A. J. R. 1998. Review of the application of isotopic studies to the genesis of Cu-Au mineralisation at Olympic Dam and Au mineralisation at Porgera, the Tennant Creek district and Yilgarn Craton. *Australian Journal of Earth Sciences,* **45**, 201-218.

Candela, P. A., 1997. A review of shallow, ore-related granites: textures, volatiles and ore metals. *Journal of Petrology*, **38**, 1619-1633.

Carter, J. D., 1982. Mortimer Hills pegmatite uranium prospect: a Rossing-style uranium deposit in the Gascoyne Province. *Geological Survey of Western Australia Professional Paper*, **12**, 27-31.

Carter, L. S., Kelly, S. A., Blackwell, D. D. and Naeser, N. D., 1998, Heat flow and thermal history of the Anadarko Basin, Oklahoma, *American Association of Petroleum Geologists Bulletin*, **82,** 291-316.

Cermak, V., Huckenholz, H. G., Rybach, L., Schmid, R., Schopper, J. R., Schuch, M., Stoffler, D. and Wohlenberg, J., 1982. Thermal conductivity and specific heat of minerals and rocks. In: Angenheister, G. (ed), Physical Properties of Rocks, Springer-Verlag Berlin, New York, 30-370.

Chabiron, A., Alyoshin, A. P., Cuney, M., Deloule, E., Golubev, V. N., Velitchkin, V. I. and Poty, B., 2001. Geochemistry of the rhyolitic magmas from the Streltsovka caldera (Transbaikalia, Russia): a melt inclusion study. *Chemical Geology*, **175,** 273-290.

Chabiron, A., Cuney, M. and Poty, B., 2003. Possible uranium sources for the largest uranium district associated with volcanism: the Streltsovka caldera (Transbaikalia, Russia). *Mineralium Deposita*, **38**, 127-140.

Chambefort, I., McPhie, J., Kamenetsky, V., Ehrig, K. and Green, N., 2009. Diverse mafic facies in the Olympic Dam Cu-Au-U deposit, South Australia. In: Williams, P.J. *et al*. (eds), Smart Science for Exploration and Mining, *Society for Geology Applied to Ore Deposits* Conference, Townsville, 614-616.

Champion, D. C. and Heinemann, M. A., 1994. Igneous rocks of northern Queensland: 1:500 000 map and explanatory notes. *Australian Geological Survey Organisation Record*, **1994/11**, 82pp.

Chapman, D. S. and Furlong, K.P., 1977. Continental heat flow-age relationships. EOS, 58, 1240.

Chernyshev, I. V. and Golubev, V. N., 1996. The Strel'tsovkoe deposit, eastern Transbaikalia: isotope dating of mineralisation in Russia's largest uranium deposit (in Russian). *Geokhimiya*, **10**, 924-937.

Chopra, P. N. and Holgate, F., 2005. A GIS analysis of temperature in the Australian crust, *Proceedings of the World Geothermal Congress*, Anatalya, Turkey, 1-7.

Clark, C., Schmidt Mumm, A., and Faure, K., 2005. Timing and nature of fluid flow and alteration during Mesoproterozoic shear zone formation, Olary Domain, South Australia. *Journal of Metamorphic Petrology*, **23**, 147-164.

Clark, G.L., Guiraud, M., Powell, R. and Burg, J. P. 1987. Metamorphism in the Olary Block, South Australia: compression with cooling in a Proterozoic fold belt. *Journal of Metamorphic Geology* **5**, 291-306.

Coats, R. P., 1964. The geology and mineralisation of the Blinman Dome Diapir. *Geological Survey of South Australia Report of Investigations*, **26**, 52pp.

Coats, R. P., 1973. COPLEY, South Australia, sheet SH54-9. South Australia Geological Survey 1:250 000 Series Explanatory Notes.

Coats, R. P. and Preiss, W. V. 1987, Stratigraphy of the Umbertana Group. In: Preiss, W. V. (ed), The Adelaide Geosyncline — later Proterozoic stratigraphy, sedimentation, palaeontology and tectonics. *Geological Survey of South Australia Bulletin*, **53**, 125-209.

Conor, C. H. H. and Preiss, W. V. 2008. Understanding the 1720-1640 Ma Paleoproterozoic Willyama Supergroup, Curnamona Province: implications for tectonics, basin evolution and ore genesis. *Precambrian Research*, **166**, 297-317.

Conor, C. H. H., 2006. Lithostratigraphy of the Olary and Mulyungarie domains – 2006. *Geoscience Australia Record*, **2006/21**, 26-33.

Conor, C.H.H. 1995. Moonta-Wallaroo region: An interpretation of the geology of the Maitland and Wallaroo 1:100 000 sheet areas. Adelaide, *South Australia Department of Primary Industries and Resources*, 537 pp.

Conor, C. H. H., 2003. The Paleo-Mesoproterozoic geology of northern Yorke Peninsula, South Australia: Hiltaba Suite-related alteration and mineralisation of the Moonta-Wallaroo Cu-Au district. Resources '96 Geological Field Guidebook, *South Australia Department of Primary Industries and Resources Report Book*, **2002/007**.

Conor, C. H. H., 2006. Lithostratigraphy-related mineralisation of the Olary and Mulyungarie domains. In: Korsch, R.J. and Barnes, R.G. (compilers), Broken Hill Exploration Initiative, Absracts for the September 2006 Conference, *Geoscience Australia Record*, **2006/21**, 22-25.

Conor, C. H. H., Raymond, O., Baker, T., Teale, G., Say, P. and Lowe, G., 2010. Alteration and mineralisation in the Moonta-Wallaroo copper-gold mining field region, Olympic Domain, South Australia. In: Porter, T.M., (ed.), Hydrothermal Iron Oxide Copper-Gold & Related Deposits: A Global Perspective, Volume 3, Advances in the Understanding of IOCG Deposits. *PGC Publishing*, Adelaide, in press.

Cook, N. D. J. and Ashley, P. M., 1992. Meta-evaporite sequence, exhalative chemical sediments and associated rocks in the Proterozoic Willyama Supergroup, South Australia: implications for metallogenesis. *Precambrian Research*, **5**6, 211-226.

Cowley, W. M., 1993. Cariewerloo Basin, Pandurra Formation. In: Drexel, J. F., Preiss, W. V. and Parker, A.J. (eds), The Geology of South Australia. Volume 1, The Precambrian. *Geological Survey of South Australia Bulletin*, **54(1)**, 139-142.

Cowley, W. M., 1991, The Pandurra Formation. *Geological Survey of South Australia Report Book*, **90/16.**

Cowley, W. M. (compiler), 2006. Solid Geology of South Australia. *Department of Primary Industries and Resources South Australia Mineral Exploration Data Package*, **15** (Version 1.1).

Creaser, R.A., 1995. Neodymium isotopic constraints for the origin of Mesoproterozoic felsic magmatism, Gawler Craton, South Australia. *Canadian Journal of Earth Sciences*, **32**, 460-472.

Cross, A., Jaireth, S. and. Rapp, R., 2011. Kintyre U deposit, Western Australia. *Geoscience Australia Record*, **2011/12**, 21-23.

Cross, K. C., Daly, S. J. and Flint, R. B. 1993. Mineralisation associated with the GRV and Hiltaba Suite granitoids – Olympic Dam deposit. In: Drexel, J.F., Preiss, W.V. and Parker, A.J. (eds), The Geology of South Australia. Volume 1, The Precambrian. *South Australia. Geological Survey Bulletin*, **54**, 132-138.

Cuney, M., 2010. Evolution of uranium fractionation processes through time: driving the secular variation of uranium deposit types.: *Economic Geology*, **105**, 553-569.

Cuney, M. and Kyser, K., 2008. Recent and not-so-recent developments in uranium deposits and implications for exploration. *Mineralogical Association of Canada Shortcourse Series*, **39**, 258pp.

Cuney, M., Brouand, M., Cathelineau, M., Derome, D., Frieberger, R., Hecht, L., Kister, P., Lobaev, V., Lorilleux, G., Peiffert, C. and Bastoul, A.M., 2003. What parameters control the high-grade-large tonnage of the Proterozoic unconformity related uranium deposits? Uranium Geochemistry 2003: Proceedings of Uranium Geochemistry 2003: Nancy, France, 123-126.

Cunningham, C. G., Steven, T. A., Rowley, P. D., Naeser, C. W., Mehnert, H. H., Hedge, C. E. and Ludwig, K. R., 1994. Evolution of volcanic rocks and associated ore deposits in the Marysvale Volcanic Field, Utah. *Economic Geology*, **89**, 2003-2005.

Curtis, J. L., Brunt, D. A. and Binks, P. J., 1990. Tertiary palaeochannel uranium deposits of South Australia. *Australasian Institute of Mining and Metallurgy Monograph*, **14**, 1631-1636.

Cutts, K. A., Hand, M. and Kelsey, D. E., 2011. Evidence for early Mesoproterozoic (ca. 1590 Ma) ultrahigh-temperature metamorphism in southern Australia. *Lithos*, **124**, 1-16.

Daly, S. J. and Fanning, C. M., 1993. Archaean. In: Drexel, J. F., Preiss, W. V. and Parker, A.J. (eds), The Geology of South Australia. Volume 1, The Precambrian. *Geological Survey of South Australia Bulletin* **54(1)**, 33-50.

Daly, S. J., Fanning, C. M. and Fairclough, M. C., 1998. Tectonic evolution and exploration potential of the Gawler Craton, South Australia. *AGSO Journal of Australian Geology & Geophysics*, **17**, 145-168.

Davidson, G. J., Paterson, H. L., Meffre, S. and Berry, R. G., 2007. Characteristics and Origin of the Oak Dam East Breccia-Hosted, Iron Oxide Cu-U-(Au) Deposit: Olympic Dam Region, Gawler Craton, South Australia. *Economic Geology,* **102**, 1471-1498.

Davis, M. G., Chapman, D. S., Van Wagoner, T. M. and Armstrong, P. A., 2007. Thermal conductivity anisotropy of metasedimentary and igneous rocks, *Journal of Geophysical Research*, **112**, B05216.

De Vries, S. T., Fry, N., Pryer, L., 2006. OZ SEEBASE™ Proterozoic Basins Study. Report to Geoscience Australia and consortium partners by FrOG Tech Pty Ltd. Public domain GIS and report, available from www.frogtech.com.au.

Derome, D., Cathelineau, M., Cuney, M., Fabre, C. and Lhomme, T., 2005. Mixing of sodic and calcic brines and uranium deposition at McArthur River, Saskatchewan, Canada. *Economic Geology*, **100**, 1529-1545.

Derome, D., Cathelineau, M., Fabre, C., Boiron, M., Banks, D.A., Lhomme, T. and Cuney, M., 2007. Paleo-fluid composition determined from individual fluid inclusions by Raman and LIBS; application to mid-Proterozoic evaporitic Na-Ca brines (Alligator Rivers uranium field, Northern Territories, Australia). *Chemical Geology*, **237**, 240-255.

Dickinson, S. B., 1953b. The copper deposits of the northern Flinders Ranges. In: Edwards, A. B. (ed), Geology of Australian ore deposits. Melbourne, Australasian Institute of Mining and Metallurgy, 505-516.

Dickinson, S. B., 1953a. The copper deposits of the Mount Lofty Ranges. In: Edwards, A. B. (ed), Geology of Australian ore deposits. Melbourne, Australasian Institute of Mining and Metallurgy, 476-486.

Direen, N. G. and Lyons, P., 2007. Regional crustal setting of iron oxide Cu-Au mineral systems of the Olympic Dam region, South Australia: insights from potential field modelling. *Economic Geology*, **102**, 1397-1414.

Drexel, J. F., 2008. Review of the Burra mine project, 1980-2008 a progress report. *Primary Industry and Resources, South Australia Report Book*, **2008/16**, 76 pp.

Drexel, J. F. and Major, R. B. 1987. Geology of the uraniferous breccias near Mount Painter, South Australia, and revision of rock nomenclature. *Quarterly Geological Notes of the Geological Survey of South Australia*, **104**, 14-24.

Drexel, J. F. and Major, R. B. 1990. Mount Painter uranium – rare earth deposits. *Australian Institute of Mining and Metallurgy Monograph*, **14**, 993-998.

Drexel, J. F. and McCallum, W. S., 1986. Origin and age of the Burra copper orebody. *Geological Survey of South Australia Quarterly Geological Notes*, **98**, 15pp.

Drexel, J. F. and Preiss, W. V. (eds), 1995. The geology of South Australia. Volume 2, the Phanerozoic. *Geological Survey of South Australia Bulletin*, **54(2)**, 347pp.

Drexel, J. F., Preiss, W. V. and Parker, A. J. (eds), 1993. The geology of South Australia. Volume 1, the Precambrian. *Geological Survey of South Australia Bulletin*, **54(1)**, 242pp.

Drown, C. G., 2003. The Barns gold project-discovery in an emerging district. *MESA Journal*, **28**, 4-9.

Dutch, R. A. and Hand, M., 2009. EMPA monazite constraints on the timing of deformation and metamorphism in the southern Kalinjala Mylonite Zone, Gawler Craton. *MESA Journal*, **53**, 41-46.

Dutch, R. A., Hand, M. and Kelsey, D. E., 2010. Unravelling the tectonothermal evolution of reworked Archean granulite-facies metapelites using in-situ geochronology: an example from the Gawler Craton, Australia. *Journal of Metamorphic Geology*, **28**, 293-316.

Dyson, I. A., 2001. The diapir-base metal association in the northern Flinders Ranges. *MESA Journal,* **22**, 37-43.

El Bouseily, A. M. and El Sokkary, A. A., 1975. The relation between Rb, Ba and Sr in granitic rocks. *Chemical Geology,* **16**, 207-219.

Elburg, M. A., Bons, P. D., Foden, J. and Brugger, J., 2003. A newly defined Late Ordovician magmatic-thermal event in the Mount Painter Province, northern Flinders Ranges, South Australia. *Australian Journal of Earth Sciences,* **50**, 611-631.

Fairclough, M. 2005. Geological and metallogenic setting of the Carrapateena FeO–Cu–Au prospect — a PACE success story. *Minerals and Energy South Australia Journal* **38**, 4-7.

Fairclough, M. C., Fabris, A., Hou, B. and Daly, S. J., 2006. Uranium: South Australian state of play. *MESA Journal,* **41**, 8-11.

Fanning, C. M., 1990. Single grain U-Pb zircon dating of two tuffaceous horizons from Wilgena 1. PRISE geochronology report 89-020 (unpublished).

Fanning, C. M., Ashley, P., Cook, N., Teale, G. S. and Conor, C., 1998. A geochronological perspective of crustal evolution in the Curnamona Province. *Australian Geological Survey Organisation Record,* **1998/25**, 30-35.

Fanning, C. M., Flint, R. B. and Preiss, W. V., 1983. Geochronology of the Pandurra Formation. South Australia. *Geological Survey of South Australia Quarterly Geological Notes,* **88**, 11-16.

Fanning, C. M., Ludwig, K R., Forbes, B. G. and Preiss, W.V., 1986. Single and multiple grain U-Pb zircon analyses for the early Adelaidean Rook Tuff, Willouran Ranges, South Australia. *Geological Society of Australia Abstracts,* **15**, 71-72.

Fanning, C. M., Reid, A. J. and Teale, G. S., 2007. A geochronological framework for the Gawler Craton, South Australia. Geological Survey of South Australia Bulletin, 55, 258pp.

Farquhar, J., Wu, N., Canfield, D. E. and Oduro, H., 2010, Connections between sulfur cycle evolution, sulfur isotopes, sediments, and base metal sulfide deposits. *Economic Geology*, **105**, 509-533.

Ferris, G. M. and Schwarz, M. P., 2003. Proterozoic gold province of the central Gawler craton. *MESA Journal*, **30**, 4-12.

Ferris, G. M., Schwarz, M. P. and Heithersay, P., 2002. The geological framework, distribution and controls of Fe-oxide and related alteration, and Cu-Au mineralisation in the Gawler Craton, South Australia. Part I: geological and tectonic framework. In: Porter, T. M. (ed), Hydrothermal Iron Oxide Copper-Gold and Related Deposits: a Global Perspective. PGC Publishing, Adelaide, 9-31.

Fraser, G. L. and Lyons, P., 2006. Timing of Mesoproterozoic tectonic activity in the northern Gawler Craton constrained by $^{40}Ar/^{39}Ar$ geochronology. *Precambrian Research,* **151**, 160-184.

Fraser, G. L. and Neumann, N. L., 2010. New SHRIMP U-Pb zircon ages from the Gawler Craton and Curnamona Province, South Australia, 2008 – 2010. *Geoscience Australia Record,* **2010/16**, 256pp.

Fraser, G. L., Skirrow, R. G., Schmidt-Mumm, A. and Holm, O., 2007. Mesoproterozoic Gold in the Central Gawler Craton, South Australia: Geology, Alteration, Fluids and Timing. *Economic Geology,* **102**, 1511-1539.

Fraser, G. L., McAvaney, S., Neumann, N., Szpunar, M. and Reid, A. J., 2010a. Discovery of early Mesoarchean crust in the eastern Gawler Craton, South Australia. *Precambrian Research,* **179**, 1-21.

Fraser, G. L., Blewett, R. S., Reid, A. J., Korsch, R. J., Dutch, R., Neumann, N. L., Meixner, A. J., Skirrow, R. G., Cowley, W. M., Szpunar, M., Preiss, W. V., Nakamura, A., Fomin, T., Holzschuh, J., Theil, S., Milligan, P. R., and Bendall, B. R., 2010b. Geological interpretation of deep seismic reflection and magnetotelluric line 08GA-G1. Geoscience Australia Record, 2010/10, 81-95.

Freeman, M.J., Shergold, J. H., Morris, D.G. and Walter, M. R., 1990. Later Proterozoic and Palaeozoic basinc of central and northern Australia — regional geology and mineralisation. *Australasian Institute of Mining and Metallurgy Monograph,* **14**, 1125-1134.

Fricke, C., 2008. Definitions of Mesoproterozoic igneous rocks of the Curnamona Province: The Ninnerie Supersuite. *Primary Industry and Resources, South Australia Report Book,* **2008/4**, 86pp.

Fricke, C. E., 2009. 1590 Ma magmatism in the Curnamona Province: Mineral potential of the Ninnerie Supersuite. *Geoscience Australia Record,* **2009/28**, 38-41.

Fricke, C. and Conor, C. H. H., 2010. Building granite plutons in the Olary Domain, South Australia: a ring dyke model. *Primary Industry and Resources, South Australia Report Book,* **2010/11**, 55pp.

Galson, D. A., Wilson, N. P., Scharli, U. and Rybach, L., 1987. A comparison of the divided-bar and QTM methods of measuring thermal conductivity. *Geothermics*, **16,** 215-222.

George-Aniel, B., Leroy, J. L. and Poty, B., 1991. Volcanogenic uranium mineralizations in the Sierra Pena Blanca district, Chihuahua, Mexico: three genetic models. *Economic Geology,* **86**, 233-248.

Geoscience Australia, 2009. Australia's Identified Mineral Resources 2009. Geoscience Australia, Canberra, Australia, 105pp.

Geoscience Australia, 2010. Mineral resource potential assessment of the Woomera Prohibited Area, South Australia. Geoscience Australia report to Department of Resources, Energy and Tourism, 63pp. http://www.ga.gov.au/image_cache/GA18686.pdf

Gibson, G. M. and Nutman, A. P., 2004. Detachment faulting and bimodal magmatism in the Paleoproterozoic Willyama Supergroup, south-central Australia: keys to recognition of a multiply deformed Precambrian metamorphic core complex. *Journal of the Geological Society of London,* **161**, 55-66.

Gibson, H., Seikel, R., and Meixner, T., 2010. Characterising uncertainty when solving for 3D temperature: New tools for the Australian geothermal energy exploration sector. *21st Australian Society of Exploration Geophysicists Conference*, Extended Abstracts.

Gibson, H., Stüwe, K., Seikel, R., FitzGerald, D., Calcagno, P., Argast, S., McInerney, P., and Budd, A., 2008. Forward prediction of spatial temperature variation from 3D geology models. *PESA Eastern Australian Basins Symposium III*. Sydney 14-17 September 2008.

Goleby, B. R., Lyons, P., Drummond, B. J., Schwarz, M., Shearer, A. J., Fairclough, M. C., Korsch, R. J. and. Skirrow, R. G., 2003. General Basement interpretation (18 s DATA). *Geoscience Australia, Record,* **2005/19.** 68-72.

Gow, P. A., Wall, V. J, Oliver. N. H. S., and Valenta, R. K., 1994. Proterozoic iron oxide (Cu-UAu-REE) deposits: Further evidence of hydrothermal origins. *Geology,* **22**, 633-636.

Groves, D. I., Bierlein, F. P., Meinert, L. D. and Hitzman, M. W., 2010. Iron oxide copper-gold (IOCG) deposits through Earth history: implications for origin, lithospheric setting, and distinction from other epigenetic iron oxide deposits. *Economic Geology,* **105**, 641-654.

Hampton, S., 1997. A study of the paragenesis and controls on Proterozoic (Cu-Fe-Au-REE) mineralisation at the Manxman A1 and Joes Dam South prospects, Mount Woods Inlier, South Australia. Unpublished Honours thesis, Townsville, James Cook University of North Queensland, 146 pp.

Hand, M., Reid, A. and Jagodzinski, E., 2007. Tectonic framework and evolution of the Gawler Craton, Southern Australia. *Economic Geology,* **102**, 1377-1395.

Haynes, D. W., 2000. Iron oxide copper (-gold) deposits: their position in the ore deposit spectrum and modes of origin. In: Porter, T.M. (ed.) Hydrothermal iron oxide copper-gold and related deposits: A global perspective, **1**. *PGC Publishing*, Adelaide, 71-90.

Haynes, D. W., Cross, K. C., Bills, R. T. and Reed, M. H., 1995. Olympic Dam ore genesis: a fluid mixing model. *Economic Geology,* **90**, 281-307.

Haynes, R. W., 1975. Beverley sedimentary uranium orebody, Frome embayment, South Australia. *Australasian Institute of Mining and Metallurgy Monograph*, **5**, 808-813.

Hayward, N. and Skirrow, R. G., 2010. Geodynamic Setting and Controls on Iron Oxide Cu-Au (±U) Ore in the Gawler Craton, South Australia. In: Porter, T.M., (ed.), Hydrothermal Iron Oxide Copper-Gold & Related Deposits: A Global Perspective, Volume **3**. Advances in the Understanding of IOCG Deposits. *PGC Publishing*, Adelaide, in press.

Heinson, G. S., Direen, N. G. and Gill., R. M., 2006. Magnetotelluric evidence for a deep-crustal mineralizing system beneath the Olympic Dam iron oxide copper-gold deposit, southern Australia. *Geology*, **34**, 573-576.

Henson, P., 2010. 3D Map and Supporting Geophysical Studies in the Gawler Craton and Curnamona Province. https://www.ga.gov.au/products/servlet/controller?event=GEOCAT_DETAILS&catno=70612

Hibburt, J. E., 1995. Arckaringa Basin. In: Drexel, J. F. and Preiss, W. V. (eds), The geology of South Australia. Volume 2, The Phanerozoic. *Geological Survey of South Australia Bulletin*, **54(2)**, 73-7.

Hitzman, M. W. and Valenta, R. K., 2005. Uranium in iron oxide-copper-gold (IOCG) systems. *Economic Geology*, **100**, 1657-1661.

Hitzman, M.W., Oreskes, N., and Einaudi, M.T., 1992. Geological characteristics and tectonic setting of Proterozoic iron oxide (Cu-U-Au-LREE) deposits. *Precambrian Research*, **58**, 241–287.

Hitzman, M., Kirkham, R., Broughton, D., Thorson, J. and Selley, D., 2005. The sediment-hosted stratiform copper ore system. *Economic Geology 100th Anniversary Volume*, 609-642.

Hoeve, J., Sibbald, T. I. I., Ramakers, P. and Lewry, J. F., 1980. Athabasca Basin unconformity-type uranium: a special type of sandstone-type deposits?, In Furguson, J. and Goleby, A. B. (eds) Uranium in the Pine Creek Geosyncline.: Vienna International Atomic Energy Agency, p. 575-594.

Houseman, G. A., Cull, J. P. Muir, P. M. and Peterson, H. L., 1989. Geothermal signatures and uranium ore deposits on the Stuart Shelf of South Australia. *Geophysics*, **54**, 158-170.

Howard, K. E, Hand, M., Barovich, K. M., Payne, J. L. and Belousova, E. A., 2011. U-Pb, Lu-Hf and Sm-Nd isotopic constraints on provenance and depositional timing of metasedimentary rocks in the western Gawler Craton: Implications for Proterozoic reconstruction models. *Precambrian Research*, **184**, 43-62.

Howard, L. E. and Sass, J. H., 1964. Terrestrial heat flow in Australia. *Journal of Geophysical Research*, **69**, 1617-26.

Hurtig, E and Schlosser, P., 1979. Vertical changes of heat flow in boreholes in the north German sedimentary basin. *KAPG Geophysical Monograph*, Budapest, Akademiai Kiado, 398-401.

Huston, D. L. (ed), 2010. An assessment of the uranium and geothermal p9otential of north Queensland. *Geoscience Australia Record*, **2010/14**, 108pp.

Huston, D. L., Maas, R. and Czarnota, K., 2007. The age and genesis of the Nifty copper deposit: back to the future. *Geocience Australia Professional Opinion*, **2007/03**. 22pp.

Huston, D. L., Maas, R., Miggins, D., Maidment, D., Czarnota, K., Preiss, W. and Cassidy, K., 2009. Neoproterozoic mineralisation in Australia: timing and geodynamic setting. In: Williams, P. J. *et al*. (eds), Smart science for exploration and mining, Proceedings of the Tenth Biennial SGA Meeting, Townsville, 2009, p. 285-287.

IAEA, 2009. World distribution of uranium deposits (UDEPO) with a uranium deposit classfication. *International Atomic Energy Agency Technical Document*, **1629**, 117pp.

Idnurm, M., 2000. Towards a high resolution late Paleoproterozoic-earliest Mesoproterozoic apparent polar wander path for northern Australia. *Australian Journal of Earth Sciences*, **47**, 405-429.

Jagodzinski, E. J., 2005. Compilation of SHRIMP U-Pb geochronological data, Olympic Domain, Gawler Craton, South Australia, 2001-2003. *Geoscience Australia Record,* **2005/20**, 197 pp.

Jaireth, S., 2009. Uranium deposits of the Lake Frome region. In: Skirrow, R.G. (ed), Uranium ore-forming systems of the Lake Frome region, South Australia: regional controls and exploration criteria. *Geoscience Australia Record,* **2009/40,** 57-66.

Jaireth, S., Mckay, A., Lambert, I. 2008. Association of large sandstone uranium deposits with hydrocarbons. *AusGeoNews,* **89**, 8-12.

Jaupart, C., 1983. Horizontal heat transfer due to radioactivity contrasts: causes and consequences of the linear heat flow relation. *Geophysical Journal of the Royal Astronomical society,* **75**. 411-435.

Johnson, J. P. 1993. The geochronology and radiogenic isotope systematics of the Olympic Dam copper-uranium-gold-silver deposit, South Australia. Unpublished Ph.D. thesis, Australian National University, Canberra, Australia, 252 pp.

Johnson, J. P. and Cross, K. C., 1995. U-Pb geochronological constraints on the genesis of Olympic Dam Cu-Au-U-Ag deposit, South Australia. Economic Geology, **90**, 1046-1063.

Johnson, J.P. and McCulloch, M.T. 1995. Sources of mineralizing fluids for the Olympic Dam deposit, (South Australia): Sm-Nd isotopic constraints. *Chemical Geology* **121**, 177- 199.

Johnston, J. D., 1984. Structural evolution of the Pine Creek Orogen and mineralisation therein, Northern Territory, Australia. Unpublished Ph.D. thesis, Melbourne, Monash University. 335pp.

Johnston, A., 2007. Algebuckina ELs 3226 and 3411, project DPY3-15 final report, Red Metal Ltd., *South Australia Department of Primary Industries and Resources Open File Envelope,* **11376**.

Kappelmeyer, O. and Haenel, R. 1974, Geothermics with special reference to practical application, *Geoexploration Monographs,* **1,** No. 4**.** Borntraeger, Berlin, 238pp.

Kent, A. J .R., Ashley, P. M. and Fanning, C. M., 2000. Metasomatic alteration associated with regional metamorphism: an example from the Willyama Supergroup, South Australia. *Lithos*, **54**, 33-62.

King, D., 1954. Geology of the Crockers Well uranium deposits. *Geological Survey of South Australia Bulletin,* **30**, 70-78.

Kinnaird, J. A. and Nex, P. A. M., 2007. A review of geological controls on uranium mineralisation in sheeted leucogranites within the Damara Orogen, Namibia. *Institute of Mining and Metallurgy Transactions, Section B, Applied Earth Sciences,* **B116**, 68-85.

Knox-Robinson, C. M. and Wyborn, L. A. I., 1997. Towards a holistic exploration strategy: using geographic information systems as a tool to enhance exploration. *Australian Journal of Earth Sciences,* **44**, 453-463.

Knutson, J., Donnelly, T. H. and Tonkin, D. G., 1983. Geochemical constraints on the genesis of copper mineralization in the Mount Gunson area, South Australia. *Economic Geology,* **78**, 250-274.

Korsch, R.K. and Kositcin, N. (eds) 2010a. South Australian seismic and MT workshop 2010. *Geoscience Australia Record,* **2010/10**, 124 pp.

Korsch, R.K. and Kositcin, N. (eds) 2010b. GOMA (Gawler Craton-Officer Basin-Musgrave Province-Amadeus Basin) seismic and MT workshop 2010. *Geoscience Australia Record,* **2010/39**, 162 pp.

Korsch, R. J., Preiss, W. V., Blewett, R. S., Fabris, A. J., Neumann, N. L., Frick, C. E., Fraser, G. L., Hozshuh, J., Milligan, P. R., and Jones, L. E. A., 2010. Geological interpretation of deep seismic reflection and magnetotelluric line 08GA-C1: Curnamona Province, South Australia. *Geoscience Australia Record*, **2010/10,** 42-53.

Kositcin, N., 2010. Geodynamic synthesis of the Gawler Craton and Curnamona Province. *Geoscience Australia Record,* **2010/27**, 113pp.

Krieg, G. W., Alexander, E. M., Rogers, P. A., 1995. Eromanga Basin. In: Drexel, J. F. and Preiss, W. V. (eds), The geology of South Australia. Volume 2, The Phanerozoic. *Geological Survey of South Australia Bulletin*, **54(2)**, 101-130.

Kwitko, G., 1982. The investigation of Tertiary coal in the Walloway Basin, South Australia. *Geological Survey of South Australia Report Book*, **82/26**.

Kyser, T. K., 2007. Fluids, basin analysis, and mineral deposits. *Geofluids*, **7**, 238-257.

Lachenbruch, A.H., 1968. Preliminary geothermal model of the Sierra Nevada. *Journal of Geophysical Research* **73**. 6977-6989.

Lacy, W. C., 1974. A view of upper Palaeozoic metallogeneis in the northern part of the Tasman Orogenic Zone. In: Denmead, A. K., Tweedale, G. W., and Wilson, A. F. (eds), The Tasman Geosyncline — a symposium. Geological Society of Australia, Queensland Division, 221-243.

Lambeck, A., Mernagh, T. P. and Wyborn, L., 2011. Are iron-rich sedimentary rocks the key to the spike in orogenic gold mineralization in the Paleoproterozoic? *Economic Geology*, **106**, 321-330.

Lambert, I. B., Donnelly, T. H. and Rowlands, N. J., 1980. Genesis of upper Proterozoic stratabound copper mineralization, Kapunda, South Australia. *Mineralium Deposita*, **15**, 1-18.

Lambert, I. B., Drexel, J. F., Donnelly, T. H. and Knutson J., 1982. Origin of breccias in the Mount Painter area, South Australia. *Journal of the Geological Society of Australia*, **29**, 115-125.

Lambert, I. B., Knutson, J., Donnelly, T. H. and Etiman, H., 1987. Stuart Shelf-Adelaide Geosyncline copper province, South Australia. *Economic Geology*, **82**, 108-123.

Lambert, I., Jaireth, S., McKay, A. and Meizitis, Y., 2005. Why Australia has so much uranium, *AusGeoNews*, **80**, 7-10.

Laverov, N. P., Velitchkin, V. I. and Shumilin, M. V., 1992. Uranium deposits of the Commonwealth of Independent States: the main economic genetic types and their distribution (in Russian). *Geologiya Rudnykh Mestorozhdenii*, **2**, 3-18.

Lindal, B., 1973. Industrial and other applications of geothermal energy. Geothermal Energy: Review of Research and Development, LC No. 72-97138. Paris, UNESCO. 135-148.

Loiselle, M. C. and Wones, D. R., 1979. Characteristics and origin of anorogenic granites. *Geological Society of America Abstracts with Programs*, **11**, 468.

Lottermoser, B. G. and Ashley, P. M., 1996. Geochemistry and exploration significance of ironstones and barite-rich rocks in the Proterozoic Willyama Supergroup, Olary Block, South Australia. *Journal of Geochemical Exploration*, **57**, 57-73.

Ludwig, K. R. and Cooper, J. A., 1984. Geochronology of Precambrian granites and associated U-Ti-Th mineralization, northern Olary province, South Australia. *Contributions to Mineralogy and Petrology*, **86**, 298-308.

Lyons, P. and Goleby, B.R. (compilers), 2005. The 2003 Gawler Craton seismic survey; notes from the seismic workshop. *Geoscience Australia Record*, **2005/19**, 81pp.

Maas, R., 1989. Nd-Sr isotope constraints on the age and origin of unconformity-type uranium deposits in the Alligator Rivers uranium field, Northern Territory, Australia. *Economic Geology*, **84**, 64-90.

Magoon, L. B. and Dow, W. G. (eds), 1994. The petroleum system – from source to trap. *American Association of Petroleum Geologists Memoir*, **60**, 655pp.

Marsland-Smith, A., 2005. Geological setting and minerology of uranium mineralisation at the Beverley deposit, Frome Basin, SA. *Geological Society of South Australia Abstracts*, **78**, 16-17.

Matthews, C., and Beardsmore, G., 2007. Hew heat flow data from south-eastern South Australia. *Exploration Geophysics* **38**, 260-269.

McConachy, G., Mcinnes, D. and Paine, J., 2006. Airborne electromagnetic signature of the Beverley Uranium deposit, South Australia. Society of Exploration Geophysicists Annual Conference and Exhibition, New Orleans, October, 790-794.

McCuaig, T. C., Beresford, S. and Hronsky, J., 2010. Translating the mineral systems approach into an effective exploration targeting system. *Ore Geology Reviews*, **38**, 128-138.

McDermott, F., Harris, N. B. W. and Hawkesworth, C. J., 1996. Geochemical constraints on crustal anatexis: a case study from the Pan-African Damara granitoids of Namibia. *Contributions to Mineralogy and Petrology*, **123**, 406-423.

McKay A., 2008, Uranium. Australia's Identified Mineral Resources 2008. Geoscience Australia, Canberra, 70-77.

McKay, A. D. and Miezitis, Y., 2001. Australia's uranium resources, geology and development of deposits. *AGSO-Geoscience Australia Mineral Resource Report*, **1**, 184pp.

McLaren, S., Sandiford, M., Hand, M., Neumann, N., Wyborn, L., and Bastrakova, I., 2003. Chapter 12-The hot southern continent: heat flow and heat production in Australian Proterozoic terranes. *Geological Society of Australia Special Publication*, **22**, 151-161.

McLaren, S., Sandiford, M., Powell, R., Neumann, N. and Woodhead, J. 2006. Paleozoic intraplate crustal anatexis in the Mount Painter Province, South Australia: Timing, thermal budgets and the role of crustal heat production. *Journal of Petrology*, doi: 10.1093/petrology/eg1044.

McPhie, J., Kamenetsky, V., Chambefort, I., Ehrig, K. and Green, N., 2010. The origin of Olympic Dam: A revolutionary new view. In: Cook *et al*. (Eds), Giant Ore Deposits Downunder, *17th Quadrennial IAGOD Symposium*, Adelaide, Symposium Proceedings, 76-77.

McPhie, J., Kamenetsky, V., Chambefort, I., Ehrig, K. and Green, N., 2011. Origin of the supergiant Olympic Dam Cu-U-Au-Ag deposit, South Australia: Was a sedimentary basin involved? *Geology* **39**, 795-798.

Meffre, S., Ehrig, K., Kamenetsky, V., Chambefort, I., Maas, R. and McPhie, J., 2010. Pb isotopes at Olympic Dam: Constraining sulphide growth. In: Cook *et al*. (Eds), Giant Ore Deposits Downunder, *17th Quadrennial IAGOD Symposium, Adelaide, Symposium Proceedings*, 78-79.

Meixner, A. J., and Roy, I.G., 2010. Depth to magnetic basement map of the Gawler-Curnamona region, South Australia (First Edition), 1:750 000 scale, *Geoscience Australia*, Canberra. www.ga.gov.au/products/servlet/controller?event=GEOCAT_DETAILS&catno=70594

Mernagh, T. P., Heinrich, C. A., Leckie, J. F., Carville, D. P ., Gilbert, D. J., Valenta, R. K. and Wyborn, L. A. I., 1994. Chemistry of the low-temperature hydrothermal gold, platinum, and palladium (± uranium) mineralization at Coronation Hill, Northern Territory, Australia. *Economic Geology*, **89**, 1053-1073.

Mernagh, T. P., Wyborn, L. A. I. and Jagodzinski, E. A., 1998. "Unconformity-related" U ± Au ± platinum-group-element deposits. *AGSO Journal*, **17**, 197-205.

Minty, B. R. S., Franklin, R., Milligan, P. R., Richardson, L. M., and Wilford, J., 2010. Radiometric Map of Australia (Second Edition), scale 1:15 000 000. Geoscience Australia, Canberra.

Morales, R. S., Both, R. A. and Golding, S., 2002. A fluid inclusion and stable isotope study of the Moonta copper-gold deposits, South Australia: Evidence for fluid immiscibility in a magmatic hydrothermal system. *Chemical Geology*, **192**, 211-226.

Morgan, P. 1984. The thermal structure and thermal evolution of the continental lithosphere. *Physics and Chemistry of the Earth*, **15**, 107–185.

Mortimer, G. E., Cooper, J. A. and Oliver, R. L., 1988 - The geochemical evolution of Proterozoic granitoids near Port Lincoln in the Gawler orogenic domain of South Australia. *Precambrian Research*, **40/41**, 387-406.

Nash, J. T., 2010. Volcanogenic uranium deposits – geology, geochemical processes, and criteria for resource assessment. *United States Geological Survey Open-File Report*, **2010-1001**, 99pp.

Neumann, N., Sandiford, M. and Foden, J., 2000. Regional geochemistry and continental heat flow: implications for the origin of the South Australian heat flow anomaly. *Earth and Planetary Science Letters*, **183**, 107-120.

Neumann, N. L., Hore, S., Fraser, G. L., 2009. New SHRIMP geochronology from the Mount Painter Province, South Australia. *Geoscience Australia Record*, **2009/28**, 136-139.

Nex, P. A. M., Kinnaird, J. and Oliver, G. J. H., 2001. Petrology, geochemistry and uranium mineralisation of post-collisional magmatism around Goanikontes, southern Central Zone, Damaran Orogen, Namibia. *Journal of African Earth Sciences,* **33**, 481-502.

Nex, P., Herd, D. and Kinnaird, J., 2002. Fluid extraction from quartz in sheeted leucogranites as a monitor to styles of uranium mineralization: an example from the Rössing area, Namibia. *Geochemistry: Exploration, Environment, Analysis*, **2**, 83-96.

Nixon, L. G. B. and Townend, R., 1966. The occurrence and petrology of syenite porphyry at the Burra copper mine. *Geological Survey of South Australia Quarterley Geological Notes*, **17**, 1-5.

Noble, R. J., Just, J. and Johnson, J. E., 1983. Catalogue of South Australian Minerals - 1983. Adelaide, D. J. Woolman, Government Printer, 248 pp.

Noorollahi, Y., Itoi, R., Fujii, H. and Tanaka, T., 2007. GIS model for geothermal resources exploration in Akita and Iwate Prefecture, northern Japan. *Computer and Geosciences,* **33** 1008-1021.

Norden, B. and Forster, A., 2006. Thermal conductivity and radiogenic heat production of sedimentary and magmatic rocks in the Northeast German Basin. *American Association of Petroleum Geologists Bulletin,* **90**, 939-962.

Nutman, A. P. and Ehlers, K., 1998. Evidence for multiple Paleoproterozoic thermal events and magmatism adjacent to the Broken Hill Pb-Zn-Ag orebody, Australia. *Precambrian Research,* **90**, 203-238.

OECD Nuclear Energy Agency, 2008. Uranium 2007 - Resources, production and demand. Organisation for Economic Cooperation and Development Publishing, Paris. 420pp.

Oliver, N. H. S., Cleverley, J. S., Mark, G., Pollard, P. J., Fu, B., Marshall, L. J., Rubenach, M. J., Williams, P. J. and Baker, T., 2004. Modelling the role of sodic alteration in the genesis of iron oxide – copper – gold deposits, eastern Mt Isa Block, Australia. *Economic Geology,* **99**, 1145-1176.

Oreskes, N. and Einaudi, M. T. 1992. Origin of hydrothermal fluids at Olympic Dam: Preliminary results from fluid inclusions and stable isotopes. *Economic Geology,* **87**, 64-90.

Page, R. W. and Laing, W. P., 1992. Felsic metavolcanic rocks related to the Broken Hill Pb-Zn-Ag orebody, Australia: geology, depositional age, and timing of high-grade metamorphism. *Economic Geology,* **87**, 2138-2168.

Page, R. W., Stevens, B. P. J. and Gibson, G. M., 2005. Geochronology of the sequence hosting the Broken Hill Pb-Zn-Ag orebody, Australia. *Economic Geology*, **100**, 633-661.

Page, R. W., Stevens, B. P. J., Gibson, G. M. and Conor, C. H. H., 2000. Geochronology of Willyama Supergroup rocks between Olary and Broken Hill, and comparison to northern Australia. *AGSO* Record **2000/10**, 72-75.

Parker, A. J., 1993. Palaeoproterozoic, In: Drexel, J. F., Preiss, W. V. and Parker, A. J. (eds), The geology of South Australia. Vol. 1, The Precambrian. *Geological Survey of South Australia Bulletin,* **54(1)**, 51-105 .

Parker, A. J. and Fanning, C. M., 1998. WHYALLA, South Australia, sheet S153-8, South Australia.Department of Primary Industries and Resources. 1:250 000 Series – Explanatory Notes, South Australia.Department of Primary Industries and Resources.

Payne, J. L., Barovich, K. and Hand, M., 2006. Provenance of metasedimentary rocks in the northern Gawler Craton, Australia: implications for Paleoproterozoic reconstructions. *Precambrian Research,* **148**, 275-291.

Payne, J. L., Ferris, G., Barovich, K. M. and Hand, M., 2009. Pitfalls of classifying ancient magmatic suites with tectonic discrimination diagrams: An example from the Paleoproterozoic Tunkillia Suite, southern Australia. *Precambrian Research,* **177**, 227-240.

Payne, J. L., Hand, M., Barovich, K. M. and Wade, B. P., 2008. Temporal constraints on the timing of high-grade metamophism in the northern Gawler Craton: implications for assembly of the Australian Proterozoic. *Australian Journal of Earth Sciences,* **55**, 623-640.

Peiffert, C., Nguyen-Trung, C. and Cuney, M., 1996. Uranium in granitic magmas: Part 2. Experimental determination of uranium solubility and fluid-melt partition coefficients in the uranium oxide-haplogranite-H_2O-NaX (X = Cl, F) system at 770°C, 2 kbar. *Geochimica et Cosmochimica Acta*, **60**, 1615-1529.

Petford, N., Cruden, A. R., McCaffrey, K. J. W. and Vigneresse, J.-L., 2000. Granite magma formation, transport and emplacement in the Earth's crust. *Nature*, **408**, 669-673.

Pidgeon, R.T. 1979. Report on the U-Pb age of monazite samples 930, 931 and 932 (from the Mount Painter area). *South Australian Department of Mines and Energy*, *Open File Envelope*,***3931*** .

PIRSA, 2002. Petroleum Basins and Provinces. https://sarig.pir.sa.gov.au/sarig/frameSet.jsp (accessed December 2010)

PIRSA, 2006a. Mineral Geological Provinces. https://sarig.pir.sa.gov.au/sarig/frameSet.jsp (accessed December 2010).

PIRSA, 2006b. Cooper and Eromanga Basins - Consolidated Data Package. http://www.pir.sa.gov.au/petroleum/home/access_to_data/free_data/cooper__and__eromanga_consolidated_data_package (Accessed March 2008)

PIRSA, 2010a. Curnamona Province – 3D sedimentary basin model. http://www.pir.sa.gov.au/minerals/geology/3d_geological_models/curnamona_sedimentary_basin_model (accessed December 2010)

PIRSA, 2010b. Petroleum and Geothermal in South Australia 2010, data package DVD.

PIRSA, 2010c. Petroleum – Basin and Province Information, http://www.pir.sa.gov.au/petroleum/prospectivity/basin_and_province_information (accessed March 2011).

PIRSA, 2011. Arrowie Basin (and the Central Adelaide Geosyncline). http://www.petroleum.pir.sa.gov.au/__data/assets/pdf_file/0006/26916/prospectivity_arrowie.pdf (accessed April 2011)

Plant, J. A., Simpson, P. R., Smith, B. and Windley, B. F., 1999. Uranium ore deposits: products of the radioactive earth. *Reviews in Mineralogy and Geochemistry*, **38**, 255-319.

Polito, P. A., Kyser, T. K., Rheinberger, G. and Southgate, P. N., 2005a. A Paragenetic and Isotopic Study of the Proterozoic Westmoreland Uranium Deposits, Southern McArthur Basin, Northern Territory, Australia. *Economic Geology*, **100**, 1243-1260.

Polito, P. A., Kyser, T. K., Thomas, D., Marlatt, J. and Drever, G., 2005b. Re-evaluation of the petrogenesis of the Proterozoic Jabiluka unconformity-related uranium deposit, Northern Territory, Australia. *Mineralium Deposita*, **40**, 257-288.

Polito, P. A., Kyser, T. K., and Jackson, M. J., 2006. The role of sandstone diagenesis and aquifer evolution in the formation of uranium and zinc-lead deposits, southern McArthur Basin, Northern Territory, Australia. *Economic Geology*, **101**, 1189-1209.

Preiss, W. V., 1985. Stratigraphy and tectonics of the Worumba anticline and associated intrusive breccias. *Geological Survey of South Australia Bulletin*, **52**, 85pp.

Preiss, W. V., 1987 (Compiler). The Adelaide Geosyncline – late Proterozoic stratigraphy, sedimentation, palaeontology and tectonics. *Geological Survey of South Australia Bulletin*, **53**, 105pp.

Preiss, W. V., 1993. Neoproterozoc. In: Drexel, J. F., Preiss, W. V. and Parker, A.J. (eds.), The Geology of South Australia. Volume 1, The Precambrian. *Geological Survey of South Australia Bulletin* **54(1)**, 171-203.

Preiss, W. V., 2000. The Adelaide Geosyncline of South Australia, and its significance in continental reconstruction. *Precambrian Research*, **100**, 21-63.

Preiss, W. V., 2010. Geology of the Neoproterozoic to Cambrian Adelaide Geosyncline and Cambrian Delamerian Orogen. *Geoscience Australia Record*, **2010/10**, 34-41.

Preiss, W. V. and Robertson, R. S., 2006. Adelaide Geosyncline and Stuart Shelf. In: Cooper, B. J. and McGeough, M. A. (eds), South Australia mineral explorers guide, second edition. *Primary Industries and Resources, South Australia Mineral Exploration Data Package*, **11**, ch. 7.

Preiss, W. V., Korsch, R. J., Blewett, R. S., Fomin, T., Cowley, W. M., Neumann, N. L. and Meixner, A. J., 2010. Geological interpretation of deep seismic reflection line 09GA-CG1: the Curnamona Province-Gawler Craton Link Line, South Australia. *Geoscience Australia Record*, **2010/10**, 66-76.

Radke, B. M., Feguson, J., Cresswell, R. G., Ransley, T. R. and Haberbehl, M. A., 2000. Hydrochemistry and implied hydrodynamics of the Cadna-owie Hooray Aquifer, Great Artesian Basin, Australia. Bureau of Rural Sciences, Canberra, 229pp.

Raymond, O. L., 2003. Yorke Peninsula (Moonta Subdomain) pre-Neoproterozoic geology. 1:250,000 scale map, 2nd edition. *Geoscience Australia*, Canberra. www.ga.gov.au/products/servlet/controller?event=GEOCAT_DETAILS&catno=68741

Raymond, O. L., and Retter, A. J., (eds), 2010. Surface geology of Australia 1:1,000,000 scale, 2010 edition [Digital Dataset]. Geoscience Australia, Canberra. http://www.ga.gov.au.

Raymond, O. L., Fletcher, I. and McNaughton, N., 2002. Copper-gold mineral systems in the southeastern Gawler craton – another Mt Isa Eastern Succession? [abs]. *Geological Society of Australia Abstracts*, **67**, 69.

Raznjevic, K., 1976, Handbook of Thermodynamic Tables and Charts, Washington DC: Hemisphere Publishing Corporation.

Reeve, J. S., Cross, K. C., Smith, R. N. and Oreskes, N., 1990. Olympic Dam copper-uranium-gold-silver deposit. *Australasian Institute of Mining and Metallurgy Monograph*, **14**, 1009-1035.

Reid, A.J., 2010. PACE geochronology. Presentation to SAREIC Technical Forum, 2010. http://www.pir.sa.gov.au/_data/assets/pdf_file/0008/132749/Reid.pdf (Accessed March 2011)

Reid, A., Hand, M., Jagodzinski, E., Kelsy, D. and Pearson, N., 2008. Palaeoproterozoic orogenesis in the southeastern Gawler Craton, South Australia. *Australian Journal of Earth Sciences*, **55**, 449-471.

Reid, P. W., McAllister, L., and Messeiller, M., 2010. Status of the Paralana 2 Hydraulic Stimulation Program. *Australian Geothermal Conference, Adelaide 2010*, extended abstract.

Reynolds, L. J., 2000. Geology of the Olympic Dam Cu-U-Au-Ag-REE deposit. In: Porter, T. M., Ed., Hydrothermal iron oxide copper-gold and related deposits: A global perspective, Volume **2**. Adelaide, *Porter GeoConsultancy Publishing*, 93-104.

Robertson, R. S., 1995. Copper and gold in South Australia. *Geological Survey of South Australia Report Book*, **95/41**, 23 pp.

Roger, J. J. W. and Adams, J. A. S., 1969. Uranium. 92-E. Abundance in common igneous rocks. *Handbook of Geochemistry*, 92-E-1 to 92-E-8.

Rogers, P. A., Lindsay, J. M., Alley, N. F., Barnett, S. R., Lablack, K. L., Kwitko, G., 1995. Murray Basin. In: Drexel, J. F. and Preiss, W. V. (eds), The geology of South Australia. Volume 2, The Phanerozoic. *Geological Survey of South Australia Bulletin*, **54(2)**, 157-163.

Rowlands, N. J., Drummond, A. J., Jarvis, D. M., Warin, O. N., Kitch, R. B. and Chuck, R .G., 1978. Gitological aspects of some Adelaidean stratiform copper deposits. *Minerals Science and Engineering*, **10**, 258-277.

Rozsypal, C. 2009. Etude expérimentale et modélisation, en fonction du pH et de la concentration en NaCl, du système ternaire U(VI)-NaCl-H_2O à T = 155°C et pression de vapeur saturante. Unpublished Ph.D. thesis, Université Henri Poincaré, Nancy, France. http://scd.uhp-nancy.fr/docnum/SCD_T_2009_0127_ROZSYPAL.pdf,

Rudnick, R. L. and Gao, S., 2003. Composition of the Continental Crust. *Treatise of Geochemistry*, **3**, 1–64.

Rutherford, L. S., Burtt, A., Hatch, K. M., Hand, M. P. and Foden, J. D. 2007. Billeroo North alkaline magmatic complex: geology and economic significance. *MESA Journal* **45**, 33-39.

Ruzicka, V., 1993. Unconformity-associated uranium deposits. *Geological Association of Canada Special Paper*, **40**, 125-149.

Sandiford, M., Hand, M. and McLaren, S. N., 1998. High geothermal gradient metamorphism during thermal subsidence. *Earth and Planetary Science Letters*, **163**, 149-165.

Sass, J. H., 1964. Heat-flow values from the Precambrian Shield of Western Australia. *Journal of Geophysical Research*, **69**, 299-308.

Schmidt Mumm, A., Clark, C. and Skirrow, R. G. 2006. Mineral exploration under cover: characterising mineralising fluid systems. *Journal of Geochemical Exploration* **89**, 359-362.

Schofield, A., 2009. Uranium content of igneous rocks of Australia 1:5 000 000 maps: explanatory notes and discussion. *Geoscience Australia Record*, **2009/17**, 20pp.

Schofield, A., 2010a. Investigation of drill holes in the vicinity of the 08GA-C1 seismic line in the Curnamona Province, South Australia. *Geoscience Australia Record*, **2010/21**, 33pp.

Schofield, A., 2010b. Potential for magmatic-related uranium mineral systems in Australia. *Geoscience Australia Record*, **2010/20**, 56pp.

Schofield, A. and Huston, D., 2010. Magmatic-related uranium systems. In: Huston, D.L. (ed), An assessment of the uranium and geothermal potential of north Queensland. *Geoscience Australia Record*, **2010/14**, 54-67.

Schofield, A., Le Gleuher, M., Cross, A. and Jaireth, S., 2009. Four Mile uranium deposit: mineralogy. In: Skirrow, R.G. (ed.), Uranium ore-forming systems of the Lake Frome region, South Australia: regional controls and exploration criteria. *Geoscience Australia Record* **2009/40** 67-79.

Selley, D., Broughton, D., Scott, R., Hitzman, M., Bull, S., Large, R., McGoldrick, P., Croaker, M., Pollington, N. and Barra, F., 2005. A new look at the geology of the Zambian copper belt. *Economic Geology 100th Anniversary Volume*, 965-1000.

Skidmore, C., 2005. Geology of the Honeymoon uranium deposit. *Geological Society of South Australia Abstracts*, **78**, 8-10.

Skirrow, R. G. (ed), 2009. Uranium ore-forming systems of the Lake Frome region, South Australia: regional spatial controls and exploration criteria. *Geoscience Australia Record*, **2009/40**, 151pp.

Skirrow, R. G., 2010. 'Hematite-group' IOCG±U ore systems: Tectonic settings, hydrothermal characteristics, and Cu-Au and U mineralizing processes. In: Corriveau, L. and Mumin, H. (eds), Exploring for Iron Oxide Copper-Gold Deposits: Canada and Global Analogues. *Geological Association of Canada Shortcourse Notes*, **20**, 39-58.

Skirrow, R. G., 2011. Controls on uranium in iron oxide copper-gold systems: insights from Proterozoic and Paleozoic deposits in southern Australia. *Proceedings of Society for the Geology Applied to Ore Deposits 11th Biennial Meeting*, Antofagasta, Chile, 26-29th September 2011, in press.

Skirrow, R. G. and Ashley, P. M., 1998. Copper-gold mineral systems and regional alteration, Curnamona Craton. *AGSO* Record, **1998/25**, 104-108.

Skirrow, R. G., Ashley, P. M., McNaughton, N. J. and Suzuki, K., 2000. Time-space framework of Cu-Au(-Mo) and regional alteration systems in the Curnamona Province. *AGSO* Record **2000/10**, 83-86.

Skirrow, R. G., Bastrakov, E., Davidson, G., Raymond, O., Heithersay, P. 2002. Geological framework, distribution and controls of Fe-oxide Cu-Au deposits in the Gawler Craton. Part II. Alteration and mineralisation. In: Porter, T.M. (Ed.), Hydrothermal iron oxide copper-gold and related deposits, Volume **2**, *PGC Publishing*, Adelaide, 33-47.

Skirrow, R. G., Fairclough, M. C., Budd, A. R., Lyons, P., Raymond, O., Milligan, P., Bastrakov, E., Fraser, G., Highet, L., Holm, O., Williams, N., 2006. Iron oxide Cu-Au (-U) potential map of the Gawler Craton, South Australia (1st Edition), 1:500 000 scale. *Geoscience Australia*, Canberra. www.ga.gov.au/products/servlet/controller?event=GEOCAT_DETAILS&catno=64165

Skirrow, R. G., Bastrakov, E. N., Barovich, K, Fraser, G. L, Creaser, R. A., Fanning, C. M., Raymond, O. L., and Davidson, G. J., 2007. Timing of iron oxide Cu-Au-(U) hydrothermal activity and Nd isotopic constraints on metal sources in the Gawler Craton, South Australia. *Economic Geology,* **102**, 1441-1470.

Skirrow, R. G., Jaireth, S., Huston, D. L., Bastrakov, E. N., Schofield, A., van der Wielen, S. E. and Barnicoat, A. C. 2009. Uranium mineral systems: Processes, exploration criteria, and a new deposit framework. *Geoscience Australia* Record **2009/20**.

Skirrow, R. G., Creaser, R. and Hore, S. B., 2011. Mt Gee-Armchair U-REE deposits, South Australia. In: Skirrow, R.G. (editor), Timing of uranium mineralisation events in Australia. *Geoscience Australia Record*, **2011/12**, 36-58.

Skvarla, M. J., Vandersande, J. W., Linvill, M. L., and Pohl, R. O., 1981. Thermal conductivity of selected repository minerals. *Scientific Basis for Nuclear Waste Management,* **3**, 43–50.

Sørensen, H., 2001. Brief introduction to the geology of the Ilímaussaq alkaline complex, south Greenland, and its exploration history. *Geology Survey of Greenland Bulletin,* **190**, 7-23.

Spalding, R. F., Druliner, A. D., Whiteside, L. S. and Struempler, A. W., 1984. Uranium geochemistry in groundwater from Tertiary sediments. *Geochemical et Cosmochimica Acta,* **48**, 2679- 2692.

Staatz, M. H., 1978. I and L uranium and thorium vein system, Bokan Mountain, southeastern Alaska. *Economic Geology*, **73**, 512-523.

Stevens, B. P., Barnes, R. G., Brown, R. E., Stroud, W. J. and Willis, I. L., 1988. The Willyama Supergroup in the Broken Hill and Euriowie Domains, New South Wales. *Precambrian Research*, **40-41**, 297-327.

Stevens, B. P. J and Stroud, W. J. (eds) 1983. Rocks of the Broken Hill Block: Their classification, nature, stratigraphic distribution, and origin. *Records of the Geological Survey of New South Wales*, **21**(1).

Stoian, L., 2010. Palynology: examples and applications from recent projects. SAREIC 2010—Technical Forum. http://www.minerals.pir.sa.gov.au/__data/assets/pdf_file/0003/132753/Liliana_Stoian.pdf

Stüwe, K., 2007. Geodynamics of the Lithosphere. An Introduction. 2nd edition. Springer Verlag, 493 p.

Sun, S.-S. and McDonough, W. F., 1989. Chemical and isotope systematics of oceanic basalts: implication for mantle composition and processes. *Geological Society of London Special Paper*, **42**, 323-346.

Szpunar, M. and Fraser, G., 2010. Age of deposition and provenance of Palaeoproterozoic basins on north-eastern Eyre Peninsula. *Department of Primary Industries and Resources, South Australia. Report Book*, **2010/08**.

Szpunar, M., Hand, M., Barovich, K., Jagodzinski, E., Belousova, E., 2011. Isotopic and geochemical constraints on the Paleoproterozoic Hutchison Group, southern Australia: Implications for Paleoproterozoic continental reconstructions. *Precambrian Research*, **187**, 99–126.

Taylor, S. R., and McLennan, S. M., 1985. The Continental Crust: Its Composition and Evolution. Blackwell, Oxford.

Teale, G. S. and Fanning, C. M., 2000. The timing of Cu-Au mineralisation in the Curnamona Province. *AGSO* Record **2000/10**, 98-100.

Tester, J. W. 1982. Energy Conversion and Economic Issues for Geothermal Energy. Handbook of Geothermal Energy. Gulf Publishing Co., Houston, Texas. 471–586.

Thompson, T. B., 1988. Geology and uranium-thorium mineral deposits of the Bokan Mountain granite complex, southeastern Alaska. *Ore Geology Reviews*, **3**, 193-210.

Thompson, T. B., Pierson, J. R. and Lyttle, T., 1982. Petrology and petrogenesis of the Bokan Granite Complex, southeastern Alaska. *Geological Survey of America Bulletin*, **93**, 898-908.

Tonkin, D.G., and Creelman, R. A., 1990. Mount Gunson copper deposits. *Australasian Institute of Mining and Metallurgy Monograph*, **14**, 1037-1043.

van der Weilen, S. E., Kirkby, A., Britt, A. F., Nicoll, M. G., and Skirrow, R., 2011. An integrated 3D map for the greater Eromanga Basin, Australia. Geoscience Australia Record. in preparation.

Walshe, J. L., Cooke, D. R. and Neumayr, P., 2005. Five questions for fun and profit: a mineral systems perspective on metallogenic epochs, province and magmatic hydrothermal Cu and Au deposits. In: Mao, J. and Bierlein, F. P. (eds), Mineral Deposit Research: Meeting the Global Challenge. Springer, Berlin, 477-480.

Walter, M. R., Veevers, J. J., Calver, C. R., and Gray, K., 1995. Neoproterozoic stratigraphy of the Centralian Superbasin, Australia. *Precambrian Research*, **73**, 173-195.

Ward, L. K. and Jack, R. L., 1916. the Yudnamutana mining field. *Geological Survey of South Australia Report*, **3**, 20pp.

Watson, E. B. and Harrison, T. M., 1983. Zircon saturation revisited: temperature and composition effects in a variety of crustal magma types. *Earth and Planetary Science Letters*, **64**, 295-304.

Webb, B. P., 1960. Diapiric structures in the Flinders Ranges, South Australia. *Journal of the Geological Society of Australia*, **22**, 9.

Webb, B. P., 1961, The geological structure of the Blinman Dome. *Transactions of the Royal Society of South Australia*, **85**, 1-6.

Wedepohl, K. H., 1974. Copper. 29-E. Abundance in common igneous rock types; crustal abundances. *Handbook of Geochemistry*, 29-E-1 to 29-E-13.

Weste, G. 1996. Geology of the Roopena and Uno 1:100 000 scale map sheets, eastern Gawler Craton. *Primary Industry and Resources, South Australia Open File Envelope*, **9025**, 348 pp.

Whitaker, A. J., Glanville, H. D., English, P. M., Stewart, A. J., Retter, A. J., Connolly, D. P., Stewart, G. A., and Fisher, C. L., 2008. Surface geology of Australia 1:1,000,000 scale, South Australia [Digital Dataset]. Geoscience Australia. http://www.ga.gov.au.

Whittle, A. W. G., 1954. Petrology of Crockers Well uranium deposit. *Geological Survey of South Australia Bulletin*, **30**, 79-83.

Williams, N. C., Lane, R., and Lyons, P. 2004. Regional constrained 3D inversion of potential field data from the Olympic Cu-Au province, South Australia. *Preview*, **109**, 30-33.

Williams, P. J. and Skirrow, R. G., 2000. Overview of iron oxide-copper-gold deposits in the Curnamona Province and Cloncurry district (eastern Mount Isa Block), Australia. In: Porter, T.M. (ed), Hydrothermal iron oxide copper-gold and related deposits, Volume **1**. *Australian Mineral Foundation*, Adelaide, 105-122.

Williams, P. J., Barton, M. D., Johnson, D. A., Fontboté, L., De Haller, A., Mark, G., Oliver, N. H. S. and Marschik, R. 2005. Iron Oxide Copper-Gold Deposits: Geology, Space-Time Distribution, and Possible Modes of Origin. *Economic Geology 100th Anniversary Volume*, 371-405.

Wilson, T. and Fairclough, M., 2009. Uranium and uranium mineral systems in South Australia. *Primary Iindustry and Resources, South Australia Report Book*, **2009/14**, 182pp.

Wilson, T., Bosman, S., Heath, P., Gouthas, G., Cowley, W., Mauger, A., Baker, A., Gordon, G., Dhu, T., Fairclough, M. and Delaney, G., 2010. The search for unconformity-related uranium mineralisation in the Pandurra Formation, South Australia: an international multidisciplinary collaboration. *MESA Journal*, **58**. 9-15.

Wingate, M. T. D., Campbell, I. H., Compston, W. and Gibson, G. M., 1998. Ion-probe U-Pb ages for Neoproterozoic basaltic magmatism in south-central Australia and implications for the breakup of Rodinia. *Precambrian Research*, **87**, 135-159.

World Nuclear Association, 2010. Geology of Uranium Deposits, World Nuclear Association. http://www.world-nuclear.org/info/inf26.html

Wülser, P.-A., 2009. Uranium metallogeny in the North Flinders Ranges region of South Australia. Unpublished Ph.D. thesis, The University of Adelaide, 237pp.

Wyborn, L. A. I., Heinrich, C. A. and Jaques, A. L., 1994. Australian Proterozoic mineral systems: essential components and mappable criteria. *Australasian Institute of Mining and Metallurgy Publications Series*, **5/94**, 109-115.

Yang, K. and Ashley, P. M., 1994. Stratabound breccias in the Willyama Supergroup, Olary Block, South Australia. *Australian Mineral Foundation*, Proceedings, Australian Research on Ore Genesis Symposium, Adelaide, December 1994, 16.1-16.5.